Modulation of synaptic transmission by interacting proteins and transporters

Daniela Billups

A thesis submitted to the University of London
for the degree of
Doctor of Philosophy

Department of Physiology, University College London

February 2002

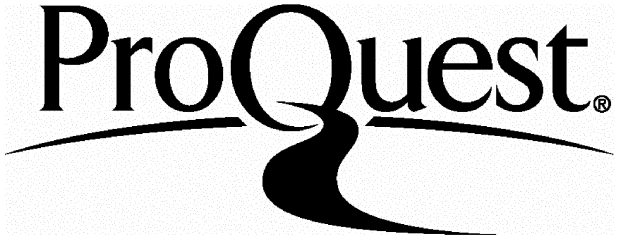

Abstract

The properties of synaptic transmission may be modulated by transporters which regulate neurotransmitter and ion concentrations, and by proteins which interact with ion channels and transporters. I have investigated this for inhibitory and excitatory synapses in the retina and the cerebellum, using electrophysiological (patch-clamp) techniques. For inhibitory synaptic transmission, I have (1) discovered that $GABA_C$ receptors in retinal bipolar cells are modulated by the intracellular cytoskeletal protein MAP-1B, and shown that disrupting the interaction between MAP-1B and the $GABA_C$ receptor increases the sensitivity of the receptor to GABA, which is expected to alter the duration of the inhibitory postsynaptic current in these cells; and (2) studied the possibility that chloride transporters maintain a non-uniform intracellular chloride distribution in retinal bipolar cells, which determines the direction and magnitude of the GABA evoked membrane potential changes in the cell. For excitatory synaptic transmission I have (1) studied glutamatergic synaptic transmission in the cerebellum of transgenic mice lacking either of the glutamate transporters GLT-1 or GLAST, and demonstrated that GLAST knockout prolongs the synaptic current at the parallel fibre to Purkinje cell synapse, but that knocking out GLT-1 or GLAST does not alter the mossy fibre to granule cell synaptic current; (2) studied the effect of glycine on mossy fibre to granule cell synaptic transmission in the cerebellum of the rat, showing that the NMDA receptor glycine site is saturated even when no glycine is added to the superfusing solution; and (3) studied the properties of the LIM protein Ajuba, which interacts with the major glial glutamate transporter GLT-1, and shown that Ajuba does not modulate the transporter's glutamate sensitivity, its associated anion channel, or the number of transporters in the plasma membrane.

Acknowledgements

I would like to sincerely thank David Attwell for giving me the opportunity to join his lab, for supporting, helping and trusting me and for giving me a great chance to gather lots of scientific and non-scientific experience.

Thanks also to the people whom I directly collaborated with over the past three years – Jonathan Hanley, Helene Marie and Paikan Marcaggi. Thanks also to Jonathan Ashmore for being my second supervisor and for lending me the pico-spritzer used in Chapter 4, to Blair Grubb for helping me take the retinal pictures with the confocal microscope and to Steven McGuinness for taking over the genotyping of the mice.

I am especially happy to have had the chance to share three years with Celine Auger, Marina Catsicas and Martine Hamann - thanks for the many discussions and chats, for the encouragement, friendship, the real coffee and for keeping me sane, girls!

I am also very grateful to all the other members of the lab for their support, encouragement and friendly atmosphere - Nicola Allen, Nana Luneborg, Peter Mobbs, Monique Sarantis, David Rossi, Rachael Pearson and Orfeus Warr.

Besonderen Dank auch an meine Eltern, die meine Freude, Neugierde und Begeisterung an der Natur und den Naturwissenschaften geweckt haben, und die mich in den Jahren vor und waehrend meiner Doktorarbeit immer ermutigt und unterstuetzt haben.

A very special thanks to Brian!

I am grateful to the Wellcome Trust for funding my PhD.

Table of Contents

List of Figures

List of Tables

CHAPTER 1

Introduction

Information processing in the central nervous system depends on neurones communicating with each other via fast chemical synaptic transmission. An invading action potential depolarizes the cell's presynaptic terminal, leading to the opening of voltage-gated calcium channels. The resulting influx of calcium ions causes the exocytosis of synaptic vesicles, the contents of which are released into and diffuse across the synaptic cleft to the postsynaptic cell, where they bind to specific neurotransmitter receptors. These are often membrane-spanning proteins which contain an ion channel within their structure. Upon binding of the appropriate ligand, these channels open and permit the passage of ions. This results in a change of the postsynaptic membrane potential, which spreads across the cell's membrane and integrates with membrane potential changes produced by other synaptic inputs. At excitatory synapses the postsynaptic membrane is depolarized, while at inhibitory synapses the postsynaptic membrane is hyperpolarized or is stabilized at the cell's resting potential ("shunting inhibition") making it harder for the cell to fire an action potential. The sum of all the potential changes produced by the excitatory and inhibitory synaptic inputs to a cell determines whether the cell fires an action potential. The most common excitatory neurotransmitter in the mammalian central nervous system is glutamate (for a review see for example Watkins, 2000), and the most common inhibitory transmitter in higher brain regions is GABA. The action of these two neurotransmitters is terminated by their removal from the site of action (by diffusion and by uptake into cells), rather than by extracellular enzymatic degradation.

Figure 1.1: Modulation of synaptic transmission by transporters and interacting proteins: the mechanisms studied in this thesis

This is a schematic drawing of a hypothetical composite excitatory and inhibitory synapse, to show the mechanisms studied in this thesis. GABAergic transmission is on the left (red colours), glutamatergic transmission is on the right hand side of the scheme (green colours).

During GABAergic synaptic transmission GABA is released from the presynaptic terminal by vesicular exocytosis. It can bind to postsynaptic $GABA_A$ (dark red cylinder) or $GABA_C$ (light red cylinder) receptors, which open and permit the passage of chloride ions. $GABA_C$ receptors interact with the microtubule associated protein MAP-1B (which in turn binds to microtubules and actin) and possibly with the glycine transporter splice variant GLYT-1E/F (yellow), as studied in chapter 3. Chloride transporters (KCC-2 and NKCC-1; blue) set the gradient for GABA responses, as studies in chapters 4. GABA is removed from the extracellular space by GABA transporters (GAT; orange) located for example in glial cells. During glutamatergic synaptic transmission, glutamate is released from the presynaptic terminal via vesicular exocytosis. It can bind to postsynaptic AMPA (dark green cylinder) and NMDA (light green cylinder) receptors, which permit the passage of cations (as studies in chapters 6 and 7). Glutamate is removed from the extracellular space by glutamate transporters (studied in chapter 6) such as GLAST and GLT-1 (located in glial cells; green), the latter of which interacts with a cytosolic protein called Ajuba (which is studied in chapter 5). NMDA receptors require the binding of glutamate and glycine or D-serine in order to be activated. D-serine may be released from glial cells. The extracellular glycine concentration is controlled by glycine transporters such as GLYT-1 in glial cells (yellow), the activity of which may modulate NMDA receptors. Glycine can be co-released with GABA from GABAergic terminals and may spill-over to glutamatergic synapses (chapter 7).

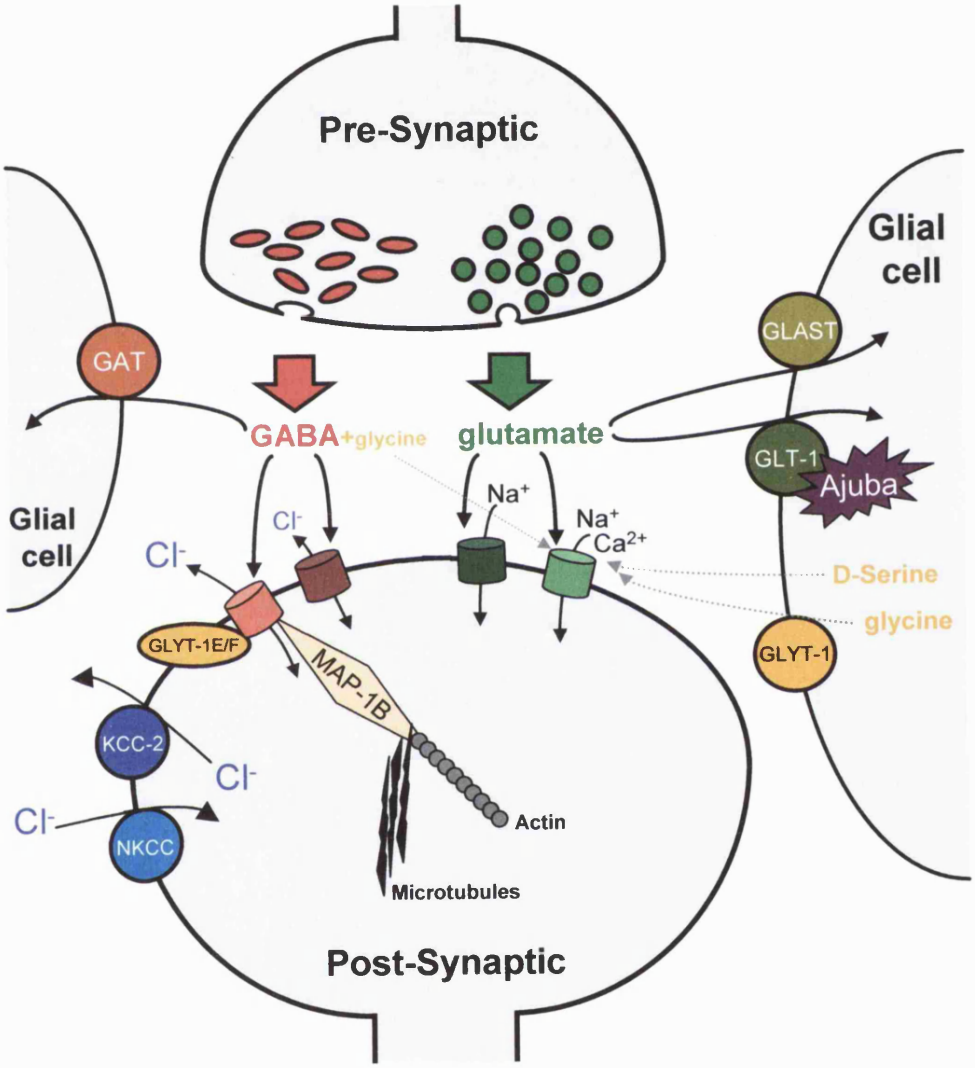
Pre-Synaptic
Glial cell
GAT
GABA+glycine
glutamate
GLAST
GLT-1
Ajuba
Glial cell
Na+
Cl-
Na+
Ca2+
Cl-
D-Serine
glycine
GLYT-1E/F
MAP-1B
GLYT-1
KCC-2
Cl-
Cl-
NKCC
Actin
Microtubules
Post-Synaptic

The properties of synaptic transmission may be modulated by transporters that regulate neurotransmitter and ion concentrations, and by proteins that interact with ion channels and transporters (Figure 1.1). For example, as reviewed below, transporters regulating neurotransmitter concentration help to control the duration of transmitter action, while transporters controlling the concentrations of ions that pass through a ligand-gated channel determine the magnitude and sign of the synaptic current. Interacting proteins can control the activity and subcellular location of ion channels and transporters, and thus modulate synaptic currents, as described below. In this thesis I have investigated these modulatory influences for inhibitory (chapters 3 and 4) and excitatory (chapters 5, 6 and 7) synapses in the retina and the cerebellum. In this chapter I will review some of the properties of the receptor and transporter proteins that were investigated, and the structures of the brain areas that were studied, to provide the essential background needed to understand the experiments I carried out. This review is broken down, first of all into an account of the relevant properties of excitatory and inhibitory transmission, and then describes the properties of the cerebellum and the retina in which I studied these two types of signalling.

1.1 Glutamate receptors

The synaptic currents I studied at excitatory synapses in chapters 6 and 7 were mediated by glutamate receptors. There are several different types of glutamate receptors, broadly divided into ionotropic and metabotropic receptors. Whereas ionotropic glutamate receptors (iGluRs) mediate fast excitatory synaptic transmission and contain an ion channel within their structure, metabotropic glutamate receptors (mGluRs) are coupled to GTP-binding proteins (G-proteins) and modulate second messenger-mediated processes inside the cell. All classes of glutamate receptors are found throughout the brain. Ionotropic receptors are primarily located at postsynaptic sites but can also be found at presynaptic terminals, whereas mGluRs are distributed

pre- and postsynaptically. Additionally, glutamate receptors can be found in glial cells (see Mayer and Westbrook, 1987a; Collingridge and Lester, 1989; Hollmann and Heinemann, 1994; McBain and Mayer, 1994; Michaelis, 1998; Ozawa et al., 1998; Dingledine et al., 1999 for reviews on glutamate receptors).

1.1.1 Ionotropic glutamate receptors

Due to their distinctive molecular biological, electrophysiological and pharmacological properties, ionotropic glutamate receptors can broadly be classified into three groups, termed NMDA (*N*-methyl-D-aspartate), AMPA (α-amino-3-hydroxy-5-methyl-isoxazole-4-proprionate) and KA (kainate) receptors. AMPA and KA receptors are pharmacologically similar and are often collectively referred to as non-NMDA receptors (Hollmann and Heinemann, 1994; Ozawa et al., 1998).

1.1.1.1 Structure of ionotropic glutamate receptor subunits

Ionotropic glutamate receptors are multimeric membrane-spanning proteins, composed of different subunits, and contain a cation-conducting pore within their structure. It was originally thought that, as for the super-family of ligand-gated chloride channels (see section 1.4), five subunits must assemble in order to form a functional ionotropic glutamate receptor channel (Hollmann and Heinemann, 1994; Premkumar and Auerbach, 1997). However, recent studies suggests that ionotropic glutamate receptors form and work as heteromeric tetramers (Laube et al., 1998; Mano and Teichberg, 1998; Rosenmund et al., 1998; Robert et al., 2001). The exact stoichiometry of subunit assembly of many of the ionotropic glutamate receptors is unclear, but the subunit composition is important for determining their properties and varies between different areas of the brain as well as at different stages of development (for a review see Ozawa et al., 1998; for a specific example see the description of developmental changes in the expression of the NMDA receptor NR2

subunits in cerebellar granule cells in section 1.9.3.1).

To date 16 different ionotropic glutamate receptor subunits have been identified, and characterised to varying extents. Four of those are present in AMPA receptors (GluR1, GluR2, GluR3 and GluR4), five in kainate receptors (GluR5, GluR6, GluR7, KA1 and KA2) and seven in NMDA receptors (NR1, NR2A, NR2B, NR2C, NR2D, NR3A and NR3B). Additionally, two other glutamate receptor subunits have been identified, namely δ1 and δ2 (Yamazaki et al., 1992; Lomeli et al., 1993). The δ subunits are mainly expressed by Purkinje cells (Araki et al., 1993) and located at the postsynaptic side of the parallel fibre to Purkinje cell synapse (Mayat et al., 1995; Landsend et al., 1997; Zhao et al., 1997) where they appear to play a role in long-term depression (Kashiwabuchi et al., 1995; Jeromin et al., 1996). However, δ1 and δ2 do not form functional channels when expressed on their own, and their properties and exact physiological function are unclear; they are also referred to as "orphan receptors" (Dingledine et al., 1999).

Although the various ionotropic glutamate receptor subunit types differ in their amino acid sequence, they share a similar structure and membrane topology. Each subunit is thought to possess a large extracellular amino-terminus with several (up to 12) glycosylation sites, which does not seem to be important for receptor subunit assembly but may be required for proper channel function (Dingledine et al., 1999). Three segments (TM1, TM3, TM4) traverse through the membrane and another forms a hairpin loop within the membrane (M2; Hollmann et al., 1994; Bennett and Dingledine, 1995). M2 is a candidate for lining the channel pore when the different subunits assemble to form the receptor, and some of its amino acid residues control the permeation properties of the channel (Ozawa et al., 1998). A large extracellular loop between TM3 and TM4 contains regions which determine some of the channel properties, such as desensitization kinetics. The relatively short intracellular C-terminus contains binding sites for intracellular proteins, and may thus be important for receptor targeting, as well as several putative phosphorylation

sites which may allow modulation of the receptor (Hollmann and Heinemann, 1994; Ozawa et al., 1998; Dingledine et al., 1999).

1.1.1.2 Non-NMDA receptors

In chapter 6 I investigate the role of glutamate transporters in terminating synaptic currents mediated by non-NMDA receptors. Non-NMDA receptors are low affinity glutamate receptors and have an EC_{50} for glutamate of about 0.5-1 mM for the peak response to rapid glutamate application, and less than 20 μM for the steady state response (Trussell and Fischbach, 1989; Patneau and Mayer, 1990). The main ions permeating the receptor channels are Na^+, K^+ and, depending on subunit composition (see below), Ca^{2+}. Their single-channel conductance is relatively small and varies, depending on the assembled subunits of the channel (see below), between about 200 fS and 25 pS (Dingledine et al., 1999). The channel conductance depends also on the number of glutamate molecules bound to the receptor, increasing in a step like fashion as each glutamate binds (Rosenmund et al., 1998; Smith and Howe, 2000). In response to agonist application the channels usually mediate rapidly activating and deactivating ($\tau \sim 1$ ms) currents, which desensitize rapidly ($\tau \sim$ 1-10 ms) (Trussell and Fischbach, 1989; Dingledine et al., 1999).

AMPA (GluR1-4) and kainate (GluR5-7 and KA1-2) receptor subunits share only around 40% amino acid sequence identity – this compares to around 70% identity between the four AMPA receptor subunits (GluR1-4), around 80% between the three low affinity kainate receptor subunits (GluR5-7), 70% between the two high affinity kainate receptor subunits (KA1-2) and only around 40% between the low and the high affinity kainate receptors (Hollmann and Heinemann, 1994). Each subunit contains around 900 amino acids and has a molecular mass of around 100 kDa (Hollmann and Heinemann, 1994). Most non-NMDA receptors function as homo- as well as heteromers, but it is believed that the latter are formed *in vivo* (Boulter et al., 1990; Dingledine et al., 1999). However, AMPA and kainate receptor subunits do

not co-assemble. The diversity of the AMPA (GluR1-4) as well as the kainate (GluR5-7 and KA1-2) receptor proteins and their properties is further increased by post-transcriptional modifications, such as alternative splicing ("flip" and "flop": Sommer et al., 1990; Monyer et al., 1991; Mosbacher et al., 1994) and RNA editing (Sommer et al., 1991; Lomeli et al., 1994), and by post-translational modifications, such as phosphorylation by certain protein kinases (Dingledine et al., 1999).

RNA editing results in the exchange of single amino acids in the receptor subunit, and occurs at several sites in the AMPA and kainate receptor subunits. The best studied example, which occurs in GluR2, GluR5 and GluR6 subunits (Dingledine et al., 1999), results in the exchange of a glutamine encoded in the DNA to an arginine in the M2 pore region of the channel (the "Q/R site"; Hume et al., 1991; Sommer et al., 1991; Verdoorn et al., 1991), and determines the channel's calcium permeability and sensitivity to polyamine block. Non-NMDA receptors are permeable to monovalent cations, primarily sodium and potassium *in vivo*, but are also permeant to calcium if the receptor subunits possess a glutamine (Q) at the Q/R site in M2. In addition, they are sensitive to polyamine block if the Q/R site is unedited (Burnashev et al., 1992; Egebjerg and Heinemann, 1993; Burnashev et al., 1996). The Q/R editing of the three subunits differs and is also developmentally regulated: GluR5 and GluR6 editing increases during development, so that about 50% of GluR5 and 80% of GluR6 are edited in the adult, while GluR2 is almost always edited. This means that AMPA receptors are calcium permeable when GluR2 is absent (Hollmann et al., 1991; Jonas et al., 1994). Non-NMDA receptors (GluR2-4) can also be edited at an R/G site: editing the arginine to a glycine at this site results in channels which recover faster from desensitization (Lomeli et al., 1994).

1.1.1.3 NMDA receptors

In chapters 6 and 7 I investigate the modulation by glutamate transporters and extracellular glycine of synaptic currents generated by NMDA receptors. NMDA

receptors are high affinity ionotropic glutamate receptors with an EC_{50} for glutamate of 2-3 μM for their steady state response (Patneau and Mayer, 1990). They require both the presence of an agonist (e.g. glutamate) and a co-agonist (glycine or D-serine) in order to be activated (Johnson and Ascher, 1987; Forsythe et al., 1988; Kleckner and Dingledine, 1988). The properties of the glycine binding site are described in detail in section 1.1.1.3.1. NMDA receptor channels conduct monovalent and some divalent cations, so that *in vivo* primarily sodium, potassium and calcium ions cross the membrane (Mayer and Westbrook, 1987b; Ascher and Nowak, 1988). The latter is of special interest, given the various intracellular second messenger cascades that calcium can trigger. Various agents, such as magnesium (Mayer et al., 1984; Nowak et al., 1984), zinc (Peters et al., 1987; Westbrook and Mayer, 1987), polyamines (Williams et al., 1989), protons (Tang et al., 1990; Traynelis and Cull-Candy, 1990) and arachidonic acid (Miller et al., 1992), modulate NMDA receptor channel properties. These can have significant physiological effects. The block of NMDA receptor channels by physiological concentrations of magnesium, for example, is strongly voltage-dependent (Mg^{2+} is pulled into the channel at negative membrane potentials) and is responsible for its characteristic J-shaped current-voltage relationship. This voltage dependent block by magnesium ions prevents the channel conducting ions at normal resting membrane potentials and allows the NMDA receptor to serve as coincidence detector, conducting ions only if the membrane potential is depolarized *and* the extracellular glutamate level is elevated. Similarly, protons inhibit the NMDA receptor with an IC_{50} of around pH 7.4, i.e. in the physiological range. NMDA receptor function can also be modulated by phosphorylation, by intracellular proteins and by interaction with the cytoskeleton (Rosenmund and Westbrook, 1993b; Dingledine et al., 1999). NMDA receptors generate a current with a slow kinetics of activation ($\tau \sim$ 10-20 ms), deactivation ($\tau \sim$ 100 ms to 4 seconds) and different types of desensitization (glycine dependent, calcium dependent and glycine and calcium independent desensitization; $\tau \sim$ several

seconds) (Lester et al., 1990; Sather et al., 1990; Vyklicky et al., 1990; Gibb and Colquhoun, 1991; Howe et al., 1991; Gibb and Colquhoun, 1992; Lester and Jahr, 1992; Rosenmund and Westbrook, 1993a; Monyer et al., 1994; Krupp et al., 1996; Vicini et al., 1998).

The first NMDA receptor subunit to be cloned was NR1 (Moriyoshi et al., 1991). Since then other subunits (NR2A-D) have been cloned and their molecular biological and functional properties characterised (see Hollmann and Heinemann, 1994; McBain and Mayer, 1994; Ozawa et al., 1998). More recently, the NR3A (also known as NMDAR-L or Chi-1) and NR3B subunits have also been identified (Ciabarra et al., 1995; Sucher et al., 1995; Das et al., 1998; Nishi et al., 2001; Perez-Otano et al., 2001). Binding as well as electrophysiological studies revealed that NR1 subunits are present throughout the CNS, whereas the different NR2 and NR3 subunits show a spatially as well as temporally distinct pattern of expression (NR2: Hestrin, 1992; Akazawa et al., 1994; Monyer et al., 1994; Watanabe et al., 1994; see also section 1.9.3.1; NR3: Ciabarra et al., 1995; Sucher et al., 1995; Nishi et al., 2001).

The NR1 subunit consists, like non-NMDA receptor subunits, of around 900 amino acid residues and has a molecular mass of around 100 kDa (Hollmann and Heinemann, 1994). In contrast, each of the four NR2 subunits contains a large, several hundred amino acids long intracellular C-terminus, increasing the total number of amino acid residues in the subunit to around 1200-1400, and resulting in a molecular mass of about 140-160 kDa. Although the four NR2 subunits show substantial homology with each other, only about 25% amino acid sequence identity is shared with NR1 (Hollmann and Heinemann, 1994). Thus, they are as distantly related to the NR1 subunit as are non-NMDA receptor proteins. The different NMDA receptor subunits are known to exist in various splice variants, increasing the functional diversity of the subunits. While little is known about these variants for the different NR2 and NR3 subunits, eight isoforms generated by alternative splicing

have been identified in the NR1 subunit (Dingledine et al., 1999)) which vary in their properties and are expressed in different regions of the brain and at different developmental stages (Laurie and Seeburg, 1994; Laurie et al., 1995; Dingledine et al., 1999; Prybylowski et al., 2000; Rumbaugh et al., 2000).

NMDA receptors work as heteromers, requiring the co-assembly of (probably two) NR1 and (probably two) NR2 subunits. The precise subunit stoichiometry of NMDA receptor proteins is unknown, but it has been suggested that a single NMDA receptor might contain more than one NR2 subunit type in combination with NR1 (Wafford et al., 1993; Chazot et al., 1994; Sheng et al., 1994; Vicini et al., 1998). The kinetics and pharmacological properties of the receptor channels, such as agonist/antagonist affinity, conductance (between about 30 and 50 pS; Stern et al., 1992), ion selectivity, channel gating, deactivation and desensitization kinetics, and modulation by ions or proteins, are influenced by the subunit composition (Stern et al., 1992; McBain and Mayer, 1994; Monyer et al., 1994; Ozawa et al., 1998; Dingledine et al., 1999). NR3 subunits do not form functional channels when expressed alone in Xenopus oocytes or HEK293 cells and require the presence of NR1 and NR2A to form functional channels in the plasma membrane (Ciabarra et al., 1995; Sucher et al., 1995; Nishi et al., 2001; Perez-Otano et al., 2001). The NR3A subunit can bind directly to NR1, NR2A and NR2B, and when co-expressed reduces single-channel current and the calcium permeability of the receptor (Ciabarra et al., 1995; Sucher et al., 1995; Das et al., 1998; Perez-Otano et al., 2001). The NR3B subunit has only recently been described, and also reduces the whole-cell current when co-expressed with NR1 and NR2A in HEK293 cells (Nishi et al., 2001).

1.1.1.3.1 The NMDA receptor glycine site

In chapter 7 I investigate modulation of NMDA receptor mediated synaptic currents by glycine. As mentioned above, NMDA receptors are believed to work as tetramers, composed probably of two NR1 and two NR2 subunits (Laube et al.,

1998). The glutamate binding site is located on the NR2 subunit, while the glycine binding site is on the NR1 subunit of the receptor (Wafford et al., 1995; Laube et al., 1997; Anson et al., 1998). However, the NR2 subunit influences glycine binding at the NR1 subunit, so that receptors differing in their NR2 subunit composition exhibit different sensitivities to glycine. In all cases, though, the EC_{50} values for glycine are between 90 and 800 nM (Woodward et al., 1995a; Woodward et al., 1995b). The concentration of glycine in the extracellular space has been measured by *in vivo* microdialysis to be in the low micromolar range (around 5-20 μM) (Matsui et al., 1995), a concentration which would saturate the glycine site of the NMDA receptor no matter what combination of NR1 and NR2 subunits are expressed (Danysz and Parsons, 1998). However, the local glycine levels near neurones may be more tightly regulated by glycine transporters, and Supplisson and Bergman (1997) demonstrated that when these transporters are located close to NMDA receptors (by co-expressing both in Xenopus oocytes), they can lower the local glycine concentration to values below those which saturate NMDA receptors.

There are two different classes of glycine transporter, with a distinct distribution and stoichiometry (see section 1.5). Briefly, GLYT-2 is located in neurones, predominantly in brain areas with glycinergic synapses, and has a stoichiometry in which 3 Na^+ and 1 Cl^- are co-transported into cells with each glycine, while GLYT-1 is mainly glial, and is expressed both in brain areas with glycinergic synapses and in areas lacking glycinergic synapses but containing excitatory synapses (i.e. close to NMDA receptors) and transports 2 Na^+, 1 Cl^- and 1 glycine (Roux and Supplisson, 2000). The latter stoichiometry was used by Attwell et al. (1993) to predict that these glycine transporters can lower the extracellular glycine concentration to around 150 nM, i.e. roughly at the EC_{50} for the NMDA receptor's glycine site. Consequently, with this stoichiometry, the operation of the glial transporter is set up so that if it reverses and pumps glycine into the extracellular space when the ion concentrations or the membrane potential change

during physiological conditions, then the NMDA response will be potentiated. By contrast, the extra Na^+ transported by GLYT-2 allows it to lower $[gly]_O$ to <10 nM, well below the level which will activate NMDA receptors, and as is needed for terminating glycinergic transmission (Roux and Supplisson, 2000).

There are several studies showing that adding glycine to the external medium or blocking glycine uptake increases the NMDA component of the synaptic current, i.e. suggesting that the glycine site on the NMDA receptor is not saturated in various brain regions. Thomson at al. (1989) discovered that evoked EPSPs in neocortical slices of the adult rat were increased when glycine was electrophoretically applied. Berger et al. (1998) found that miniature EPSCs recorded from motoneurones in brain stem slices of the rat were longer lasting when glycine was bath applied, implying an enhanced NMDA component to the current. They also suggested a major role for glycine transporters in regulating the glycine site occupancy at NMDA receptors at this synapse: the bath applied glycine concentration which potentiated the NMDA component of the mEPSCs was several orders of magnitude higher than expected, whereas even low concentrations of a non-transported glycine site agonist potentiated the currents. Bergeron et al. (1998) demonstrated that bath applying glycine or a GLYT-1 antagonist potentiated evoked EPSCs in CA1 pyramidal neurones in adult rat hippocampal slices.

In addition to glycine, D-serine has also been shown to be a potent agonist at the NMDA receptor's glycine site (Kleckner and Dingledine, 1989; Hashimoto and Oka, 1997) and it has been suggested that D-serine might be an endogenous modulator of the NMDA receptor (Schell et al., 1995; Wolosker et al., 1999; Mothet et al., 2000). D-serine and its synthesizing enzyme, serine racemase, are localized in astrocytes of various brain regions, and glutamate-stimulated D-serine release has been demonstrated from astrocyte cultures (Schell et al., 1995; Schell et al., 1997; Wolosker et al., 1999). In the cerebellum the migration of granule cells from the external granule cell layer through the molecular layer (along the Bergmann glia) to

the internal granule cell layer is under the control of NMDA receptor activity (Komuro and Rakic, 1993; Rossi and Slater, 1993). The developmental profile of D-serine concentration in the rat cerebellum matches that of the granule cell migration, with D-serine levels being highest at the peak of migration (around P14) and declining to undetectable levels when migration is completed (>P21) (Schell et al., 1997). It was therefore suggested that the NMDA receptor glycine site in cerebellar granule cells is activated predominantly by D-serine during postnatal development (during cell migration and synapse formation), whereas glycine would serve as a modulator of synaptic transmission in the adult animal.

1.1.2 Metabotropic glutamate receptors

Metabotropic glutamate receptors are large membrane proteins (around 1000 amino acids), which possess a large extracellular N-terminal (around 550 amino acids), a core region (7 transmembrane segments; around 250 amino acids) and an intracellular C-terminus of variable length. There are eight different mGluR subunits, which appear to work as homodimers. On the basis of their amino acid sequency homology, their pharmacological properties and the signal transduction cascades they use, the different metabotropic glutamate receptor subunits can be divided into three groups (reviewed by Hollmann and Heinemann, 1994; Ozawa et al., 1998; De Blasi et al., 2001): Group I receptors include mGluR1 and mGluR5, group II receptors include mGluR2 and mGluR3 and group III receptors include mGluR4, 6, 7 and 8. Metabotropic receptors initiate intracellular processes via activation of certain G-proteins, but may also activate signals independently of G-protein activation (Heuss and Gerber, 2000). Whereas Group I receptors activate G-proteins which trigger the PLC - IP_3 pathways and result in calcium release from internal stores, group II and group III receptors couple to G-proteins which are usually negatively coupled to the adenylyl cyclase system. Metabotropic glutamate receptors are important in regulating neuronal excitability and neurotransmitter release.

Relevant to this thesis, in the retina mGluR6 mediates synaptic transmission on ON bipolar cells (see section 1.8), while in the cerebellum mGluR1 mediates slow postsynaptic currents in Purkinje cells (see section 1.9.3.2).

1.2 Glutamatergic synaptic transmission – the time-course of the EPSC

In chapter 6 I examine the role of glutamate transporters in controlling the duration of the non-NMDA and NMDA components of the excitatory synaptic current at cerebellar synapses. It has been shown for many glutamatergic synapses in the CNS that non-NMDA and NMDA receptors are co-activated and thus co-localized at the same synapse (for example Bekkers and Stevens, 1989; Hestrin et al., 1990; Lester et al., 1990; Silver et al., 1992): the postsynaptic current response to synaptic activation (spontaneous or evoked) usually has two components – one is very fast (rise time of the order of a few hundred microseconds and decay time constant of the order of a few milliseconds) and the other one is rather slow (rise time of the order of around 10 ms and a decay constant in the range of hundreds of milliseconds). Using specific blockers the two components have been identified as resulting from synaptic activation of non-NMDA (AMPA/kainate receptors) and NMDA receptors, respectively. Metabotropic receptors can generate an even slower current component (see chapter 6; Batchelor et al., 1994; Tempia et al., 2001), but they will not be dealt with in detail here as they are not studied in this thesis.

The shape of the postsynaptic current response (EPSC) is determined by (1) the time-course of the glutamate concentration in the synaptic cleft, and (2) the channel kinetics of the postsynaptic receptors, as follows.

The rising phase of the EPSC depends on the rise time of the glutamate concentration transient in the synaptic cleft, the distribution of postsynaptic receptors (relative to the release site) and the activation kinetics of the postsynaptic receptors.

The amplitude of the EPSC depends on the receptor single channel

conductance and the maximum number of receptors which are open simultaneously, which depends on the number of receptors activated and their open probability. It was originally believed that the postsynaptic receptors are fully occupied (saturated) when a single quantum of neurotransmitter is released (Clements et al., 1992; Tang et al., 1994; Tong and Jahr, 1994b). More recently, however, a number of studies have demonstrated that neither non-NMDA nor NMDA receptors are saturated during such conditions (Tong and Jahr, 1994a; Silver et al., 1996a; Liu et al., 1999; Mainen et al., 1999), so receptor occupancy, and consequently the magnitude of postsynaptic response, can be modulated by changing the amount of glutamate in the synaptic cleft, e.g. by modulating glutamate removal (uptake) as shown by Tong & Jahr (1994a).

The decay time of the EPSC, which will influence the amount of charge transferred into the cell and thus be important for the size and duration of the postsynaptic depolarization, depends on the time-course of the glutamate transient in the synaptic cleft relative to the time-constants of the channel's deactivation and desensitization kinetics. There are three possibilities, as follows. (1) If the glutamate concentration in the synaptic cleft declines slowly (i.e. slower than receptor deactivation and desensitization), then the time-course of the EPSC decay will be set by receptor desensitization. (2) If the glutamate concentration in the synaptic cleft drops quickly (i.e. faster than receptor deactivation and desensitization), then the time-course of the EPSC decay will be set by receptor deactivation. (3) If the glutamate concentration in the synaptic cleft declines with a time-course that is slower than receptor deactivation but faster than desensitization, then the time course of the EPSC decay will be set by the time-course of the glutamate decay in the synaptic cleft (transformed through the dose-response curve for activation).

To examine what determines the shape of the EPSC decay at a given synapse, many studies have investigated the deactivation and desensitization kinetics of non-NMDA (and to some extent NMDA, see below) receptor mediated responses in

outside-out or nucleated patches from cell somata, using fast and sustained application of glutamate respectively, and compared these time-constants to the time-constant of the EPSC decay. The results varied, depending on the cell type and synapse studied, probably reflecting the presence of different receptor subunits. In some cases, the decay time-course of the non-NMDA receptor mediated EPSC was apparently determined by deactivation (Hestrin et al., 1990; Colquhoun et al., 1992; Barbour et al., 1994), in others it was apparently determined by desensitization (Trussell and Fischbach, 1989; Trussell et al., 1993; Otis et al., 1996a), and in others the time-constant of the EPSC was in between the measured deactivation and desensitization time constants (Barbour et al., 1994; Silver et al., 1996b) suggesting that the time-course of the glutamate concentration in the cleft influences the decay of the non-NMDA component of the EPSC at these synapses. This approach, however, assumes that synaptic and somatic non-NMDA receptors have similar kinetic properties, which might not be true: the subunit composition of synaptic receptors might differ from the somatic receptors, since synaptic receptors are anchored in a web of postsynaptic density proteins which could well alter their properties.

At most glutamatergic synapses the NMDA receptor-mediated component of the EPSC decays with a biexponential time course, which reflects in large part the kinetic properties of the underlying NMDA receptor channels (Keller et al., 1991; Lester and Jahr, 1992; Vicini et al., 1998). The high affinity of NMDA receptors for glutamate (Patneau and Mayer, 1990) results in glutamate staying bound to the receptor for a long time, generating prolonged bursts of channel opening (Ascher et al., 1988; Lester et al., 1990; Howe et al., 1991; Gibb and Colquhoun, 1992) and it has been suggested that no rebinding of transmitter occurs during the postsynaptic current (Hestrin et al., 1990; Lester et al., 1990). Thus, the time constants of the decay of the NMDA receptor mediated EPSC component probably reflect the slow unbinding of glutamate and the consequent temporal distribution of bursts and

clusters of channel opening events (Gibb and Colquhoun, 1992). Indeed, fast application of glutamate to membrane patches has revealed NMDA receptor deactivation time constants which are similar to the decay time constants of the NMDA component of the EPSC in the same cell type (Lester et al., 1990; Hestrin, 1992; Lester and Jahr, 1992; Rumbaugh and Vicini, 1999; Rumbaugh et al., 2000), indicating that the channel deactivation kinetics do indeed shape the NMDA receptor EPSC component.

The time-course of the glutamate concentration transient in the synaptic cleft depends on the rate of vesicular release and the rate of glutamate removal. The rate of glutamate removal is determined by the speed of glutamate diffusing down its concentration gradient (maintained by glutamate transporters), and by rapid binding of glutamate to glutamate transporters ("buffering"; Diamond and Jahr, 1997) or rapid translocation of glutamate into cells ("uptake"; Auger and Attwell, 2000), and can also be influenced by the synapse geometry (Kinney et al., 1997). It was estimated that at most (small diameter) synapses the glutamate concentration peaks at 1-5 mM and decays biexponentially with time constants of around 100 μs and 2 ms (Clements, 1996), which would allow AMPA receptor deactivation to be a major factor in shaping the EPSC decay, as observed by so many studies (see above). However, if glutamate removal from the synaptic cleft were hampered (as in the experiments I present in chapter 6, in which glutamate transporters are genetically deleted or blocked), and the glutamate concentration in the cleft remained elevated, then the decay of the synaptic current would be strongly influenced by the channel's desensitization kinetics or would follow the decay of the extracellular glutamate concentration. The postsynaptic current would then be longer lasting, and information transfer between cells would be greatly altered. It is therefore of considerable interest to understand the role of glutamate transporters in shaping synaptic transmission, and not surprising that several studies have examined this issue (see section 1.3.5).

1.3 Glutamate transporters in the plasma membrane

This section describes the necessary background on plasma membrane glutamate transporters for the experiments reported in chapter 5 investigating the effects of a protein interacting with a glial glutamate transporter, and in chapter 6 on the role of glutamate transporters in synaptic transmission.

The extracellular glutamate concentration in the CNS is controlled by glutamate transporters (reviewed by Hertz, 1979; Danbolt, 2001), which can be located either outside the synaptic area in glial cells or neurones, or at the pre- and/or postsynaptic membranes of neurones (see section 1.3.2). A low extracellular glutamate concentration is important for facilitating removal of glutamate from the synaptic cleft by diffusion, but is also critical for maintaining the extracellular glutamate concentration below neurotoxic levels: an exposure of neurones to glutamate concentrations of 100 μM for more than 5 minutes leads to irreversible neuronal damage (Choi et al., 1987), as a result of prolonged activation of NMDA receptors causing an excessive Ca^{2+} influx (Szatkowski and Attwell, 1994).

1.3.1 Structure and molecular properties of glutamate transporters

Five different types of glutamate transporters have been cloned so far: GLAST (from rat brain; Storck et al., 1992), GLT-1 (from rat brain; Pines et al., 1992), EAAC-1 (from rabbit small intestine; Kanai and Hediger, 1992), EAAT4 (from human cerebellum; Fairman et al., 1995) and EAAT5 (from human retina; Arriza et al., 1997). The human homologues of GLAST, GLT-1 and EAAC-1 have also been cloned and named as EAAT-1, EAAT-2 and EAAT-3 respectively (from human motor cortex; Arriza et al., 1994). Some of these transporters have been shown to exist in the brain as alternatively spliced variants, for example GLAST (GLAST-1a; Huggett et al., 2000) and GLT-1 (Meyer et al., 1998; Chen et al., 2000c; GLT-1v: Schmitt et al., 2002). Not much is known about these variants, but

interestingly the recently discovered GLT-1v appears to be expressed in neurones (even though GLT-1 is generally believed to be a glial transporter; see section 1.3.2). Glutamate transporters have been proposed to work as multimers (Haugeto et al., 1996), and EAAT-3 has recently been shown to form pentameric protein complexes when expressed in Xenopus oocytes (Eskandari et al., 2000). Each transporter "subunit" is around 523-573 amino acids long, resulting in a molecular weight of around 65-75 kDa. They are membrane-spanning proteins for which several different membrane topology models have been suggested: for GLAST/EAAT-1 (Storck et al., 1992; Seal and Amara, 1998; Seal et al., 2000), for GLT-1 (Pines et al., 1992; Grunewald et al., 1998; Grunewald and Kanner, 2000) and for EAAC-1 (Kanai and Hediger, 1992). In all cases the transporter is thought to span the membrane 6-11 times (α-helices), and to have intracellular amino and carboxy terminals, and a large extracellular loop joining the 3rd and 4th transmembrane segment (with two glycosylation sites). There is uncertainty over the topology of the C-terminal half of the transporter; some topological models propose simple α-helices, some propose reentrant-loops and some propose amino acid stretches which lay on the outside of the membrane. One of the more recent topology suggestions for GLT-1 is shown in Figure 5.1. Several proteins interacting with the amino and the carboxy terminal part of the transporters have been identified recently, as described in section 1.7.

1.3.2 Localization of plasma membrane glutamate transporters in the CNS

All five glutamate transporter types are expressed in the CNS (and some also in other parts of the body), but are distributed in different brain areas and in different cell types (Danbolt, 2001). Originally it was thought that GLAST and GLT-1 were exclusively expressed in glial cells, whereas EAAC-1, EAAT-4 and EAAT-5 were thought to be neuronal, but this categorization might be less rigid than previously thought. The following information is from several publications, which investigated

the regional and cellular distribution and the developmental expression profile of different glutamate transporters in the CNS (Rauen and Kanner, 1994; Rothstein et al., 1994; Chaudhry et al., 1995; Lehre et al., 1995; Rauen et al., 1996; Yamada et al., 1996; Furuta et al., 1997b; Furuta et al., 1997a; Ullensvang et al., 1997; Conti et al., 1998; Dehnes et al., 1998; Eliasof et al., 1998b; Eliasof et al., 1998a; Lehre and Danbolt, 1998; Mennerick et al., 1998; Plachez et al., 2000; Schmitt et al., 2002).

(1) GLAST/EAAT-1 appears to be a major glutamate transporter in the cerebellum and the retina, where it is located mainly in Bergmann glia and Müller cells respectively. However, it is also present in astrocytes throughout the brain and can be transiently expressed by some cultured neurones. (2) GLT-1/EAAT-2 is the most abundant glutamate transporter in the forebrain and is expressed in astrocytes throughout the CNS. In the retina GLT-1 is expressed in neurones (cone axon terminals, some cone bipolar cells and some amacrine cells) but not Müller cells. GLT-1 can also be expressed by neurones in hippocampal culture and the splice variant GLT-1v is expressed neuronally throughout the brain. (3) EAAC-1/EAAT-3 is found in neurones throughout the CNS and also in astrocytes of the cerebral cortex. (4) EAAT-4 is found mainly in cerebellar Purkinje cells, but is also present (though at very low levels) in neuronal dendrites and some astrocytes in the forebrain. (5) EAAT-5 is found only in the retina, in photoreceptor axon terminals, in some bipolar cells and in Müller cells.

The different glutamate transporter types can be expressed by the same cell. For example, most astrocytes contain GLAST and GLT-1 in their plasma membrane, in a ratio of about 1:4; by contrast in cerebellar Bergmann glia this ratio is 6:1 (Lehre and Danbolt, 1998). Retinal Müller cells express GLAST, GLT-1 and EAAT-5 (Eliasof et al., 1998b; Eliasof et al., 1998a), and Purkinje cells in the cerebellum express EAAC-1 as well as EAAT-4 (Furuta et al., 1997b). The distribution of the transporters in the cell is not random but can depend on the type of neighbouring structure. For example GLT-1 and GLAST are more abundant in regions of the

astrocyte membrane which are adjacent to nerve terminals, axons and dendritic spines than in regions of the cell which are facing other astrocytes, blood vessels, pia or dendritic shafts (Chaudhry et al., 1995). The location of the individual transporters is likely to serve certain purposes. Transporters located in glial cells may mainly function to maintain a low extracellular resting glutamate concentration, setting up a concentration gradient for glutamate to diffuse out of the synaptic cleft. Carriers located in the vicinity of synaptic areas, such as EAAT-4 and EAAC-1 in Purkinje cell spines, might play a more direct role in shaping synaptic transmission (Takahashi et al., 1996a; Otis et al., 1997; Auger and Attwell, 2000; Brasnjo and Otis, 2001).

The surface expression of the transporters can be regulated by various extracellular soluble factors; for example GLAST expression in cultured cells was upregulated by glutamate (Duan et al., 1999), expression of glial transporters was increased when they were co-cultured with neurones (Swanson et al., 1997; Schlag et al., 1998) and pituitary adenylate cyclase activating polypeptide (PACAP), a neuronally derived peptide, increased surface expression of GLAST and GLT-1 in nearby astrocytes (Figiel and Engele, 2000).

1.3.3 Stoichiometry and properties of glutamate transport and its anion conductance

Glutamate uptake is driven by the co-transport of ions down their electrochemical gradients. It has been shown that glutamate uptake depends strongly on the co-transport of sodium ions (Erecinska et al., 1983). For both the mainly glial GLT-1 and the mainly neuronal EAAT-3 it has been shown that three sodium ions (Zerangue and Kavanaugh, 1996; Levy et al., 1998) and one proton (Bouvier et al., 1992; Zerangue and Kavanaugh, 1996; Levy et al., 1998) are co-transported, whereas one potassium ion (Barbour et al., 1988; Amato et al., 1994) is counter-transported for each molecule of glutamate transported across the membrane. Glutamate uptake

is thus electrogenic, transporting two net positive charges into the cell. This results in the transport of glutamate being inhibited at depolarized membrane potentials (Brew and Attwell, 1987). Since transporters operate solely by means of the co-transport of ions down their electrochemical gradients, if these gradients change they can also run backwards and release glutamate with the same stoichiometry as described above (Szatkowski et al., 1990; Attwell et al., 1993; Billups and Attwell, 1996). This non-vesicular release of glutamate is responsible for the rise of glutamate to neurotoxic levels in severe brain ischaemia (Szatkowski et al., 1990; Attwell et al., 1993; Szatkowski and Attwell, 1994; Rossi et al., 2000).

In addition to transporting glutamate, glutamate transporters can also conduct anions (*in vivo* mainly chloride). The first to report such a chloride flux through glutamate transporters, in cones of the salamander retina, were Sarantis et al. (1988). This transporter has subsequently been cloned (EAAT-5; Arriza et al., 1997) and its high chloride permeability confirmed in expression systems. A significant chloride flux through glutamate transporters was also reported when EAAT-4 was cloned from human cerebellum and expressed in Xenopus oocytes (Fairman et al., 1995), and this chloride flux has been shown to occur when EAAT-4 is activated in Purkinje cells (Otis et al., 1997). From measurements of glutamate transporter currents (due to glutamate translocation and anion flux) in Müller cells of the salamander retina (Billups et al., 1996; Eliasof and Jahr, 1996), Purkinje cells of the cerebellum (Otis and Jahr, 1998) and EAAT-1, EAAT-2 and EAAT-3 expressed in Xenopus oocytes (Wadiche et al., 1995a) it has emerged that, although all glutamate transporters have an anion conductance within their structure, the different transporters show different degrees of anion permeability. The anion channel conductance is particularly high in EAAT-4 and EAAT-5 (Sarantis et al., 1988; Fairman et al., 1995; Arriza et al., 1997), but is much smaller in the other glutamate transporters when physiological anions (i.e. chloride) are present (Wadiche et al., 1995a). Although chloride is the most physiological anion, other ions such as nitrate or perchlorate permeate the

transporter much better and are thus often used to examine the transporters' channel properties. The anion conductance is thermodynamically uncoupled from the transport activity; this means that the movement of anions does not drive glutamate transport. The transporter can conduct anions although it does not translocate glutamate. The anion conductance is activated by (intra- or extracellular) glutamate and critically dependent on sodium; potassium does not need to be present (Figure 1.2). The physiological role of the anion conductance is unclear. In principle a glutamate activated chloride conductance might help to keep the membrane potential at negative values and thus maintain the driving force for glutamate uptake, but for most cells the current generated by the anion conductance is too small to significantly alter the membrane potential. The only exception to this is in cones, where EAAT-5 mediated chloride currents generate significant voltage changes (Sarantis et al., 1988; Picaud et al., 1995).

1.3.4 Modulation of glutamate transporters

Glutamate transporter activity has also been shown to be modulated by various endogenous molecules and mechanisms, such as zinc (Spiridon et al., 1998; Vandenberg et al., 1998; Mitrovic et al., 2001), arachidonic acid (Barbour et al., 1989; Zerangue et al., 1995), sulfhydryl oxidation (Trotti et al., 1997), phosphorylation (Casado et al., 1993; Conradt and Stoffel, 1997; Davis et al., 1998) and interaction with intracellular proteins (see section 1.7). These different types of modulation might be physiologically relevant, but their exact function in brain physiology has yet to be established.

Figure 1.2: Schematic drawing of a glutamate transporter and its anion conductance

Glutamate transporters use the electrochemical gradients for sodium, potassium and protons to translocate glutamate across the membrane. For each glutamate three sodium ions and one proton are co-transported, and one potassium ion is counter-transported. Glutamate transporters also contain an anion channel in their structure. For this channel to conduct, the transporter needs to bind sodium and glutamate (potassium and protons do not need to be bound). X^- indicates an anion, for example chloride.

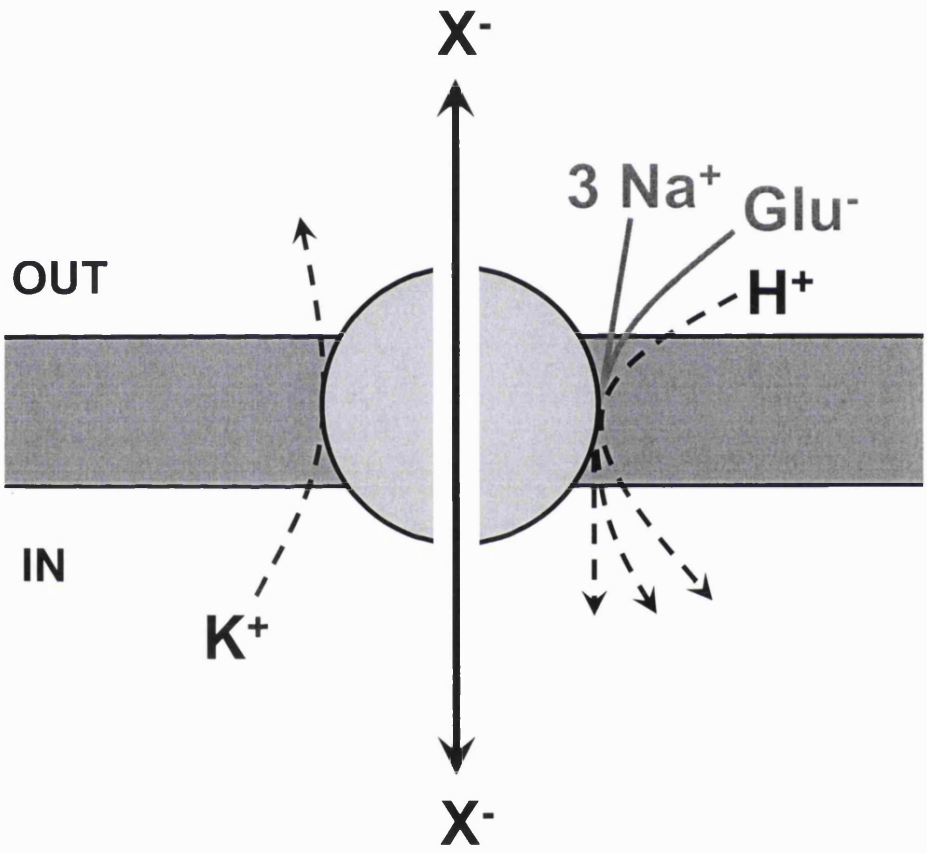
X-
3 Na+
Glu-
OUT
H+
IN
K+
X-

1.3.5 The role of glutamate uptake in the brain and during synaptic transmission

Glutamate transporters might shape synaptic currents by maintaining a low glutamate concentration around the synapse and thus producing a concentration gradient for glutamate diffusion, by providing glutamate binding sites (to act as a "buffer"), or by physically removing glutamate from the extracellular space (see section 1.2). Glutamate transporter currents have been recorded in astrocytes and Bergmann glia shortly after synaptic transmission, confirming that glutamate escapes the synaptic cleft shortly after release and is taken up by glial cells (Bergles et al., 1997; Bergles and Jahr, 1997; Clark and Barbour, 1997). Several groups have investigated the role of glutamate transporters during synaptic transmission at different synapses in the brain, by recording postsynaptic currents in brain slices. They either inhibited glutamate uptake pharmacologically, or studied mice lacking a particular glutamate transporter, to see if the postsynaptic response was altered when glutamate transport was impaired. Below I briefly review some of their findings.

1.3.5.1 Blocking glutamate transport pharmacologically

The results of different studies using pharmacological block of transporters are varied, and it appears that synapse morphology, vicinity to glial cells, recording temperature, stimulation frequency and other factors could account for this variability. There is thus no clear cut answer as to whether glutamate transporters do or don't shape the time-course of synaptic transmission, as the following examples illustrate.

Blocking glutamate uptake did not affect the kainate or AMPA receptor mediated EPSC at a thalamo-cortical synapse in the rat (Kidd and Isaac, 2001). Similarly, blocking glutamate transporters in the rat hippocampus did not affect the

time-course of the non-NMDA or NMDA receptor mediated EPSC at the Schaeffer-collateral to CA1 pyramidal cell synapse (Hestrin et al., 1990; Isaacson and Nicoll, 1993; Sarantis et al., 1993), indicating that glutamate transport does not shape the EPSC decay at this synapse. However, proper glutamate transporter function is important for limiting glutamate spill-over between synapses and consequent NMDA receptor activation (Diamond, 2001).

By contrast in the retina, where most cells encode information as graded potentials and glutamate release is prolonged, inhibiting glutamate transport has significant effects on the postsynaptic response. The light evoked voltage response (hyperpolarization) in horizontal cells of the salamander retina is reduced (and slower) when cone transporters were inhibited, suggesting that the cone transporter strongly influences the glutamate concentration at this synapse (Gaal et al., 1998; Roska et al., 1998). The electrially, as well as light evoked, non-NMDA and NMDA receptor mediated EPSCs in ganglion cells of the salamander (Higgs and Lukasiewicz, 1999) and the newt (Matsui et al., 1999) retinae were also longer lasting when glutamate uptake was blocked, although the shape of spontaneous non-NMDA receptor mediated EPSCs were not affected in either preparation. Similarly, at large synapses, such as the rat mossy-fibre to unipolar brush cell (UBC) synapse in the cerebellar granule cell layer (Kinney et al., 1997) or the calyceal synapse in the chick cochlear nucleus (onto nucleus magnocellularis (NM) cells; Otis et al., 1996b; Turecek and Trussell, 2000), the EPSC was prolonged when glutamate transporters were blocked, and glutamate transporters were important in controlling frequency dependent EPSC depression at the NM cell synapse (Turecek and Trussell, 2000).

Relevant to the experiments I report in chapter 6, the role of glutamate transporters in synaptic transmission has also been studied at a variety of synapses in the cerebellum. Sarantis et al. (1993) and Overstreet et al. (1999) investigated the mossy fibre to granule cell synapse with differing results: their findings are summarized in section 6.5. Glutamate transporters do not shape the parallel fibre to

stellate cell EPSC produced by single stimulation (Barbour et al., 1994; Carter and Regehr, 2000), but are important during repetitive stimulation and for controlling glutamate spill-over between synapses after trains (Carter and Regehr, 2000). The climbing fibre and parallel fibre to Purkinje cell EPSCs are longer lasting when glutamate transport is impaired (Barbour et al., 1994; Takahashi et al., 1995b; Takahashi et al., 1996a), and postsynaptic glutamate transporters in Purkinje cell dendrites have been shown to regulate activation of the cells metabotropic glutamate receptors and influence LTD (Brasnjo and Otis, 2001).

Glutamate transporters in glial cells can also influence neurotransmitter release by controlling the activation of presynaptic metabotropic glutamate receptors. At synapses in the hypothalamic supraoptic nucleus, blocking glutamate transport inhibited the EPSC amplitude, reduced the frequency of miniature EPSCs and affected paired-pulse facilitation. These effects were dependent on metabotropic glutamate receptor activation and the extent of the surrounding glial sheet (in which the transporters are located; Oliet et al., 2001).

1.3.5.2 Glutamate transporter knock-out mice

Several groups have generated mice lacking different glutamate transporters. These mice can provide valuable information about the role of individual glutamate transporters in the brain (by contrast many transport blockers affect all transporter subtypes). In chapter 6 I use mice lacking GLAST or GLT-1 to investigate the role of these transporters during synaptic transmission in the cerebellum. I shall therefore briefly summarize the phenotype of each knock-out mouse including, if investigated, the effect on excitatory synaptic transmission.

1.3.5.2.1 The GLAST knock-out mouse

Watase et al. (1998) generated a GLAST knock-out mouse by disrupting the gene in a position which corresponds to the start of the 4th transmembrane spanning segment of the transporter. These mice develop normally and do not show any abnormalities in their phenotype. They manage simple coordinated tasks, such as staying on a stationary or a slowly rotating rod, but fail more challenging tasks such as staying on a quickly rotating rod. The gross as well as the cellular anatomy of the cerebellum, where GLAST is normally heavily expressed, is undistinguishable from the wild type mice, and neither the granule cell density in the granule cell layer nor the number of parallel fibre to Purkinje cell synapses in the molecular layer is changed. The time-course of the single stimulus evoked parallel fibre to Purkinje cell EPSC (recorded in young and in adult mice) was not significantly different between the wild type and the knock-out mice (this is in contrast to my results, see chapter 6), nor was the paired pulse facilitation (which has presynaptic origins). However, Purkinje cells in the mutant mice remained multiply innervated by climbing fibres even at the adult stage (when in wild type mice only one climbing fibre innervates each Purkinje cell) and showed slowly rising and decaying EPSCs as well as "normal" climbing fibre to Purkinje cell EPSCs. The time-course of the single stimulus evoked "normal" climbing fibre to Purkinje cell EPSC recorded in the knock-out was indistinguishable from the ones in the wild-type though. Watase et al. (1998) also found that oedema volumes after cerebellar injury increased significantly in the mutant mice compared to wild type. Importantly, the authors did not find any evidence for upregulation of other glutamate transporters (GLT-1, EAAC-1 and EAAT-4). Taken together, their results indicate that GLAST plays an important role in climbing fibre synapse formation as well as in preventing excitotoxic cerebellar damage after acute brain injury, but suggests that GLAST does not shape synaptic transmission at the parallel or climbing fibre to Purkinje cell synapse. My data in chapter 6 contradict this suggestion.

Harada et al. (1998) used these GLAST knock-out mice to study the role of GLAST in the retina, where it is highly expressed in Müller glial cells. Neither the gross anatomy of the retina nor the Müller cell morphology was altered in the mutant mouse. However, the electroretinogram (ERG) b-wave and oscillatory potentials were reduced. Moreover, GLAST deficient mice were more prone to ischaemic damage in the retina. Their results suggest that GLAST is required for normal signal transmission in the retina and crucial for protecting retinal cells from glutamate toxicity.

1.3.5.2.2 The GLT-1 knock-out mouse

Tanaka et al. (1997) generated a mouse lacking the glial glutamate transporter GLT-1 by disrupting the gene in a position which corresponds to the start of the 3rd transmembrane spanning segment of the transporter. Prenatally the mice appeared to develop properly, so that the body weight and appearance of the knock-outs at birth was indistinguishable from the wild type mice. However, the mutant mice gained weight more slowly, showed lethal spontaneous seizures, were more prone to acute cortical injury and had a mean life span of only 6 weeks. The single stimulus evoked Schaeffer collateral to CA1 pyramidal cell EPSC was identical in both genotypes, but the glutamate transient was larger and glutamate was cleared from the synapse more slowly in knock-out mice (as assessed by using a low affinity competitive glutamate receptor antagonist). GLT-1 knock-out mice showed impaired LTP induction in the hippocampal CA1 region (Katagiri et al., 2001). Taken together, their results indicate that GLT-1 plays an important role in keeping the extracellular glutamate levels low, protects cells from epilepsy and glutamate toxicity, and participates in regulating synaptic plasticity.

Harada et al. (1998) used these GLT-1 knock-out mice to study the role of GLT-1 in the retina, where it is expressed in cones and some cone bipolar cells (Rauen and Kanner, 1994; Harada et al., 1998). The gross anatomy of the retina, the

Müller cell morphology and the electroretinogram (ERG) were indistinguishable in the two genotypes. However, GLT-1 deficient mice were more prone to ischaemic damage in the retina than wild type mice, but much less so than GLAST deficient mice (see above). Their results suggest that GLT-1 is not required for normal signal transmission in the retina, but has a neuroprotective role during retinal ischaemia.

1.3.5.2.3 The EAAC-1 knock-out mouse

Peghini et al. (1997) generated a mouse lacking the neuronal glutamate transporter EAAC-1. These mice develop normally and do not show any neurological abnormalities. They do as well at the rotorod test (motor coordination), and the Morris water maze test (spatial orientation), and are as susceptible to induced epileptic seizures, as their wild type siblings, but they do show reduced spontaneous locomotor activity. The hippocampus and the cerebellum show normal morphology and cell numbers, and the parallel fibre and climbing fibre to Purkinje cell EPSCs are not different in the wild type or knock-out mice (Wachtmann et al., 2000), suggesting that EAAC-1 does not shape synaptic transmission at these synapses. Mice lacking EAAC-1 excrete significantly more glutamate and D-aspartate than wild-type mice, suggesting that EAAC-1 transporters are important for reabsorbing glutamate and aspartate in the renal tubules.

1.3.5.2.4 Antisense knock-down of glutamate transporters

To investigate the role of the different glutamate transporters GLAST, GLT-1 and EAAC-1 in the brain, Rothstein et al. (1996) stopped the synthesis of those transporters (and thus effectively knocked them down) by injecting adult mice with antisense oligonucleotides. GLAST as well as GLT-1 antisense treatment induced progressive paralysis and tonic elevation of extracellular glutamate levels, whereas EAAC-1 deficient mice had epileptic seizures but normal extracellular glutamate

concentration. The loss of GLAST and GLT-1 (but not EAAC-1) resulted in cytotoxicity and cellular degeneration. The authors did not study the effect on synaptic transmission. They concluded that glial glutamate transporters provide the majority of functional glutamate transport and are essential for maintaining low extracellular glutamate and for preventing chronic glutamate neurotoxicity, while neuronal glutamate transporters are important for providing glutamate as a substrate for the inhibitory transmitter GABA, which is needed to prevent epileptic seizures.

1.4 GABA receptors

In chapters 3 and 4 I report experiments on membrane currents in neurones evoked by γ-aminobutyric-acid (GABA), which is a major inhibitory neurotransmitter in the adult mammalian central nervous system (CNS) (reviewed by Kaila, 1994). GABA receptors can be divided into two main classes, namely ionotropic receptors, which open anion channels, and receptors coupled to G-proteins. Ionotropic GABA receptors can be further divided into $GABA_A$ and $GABA_C$ receptors, whereas the G-protein coupled receptors are simply referred to as $GABA_B$ receptors.

1.4.1 Ionotropic GABA receptors

Ionotropic GABA receptors belong to the superfamily of ligand-gated ion channels, including the nicotinic acetylcholine receptors and glycine receptors (Luddens and Wisden, 1991; Luddens et al., 1995). They are membrane-spanning proteins, composed of different subunits, which assemble as pentamers and contain an anion conductance within their structure which is mainly permeant to chloride ions (for reviews see Kaila, 1994; Feigenspan and Bormann, 1998; Qian and Ripps, 2001; Zhang et al., 2001). In this thesis I studied mainly $GABA_C$ receptors and will therefore describe some of their properties in the following sections; I will also

highlight certain similarities and differences between $GABA_C$ and $GABA_A$ receptors.

1.4.1.1 A brief history of $GABA_C$ receptors

Johnston et al. (1975) were the first to suggest the existence of GABA activated anion channels distinct from $GABA_A$ receptors: they discovered GABA activated responses in cat spinal cord interneurones that were not inhibited by the $GABA_A$ receptor antagonist bicuculline. Sometime later bicuculline-insensitive chloride mediated GABA responses were also detected in the frog optic tectum (Nistri and Sivilotti, 1985; Sivilotti and Nistri, 1989). Furthermore, radiolabelling studies revealed GABA binding sites insensitive to bicuculline and to the $GABA_B$ agonist baclofen in rat cerebellar membranes (Drew et al., 1984; Drew and Johnston, 1992). This prompted the proposal of a novel ionotropic GABA receptor class named $GABA_C$ (Drew et al., 1984). The first thorough characterization of $GABA_C$ receptor mediated currents was performed by Polenzani et al. (1991), who discovered baclofen- and bicuculline-insensitive GABA currents in Xenopus oocytes which had been injected with bovine retinal RNA. Since then, $GABA_C$ receptor mediated currents have been further investigated in expression systems (for example Woodward et al., 1992a, b, 1993), and *in situ* in the hippocampus of young rats (Strata and Cherubini, 1994), in the superior colliculus of adult rats (Schmidt et al., 2001) and in the retina of rats (Feigenspan et al., 1993), fish (Qian and Dowling, 1993), salamanders (Lukasiewicz et al., 1994) and ferrets (Lukasiewicz and Wong, 1997). As described in detail in section 1.4.1.5, investigations on $GABA_C$ receptors in retinal cells (dissociated and in slices; for example: Feigenspan and Bormann, 1994a; Matthews et al., 1994; Dong and Werblin, 1995; Qian and Dowling, 1995; Yeh et al., 1996; Euler and Wassle, 1998; Haverkamp et al., 2000), and on cloned receptors (see below) have shown that $GABA_C$ receptors differ from $GABA_A$ receptors in having a higher affinity for GABA and showing little desensitization. Three different $GABA_C$ receptor subunits have been cloned, the human ρ1 and ρ2

(Cutting et al., 1991; Cutting et al., 1992) and the rat ρ1, ρ2 and ρ3 (Ogurusu et al., 1995; Ogurusu and Shingai, 1996; Wegelius et al., 1996), and their properties have been studied in Xenopus oocytes (for example: Shimada et al., 1992; Kusama et al., 1995; Zhang et al., 1995; Shingai et al., 1996) and in mammalian cell lines (Enz and Bormann, 1995; Enz and Cutting, 1999). Immunohistochemical work (Enz et al., 1996; Koulen et al., 1997; Fletcher et al., 1998; Koulen et al., 1998a; Wassle et al., 1998; Shields et al., 2000) and RT-PCR studies (Enz et al., 1995; Yeh et al., 1996; Boue-Grabot et al., 1998; Wegelius et al., 1998; Enz and Cutting, 1999) have investigated the localization of $GABA_C$ receptor protein and mRNA in the retina and the brain of rats, and molecular biological studies have shown interaction of $GABA_C$ receptors with different proteins (Hanley et al., 1999; Hanley et al., 2000). The physiological role of $GABA_C$ receptors in the retina (for example Lukasiewicz and Werblin, 1994; Matsui et al., 2001; Roska and Werblin, 2001) and the brain (Martina et al., 1995; Pasternack et al., 1999; Schmidt et al., 2001) is in the process of being unravelled, and investigation of the recently produced ρ1 knock-out mouse (Miller et al., 2000) should provide valuable information on this (see section 3.17.4).

1.4.1.2 Ionotropic GABA receptor subunits

To date seven different classes of $GABA_A$ receptor subunits (α1-6, β1-3, γ1-3, δ, ϵ, π, θ) and one class of $GABA_C$ receptor subunits (ρ1-3) have been cloned. $GABA_A$ receptors work as heteromers, with the most common native receptor stoichiometry being the assembly of 2α, 2β and one of γ or δ or possibly ϵ, π, θ (Barnard et al., 1998; Sieghart et al., 1999). The subunit composition determines many of the electrophysiological and pharmacological properties of the ionotropic GABA receptors (for reviews see Kaila, 1994; Feigenspan and Bormann, 1998; Qian and Ripps, 2001). Although homomeric $GABA_C$ receptors, when expressed in oocytes or mammalian cell lines, have been shown to form functional channels with pharmacological and kinetic properties similar to those found in retinal $GABA_C$

receptors, they appear to form and work as heteromers *in vivo* (Enz and Cutting, 1999). One interesting exception is the rat ρ2 subunit, which does not form functional homomeric $GABA_C$ receptor channels when expressed in Xenopus oocytes (Zhang et al., 1995) or native cells: single-cell RT-PCR combined with patch-clamp experiments showed that while bipolar cells contain mRNA for ρ1 and ρ2 and mediate $GABA_C$ receptor currents, ganglion cells do not exhibit $GABA_C$ receptor currents despite containing ρ2 mRNA. This suggests that functional $GABA_C$ receptors *in vivo* require the ρ1 subunit and pharmacological evidence described in section 1.4.1.4 implies that they are most likely assembled of ρ1/ρ2 heteromers (Yeh et al., 1996). $GABA_A$ and $GABA_C$ receptor subunits are present within the same cell type (Greferath et al., 1995; Yeh et al., 1996; Fletcher et al., 1998) and can co-assemble within one channel when co-expressed in Xenopus oocytes (Qian and Ripps, 1999; Pan et al., 2000). However, it is still controversial whether they do so *in vivo* (Enz and Cutting, 1998). Moreover, $GABA_A$ receptor subunits failed to co-immunoprecipitate with $GABA_C$ receptor subunits *in vitro* (Hackam et al., 1998), and immunolabelling studies in rat retinal slices show that the two receptor types localize in discrete puncta (Koulen et al., 1998a), suggesting that they form separate receptor channel populations and do not co-assemble.

1.4.1.3 Structure of ionotropic GABA receptor subunits

As reviewed by Feigenspan & Bormann (1998), Enz & Cutting (1998) and Zhang et al. (2001), each $GABA_A$ and $GABA_C$ receptor subunit is made up of around 500 amino acids and consists of four membrane spanning α-helices. The second transmembrane segment (TM2) lines the pore and is important for gating and ion selectivity of the channel. Both the very long amino- and the short carboxy-terminal are located on the extracellular side of the membrane. Each subunit has a large intracellular loop between the TM3 and TM4 (see Figure 3.1), which contains several putative phosphorylation sites which may allow modulation by intracellular

protein kinases such as PKA, PKC and tyrosine kinase. In addition, this loop has also been shown to be important for interaction with intracellular proteins, such as GABARAP for $GABA_A$ receptors (Wang et al., 1999) and MAP-1B for $GABA_C$ receptors (Hanley et al., 1999); the function of these interacting proteins is described in section 1.7 and in chapter 3.

1.4.1.4 Pharmacological properties of ionotropic GABA receptors

$GABA_A$ and $GABA_C$ receptors are classically differentiated by their different pharmacological properties, most notably the insensitivity of $GABA_C$ receptors to the competitive $GABA_A$ receptor antagonist bicuculline (see section 1.4.1.1). $GABA_C$ receptors are also insensitive to some well-known modulators of $GABA_A$ receptors, such as barbiturates, benzodiazepines and steroids, which potentiate the action of GABA on those receptors (Polenzani et al., 1991; Bormann and Feigenspan, 1995; Feigenspan and Bormann, 1998). On the other hand, protons and zinc inhibit both types of receptors (Dong and Werblin, 1995; Feigenspan and Bormann, 1998; Kaneda et al., 2000; Rivera et al., 2000). Picrotoxin, a chloride channel blocker, acts on $GABA_A$ as well as on most $GABA_C$ receptor channels, the exception being receptors containing the rat ρ2 subunit (Zhang et al., 1995; Enz and Cutting, 1999), which contains an amino acid alteration compared to ρ1 (T299M) which creates the insensitive to picrotoxin. It is interesting to note that $GABA_C$ receptors in rat retinal bipolar cells display picrotoxin insensitivity (Feigenspan et al., 1993; Pan and Lipton, 1995), suggesting that they contain the ρ2 subunit. Considering that rat ρ2 subunits do not form functional channels when expressed as homomers in Xenopus oocytes (Zhang et al., 1995), the picrotoxin-insensitivity of $GABA_C$ receptors in bipolar cells suggests that these receptors work as heteromers, containing both ρ1 and ρ2 subunits (mRNA for both receptor subunits is present in the same bipolar cell: Enz et al., 1995; Yeh et al., 1996; see section 1.4.1.2). The only specific $GABA_C$ receptor blocker available so far is TPMPA (Ragozzino et al., 1996).

1.4.1.5 Electrophysiological properties of ionotropic GABA receptor channels

One of the most striking differences between $GABA_A$ and $GABA_C$ receptors properties is the much higher sensitivity of $GABA_C$ receptors to GABA. The EC_{50} for GABA depends on the subunit composition, but ranges from around 10 to 100 μM for $GABA_A$ receptors (Kaila, 1994; Feigenspan and Bormann, 1998) and 1 to 5 μM for $GABA_C$ receptors (Polenzani et al., 1991; Calvo et al., 1994; Feigenspan and Bormann, 1994a; Wang et al., 1994; Zhang et al., 1995). Rat retinal bipolar cells contain $GABA_A$ receptors which have an EC_{50} of 27 μM (and a Hill coefficient of 1.7), and $GABA_C$ receptors which have an EC_{50} of 4 μM (and a Hill coefficient of 1.5; see also chapter 3). The Hill coefficients of around 2 suggest that ionotropic GABA receptors require the binding of at least two GABA molecules for activation (Feigenspan et al., 1993; Feigenspan and Bormann, 1994a).

Another prominent difference between $GABA_A$ and $GABA_C$ receptors is their current kinetics (Polenzani et al., 1991; Feigenspan et al., 1993; Qian and Dowling, 1993; Kaila, 1994; Chang and Weiss, 1999; Enz and Cutting, 1999). Whereas $GABA_A$ receptors desensitize rapidly in the maintained presence of GABA, $GABA_C$ receptors show no or only very little desensitization, and deactivate very slowly after the GABA concentration falls (possibly reflecting a low unbinding rate constant, which confers their high affinity). They can therefore mediate sustained current responses (Lukasiewicz and Shields, 1998).

Single channel analysis has also revealed major differences between the two receptor types: in rat retinal bipolar cells $GABA_A$ receptors have a larger single channel conductance, but a shorter mean open time than $GABA_C$ receptors ($GABA_A$: 27-30 pS and 30 ms; $GABA_C$: 7 pS and 150ms (Feigenspan et al., 1993)).

Both ionotropic GABA receptor types conduct anions (Bormann et al., 1987; Feigenspan et al., 1993; Feigenspan and Bormann, 1994a), which *in vivo* are mainly chloride and bicarbonate. The permeability ratio of bicarbonate vs chloride (P_{HCO3}/P_{Cl}) depends on the subunit composition of the receptor, and varies between

different regions and cells of the CNS, as well as at different developmental stages, but is of the order of 0.1 to 0.3 (Kaila, 1994; Feigenspan and Bormann, 1998).

1.4.1.6 Localization of ionotropic GABA receptor subunits

The subunit composition of GABA receptors, and thus their properties, varies greatly in different regions and cells of the CNS. Whereas $GABA_A$ receptors seem to be expressed on almost every neurone in the CNS (Kaila, 1994), $GABA_C$ receptor expression in the adult animal is most prominent within the visual system, especially the retina. The $GABA_C$ receptor transcripts (for the ρ1 and ρ2 subunits) have been found in the retina, especially in bipolar cells, but also in the dorsal lateral geniculate nucleus (dLGN), the superior colliculus and the visual cortex. The mRNA for ρ2 can also be found in other brain region, such as the cerebellum, hippocampus and cortex, and ρ1 and ρ3 transcripts are, albeit very weakly, also found in some of those areas (Enz et al., 1995; Yeh et al., 1996; Boue-Grabot et al., 1998; Wegelius et al., 1998; Enz and Cutting, 1999). Antibody labelling for ρ has mainly been performed in the retina (Enz et al., 1996; Koulen et al., 1997; Fletcher et al., 1998; Koulen et al., 1998a; Wassle et al., 1998; Shields et al., 2000), where it confirmed the presence of ρ in all strata of the inner plexiform layer and also in the outer plexiform layer. The ρ subunit appears in hot spots at rod and cone bipolar cell axon terminals, and is located in discrete puncta at synaptic sites. Moreover, as mentioned above (section 1.4.1.1), $GABA_C$ receptor mediated currents have been recorded in the retina and also some other areas of the CNS, indicating that they are functional. In this thesis I recorded GABA-evoked currents mainly from rat rod bipolar cells (Chapters 3 and 4), which do not only contain the $GABA_C$ receptor subunits ρ1 and ρ2 (Enz et al., 1995; Yeh et al., 1996), but also the $GABA_A$ receptor subunits α1, α3, β2/3 and γ2 (Greferath et al., 1994; Yeh et al., 1996; Fletcher et al., 1998). However these cells (in rat) express neither $GABA_B$ receptors (Heidelberger and Matthews, 1991; Koulen et al., 1998b) nor any of the high affinity GABA transporters (GAT-1, 2, or 3:

Brecha and Weigmann, 1994; Ruiz et al., 1994; Honda et al., 1995; Johnson et al., 1996).

1.4.2 G-protein coupled GABA receptors

Unlike ionotropic $GABA_A$ and $GABA_C$ receptors, $GABA_B$ receptors do not contain an ion channel within their structure, but are coupled to cation channels via G-proteins (for reviews see Bowery, 1989; Marshall et al., 1999; Mohler and Fritschy, 1999). Like other members of the G-protein coupled receptor family, $GABA_B$ receptor subunits have a structure of seven membrane-spanning segments. So far two types of $GABA_B$ receptors have been cloned ($GABA_BR1$ and $GABA_BR2$) and shown to work as heteromeric dimers (Kaupmann et al., 1997; Kaupmann et al., 1998). $GABA_B$ receptors are expressed throughout the whole central nervous system and can be found on post- as well as presynaptic sites. Broadly speaking, $GABA_B$ receptor activation results in inhibition – either by activation of potassium channels or by decreasing activation of voltage-gated calcium channels (thus reducing neurotransmitter release).

1.5 GABA and glycine transporters

In chapter 3 I investigate the effect on $GABA_C$ receptor function of inhibiting GABA transporters, and investigate a possible interaction between a glycine transporter and $GABA_C$ receptors. Furthermore, understanding glycine transporters is important for understanding how the glycine concentration is controlled near NMDA receptors, which I investigate in chapter 7 (section 1.1.1.3.1). Accordingly, here I briefly review the properties of these transporter types.

GABA and glycine are taken up into cells by GABA and glycine transporters, which are members of the Na^+/Cl^--dependent transporter family. As recently reviewed by Gadea & Lopez-Colome (2001a), Gadea & Lopez-Colome

(2001b) and Masson et al. (1999), they share a similar membrane topology, having twelve transmembrane spanning segments, large extracellular loops and intracellular amino- and carboxy-termini. There are three different high affinity GABA transporters cloned, called GAT-1, GAT-2 and GAT-3 in rat (the names vary between species, so the rat GAT-2 and GAT-3 are called GAT-3 and GAT-4 respectively in mice; I will refer to the rat names in this thesis), one low affinity GABA transporter, called BGT-1 in rat (called GAT-2 in mice), and two glycine transporters, called GLYT-1 and GLYT-2. GLYT-2 has two splice variants, GLYT-2A and GLYT-2B. For GLYT-1 the splice variants produce transporters which differ in their amino terminus, and are distinguished as GLYT-1A, GLYT-1B and GLYT-1C. More recently another splice variant, which differs in its carboxy terminal, has been found in the bovine retina and was named GLYT-1E/F (Hanley et al., 2000). This variant was shown to interact with the intracellular loop of the $GABA_C$ receptor subunit ρ1 but, as nothing is known about the function of this interaction, in chapter 3 I investigate whether glycine transporter activation modulates $GABA_C$ receptor properties.

GABA transporters are located throughout the CNS, and although it has long been believed that the three high affinity transporter types have a distinct cell expression pattern (e.g. GAT-1 being neuronal and GAT-3 being glial), GAT-1, GAT-2 and GAT-3 have each been shown to be expressed by both neurones and glial cells, depending on the animal species used and the brain area investigated. BGT-1 is expressed mainly in glial cells. Glycine transporters also are expressed in large areas of the CNS, with GLYT-1 and GLYT-2 being mainly glial and neuronal, respectively. Whereas GLYT-2 is expressed in presynaptic terminals of glycinergic neurones (in the spinal cord, brain stem and cerebellum), GLYT-1 can be found in brain areas which are devoid of glycinergic synaptic transmission as well as in the same areas as GLYT-2 (Zafra et al., 1995). The co-localization of glycine transporters and NMDA receptors led to the suggestion that the extracellular glycine

concentration, and hence the size of the NMDA component of the EPSC at excitatory synapses, can be modulated by glycine transporters (Smith et al., 1992; see also section 1.1.1.3.3). In chapter 7, I examine whether glycine can modulate NMDA receptor activity at the mossy fibre to granule cell synapse in the cerebellum. This is a glutamatergic synapse (see section 1.9) where both glycine transporter subtypes are present: electron microscopy and immunolabelling revealed that GLYT-1 is present in glial cell processes surrounding granule cells, whereas GLYT-2 is present in the Golgi cell terminal membranes apposed to granule cell dendrites (Zafra et al., 1995).

GABA and glycine transporters use the electrochemical gradients for sodium and chloride in order to translocate GABA/glycine against their concentration gradients across the membrane. It was originally thought that all members of the Na^+/Cl^--dependent transporter family share the same stoichiometry, i.e. 2 Na^+ and 1 Cl^- translocate for each GABA/glycine. This stoichiometry produces a transporter which is electrogenic, and indeed GABA and glycine transporters have been studied electrophysiologically. However, it was recently shown that GLYT-2 has a different stoichiometry to GLYT-1, in that it co-transports 3 Na^+ and 1 Cl^- with each glycine molecule (Roux and Supplisson, 2000). This provides much greater accumulative power for glycine, and makes GLYT-2 much less likely to reverse, consistent with a role of this transporter subtype in terminating inhibitory glycinergic synaptic transmission. On the other hand, the stoichiometry of GLYT-1 allows the transporter to reverse relatively easily, for example during neuronal activity when $[K^+]_o$ rises and cells depolarize. Reversal of GLYT-1 will release glycine into the extracellular space, consistent with a role for this transporter in modulating excitatory synaptic transmission (see previous paragraph and section 1.1.1.3.1).

1.6. Chloride homeostasis and the polarity of GABA responses

In chapter 4, I investigate how the transmembrane chloride concentration

gradient, which drives $GABA_A$ and $GABA_C$ receptor currents, is controlled in retinal bipolar cells. Here I review previous work on this topic.

The membrane potential of a cell depends on the concentrations of ions on either side of the membrane and the relative permeability of the membrane to those ions. Whenever ion channels open, the permeability of the membrane to the relevant ion increases, and the membrane potential shifts towards the reversal potential of that ion. As mentioned in section 1.4, ionotropic GABA receptors conduct anions when activated, *in vivo* mainly chloride and bicarbonate (Bormann et al., 1987). The permeability to bicarbonate depends on the subunit composition of the GABA receptor, but is in most cases about 0.1 to 0.3 of that to chloride (for example Kaila, 1994; Feigenspan and Bormann, 1998). So when GABA receptor ion channels open, the membrane potential (V_m) shifts towards the reversal potential of the GABA evoked conductance (E_{GABA}), which is between the reversal potential for chloride (E_{Cl^-}) and the reversal potential for bicarbonate (E_{HCO3^-}), and due to the higher permeability for chloride it is much closer to E_{Cl^-} than to E_{HCO3^-}. The GABA response is hyperpolarizing when E_{GABA} is more negative, and depolarizing when it is more positive than V_m. Additionally, GABA can also evoke biphasic responses consisting of a hyperpolarization followed by a depolarization (these biphasic responses required the presence of bicarbonate in the solution), for example during intense neuronal activity or the prolonged presence of GABA. This means that E_{GABA} shifts from being more negative than V_m to being more positive, which may be explained by chloride accumulating inside the cell during prolonged channel opening, along with a significant bicarbonate permeability to the channel (Staley et al., 1995; Backus et al., 1998; Dallwig et al., 1999; Frech et al., 1999).

During development GABA responses are often excitatory (for example Cherubini et al., 1990; Cherubini et al., 1991; Chen et al., 1996; Owens et al., 1996), i.e. E_{GABA} is significantly more positive than V_m, and can depolarize the membrane potential sufficiently to activate voltage gated calcium channels (Reichling et al.,

1994; Owens et al., 1996). Calcium entry evoked by such GABA evoked depolarization is believed to be important for neuronal proliferation, migration and synaptogenesis. In the adult animal GABA responses are usually inhibitory (Kaila, 1994): this is either due to E_{GABA} being more negative than V_m (so that GABA hyperpolarizes the membrane and moves the membrane potential further away from the threshold of many voltage gated cation channels) or due to E_{GABA} being close to (only slightly more negative or positive) or equal to V_m (so that GABA stabilizes the membrane potential at or around its resting value, this is termed "shunting inhibition"). The developmental shift of E_{GABA} appears to be mainly due to a shift of E_{Cl}, with the intracellular chloride concentration ($[Cl^-]_i$) being higher in younger animals. This has been proposed for some time but was only recently directly demonstrated in cells of mammalian brain slices using the gramicidin perforated patch-clamp technique (for example: Owens et al., 1996; Ehrlich et al., 1999; Kakazu et al., 1999).

The intracellular chloride concentration in neurones is usually not determined by passive chloride movement through chloride conducting channels, but is regulated by specific chloride transporters, such as the Cl^--ATPase (extruding chloride), the Cl^-/HCO_3^--exchanger (usually accumulating chloride), the Na^+-dependent Cl^-/HCO_3^--exchanger (usually extruding chloride) and transporters of the electroneutral cation-chloride co-transporter family (Kaila, 1994; Delpire, 2000). The latter family has seven members, but the two most important ones for neurophysiology appear to be the sodium-potassium-chloride cotransporter NKCC-1 and the brain specific potassium-chloride co-transporter KCC-2 (Payne et al., 1996), both of which have been shown to control $[Cl^-]_i$ in a variety of neurones (for example Kakazu et al., 1999; Rivera et al., 1999; DeFazio et al., 2000; Sung et al., 2000; Hubner et al., 2001b; Martina et al., 2001). During each transport cycle, NKCC-1 transports 1 sodium, 1 potassium and 2 chloride ions across the membrane (Russell, 2000), whereas KCC-2 co-transports 1 potassium with each chloride ion (Payne, 1997).

Thus, both transporters are electroneutral. During physiological conditions the ion concentrations are such that NKCC-1 accumulates chloride, whereas KCC-2 extrudes it from the cell (see Figure 4.6B for the energy changes associated with chloride transport by these carriers). Thus the presence of NKCC-1 in the cell membrane could aid in depolarizing E_{GABA}, whereas the presence of KCC-2 could aid in hyperpolarizing GABA responses. Interestingly the expression for NKCC-1 and KCC-2 show cellular, subcellular and developmental differences. The overall brain expression levels of NKCC-1 are high at birth and decline during early postnatal development (Plotkin et al., 1997). The presence of this transporter in the neurones of young animals explains their high internal chloride level, more positive E_{GABA} and depolarizing, excitatory GABA responses. By contrast, KCC-2 levels are low at birth and increase during postnatal development (Lu et al., 1999). The increase in KCC-2 expression was shown to coincide with, and be responsible for, the switch from depolarizing to hyperpolarizing GABA responses, and is regulated by the extracellular GABA concentration (Rivera et al., 1999; Ganguly et al., 2001). NKCC-1 can be found in neurones and glial cells, whereas KCC-2 is expressed only by neurones (Payne et al., 1996; Hubner et al., 2001a). When present in the same cell, NKCC-1 and KCC-2 can be found at different subcellular locations; for example NKCC-1 was found mainly in the dendrites, whereas KCC-2 was found mainly in the axon terminals of retinal rod (ON) bipolar cells, suggesting compartmentalized chloride concentration in this neurone (Vardi et al., 2000a; Vu et al., 2000). As described in detail in section 4.1, this distribution could make E_{Cl} more positive at the dendrites than at the synaptic terminals of the bipolar cells, which would be appropriate for generating the observed receptive field structure and light response transience in these cells. In Chapter 4, I examine whether the intracellular chloride concentration is, as suggested by the chloride transporter distribution, different in the dendrites and the axon terminal of retinal rod bipolar cells.

1.7. Proteins interacting with receptors and transporters

In chapter 3 and 5, I report experiments studying the effect of proteins interacting with $GABA_C$ receptors and glutamate transporters. In this section I review our current knowledge of proteins interacting with synaptic receptors and transporters.

For synaptic transmission to work properly, ion channels, neurotransmitter receptors and transporters have to be located at the appropriate part of the cell, and stabilized in the plasma membrane. Many neurotransmitter receptors are coupled to intracellular signalling pathways and the physical proximity of the receptor to an intracellular protein is crucial for converting binding of the extracellular neurotransmitter into an intracellular signal. Proteins interacting with ion channels, receptors and transporters regulate their subcellular location, activity and intracellular signalling (for recent reviews see: Garner et al., 2000; Gundelfinger and tom Dieck, 2000; Kennedy, 2000; Sheng and Pak, 2000; Sheng and Sala, 2001).

1.7.1 Interactions with ion channels and receptors

For K^+ channels, interaction of their C-terminus with scaffolding proteins containing PDZ domains determines whether they are expressed in the dendrites or axon of neurones (Arnold and Clapham, 1999), and confers sensitivity to modulation by G proteins (Hibino et al., 2000). Protein interactions at glutamatergic synapses are only sparsely studied for the presynaptic terminal (for a recent review see Gundelfinger and tom Dieck, 2000), but a great deal is known about the postsynaptic side (for recent reviews see Sheng, 2001a, b; Sheng and Sala, 2001). The postsynaptic density (PSD) is a specialized structure densely packed with an array of cytoskeletal and signalling proteins. It is formed by a mesh of supramolecular complexes, in which proteins such as the PDZ protein PSD-95 (just beneath the membrane) and Shank (in the deeper part of the PSD) form a scaffold to cluster

receptors and bring many proteins important for neurotransmission and downstream signalling into close proximity. For example, NMDA receptors interact with α-actinin-2 (via the C-terminal tail of the NR1 subunit), which tethers them to the cytoskeleton and controls their Ca^{2+}-dependent desensitization (Krupp et al., 1999), they interact with CaMKII (via the C-terminal tail of the NR2 subunit), and with a network of other proteins (Husi et al., 2000) including PSD-95, which locates downstream signalling enzymes such as nNOS (neuronal nitric oxide synthase) close to the channel (Brenman et al., 1996; Sheng and Lee, 2000). Similarly, AMPA receptors interact with proteins such as GRIP/APB (Dong et al., 1997; Srivastava et al., 1998; Srivastava and Ziff, 1999), PICK-1 (Xia et al., 1999), Stargazer (Chen et al., 2000b) and NSF (Nishimune et al., 1998; Noel et al., 1999); the latter interaction is particularly intriguing as NSF is implicated in vesicle fusion and probably controls the number of AMPA receptors present in the membrane (see also chapter 3.17.2). Finally, metabotropic glutamate receptors (mGluR) can be localized close to their downstream effector (the IP_3 receptor) by binding to the Homer class of proteins, which also bind to the IP_3 receptor of the smooth endoplasmic reticulum and thus regulate intracellular calcium release (Brakeman et al., 1997; Tu et al., 1999). Homer also binds to Shank, which in turn binds to GKAP (guanylate kinase associated protein). Shank can thus link the NMDA–PSD-95–GKAP complex to the mGluR–Homer–IP3 complex (Lim et al., 1999; Naisbitt et al., 1999; Tu et al., 1999; Sheng and Kim, 2000).

By contrast, much less is known about proteins interacting with glycine and GABA receptors and their role in constructing inhibitory synapses (for a recent review see Sheng and Pak, 2000; Moss and Smart, 2001). The only binding partner for glycine receptors (via the β subunit) identified so far is gephyrin (Kirsch et al., 1993; Meyer et al., 1995), which anchors the receptor to the cytoskeleton by interacting with microtubules and actin, and might provide a link to intracellular signalling proteins with which it interacts. $GABA_A$ receptors bind to GABARAP

(Wang et al., 1999; Chen et al., 2000a; Kneussel et al., 2000; Wang and Olsen, 2000), GRUB (Bedford et al., 2000), Plic-1 (Bedford et al., 2001), RACK-1 (receptor for activated C kinase) and PKCβII (Brandon et al., 1999). These proteins appear to modulate the receptor activity or participate in targeting, trafficking and insertion of the receptor into the membrane (see also section 3.17.1 and 3.17.2), but an anchoring protein for $GABA_A$ receptors has not been found yet.

Of most relevance to this thesis, two protein binding partners have been identified for $GABA_C$ receptors: the glycine transporter GLYT-1E/F splice variant (Hanley et al., 2000) and the microtubule associated protein MAP-1B (Hanley et al., 1999). The purpose of the GLYT-1E/F interactions remains unknown (see also chapter 3.17.5), but MAP-1B could link the receptor to the cytoskeleton by interacting with microtubules and actin. In chapter 3, I show that it also modulates $GABA_C$ receptor sensitivity (Billups et al., 2000). MAP-1B and $GABA_C$ receptors have been shown to co-localize in mammalian retinal bipolar cells (Hanley et al., 1999) and cone photoreceptors (Pattnaik et al., 2000). MAP-1B is a high molecular weight protein of around 200-300 kDa (255 kDa), has 2468 amino acids and forms a complex of three proteins: the heavy chain (HC) and two light chains (LC1 and LC3) (Schoenfeld et al., 1989; Hammarback et al., 1991; Langkopf et al., 1992). The heavy chain contains a microtubule binding region (amino acids 589-787) as well as the $GABA_C$ receptor binding region (amino acids 460-565), and can bind microtubules, actin and ρ at the same time (Hanley et al., 1999). MAP-1B is a long, flexible, filamentous molecule and appears to have a rod like structure in electron microscopy studies (Sato-Yoshitake et al., 1989; Wiche et al., 1991), which might allow it to stretch to just underneath the membrane when it binds to the $GABA_C$ receptor. MAP-1B is expressed at high levels throughout the nervous system in the new-born animal and declines during development (Schoenfeld et al., 1989), which has resulted in most efforts going into studying its function in the developing neurone. However in some areas, such as parts of the cerebellum, hippocampus,

spinal cord, olfactory bulb and retina, the expression remains at significant levels in the adult (Schoenfeld et al., 1989; Tucker et al., 1989; Hanley et al., 1999). The function of MAP-1B, especially in the adult brain, is unclear, but during development it appears to regulate microtubule dynamics during neurite outgrowth. Its efficiency of binding to microtubules is regulated by phosphorylation (Pedrotti et al., 1996) by casein kinase II (CKII) and proline-directed protein kinase (PDPK), but it can also be phosphorylated by protein kinase A (PKA) and protein kinase C (PKC) (Diaz-Nido et al., 1988; Kennelly and Krebs, 1991). Two groups have generated MAP-1B knock-out mice, the properties of which are discussed in section 3.17.4.

1.7.2 Interactions with glutamate transporters

Proteins interacting with neurotransmitter transporters are likely to play as important a role in CNS function as proteins interacting with ion channels. The existence of proteins interacting with glutamate transporters has been shown by several lines of evidence. First, the retinal transporter EAAT-5 has a C-terminal motif appropriate for binding to PDZ proteins (Arriza et al., 1997). Second, dialysing retinal glia with peptides mimicking the C-terminus of GLAST transporters increases the glutamate affinity of these transporters (Marie and Attwell, 1999) presumably by displacing an endogenous protein which interacts with the C-terminus and decreases the affinity. Third, the subcellular localization of glial GLT-1 transporters is highly controlled: more transporters are located in membrane facing the synaptic terminals, axons and spines of neurones than in membrane facing capillaries, pia or main dendrites (Chaudhry et al., 1995), presumably because of interaction with cytoskeletal tethering molecules. Indeed, the surface membrane density of transporters is regulated by interaction with intra- and extracellular messengers (Sims et al., 2000), suggesting controlled insertion of transporters into the membrane: a process which for AMPA receptors is controlled by interacting proteins such as NSF (Nishimune et al., 1998) and for $GABA_A$ receptors by interaction with Plic-1

(Bedford et al., 2001). Finally, proteins interacting with EAAC-1, EAAT-4 and GLT-1 have recently been described, as summarized below.

GTRAP3-18 has been identified as a binding partner for the C-terminus of the widespread neuronal glutamate transporter EAAC-1 (Lin et al., 2001). When co-expressed with EAAC-1 in HEK293 cells, this protein modulates glutamate transport activity by decreasing the glutamate affinity. GTRAP41 and GTRAP48 are binding partners for the C-terminus of the glutamate transporter EAAT-4 (Jackson et al., 2001), which is mainly expressed at perisynaptic sites on cerebellar Purkinje cell spines. Interaction with either of these proteins modulates glutamate transport activity by decreasing the glutamate affinity and increasing the maximum uptake rate (either by increasing the catalytic rate or by increasing its surface availability), and stabilizes the transporter in the membrane. In addition, by interacting with GTP binding proteins, GTRAP48 appears to link the transporter to downstream signalling pathways. The serine/threonine kinase PCTAIRE-1 interacts with the N-terminus (Law and Rothstein, 2000) of EAAT-4, and may link the transporter to intracellular signalling cascades.

Finally, and most relevant to the experiments reported in chapter 5, the cytosolic LIM protein Ajuba was identified by another student in this laboratory (Marie et al., 2002) as a binding partner for the N-terminal part of the glutamate transporter GLT-1 (see section 5.1). Not much is known about this protein, as it has only recently been identified and characterized (Goyal et al., 1999; Kanungo et al., 2000; Marie et al., 2002). It consists of 547 amino acids and has a molecular weight of about 58 kDa. Ajuba contains three LIM domains which are zinc-containing motifs mediating protein-protein and possibly protein-DNA interactions, named after the transcription factors Lin-11, Isl-1 and Mec-3 in which they were first found (for reviews see: Dawid et al., 1998; Bach, 2000). It also contains two potential SH3-recognition motifs as well as two nuclear export signal motifs within its pre-LIM domain (the part of the protein which is N-terminal to the LIM domains). Ajuba has

been shown to shuttle between the cytosol and the nucleus, where it inhibits proliferation and alters the cell fate, suggesting that it transfers intracellular signals to the nucleus (Kanungo et al., 2000). Ajuba has also been shown to participate in intracellular signalling, activating mitogen-activated protein kinase (MAP kinase) pathways via interaction with Grb2 (Goyal et al., 1999). In chapter 5, I examine if Ajuba might have another role, in modulating the properties of GLT-1.

1.8 Anatomy and neuronal circuits in the retina

The experiments reported in chapters 3 and 4 were carried out on bipolar cells in retinal slices. As a background to these experiments, here I review the neural wiring of the retina and light response properties of bipolar cells.

The retina has a lamina structure (Figure 3.21). Its thickness is around 100-200 μm, and in retinal slices (see Figure 3.11) one can easily discriminate two layers of synaptic connections (the outer plexiform layer (OPL) and the inner plexiform layer (IPL)), which separate three layers of cell bodies (the outer nuclear layer (ONL), inner nuclear layer (INL) and ganglion cell layer (GCL)). The retina contains a variety of cell types, each of which serves different functions in visual processing (reviewed by: Shepherd, 1998; Bloomfield and Dacheux, 2001; Masland, 2001a, b). The ONL consists of photoreceptor cell bodies, the INL contains the somata of bipolar, amacrine, horizontal, interplexiform and Müller cells, and the GCL is composed of ganglion cell bodies and displaced amacrine cells. The plexiform layers are regions in which the different cell types form synaptic contacts with each other, as outlined below. I will focus on the main connections made onto and by bipolar cells, the cells studied in this thesis.

The principal flow of visual information is through the entire thickness of the retina. Light passes through all layers of the retina before being absorbed by photopigment, which is located in the most distal part of the retinal photoreceptors. There are two types of photoreceptors, serving different purposes and allowing the

retina to detect light over a wide range of intensities: rods are highly sensitive to light and important for scotopic (night) vision, cones have a higher threshold and are important for photopic (day) vision. Rods and cones hyperpolarize in response to light; in the dark, when they are depolarized, rods and cones release glutamate from their synaptic terminals onto the dendrites of postsynaptic bipolar and horizontal cells in the OPL (Slaughter and Miller, 1983; Bloomfield and Dowling, 1985a; Wu and Maple, 1998).

There are two main classes of bipolar cells - ON and OFF bipolar cells - which have several characteristic anatomical and physiological properties. Whereas the somata of ON bipolar cells are located in the outer part of the INL and their axons travel through most of the IPL to branch near the ganglion cells (in sub-lamina b of the IPL), the cell bodies of OFF bipolar cells are located in the inner part of the INL and have relatively short axons which branch in sub-lamina a of the IPL which is nearer the bipolar and amacrine cell bodies (Nelson et al., 1978; Kolb, 1979; Bloomfield and Miller, 1986). In response to light falling in the centre of their receptive fields, ON bipolar cells depolarize, whereas OFF bipolar cells hyperpolarize. This is due to different receptor types being present on the bipolar cell dendrites, i.e. metabotropic glutamate receptors (mGluR6) on the ON bipolar cells (Slaughter and Miller, 1981, 1985; Tian and Slaughter, 1994; Vardi and Morigiwa, 1997; Vardi et al., 2000b), and ionotropic glutamate receptors (of the non-NMDA type) on the OFF bipolar cells (Brandstatter et al., 1994; Euler et al., 1996; Brandstatter et al., 1997; DeVries and Schwartz, 1999; Marc, 1999; Qin and Pourcho, 2001). When activated by glutamate (i.e. in the dark), mGluR6 receptors on the ON bipolar cell dendrites cause, via a G-protein activated second messenger cascade and subsequent drop in cGMP levels, the closure of cation-conducting nucleotide-gated ion channels and thus hyperpolarization of the membrane (Nawy and Jahr, 1990; Shiells and Falk, 1990; Nawy and Jahr, 1991; Nawy, 1999). Conversely, when glutamate levels are low (i.e. in the light), less mGluR6 receptors

are activated, leading to an increase in cGMP levels, so that the nucleotide-gated cation channels open and the cell membrane depolarizes. In contrast, OFF bipolar cells contain ionotropic glutamate receptors, so when glutamate levels are high (i.e. in the dark), these channels conduct and depolarize the membrane, and when glutamate levels are low (i.e. in the light) these channels close and the cell membrane hyperpolarizes.

ON and OFF bipolar cells can also be categorized into rod or cone bipolar cells, depending on which photoreceptor type, rods or cones, they receive input from. In the rat one can distinguish 10 types of bipolar cells, 9 of which are cone bipolar cells (5 OFF and 4 ON) and only 1 of which is a rod bipolar cell (ON) (Euler and Wassle, 1995; Euler et al., 1996; Hartveit, 1997; Euler and Wassle, 1998).

Bipolar cells are glutamatergic (Bloomfield and Dowling, 1985b; Wu and Maple, 1998), and when depolarized they release glutamate onto postsynaptic cells in the IPL. Cone bipolar cells form synapses with the dendrites of ganglion cells, of which there are 10-15 types, and amacrine cells, of which there are 25-30 types (Masland, 2001b). The properties of the complex cone pathways are largely unknown (Bloomfield and Dacheux, 2001), but the cone signal is transferred to the inner retina by many different cone bipolar cells, i.e. via many parallel channels (Masland, 2001a). Rod bipolar cells, on the other hand, do not appear to form direct synapses with ganglion cells, but contact two or three types of amacrine cells (Kolb, 1979; Strettoi et al., 1990; Strettoi et al., 1992; Bloomfield and Dacheux, 2001). One of these, the AII amacrine cell, makes electrical connections (gap junctions) with cone ON bipolar cells (see Figure 3.21), linking in this way the rod pathway to the ganglion cells (Strettoi et al., 1994). Thus, the most straightforward cone pathway through the retina is: cone – cone bipolar cell (ON or OFF) – ganglion cell (ON or OFF), while the most straightforward rod pathway is: rod – rod bipolar cell – AII amacrine cell – cone ON bipolar cell – ON ganglion cell (Bloomfield and Dacheux, 2001; Masland, 2001a). Ganglion cells are the only output of the retina, and their

axons transfer the visual information to higher centres of the brain.

The vertical information flow through bipolar cells is modulated by GABA acting on $GABA_A$ and $GABA_C$ receptors located on the bipolar cell dendrites and axon terminals, in the OPL and IPL. The two cell types which play a crucial role in this early visual processing are horizontal cells and amacrine cells. Horizontal cells modulate the information flow at outer retina by "lateral inhibition" (see section 4.1 and 4.8 for a more detailed description), which generates the classical centre-antagonistic surround organization of the receptive field. Amacrine cells modulate information flow in the inner retina by "vertical inhibition" which induces transience into the bipolar cell response (see section 3.17.4 for a more detailed description).

1.9 Anatomy of and neuronal circuits in the cerebellar cortex

In chapters 6 and 7, I describe experiments on two synapses in the cerebellum, the mossy-fibre to granule synapse and the parallel fibre to Purkinje cell synapse. Here I present the anatomical and physiological background needed to understand these experiments.

The cerebellum is an important motor control centre and is believed to be important for motor learning (Marr, 1969). The cerebellar cortex is greatly invaginated, forming different lobes (there are ten main lobes (I-X)). Each lobe displays a highly laminated structure and a well-conserved cellular organisation and microcircuitry (Eccles et al., 1967; Palay and Chan-Palay, 1974; Carpenter and Sutin, 1983), and one can distinguish three different layers in each lobe – the molecular layer, the Purkinje cell layer and the granule cell layer – which are characterised by different types of neurones (Figure 1.3). In the middle of each lobe is the white matter, i.e. bundles of afferent and efferent fibres (see below).

Figure 1.3: Diagram of the cerebellar cortex

Schematic drawing of the cerebellar cortex (in the adult), in the sagittal and transverse planes, showing the major organizational features of cells and fibres (from Eccles et al., 1967). Purkinje cells are shown in red, excitatory granule cells and parallel fibres are shown in green and climbing fibres (Cl) and mossy fibres (Mo) are shown in blue. Inhibitory stellate cells (St), basket cells (Ba) and Golgi cells (Go) are in black.

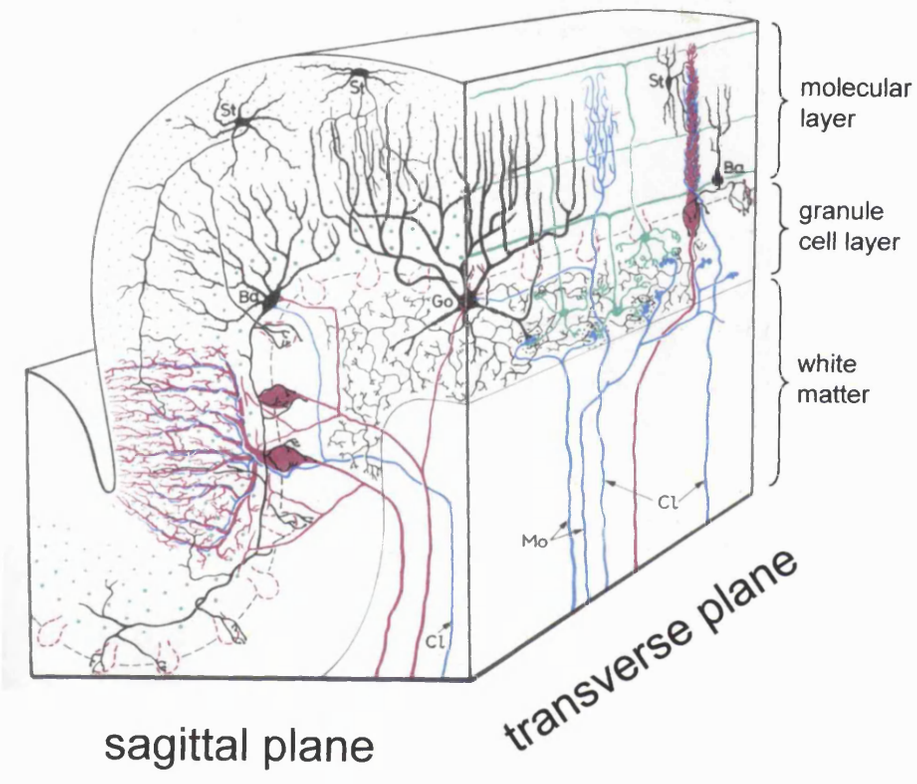
molecular layer
granule cell layer
white matter
St
St
St
Bc
Bc
Go
Cl
Cl
Mo
sagittal plane
transverse plane

1.9.1 Cell types

Surrounding the white matter is the granule cell layer. The most abundant cell type in this layer is an excitatory interneurone, the granule cell. Each granule cell has a small soma of about 5–8 μm in diameter, contains on average 4–5 relatively short dendrites and projects its long axon into the molecular layer, where it bifurcates (into a T-shape) and travels for some distance parallel to the surface (in the transverse plane) as parallel fibre (see below). Intermingled between the small somata of the numerous granule cells are larger inhibitory interneurones, the Golgi cells. These cells have soma about 9–16 μm in diameter, an extensive denditic tree which runs through all three layers of the cortex and a highly branched axon which is confined to the granule cell layer. In some lobes (mainly lobe X, but recent studies have indicated a more widespread distribution: personal communication with Traverse Slater), there is another class of excitatory interneurone, which is restricted to the granule cell layer – the unipolar brush cell. This cell type has a medium sized soma (about 7–10 μm in diameter), a relatively large dendritic brush and an axon with a couple of collaterals, each of which ends in a large bulbous axon terminal within the granule cell layer (reviewed by Mugnaini et al., 1997; Slater et al., 1997; Dino et al., 2000a).

Adjacent to the granule cell layer is the Purkinje cell layer, which consists of a single layer of Purkinje cell bodies, the somata of Bergmann glia and some Lugaro cells. Purkinje cells have a large soma of about 20–40 μm diameter, a highly branched dendritic tree which extends though the molecular layer (in the parasagittal plane) and a long axon which forms the only output of the cerebellar cortex. The somata of Bergmann glia are smaller than those of Purkinje cells and are electrically coupled to each other; their processes extend radially through the molecular layer. Lugaro cells can be seen from time to time at the lower edge of the Purkinje cell layer. These have elongated cell bodies, send long dendrites below and in between

the Purkinje cell bodies and send two axonal plexi into the molecular layer (Laine and Axelrad, 1996, 1998; Dieudonne and Dumoulin, 2000; Dumoulin et al., 2001).

The outermost layer of the cerebellar cortex is the molecular layer, which is rich in neuropil and contains two types of inhibitory interneurones, the stellate and the basket cells. The stellate cells are located in the outer two thirds of the molecular layer, have a medium sized soma (around 10 μm in diameter), radial extending dendrites and a long axon terminating in the molecular layer. Basket cells are located in the lower part of the molecular layer, and have a similar soma size to stellate cells and dendrites ascending into the molecular layer. Their axons run along the Purkinje cell layer and send off axon collaterals which embrace the soma of Purkinje cells.

Astrocytes and oligodendrocytes are diffusely located throughout the granule cell layer and white matter, whereas the radial Bergmann glia span the molecular layer of the cerebellar cortex.

1.9.2 Synaptic connections

Climbing fibres and mossy fibres are the only afferent pathways to the cerebellum. As well as innervating the cerebellar cortex (see below), both send collaterals to form excitatory (glutamatergic) contacts with cells in the deep cerebellar nuclei (DCN). Climbing fibres originate from cells located in the inferior olive, whereas mossy fibres arise from cells in many regions of the central nervous system (such as the cerebral cortex, the vestibular nuclei, the reticular formation and the spinal cord). Once in the cerebellar cortex, each climbing fibre branches off to terminate on the soma and the proximal (central) part of the dendritic tree of Purkinje cells and forms as many as 200–1200 synaptic contacts with a single cell. Climbing fibres are glutamatergic and very reliable in making a Purkinje cell fire.

Mossy fibres on the other hand terminate in the granule cell layer of the cerebellar cortex and contact a large number of neurones in arrangements termed 'cerebellar glomeruli' (Figure 1.4) (Hamori and Somogyi, 1983; Jakab and Hamori,

1988; Jakab, 1989; Hamori et al., 1997). These are specialised structures located throughout the granule cell layer, and measure about 10 μm in diameter. Each glomerulus contains a single mossy fibre rosette at its core, a large number of cellular processes arising from granule cells, Golgi cells and sometimes unipolar brush cells, and a surrounding sheath of glial cells in which neurotransmitter transporters (e.g. GLT-1 and GLAST) are localized. Each mossy fibre terminal makes (glutamatergic) synaptic contact with each of the 4–5 dendritic digits of about 50–60 granule cell dendrites, whereas an individual granule cell receives input from 4–5 different mossy fibre terminals. More than 1 mossy fibre need to be active simultaneously to make a granule cell fire (D'Angelo et al., 1995). Granule cell firing can result from repetitive mossy fibre activity which produces temporal summation (Overstreet et al., 1999) or from spatial summation via the activation of several simultaneously active inputs (D'Angelo et al., 1995). The purpose of the granule cell is thus to integrate afferent synaptic input from extrinsic mossy fibres, and serve as a feedforward glutamatergic interneurone projecting to populations of GABAergic interneurones and Purkinje cells. Golgi cell dendrites also receive excitatory input from mossy fibres; their axons make inhibitory (GABAergic) synapses onto granule cell dendrites in the glomerulus (Jakab and Hamori, 1988). In some cases the mossy fibre rosette in a glomerulus also forms a large synaptic contact with the dendritic digits of the dendritic brush of a unipolar brush cell (Rossi et al., 1995); these in turn form excitatory (glutamatergic) synapses with granule cells and other unipolar brush cells, producing feed-forward excitation in the granule cell layer (Dino et al., 2000a; Dino et al., 2000b; Nunzi et al., 2001).

As mentioned in section 1.9.1, each granule cell sends its axon into the molecular layer, where it bifurcates and travels perpendicular to the dendritic trees of Purkinje cells. Since the axons of many granule cells run parallel to each other in the molecular layer, they are usually referred to as 'parallel fibres'. Each parallel fibre makes excitatory (glutamatergic) synaptic contact with around 300 different Purkinje

Figure 1.4: Drawing of a cerebellar mossy fibre glomerulus

Schematic drawing of a cerebellar mossy fibre glomerulus (in the adult) in the granule cell layer (from Carpenter and Sutin, 1983). A mossy fibre rosette forms the core of the glomerulus, making excitatory (glutamatergic) synaptic contact with granule cell and Golgi cell dendrites. Golgi cell axons also protrude into the glomerulus, making inhibitory (GABAergic) synaptic contact with granule cell dendrites (but not with the Golgi cell dendrites or the mossy-fibre rosette: Eccles et al., 1967). The whole structure is enclosed in a glial capsule, in which glutamate transporters such as GLT-1 and GLAST are located.

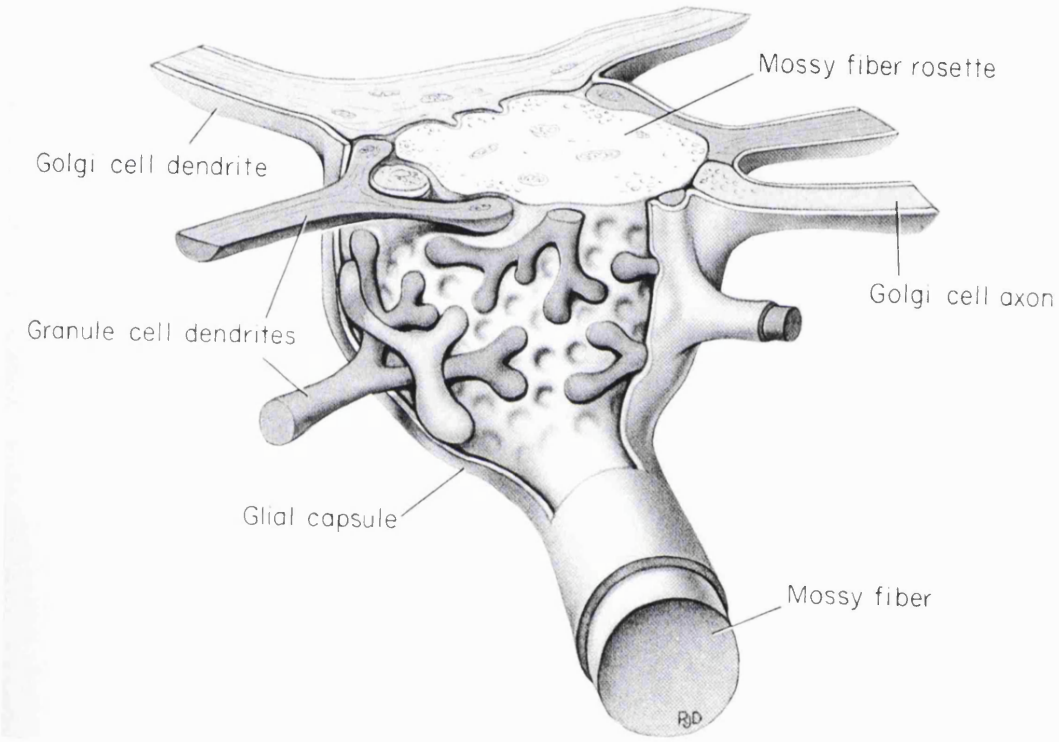
Mossy fiber rosette
Golgi cell dendrite
Golgi cell axon
Granule cell dendrites
Glial capsule
Mossy fiber

cells, but there is only one contact per Purkinje cell. Although about 150,000 granule cell axons (parallel fibres) form excitatory (glutamatergic) synaptic contacts with a single Purkinje cell dendrite, only about 50 granule cells need to be active to make a Purkinje cell fire an action potential (Barbour, 1993). Parallel fibres form also glutamatergic synapses with stellate, basket and Golgi cell dendrites in the molecular layer, and the Golgi cells in turn inhibit, via a negative feedback loop, the granule cells in the granule cell layer. Basket and stellate cells both receive excitatory input from the parallel fibres and form inhibitory synapses with Golgi cells and Purkinje cells. Each basket cell axon travels along the Purkinje cell layer and its collaterals embrace the soma and initial segment of several Purkinje cells, which they inhibit via axo-somatic (GABAergic) synapses and via so called *pinceau terminal* synapses at the axon hillock (Southan and Robertson, 1998). Basket, stellate and Golgi cells are also contacted by Lugaro cells (Laine and Axelrad, 1996, 1998; Dieudonne and Dumoulin, 2000), but so far only Golgi cells have been demonstrated to receive inhibitory (mixed GABAergic and glycinergic) input from these cells (Dumoulin et al., 2001).

The only output of the cerebellum is via the Purkinje cell axon, which makes inhibitory (GABAergic) synapses with the deep cerebellar nuclear cells.

1.9.3 Some properties of the synapses studied in this thesis

In this thesis (chapters 6 and 7) I studied the mossy fibre to granule cell as well as the parallel fibre to Purkinje cell synapses and will therefore briefly describe some of the main properties of these synapses.

1.9.3.1 The mossy fibre to granule cell synapse

Most of the mossy fibre to granule cell synapse formation in the rat takes place in the first three weeks after birth, when granule cells migrate from the external

granule cell layer along Bergmann radial glia through the molecular layer (where their processes form the parallel fibres) towards their final destination, the granule cell layer (Altman, 1972a; Hamori and Somogyi, 1983). Here the mossy fibres form excitatory synapses with granule cells and the maturation of the cerebellar glomeruli takes place (Hamori and Somogyi, 1983). Mossy fibres release glutamate as their neurotransmitter, which acts on postsynaptic AMPA and NMDA receptors (Garthwaite and Brodbelt, 1989; Silver et al., 1992; D'Angelo et al., 1993). The AMPA component is very brief, with a 10-90% rise time of around 200 μs, and a decay time constant of 1-2 ms (Silver et al., 1992). The NMDA component of the postsynaptic current changes during postnatal development (Rumbaugh and Vicini, 1999; Cathala et al., 2000), as the NR2 subunit expression of the NMDA receptors in granule cells changes during the first two postnatal weeks (Akazawa et al., 1994; Farrant et al., 1994; Monyer et al., 1994; Watanabe et al., 1994; Wang et al., 1995; Takahashi et al., 1996b): granule cells in rat cerebellum undergo a switch in NR2 expression from NR2B (from birth until around P14) to NR2A/NR2C (starting gradually from around P8) to mainly NR2C (in the adult). The NR1 subunit is expressed throughout this period, but the first mossy fibre synapses form only at the end of the first postnatal week (Altman, 1972b).

The properties of the mossy fibre to granule cell synapse can be modulated in the short term by, for example, metabotropic glutamate and GABA receptors. GABA released from Golgi cell terminals can spill over onto $GABA_B$ receptors on the mossy fibre terminal, decreasing the amount of glutamate release and thus the amplitude of the postsynaptic current (Mitchell and Silver, 2000a). Conversely, glutamate released from mossy fibres has also been shown to spill over and activate mGluRs (of type I and II) on neighbouring Golgi cell axon terminals, decreasing GABA release and thus reducing the inhibition onto granule cells (Mitchell and Silver, 2000b). Additionally, granule cells express metabotropic glutamate receptors of groups I and III (Vetter et al., 1999), which couple to the PLC-IP_3/DAG and the

cAMP pathways.

The mossy fibre to granule cell synapse exhibits a longer lasting plasticity, i.e. an mGluR dependent form of long-term potentiation (LTP), which requires NMDA receptor activation (rossi et al., 1996; D'Angelo et al., 1999; Armano et al., 2000). It can be elicited either by (1) application of an mGluR agonist (t-ACPD; for around 2 minutes) while NMDA receptors are synaptically activated at low frequency (0.1 Hz, recorded in voltage clamp; Rossi et al., 1996), by (2) theta burst stimulation (8 bursts of 10 stimuli at 100 Hz repeated every 250 ms) or a 1 second train (100 Hz) while the granule cell is depolarized (–40 mV; to allow NMDA receptor activation; recorded in voltage clamp; D'Angelo et al., 1999) or by (3) theta burst stimulation (4 bursts of 10 stimuli at 100 Hz repeated every 250 ms) when recorded in current clamp (resting potential was –70 mV; Armano et al., 2000). After any of these protocols the amplitudes of the non-NMDA and the NMDA components of the EPSC/EPSP were potentiated (for >45 minutes) by around 40-100 %. Experiments using pharmacological blockers show that this form of LTP requires the activation of mGluRs, NMDA receptors and PKC, as well as a rise in the intracellular calcium concentration (D'Angelo et al., 1999). LTP protocols at the mossy fibre to granule cell synapse did not only augment the synaptic strength, but increased also the intrinsic excitability of the granule cell (i.e. the threshold to fire an action potential was decreased and the input resistance was increased; Armano et al., 2000). However, LTP was not induced if GABAergic inhibition was intact, i.e. when recordings were made in bicuculline-free solution.

1.9.3.2 The parallel fibre to Purkinje cell synapse

Parallel fibres release glutamate when granule cells fire, which activates ionotropic AMPA receptors (Konnerth et al., 1990; Perkel et al., 1990; Llano et al., 1991), metabotropic glutamate receptors (Batchelor et al., 1994; Tempia et al., 2001) and possibly also glutamate transporters (Canepari et al., 2001) on the Purkinje cell.

The parallel fibre to Purkinje cell EPSC is thus mediated by a fast rising and decaying AMPA component (as documented in chapter 6) and a slowly rising and decaying mGluR (mGluR1) component. Synaptic activation of the mGluR1 receptors (which belong, as mentioned in section 1.1.2, to the group I of mGluRs) leads to an intracellular calcium concentration rise via IP_3 signalling in the Purkinje cell spine (Finch and Augustine, 1998; Takechi et al., 1998), to opening of a cation channel (Canepari et al., 2001) and to release of endogenous cannabinoids, which can act on presynaptic CB1 receptors to reduce the amount of neurotransmitter release from parallel fibres (Kreitzer and Regehr, 2001), climbing fibres (Maejima et al., 2001) and interneurone axon terminals (Diana et al., 2002). Purkinje cell spines also express the δ2 glutamate receptors (Landsend et al., 1997; Zhao et al., 1997), which may be important during synaptogenesis and plasticity. There are no functional postsynaptic NMDA receptors at this synapse after about P10 (Rosenmund et al., 1992; Momiyama et al., 1996; Cull-Candy et al., 1998), but it has recently been shown that the presynaptic parallel fibre terminals express NMDA receptors (Casado et al., 2000). The parallel fibre also expresses $GABA_B$ and A1 receptors which, when activated by GABA and adenosine respectively, modulate presynaptic calcium channels and result in reduced glutamate release (Takahashi et al., 1995b; Dittman and Regehr, 1996, 1997).

The granule cell to Purkinje cell synapse shows short term plasticity (on a second time scale: paired pulse facilitation (PPF; Konnerth et al., 1990; Atluri and Regehr, 1996; Kreitzer and Regehr, 2000)) and long term (hour time scale) potentiation (LTP; Salin et al., 1996) and depression (LTD; Ito and Kano, 1982; Ito, 2001)). The short term facilitation can be elicited by a pair of stimuli (less than about 1 second apart; the facilitation decays with a time constant of around 200 ms) or a train of stimuli (for example 10 stimuli at 1-50 Hz as in Kreitzer and Regehr, 2000). It facilitates the EPSC up to 2.5 times over the millisecond to second time scale and is critically dependent on the residual calcium concentration in the presynaptic

terminal (Atluri and Regehr, 1996; Kreitzer and Regehr, 2000; Carter et al., 2002). LTP can be induced by low frequency stimulation of the parallel fibres (about 2-8 Hz) and is dependent on presynaptic activation of calcium sensitive adenylate cyclase and PKA activation (Salin et al., 1996). LTP is not only induced but also expressed presynaptically (reviewed by Hansel et al., 2001). Purkinje cell to parallel fibre LTD can be induced by simultaneous low frequency stimulation of parallel fibres and climbing fibres (Ito and Kano, 1982). It depresses the synapse by up to 50% and is dependent on (1) calcium influx via voltage gated calcium channels (thought to be the result of climbing fibre activity), (2) activation of postsynaptic AMPA and mGluR1, and presynaptic NMDA receptors (Casado et al., 2002) by glutamate (as result of parallel fibre activity) and (3) transient PKC activation. Postsynaptic glutamate transporters appear to regulate mGluR (and possibly also presynaptic NMDA receptor) activation and induction of LTD (Brasnjo and Otis, 2001). Long term depression seems to result from a reduction of the number of AMPA receptors in the Purkinje cell membrane due to clathrin mediated endocytosis (reviewed by Hansel et al., 2001). Purkinje cell to parallel fibre LTD appears thus to be induced partly pre- and partly postsynaptically, and expressed postsynaptically. It has long been postulated to play an important role in motor learning (Marr, 1969).

CHAPTER 2

Methods

This chapter describes the general methods used for experiments throughout the thesis. Particular methological details which are important for understanding specific experiments are described in detail in the relevant Results chapters.

The experiments in this thesis were carried out on three cell types: retinal cells, cultured COS cells and cerebellar cells. The preparation of these different cell types will be described in turn.

2.1 Cell preparation

2.1.1 Retina

Retinal slices and isolated cells from postnatal day 35 (P35) Sprague-Dawley rats, as used in Chapter 3 to study the effect of MAP-1B on $GABA_C$ currents in bipolar cells and in Chapter 4 to study how the intracellular chloride concentration is controlled in bipolar cells, were obtained as follows.

2.1.1.1 Dissection

The rats were killed by cervical dislocation, followed by decapitation. The eyes were removed immediately and stored submerged in cold external incubation medium (Table 2.1 Solution B, or Table 2.2 Solution A) until dissection of the retina a few minutes later. Each eye was cut open and dissected along the ora serrata, using a razor blade and ophthalmological scissors. The anterior part of the eye, the lens and vitreous humour were removed using fine forceps, and the rest of the eye cup, containing the sclera, pigment epithelium and retina, were transferred to and stored

in a chamber containing oxygenated incubation medium (Table 2.1 Solution B, or Table 2.2 Solution A) at room temperature. The retinae were used within 8 hours after the animal was killed. To prepare isolated cells or retinal slices, one of the stored eye-cups was cut into quarters, and the retina was separated from the sclera and any remaining vitreous humour.

2.1.1.2 Preparation of isolated retinal cells

Retinal cells were isolated by papain dissociation following the method of Bader et al. (1979) with solutions adapted to the correct tonicity for mammalian cells. A piece of isolated retinal tissue was incubated at 34^{O}C for 20 minutes in 2 ml of mammalian dissociation medium (calcium-free to uncouple Ca^{2+}-dependent cell adhesion molecules: Table 2.1 Solution A) containing 15 µl of the proteolytic enzyme papain (Sigma, P3125). The retina was then washed 4 times in 4 ml of incubation medium (Table 2.1 Solution B), broken up by passing it in and out of a fire polished Pasteur pipette (i.e. triturated), and plated directly onto the bottom of the recording chamber. The cells were allowed to settle for 15 minutes before perfusing with recording medium (Table 2.1 Solution C). Bipolar cells were easily identified by their morphology (Figure 3.5 shows a picture of a dissociated bipolar cell).

2.1.1.3 Preparation of retinal slices

Retinal slices were obtained using a hand operated chopper: this uses a vertically moving razor blade to cut slices off the retina as the retina is moved underneath. The piece of isolated retina was laid flat on the bottom of a glass petri-dish, ganglion cell side up, and covered only by a thin film of Ringer. A rectangular piece of Millipore filter paper was used to pick up and transfer the retina to the slicing chamber, where it was secured by two strips of Vaseline and covered by

incubation medium (Table 2.1 Solution B, or Table 2.2 Solution A). The filter paper with the attached retina was chopped to obtain about 200 μm thick slices. Each slice was picked up by the sliced piece of filter paper (to which the slice remained attached) with forceps, tilted through 90^{O} so that it was viewed from the side of the slice, and transferred to the recording chamber where it was held in place by two Vaseline strips. All the layers of the retina could easily be identified (Chapter 3, Figure 3.11).

2.1.2 Cultured COS cells

COS cells were used as an expression system for the experiments described in chapter 5 on a protein interacting with the glutamate transporter GLT-1.

2.1.2.1 Cell culturing

COS-7 cells were cultured in a humidifying incubator (5% CO_2) at $37^{O}C$ in DMEM (Dulbecco's Modified Eagle Medium, Gibco) supplemented with 10% foetal calf serum (Gibco), 0.1 μg/ml penicillin and 0.1 μg/ml streptomycin. The cells were split and re-plated the day before they were injected with cDNA for the proteins to be expressed. The confluent cells were detached from the petri-dish by trypsin, transferred to sterile tubes and pelleted at 1000 rpm for 2 minutes. They were then resuspended in fresh medium and plated at a density of about $2x10^{6}$ cells/10 cm dish on poly-L-lysine coated cover slips.

2.1.2.2 DNA injection

The cDNA stocks were stored at 1 mg/ml at $-20^{O}C$ or $-80^{O}C$. The glial glutamate transporter GLT-1 was expressed using the vector PRK5-GLT-1 (obtained from Niels Danbolt, Oslo), the LIM protein Ajuba was expressed using the vector PCS2-Ajuba (obtained from Greg Longmore, Washington University) and GFP was

expressed as its S65T mutant with enhanced fluorescence (Cubitt et al., 1995; Heim et al., 1995). On the day of the injection each of these stocks was diluted in phosphate buffered saline (PBS) to a concentration of 50 ng/μl. The COS cells which would express GLT-1 were injected with 50 ng/μl of the PRK5-GLT-1 cDNA and 50 ng/μl of the GFP cDNA; the cells which would express GLT-1 and Ajuba were injected with 50 ng/μl of the PRK-5 GLT-1 cDNA, 50 ng/μl PCS2-Ajuba cDNA and 50 ng/μl of the GFP cDNA. GFP was co-injected to identify cells successfully expressing the injected cDNA: it was assumed that if a cell expressed GFP it would also express the other co-injected cDNA (GLT-1 or Ajuba). This was validated by the observation that glutamate transport currents were almost always seen in cells showing GFP fluorescence but never in cells lacking GFP fluorescence (see chapter 5 section 5.3). Glass pipettes (about 30 MΩ open tip resistance when filled with PBS and immersed in PBS) were used to inject the cDNAs into the nuclei of single cells. About 100 cells per petri-dish were injected. The cells were left for about 24 hours in the incubator ($37^{O}C$, 5% CO_2) before they were used in the electrophysiology experiments. About 20 out of the 100 injected cells per dish showed GFP fluorescence and thus successful transfection.

2.1.3 Preparation of cerebellar slices

Sprague-Dawley rats (aged postnatal day 14 (P14)), or mice with particular glutamate transporters knocked out (aged P11-P15 for GLT-1 KO mice, P16-P20 for the GLAST KO mice used to study Purkinje cells and P29-P31 for the GLAST KO mice used to study granule cells), were used for the preparation of cerebellar brain slices. The animals were killed by cervical dislocation followed by decapitation, and the head was immediately transferred into chilled slicing medium (Table 2.4 Solution A). The scalp was removed and the skull opened from the dorsal surface by a transverse cut through the brain just posterior to the olfactory bulb, and lateral cuts on either side of the head from the anterior to the posterior running well behind the

lambdoid suture. The parietal bones and the occipital bone were carefully raised with forceps, and the whole brain was quickly removed and placed in ice-cold oxygenated slicing medium (with a lowered [Na^+] to reduce cell death; Table 2.4 Solution A). To obtain parasagittal slices of the cerebellar vermis, a transverse cut was made through the inferior colliculus and a parasagittal cut through one of the cerebellar hemispheres. This cerebellar block was mounted on the stage of a vibrating tissue slicer (Vibratome), cemented with Superglue and mechanically stabilised by an agar block attached to the Vibratome stage. The brain was immersed in ice-cold oxygenated slicing medium throughout the cutting process, which was exchanged every 3-5 slices made. Parasagittal slices of the cerebellar vermis, 200-225 μm thick, were cut, placed in oxygenated incubation medium (Table 2.4 Solution B) and stored at 35-37^{O} for about 30 minutes. The slices were then kept at room temperature until used for recording, not more than 8 hours after the animal was killed. For the experiment, a cerebellar slice was placed in the recording chamber (1 ml volume) and held in place by a "harp" made of a parallel array of nylon threads, separated from each other by 0.5-1.0 mm, strung on a platinum frame.

2.2 Mechanical and optical set-up

The recording chamber containing retinal slices or isolated cells, cerebellar slices or COS cells was placed on the stage of an upright microscope (Axioscope, Zeiss) and connected to an inlet tube and a sucker (connected to a vacuum pump), so that the slices/isolated cells were constantly superfused with oxygenated solution. The inlet was either gravity fed from 50 ml syringes (flow rate around 6-8 ml/min) or driven by a peristaltic pump (flow rate around 3-5 ml/min). Cells were viewed using a 40x water immersion objective with differential interference contrast (DIC) (Normarski optics). The microscope was equipped with a xenon lamp and appropriate fluorescence filters (FITC; excitation: 425 nm, emission: 515 nm) to view cells COS transfected with GFP (Chapter 5) or cells filled with Lucifer Yellow

(all other results chapters).

2.3 Pipettes and electrical set-up

Patch pipettes were made of filament-containing borosilicate glass capillaries. These were either thick-walled (outer diameter 1.5 mm, inner diameter 0.86 mm, type GC150F-10 from World Precision Instruments) for granule cells and bipolar cells, or thin walled (outer diameter 1.5 mm, inner diameter 1.17 mm, type GC150TF-10) for Purkinje cells and COS cells. The patch pipettes were produced by pulling the capillaries either in a two step horizontal puller (BB-CH), or using a two step vertical puller (Narishige PC-10). Patch pipettes were filled with the appropriate intracellular solution (Table 2.5). The membrane potential applied to the cell is slightly more negative than that measured by the patch-clamp apparatus, due to the presence of a liquid junction potential at the boundary between the electrode solution and bath solution before a seal is made on a cell, which is not present after the seal is made (Fenwick et al., 1982). For my internal solutions, which contain a high chloride concentration this potential was measured as approximately –2 mV. This was not compensated for in most of the data shown (because the error is so small) but it was added onto the measured voltage for all the experiments determining the reversal potential of GABA-evoked currents at different locations in retinal bipolar cells (chapter 4) for which a few millivolts error could be important.

The recording electrode was mounted into the pipette holder of a patch-clamp headstage (Axopatch CV202AU, Axon Instruments), which was attached to and moved by an electric micro-manipulator (SMI, Luigs & Neumann, Germany). A chlorided silver wire (or in some experiments, where the external chloride concentration was altered, a 4M NaCl filled Agar bridge, to prevent changes of bath electrode potential) was placed in the recording chamber to serve as the bath electrode. Membrane currents were recorded with an Axopatch 200A amplifier (filtered at 10 kHz, -3dB, four-pole, low-pass Bessel filter), digitised using a

Digidata 1200 Interface (Axon Instruments) and stored either via a digital data recorder (PCM701ES, Sony) on video tape or directly onto a personal computer (using pClamp 5 or pClamp 8), on which the data were analysed off-line using Clampfit 6 or 8 (Axon Instruments). Additionally, all data were recorded continuously using a chart recorder.

2.4 Patch-clamp recordings

All recordings were performed either in the conventional or the perforated whole-cell configuration (Hamill et al., 1981; Edwards et al., 1989). The general principle of the patch-clamp technique is the obtaining of a high resistance seal (usually 1-10 GΩ) between the cell membrane and the tip of the glass patch pipette, so that most of the current flowing through the membrane patch flows directly into the pipette to the patch clamp amplifier and is therefore recorded with a high signal to noise ratio. The gigaohm-seal can be obtained by attaching the pipette onto the cell surface and sucking gently. The chances of formation of a gigaohm-seal can be increased by applying positive pressure to the pipette before contacting the cell to keep the pipette tip clean, so that the attachment of any kind of debris flowing in the bath solution, or of tissue when entering the slice, is prevented (for a description of slice patching see Edwards et al., 1989). After formation of a high resistance seal in the cell-attached mode, and compensation of the pipette capacitance transient, further suction is applied to the pipette to rupture the membrane patch below the pipette tip to achieve a low resistance access to the cell's interior. In this conventional whole-cell patch-clamp mode the cell interior is in direct contact with the pipette interior. Ions of the cytoplasm will diffuse into the pipette, and vice versa, resulting in the cell becoming dialysed within several minutes after the membrane patch is broken (see section 2.7 for estimates of the time needed for this). In this way the intracellular solution composition can be controlled by the pipette solution.

Whole-cell clamping was used for the majority of the experiments in this

thesis. However, for the experiments in chapter 4 determining the chloride concentration in retinal bipolar cells, and for some experiments on COS cells in chapter 5, it was desirable not to perturb the internal cellular environment. This was achieved by using the perforated patch technique (Horn and Marty, 1988), in which a pore-forming antibiotic such gramicidin, Amphotericin B or nystatin is included in the pipette solution. After formation of a high resistance seal in the cell-attached mode and compensation of the pipette capacitance transients, the antibiotic slowly forms pores in the membrane patch beneath the pipette tip, and thus provides electrical access to the cell's interior. Depending on the perforating agent used, the pores are permeable to different ions, so the cell gets some of its internal ions exchanged with the pipette solution. To investigate the intracellular chloride concentration in bipolar cells (chapter 4) I used gramicidin D (#G-5002, Sigma) as perforating agent since this does not alter $[Cl^-]_i$, because its pores are Cl^- impermeable but conduct cations well (Kyrozis and Reichling, 1995). To investigate the possible modulation of glutamate transporters by the intracellular protein Ajuba I used Amphotericin B (#A-4888, Sigma) as the perforating agent which produces pores permeable to monovalent cations and anions (Rae et al., 1991).

2.5 Series resistance

Series resistance is the resistance between the cell's interior and the pipette's interior when in the whole-cell patch clamp configuration. It is measured as described in the next section. A low series resistance (in the MΩ range) implies a good electrical and diffusion pathway into the cell. A good diffusion pathway is essential for the efficient exchange of molecules between the pipette and the cell. A good electrical pathway to the cell interior is important because current flowing between pipette and cytoplasm will result in a voltage drop across the pipette tip, the value of which depends on the series resistance and the size of the current. A high series resistance or large current flow will result in a high voltage drop, and the

apparent membrane potential is the sum of the real membrane potential plus the voltage drop. In most of my experiments this voltage drop is negligible (see sections 2.8.1, 2.8.3 and 2.8.4) and was not corrected for. In Chapter 4, however, it was important to correct for the voltage drop (see section 2.8.2).

2.6 Cell capacitance measurements

The cell membrane capacitance and resistance, and the series resistance can be measured by analysing the current response to a voltage step. The membrane acts as a capacitor and resistor connected in parallel, and the series resistance is in series with these (Figure 2.1). The current flow, I, through this circuit in response to a voltage step, V_s, is (Tessier-Lavigne et al., 1988):

$$I(t) = \left(\frac{V_s}{R_m + R_s}\right) \cdot \left(1 + \frac{R_m \cdot e^{-t/\tau}}{R_s}\right) \tag{2.1}$$

where t is the time after the onset of the voltage step, R_m is the membrane resistance, R_s is the series resistance, and τ, the decay time constant of the current transient, is:

$$\tau = C_m \cdot \frac{R_s \cdot R_m}{R_s + R_m} \tag{2.2}$$

At the onset of the voltage step, at t = 0, the capacitor is uncharged, all current flows through it and the voltage across it is zero. Consequently, just as the voltage step is applied, the voltage across the series resistance is the applied voltage step, and the initial current flowing allows calculation of the series resistance as:

$$R_s = \frac{V_s}{I(t = 0)} \tag{2.3}$$

At steady state, i.e. $t = \infty$, the capacitor is fully charged and no current flows through it. The membrane resistance can then be calculated from the voltage step and the current at $t = \infty$:

$$R_m = \frac{V_s}{I(t = \infty)} - R_s \tag{2.4}$$

Figure 2.1: Measurement of cell capacitance

(A) Equivalent circuit of a whole-cell patch-clamped cell. R_s is the series resistance, R_m is the membrane resistance and C_m is the membrane capacitance.

(B) Example of a current response (black) to a 5 mV voltage step (grey) of a whole-cell patch-clamped COS cell. In this cell I(t = 0) was 800 pA, I(t = ∞) was 20 pA and τ was 0.32 ms (fitted with a single exponential using Clampfit). With these values R_s = 6.25 MΩ (equation 2.3), R_m = 250 MΩ (equation 2.5) and C_m = 53 pF (equation 2.7).

A

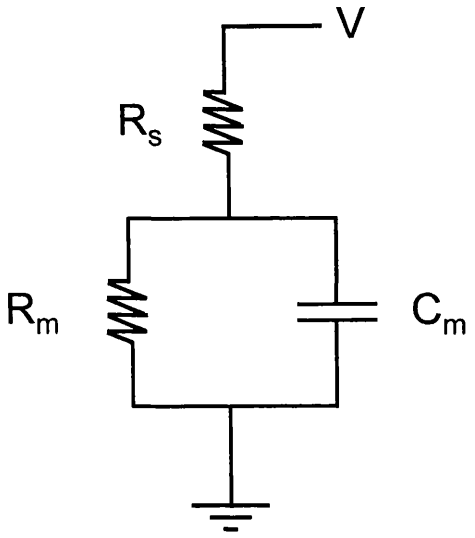

B

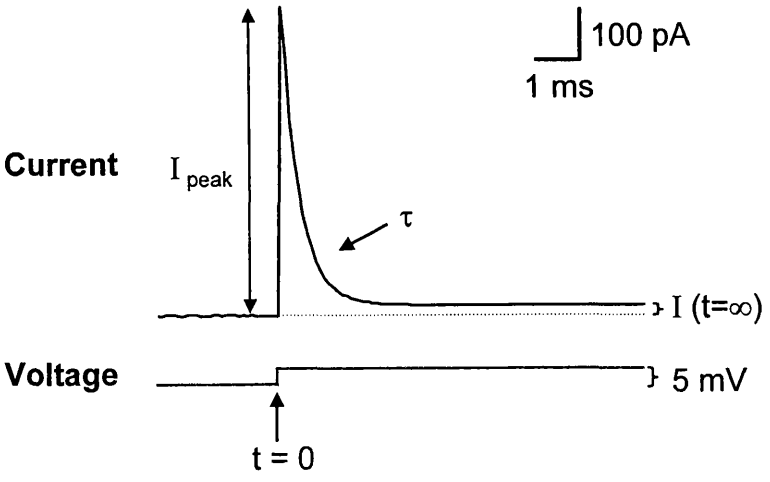

Substituting R_s from equation 2.3 gives:

$$R_m = V_s \cdot \frac{I(t=0) - I(t=\infty)}{I(t=0) \cdot I(t=\infty)} \tag{2.5}$$

The membrane capacitance can be calculated by rearranging equation 2.2 to give:

$$C_m = \tau \cdot \frac{R_s + R_m}{R_s \cdot R_m} \tag{2.6}$$

Substituting R_s from equation 2.3 and R_m from equation 2.5 gives:

$$C_m = \tau \cdot \frac{I(t=0)^2}{V_s \cdot \left(I(t=0) - I(t=\infty)\right)} \tag{2.7}$$

The time constant, τ, was obtained by fitting the current transient with a single exponential using Clampfit.

2.7 Diffusion of substances from the pipette into the cell

During whole-cell patch-clamping the intracellular ion composition is controlled by the pipette solution. The time needed for a substance to diffuse into the cell from the patch-pipette can be estimated as follows. The diffusive flux, J, of a substance along the x axis (from the pipette into the cell) is given by:

$$J = -D \cdot A \cdot \frac{dC}{dx} \tag{2.8}$$

where D is the diffusion coefficient of the substance, A is the area available for diffusion, C is the concentration of the substance at point x and dC/dx is the concentration gradient of C in the x direction. Assuming the end of the pipette to be an idealised barrier of width w and area A, equation 2.8 becomes:

$$J = D \cdot A \cdot \frac{C_{pipette} - C_{cell}}{w} \tag{2.9}$$

with $C_{pipette}$ being the concentration of the substance in the pipette and C_{cell} being the concentration of the substance in the cell. For a cell of volume V_{cell}, the amount of substance in the cell is $V_{cell}.C_{cell}$. The diffusive flux, J, tends to increase the total amount of substance in the cell, so:

$$J = \frac{d(V_{cell} \cdot C_{cell})}{dt} \tag{2.10}$$

From equations 2.9 and 2.10, the rate of increase of the substance's concentration in the cell is given by:

$$\frac{d(V_{cell} \cdot C_{cell})}{dt} = D \cdot A \cdot \frac{C_{pipette} - C_{cell}}{w} \tag{2.11}$$

The pipette series resistance across the barrier is:

$$R_s = \frac{\rho \cdot w}{A} \tag{2.12}$$

where ρ is the resistivity of the pipette solution. Putting equation (2.12) into equation (2.11) gives:

$$V_{cell} \cdot \frac{dC_{cell}}{dt} = \frac{D \cdot \rho}{R_s} \cdot (C_{pipette} - C_{cell}) \tag{2.13}$$

or, since $C_{pipette}$ is constant:

$$\frac{d(C_{cell} - C_{pipette})}{dt} = -\frac{D \cdot \rho}{V_{cell} \cdot R_s} \cdot (C_{cell} - C_{pipette}) \tag{2.14}$$

Rearranging and integrating, this gives:

$$\int_0^t \frac{1}{(C_{cell} - C_{pipette})} \cdot d(C_{cell} - C_{pipette}) = -\frac{D \cdot \rho}{V_{cell} \cdot R_s} \cdot \int_0^t dt \tag{2.15}$$

which gives:

$$\log_e\left(\frac{(C_{cell} - C_{pipette})_t}{(C_{cell} - C_{pipette})_0}\right) = -\frac{D \cdot \rho}{V_{cell} \cdot R_s} \cdot (t - 0) \tag{2.16}$$

this gives:

$$\frac{(C_{cell} - C_{pipette})_t}{(C_{cell} - C_{pipette})_0} = e^{-\frac{D \cdot \rho}{V_{cell} \cdot R_s} \cdot t} \quad (2.17)$$

If $C_{cell} = 0$ at $t = 0$, rearranging gives:

$$(C_{cell} - C_{pipette})_t = - C_{pipette} \cdot e^{-\frac{D \cdot \rho}{V_{cell} \cdot R_s} \cdot t} \quad (2.18)$$

Thus, the concentration of the substance in the cell, C_{cell}, approaches the concentration of the substance in the pipette, $C_{pipette}$, exponentially:

$$C_{cell}(t) = C_{pipette} \cdot \left(1 - e^{-t/\tau}\right) \quad (2.19)$$

with a time constant of:

$$\tau = \frac{V_{cell} \cdot R_s}{D \cdot \rho} \quad (2.20)$$

For a typical cell of diameter 10 μM and a volume 523 μm^3, a series resistance of 5 MΩ, a diffusion coefficient of 10^{-9} m^2s^{-1} (typical for small cations like Na^+, K^+ and Cl^-) and a resistivity of 0.1 Ωm, this predicts a time constant for equilibration of small ion in the cell of ~ 26 seconds. In Chapter 3 I use equation (2.20) to estimate the time constant for equilibration of small peptides into bipolar cells as ~ 248 seconds.

2.8 Protocols and data analysis

Having given an overview of the main methods used, the following sections give some methodological details specific to each results chapter.

2.8.1 Chapter 3 - $GABA_C$ currents in retinal bipolar cells

$GABA_C$ receptor mediated currents were investigated by whole-cell patch-

clamping either isolated retinal bipolar cells or bipolar cells in retinal slices. The recordings were restricted to ON bipolar cells, mainly rod bipolar cells (about 80%) and in some cases the morphologically similar cone bipolar cells type 8 or 9 (about 20%). The different types of bipolar cells were identified by their morphology (filled with Lucifer Yellow) and location in the retinal slice (see Chapters 1, 3 and 4 for classification and identification of bipolar cells). Cells were selected which had a soma in the inner nuclear layer (INL) closely apposed to the outer plexiform layer (OPL), with dendrites in the OPL and an axon heading down to the ON lamina of the inner plexiform layer (IPL), i.e. terminating in the part of the IPL closest to the ganglion cells.

To obtain GABA dose-response curves, different concentrations of GABA were bath applied and analysed as described in Chapter 3. $GABA_C$ receptor mediated currents were recorded in the presence of 300 μM bicuculline, a concentration which should be sufficient to block $GABA_A$ receptors even at the highest concentration of GABA used in these experiments (see section 3.6). To block synaptic transmission in the retinal slice calcium chloride in the superfusate was replaced by 4 mM $CoCl_2$, which blocks voltage-gated calcium channels. The intracellular solution was potassium based (Table 2.5 solution A) and included either a peptide designed to disrupt the interactions between $GABA_C$ receptors and the cytoskeletal protein MAP-1B, or a control peptide (see section 3.5). The peptides were synthesised by Altabioscience and stored as a 50 mg/ml stock (in DMSO) at $-20^{O}C$. They were diluted into the intracellular solution on the day of the experiments and used at a final concentration of 100 μM. In some cases the peptidase inhibitors leupeptin, bestatin and pepstatin (Table 2.5 solution A) were included in the pipette to prevent peptide breakdown, but no difference in the results was observed.

The open tip resistance of the pipettes measured with the pipette in the bath was 5-7 MΩ (filled with solution C or D in table 2.1, or solution A in table 2.5). The cells were whole-cell voltage-clamped at –60 mV. All through the experiment, -5

mV pulses were given to monitor the series resistance and the membrane properties of the cell. The membrane capacitance was usually ~5 pF, the membrane resistance of the cell was ~ 1 GΩ and the series resistance was ~25 MΩ. A series resistance of R_s = 25 MΩ will induce a voltage error of V_s <2.5 mV for a typical current of I <100 pA ($V_s = R_s.I$), which was were not corrected for. Series resistance compensation was not used. All experiments for this project were done at room temperature and in the light.

GABA evoked current amplitudes were measured by hand directly from the chart recorder trace.

2.8.2 Chapter 4 – Control of $[Cl^-]_i$ in retinal bipolar cells

GABA receptor mediated currents were investigated by perforated patch-clamping bipolar cells using gramicidin, in retinal slices of P35 day old rats. As for the experiments in Chapter 3, the recordings were restricted to ON bipolar cells, mainly rod bipolar cells and in some cases cone bipolar cells type 8 or 9. Cells were selected that had a soma in the INL closely apposed to the OPL, with dendrites in the OPL and an axon heading down to the IPL. Further identification was provided by checking that the cell responded when GABA was puffed onto the ON lamina of the IPL (closest to the ganglion cells) but not when it was puffed onto the OFF lamina (closest to the INL). When possible, the identity of the cell was confirmed by filling the cell with Lucifer Yellow from the patch pipette (in whole-cell mode) after the experiment was completed in perforated patch mode (as described in chapter 4).

To obtain GABA responses, 100 μM GABA was pressure applied (puffed) from a pipette controlled by a PicoSpritzer (PMI-100 pressure micro injector, Cornerstone, Dagan). The extracellular solution (bubbled with 100% oxygen) was HEPES buffered - this allowed me to convert the measured reversal potentials directly into values of intracellular chloride, without the complication of correcting for the permeability of GABA-gated channels to bicarbonate. The intracellular

solution (Table 2.5 solution B) was potassium based, to provide physiological conditions and normal operation of the K^+-dependent Cl^- transporter KCC2, and contained 0.2% Lucifer yellow to allow cell identification after the experiment was completed, and 64 μg/ml gramicidin D (Sigma, #5002). Every few days a 8 mg/ml gramicidin stock solution was prepared in DMSO, vortexed (~2 minutes), sonicated (~10 seconds) and stored in the fridge. On the day of the experiment some of this stock was diluted into intracellular solution (Table 2.5 solution B) to a final concentration of 64 μg/ml and vortexed for several minutes (giving a residual 0.8% DMSO in the pipette).

The open tip resistance of the pipettes in solutions B or C of table 2.2 was 5-7 MΩ. After forming a seal on the cell membrane, I waited ≥30 minutes for the gramicidin to make sufficient pores in the membrane to lower the series resistance to below 100 MΩ (range 30-100 MΩ, generally around 50 MΩ). A series resistance of R_s = 100 MΩ will induce a voltage error of V_s <5 mV for a typical current of I <50 pA ($V_s = R_s.I$; note that currents in this study were less than in that of chapter 3 because most of the current is generated by the applied GABA, which was locally applied here, but was applied for the whole cell for the experiments of chapter 3). For each cell this voltage error was calculated and subtracted from the apparent reversal potential of the GABA evoked current to obtain the true reversal potential. The junction potential between the electrode and the external solution before the seal was made on a cell was measured as –2 mV (as described by Fenwick et al., 1982). All membrane potentials were corrected for this, assuming that, in perforated patch mode, after cations had equilibrated across the pores formed by gramicidin in the membrane, there was no junction potential between the electrode and the inside of the cell.

The cells were normally voltage clamped at –40 mV. During the course of an experiment -5mV pulses were given from time to time to monitor changes in series resistance and the membrane properties of the cell. The membrane capacitance was

usually ~5 pF, the membrane resistance of the cell was ~1 GΩ and the series resistance was ~50 MΩ. Series resistance compensation was not used, but the resulting voltage error was corrected for as just described. All experiments for this project were done at 25-28 ^{O}C and in the light.

GABA evoked current amplitudes recorded at constant potential were measured by hand directly from the chart recorder trace. Currents during voltage ramps were analysed using Clampfit 8.

2.8.3 Chapter 5 – Interaction of the protein Ajuba with the glutamate transporter GLT-1

COS cells were cultured and injected with DNA as described in section 2.1.2. Usually four dishes of cells were prepared – two containing cells expressing GLT-1 and GFP only, and two containing cells expressing GLT-1, Ajuba and GFP. The cells were transferred from the incubator into the electrophysiological set-up 18-24 hours after the injection. Once in the recording chamber, the cultured COS cells were perfused with oxygenated (100% O_2) solution (Table 2.3 solution A). Cells successfully expressing the injected DNA were identified by their GFP fluorescence (see section 2.2). Experiments were performed on both sets of dishes, alternating between them, on the same day. Unless specifically mentioned, the cells were whole-cell voltage clamped at –60 mV, and glutamate transporter currents evoked by bath applied glutamate were recorded at room temperature. The intracellular solution was potassium based to provide the internal K^+ needed for glutamate transporter operation (table 2.5; Barbour et al., 1988).

During the course of an experiment –5 mV pulses were given from time to time to monitor changes in series resistance and the membrane properties of the cell. The membrane capacitance of COS cells was usually around 80 pF, the membrane resistance was ~150 MΩ and the series resistance was ~5 MΩ. A series resistance of R_s = 5 MΩ will induce a voltage error of V_s <2 mV for a typical current of I <400 pA

($V_s = R_s.I$), which was not corrected for.

For the experiments in section 5.9 the cells were perforated patch-clamped at –60 mV. Every couple of days a 30 mg/ml Amphotericin B stock solution was prepared in DMSO, vortexed, sonicated and stored in the fridge. Just before the experiments some of the stock was diluted into the intracellular solution (Table 2.5 solution C), vortexed (about 1 minute) and sonicated (10-20 s), producing a final concentration of 200 μg/ml (with a residual 0.7% DMSO in the pipette). Amphotericin B was used as the perforating agent, because it forms relatively large holes in the membrane (and thus allows a good electrical access) but does not permit large molecules or proteins (such as Ajuba) to leave the cell.

The open tip resistance of the pipettes filled with solution C of table 2.5 and immersed in solution A of table 2.3 was around 2 MΩ. After forming a seal on the cell membrane, I waited around 10-15 minutes for the Amphotericin B to make sufficient pores in the membrane to lower the series resistance to around 20 MΩ. A series resistance of $R_s = 20$ MΩ will induce a voltage error of $V_s < 2$ mV for a typical current of I <100 pA ($V_s = R_s.I$). This voltage error was not corrected for. Series resistance compensation was only used in the experiments described in section 6.4. All experiments were performed at room temperature.

Transporter mediated currents were analysed by measuring the amplitude on the chart recorder print out.

2.8.4 Chapter 6 & 7 – Study of synaptic transmission in the cerebellum

Synaptic transmission in the cerebellum was studied at the mossy-fibre – granule cell synapse (in rat at postnatal day 14 (P14), and in mice lacking GLAST transporters at P28-30, or lacking GLT-1 transporters at P12-15), and at the parallel-fibre – Purkinje cell synapse (in mice lacking GLAST transporters at P16-20). Experiments were at room temperature or at 37°C (as indicated in the text of

Chapters 6 and 7). Synaptic transmission was evoked by electrical stimulation using a Ringer's-filled glass pipette placed in the granule cell layer (to stimulate the mossy-fibres) or in the molecular layer (to stimulate the parallel fibres). Unless specifically mentioned, granule cells were voltage clamped at –60 mV and Purkinje cells at –70 mV. A brief (20-100 μs) voltage pulse, or trains of stimuli (10 stimuli at 100 Hz for granule cells; 10, 20 or 50 stimuli at 200 Hz for Purkinje cells) were delivered via the stimulation electrode and the resulting current response was recorded. For each holding potential, stimuli were applied 10-60 times, at intervals of 10 seconds (0.1 Hz; granule cells) or either 25 or 60 seconds (0.04 or 0.017 Hz; Purkinje cells). Currents were sampled at 20-50 kHz and low pass filtered at 10 kHz.

The extracellular solution (Table 2.4) was continuously bubbled with 95% O_2 / 5% CO_2 gas. All experiments on granule cells (Chapter 6 and 7) were performed in the presence of 20 μM bicuculline, to inhibit $GABA_A$ receptor mediated currents which occur frequently due to spontaneous Golgi cell activity and GABA release. For the experiments in Chapter 6, the extracellular solution contained 10 μM glycine, a necessary co-agonist of the NMDA receptor. For the experiments in Chapter 7, 5 μM strychnine was added to the solution to block glycine receptors. The experiments on Purkinje cells (Chapter 6) were done in the presence of 10 μM gabazine (SR95531), to block $GABA_A$ receptors. When drugs were used in an experiment, they were applied for at least 2 minutes before recording took place to allow enough time for the solutions to be exchanged within the slice. To allow a good voltage clamp, the pipette solution was cesium based (to block voltage-gated potassium currents) and contained QX314 (to block voltage-gated sodium currents). In most cases 0.2% di-potassium Lucifer Yellow was included in the pipette solution to allow visual identification of the cells.

The open tip resistance of the pipettes (filled with solution from table 2.5 and immersed in extracellular solution from table 2.4) was 5-7 MΩ for granule cells and 2-4 MΩ for Purkinje cells. Throughout the course of an experiment, changes in series

resistance and membrane properties were monitored by application of brief hyperpolarizing voltage steps (-5 mV) delivered prior to each synaptic stimulus. The series resistance was usually around ~20 MΩ for granule cells and ~ 8 MΩ for Purkinje cells. A series resistance of R_s = 20 MΩ will induce a voltage error of V_s < 2 mV for a typical current of I <100 pA ($V_s = R_s.I$) in granule cells, and this was not corrected for. Series resistance compensation was only used for Purkinje cell experiments (Chapter 6).

For analysis of EPSCs, EPSCs recorded at the same holding potential were averaged. The averaged EPSC was then analysed for its peak amplitude, the amplitude after 20 ms (to provide an estimate of the NMDA receptor mediated component of the EPSC), and the total charge transfer (area underneath the curve) using Clampfit 8.

2.9 Statistics

All values are presented as mean ± s.e.m.. Significance tests were carried out using 2-tailed Student's t-tests (paired or unpaired as appropriate).

Table 2.1: Extracellular solutions for chapter 3

Extracellular solutions used in experiments on the interaction of $GABA_C$ receptors with MAP-1B.

A = mammalian dissociation medium

B = slice and incubation medium

C = recording solution (calcium)

D = recording solution (cobalt)

All concentrations in mM

	A	B	C	D
NaCl	101	130	130	130
KCl	3.7	2.5	2.5	2.5
$MgCl_2$		2	2	2
$CaCl_2$		2	2	
$CoCl_2$				4
HEPES		10	10	10
Glucose	15	10	10	10
Na-pyruvate	1			
D,L-cysteine HCl	10			
$NaHCO_3$	25			
NaH_2PO_4	10			
pH with NaOH		7.4	7.4	7.4
Bicuculline			0.3	0.3

Table 2.2: Extracellular solutions for chapter 4

Extracellular solutions used in experiments on $[Cl^-]_i$ in bipolar cells.

A = slice and incubation solution

B = recording solution

C = recording solution, high potassium

All concentrations in mM

	A	B	C
NaCl	135	135	135
KCl	2.5	2.5	6
$MgCl_2$	3	4	4
$CaCl_2$	1		
HEPES	10	10	10
NaH_2PO_4	1	1	1
Glucose	10	10	10
Na_2EGTA		5	5
pH with NaOH	7.4	7.4	7.4
NBQX		0.02	0.02
AP-5		0.05	0.05
[Chloride]	145.5	145.5	149

Table 2.3: Extracellular solutions for chapter 5

Extracellular solutions used in COS cell experiments on the interaction of Ajuba with GLT-1.

A = recording solution (chloride)

B = recording solution (nitrate)

C = recording solution (kainate)

All concentrations in mM

	A	B	C
NaCl	140		140
$NaNO_3$		140	
KCl	2.5	2.5	2.5
$MgCl_2$	2	2	2
$CaCl_2$	2.5	2.5	2.5
HEPES	10	10	10
Glucose	10	10	10
NaH_2PO_4	1	1	1
Kainate			0.3
pH with NaOH	7.4	7.4	7.4

Table 2.4: Extracellular solutions for chapters 6 & 7

Extracellular solutions used in experiments on cerebellar synaptic transmission.

A = slicing medium

B = incubation medium

C = recording solution (granule cells; Chapter 6)

D = magnesium-free recording solution (granule cells; Chapter 6)

E = recording solution (granule cells; Chapter 7)

F = recording solution (Purkinje cells; Chapter 6)

All concentrations in mM

	A	B	C	D	E	F
NaCl		120	120	120	120	124
KCl	2.5	2.5	2.5	2.5	2.5	2.5
$NaHCO_3$	26	26	26	26	26	26
NaH_2PO_4	1	1	1	1	1	1
$CaCl_2$	0.1	0.1	2.5	2.5	2.5	3
$MgCl_2$	4	4	1.2			1
Glucose	10	10	10	10	10	10
Sucrose	240					
pH with 5% CO_2	7.4	7.4	7.4	7.4	7.4	7.4
Strychnine					0.005	
Glycine			0.01	0.01		
Bicuculline			0.02	0.02	0.02	
Gabazine						0.01

Table 2.5: Intracellular solutions

A = Chapter 3 - retinal bipolar cell $GABA_C$ – MAP-1B interaction

B = Chapter 4 - retinal bipolar cells $[Cl^-]_i$ experiments

C = Chapter 5 – Ajuba – GLT-1 interaction (COS cells)

D = Chapter 6 – synaptic transmission to Purkinje cells

E = Chapter 6 & 7 – synaptic transmission to granule cells

All concentrations in mM

	A	B	C	D	E
KCl	135	135	140		
CsCl					125
Cs-gluconate				140	
$MgCl_2$	2	2	2		4.6
$CaCl_2$	0.5	0.5	0.5	0.1	0.5
Na_2EGTA	5	5	5	0.5	5
HEPES	10	10	10	10	10
Mg-ATP	2	2	1	4	4
Na_2-GTP				0.5	0.4
QX-314					10
Bestatin	0.01				
Leupeptin	0.1				
Pepstatin	0.001				
pH with KOH	7.2	7.2	7.1		
pH with CsOH				7.3	7.2
Lucifer Yellow	0.2 %	0.2%			0.2%

CHAPTER 3

Modulation of $GABA_C$ receptor sensitivity by MAP-1B

3.1. Introduction

As described in chapter 1, $GABA_C$ receptors contribute importantly to the light response of retinal bipolar cells, and thus to early visual processing (see also section 3.17.4 and 4.1). The aim of the experiments described in this chapter was to find out whether the microtubule-associated-protein MAP-1B or the glycine transporter GLYT-1E/F influence $GABA_C$ receptor properties.

Yeast-two hybrid screening revealed MAP-1B (see section 1.7.1) as a binding partner for the $GABA_C$ receptor ρ_1 subunit (Hanley et al., 1999). Subsequently, using pull down assays, MAP-1B was shown to interact with both the ρ_1 and ρ_2 subunits of the $GABA_C$ receptor, but not with the $GABA_A$ receptor subunits α_1, β_3 and γ_2 (Billups et al., 2000). Antibody staining showed that MAP-1B co-localizes with $GABA_C$ receptors both when co-expressed in cultured COS cells, and in retinal bipolar cells, which express $GABA_C$ receptors endogenously, especially on their axon terminals (Hanley et al., 1999). Because of its ability to bind to microtubules, actin and the ρ subunit simultaneously, MAP-1B was proposed to anchor $GABA_C$ receptors to the cytoskeleton (Hanley et al., 1999; Moss and Smart, 2001). However, as has been shown for other receptor-interacting proteins (see section 1.7.1 and section 3.17.2), MAP-1B could additionally modulate the $GABA_C$ receptor's kinetic properties (altering, for example, the EC_{50} for activation by GABA, or the maximum open probability).

The glycine transporter GLYT-1E/F has also been shown to interact with the $GABA_C$ receptor subunit ρ_1 (Hanley et al., 2000), but the function of this interaction

is unclear. The transporter and MAP-1B might bind to the same site on ρ_1, and competition for this binding site might influence the cells' response to GABA or glycine uptake. Alternatively, it is possible that the glycine transporter and MAP-1B bind to separate sites on ρ_1, possibly simultaneously. Binding of the glycine transporter to ρ_1 might influence $GABA_C$ receptor kinetic properties, or alternatively $GABA_C$ receptor activation might influence glycine transporter function.

This work was done in collaboration with Jonathan Hanley, who did all of the molecular biological work, which is described briefly to provide the background to the electrophysiological work that I did.

3.2. Identification of the MAP-1B binding site on ρ_1

$GABA_C$ receptors are composed of ρ subunits and are thought to work as pentamers (see section 1.4). Each $GABA_C$ receptor subunit transverses the membrane four times and has a large intracellular amino acid loop (E^{355}-R^{454}) joining the 3rd and 4th transmembrane domains (TM3 and TM4) (Figure 3.1). Previous work (Hanley et al., 1999) has shown that MAP-1B binds to the C-terminal quarter of this intracellular loop (S^{434}-R^{454}).

My electrophysiological experiments depended on knowing the exact sequence of the binding site for MAP-1B on the ρ_1 subunit. To narrow down the location of the binding site, my collaborator Jon Hanley constructed three different GST fusion proteins containing different stretches of the TM3-TM4 intracellular loop (Figure 3.2 A, B). One construct included the C-terminal end of the loop (GST-402-R^{454}), which has been shown previously to bind to MAP-1B like the full-loop (E^{355}-R^{454}) (Hanley et al., 1999), as shown in Figure 3.4. The other two constructs contained the full-loop of ρ_1 with either the last 5 (GST-E^{355}-I^{449}) or the last 10 (GST-E^{355}-I^{444}) amino acids at the C-terminal end missing. Beads, to which these fusion proteins were attached, were used to pull down MAP-1B from rat retinal extracts (Figure 3.2 B), and binding was tested by Western blotting and probing with

Figure 3.1: Schematic drawing of a $GABA_C$ receptor subunit

Each $GABA_C$ receptor subunit is thought to have a long extracellular N-terminus, four α-helices transversing the membrane, a large intracellular loop joining the 3rd and 4th transmembrane spanning segments (TM3-TM4) and a short extracellular C-terminus. MAP-1B has been shown to bind to the last quarter of the large intracellular loop (amino acids 434-454)(Hanley et al., 1999). The stretch indicated in red indicates the last 10 amino acids of this loop (not to scale), which were investigated in the pull-down assays described in Section 3.2.

$GABA_C$ receptor subunit

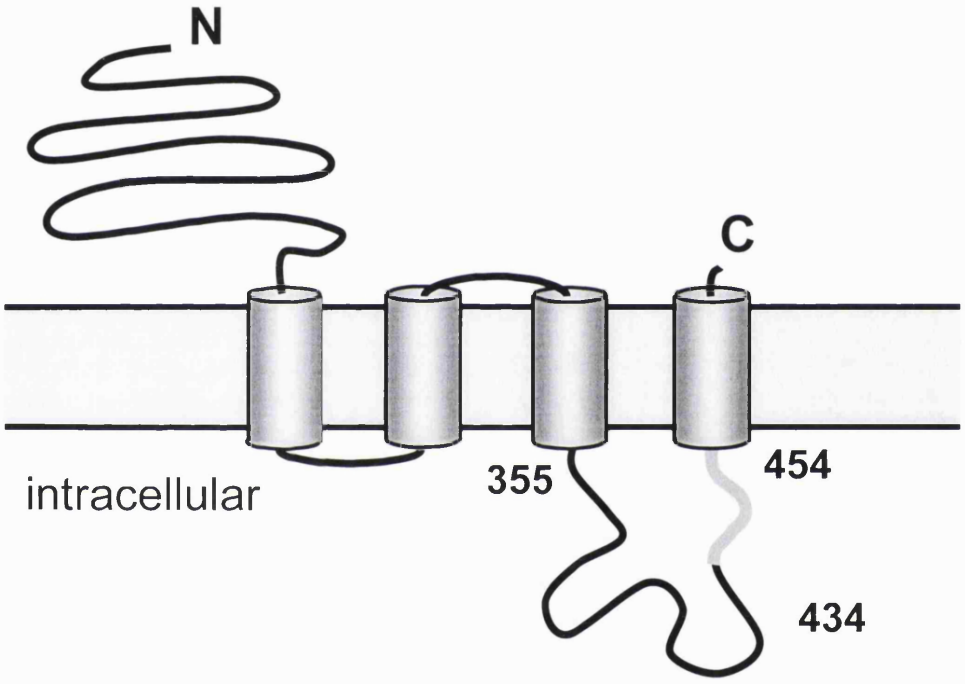

Figure 3.2: MAP-1B binds to the extreme C-terminus of the ρ_1 TM3-TM4 intracellular loop

(A) Sequence of GST fusions with the C-terminal half of the ρ_1 intracellular loop ($\rho_1^{402-454}$), and with a ten amino acid truncation ($\rho_1^{355-444}$), and a five amino acid truncation ($\rho_1^{355-449}$) of the whole loop. **(B)** Cartoon illustrating the pull-down assay performed in C. Parts of the TM3-TM4 loop are fused to GST (giving GST-ρ_1), which is then attached to beads and used to pull down proteins from retinal extracts. MAP-1B binding was detected by Western blotting. **(C) Upper gel**: binding of MAP-1B to the ten amino acid truncation fusion protein (lane 3), compared with binding to the C-terminal half of the intracellular loop $\rho_1^{402-454}$ (lane 4). Lane 2 shows lack of binding to GST and lane 1 shows the input to the assay ("in" represents the MAP-1B present in 1% of the input). **Lower gel**: Same as in the upper gel, but for the 5 amino acid truncation fusion protein

This work was carried out by my collaborator Jonathan Hanley.

A

GST-402 —— VSMRIDTHAIDKYSR[454]

GST-355 —— VSMRI[444]

GST-355 —— VSMRIDTHAI[449]

B

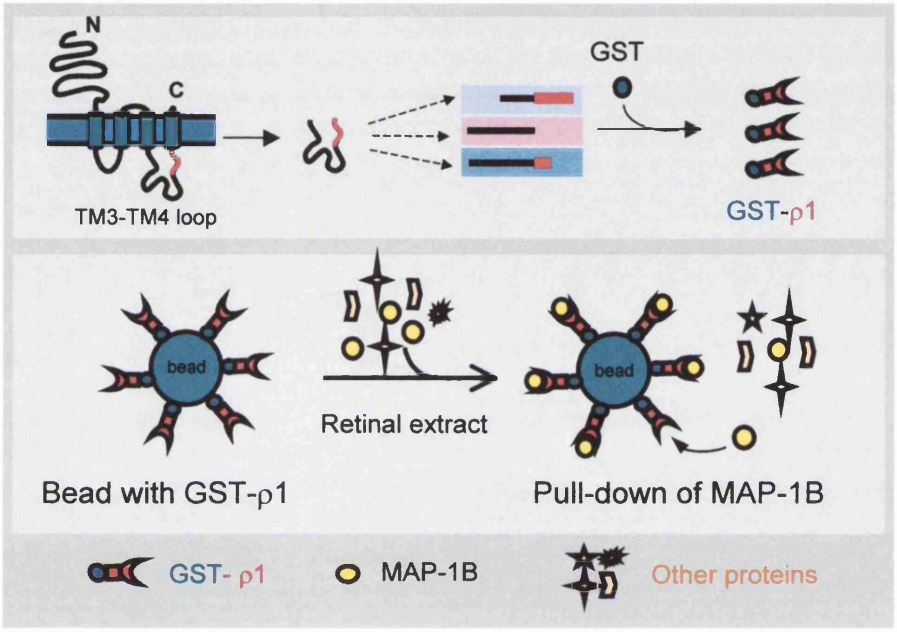

C

antibodies against MAP-1B (Figure 3.2 C). As a control it was confirmed that the beads containing GST alone (GST) did not bind MAP-1B (Figure 3.2 C, upper and lower gel, lanes 2). The construct including the C-terminal end of the loop (GST-402-R^{454}) pulled down MAP-1B (Figure 3.2 C, upper and lower gel, lanes 4), whereas the construct with the 10 amino acid truncation (GST-E^{355}-I^{444}) showed no binding (Figure 3.2 C, upper gel, lane 3), and the one with the 5 amino acid truncation (GST-E^{355}-I^{449}) only very weak binding (Figure 3.2 C, lower gel, lane 3). These data indicate that the last 10 amino acids (D^{445}-R^{454}) of the intracellular loop of ρ_1 are necessary for binding of MAP-1B, with residues within the last 5 amino acids (D^{450}-R^{454}) playing a particularly important role.

To investigate the importance for binding MAP-1B of specific amino acids within this C-terminal end of the intracellular loop, Jon Hanley carried out site-directed mutagenesis. Mutations were made in groups of three to the corresponding amino acids of the $GABA_A$ receptor α_1 subunit (Figure 3.3 A), which has been shown not to interact with MAP-1B, and COS cells were used to express the mutated full-length *myc*-tagged ρ_1. Beads with GST-MAP-1B attached (GST fused to the part of MAP-1B which binds ρ_1, i.e. amino acids 460-585) were used to pull down the mutated ρ_1 from lysates of transfected COS cells (Figure 3.3 B). Binding was determined by Western blotting and probing with a *myc* antibody (Figure 3.3 C). The most C-terminal mutation (KY–RL) prevented binding of ρ_1^{myc} (Figure 3.3 C, lane 11), indicating that these amino acids play a crucial role for the interaction between MAP-1B and ρ_1. The more N-terminal mutations (THA–VSK and RID–FNS, Figure 3.3 C, lane 9 and lane 7, respectively) reduced binding, indicating that they also play a part in the interaction. The most N-terminal mutation (VSM–KKT, Figure 3.3 C, lane 5) did not affect binding compared to the wild type (Figure 3.3 C, lane 3), indicating that those residues are outside the binding region. These data suggest that the MAP-1B binding site does not extend further N-terminally than R^{443}.

Figure 3.3: Identification of amino acid residues in the ρ_1 intracellular loop which are important for MAP-1B binding

Groups of residues in ρ_1 were mutated to the equivalent sequence of the α_1 subunit of $GABA_A$ receptors. **(A)** Alignment of the extreme C-terminal regions of the intracellular TM3-TM4 loop of the ρ_1 and α_1 subunits. The amino acid substitutions are shown in boxes; identical amino acids were not mutated. **(B)** Cartoon illustrating the pull-down assay performed in C. **(C)** Immobilized GST fusion proteins corresponding to the ρ_1-binding region of MAP-1B were incubated with extracts of COS cells transfected with mutants of full-length ρ_1^{myc}. Binding of ρ_1^{myc} mutants to GST-MAP-1B as determined by Western blotting probed with an antibody against *myc*. For each construct, "in" represents the ρ_1^{myc} present in 5% of the input, and "bd" represents protein bound to GST-MAP-1B; "GST" shows lack of binding of ρ_1^{myc} to GST alone.

This work was carried out by my collaborator Jonathan Hanley.

A


ρ1: VSM RID THA ID KY SR - (TM4)
α1: KKT FNS VSK ID RL SR - (TM4)

B

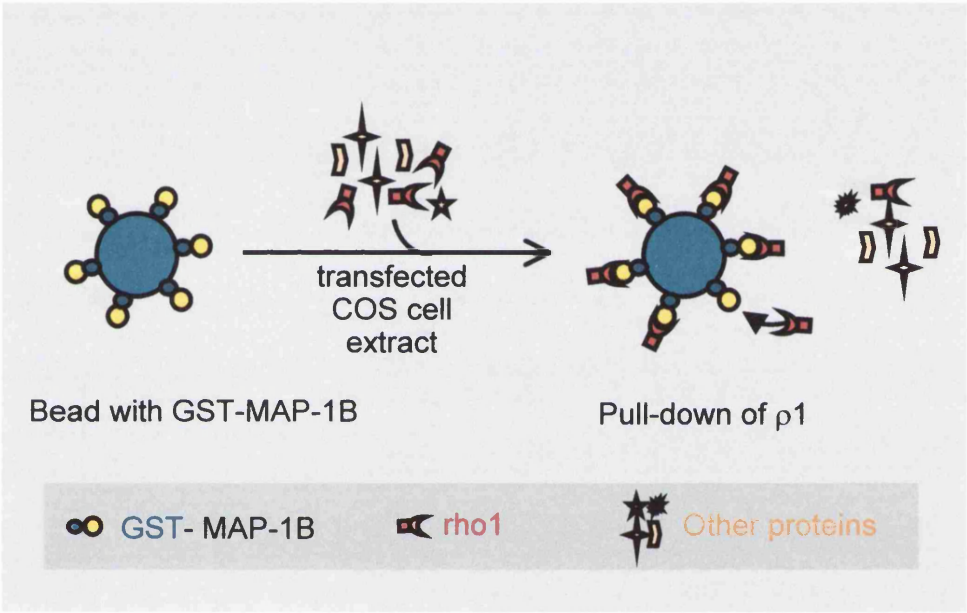
transfected
COS cell
extract
Bead with GST-MAP-1B
Pull-down of ρ1
GST- MAP-1B
rho1
Other proteins

C

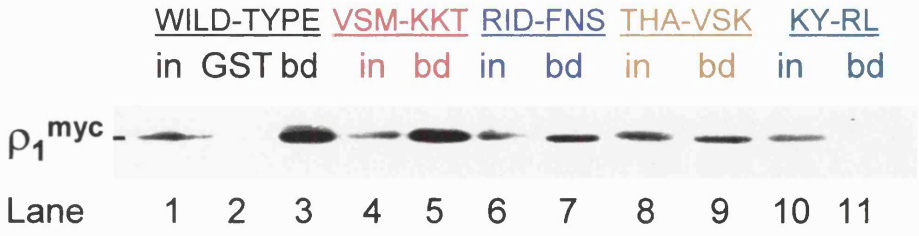
WILD-TYPE VSM-KKT RID-FNS THA-VSK KY-RL
in GST bd in bd in bd in bd in bd
ρ1myc
Lane 1 2 3 4 5 6 7 8 9 10 11

The above truncation and mutagenesis experiments suggest that MAP-1B binds to the last 12 amino acids of the ρ_1 intracellular loop joining TM3 and TM4 (R^{443}–R^{454}), with the last 5 amino acids, especially $K^{451}Y^{452}$, playing a crucial role.

3.3. Block of MAP-1B binding to ρ_1 by competition with a binding site peptide

Having identified the binding site for MAP-1B on ρ_1, the next step needed for my electrophysiological work was to show that peptides corresponding to this site could compete with ρ_1 for binding to MAP-1B, and thus disrupt the ρ_1 – MAP-1B interaction. Peptides containing the rat version of this sequence ("binding site peptide", RINTHAIDKYSR) were synthesized (the human sequence RIDTHAIDKYSR, as used in the experiments above, differs slightly from the rat sequence RINTHAIDKYSR, which was used in the following experiments since the peptide was ultimately to be used in electrophysiological recordings, which were performed on rat tissue). Pull-down assays were performed to see if the peptide competes with ρ_1 for binding to MAP-1B: beads to which GST-full-loop $\rho_1^{355–454}$ was attached, were used to pull down MAP-1B from retinal extracts in the presence of different concentrations (50 nM, 100 nM and 250 nM) of the binding-site peptide. As a control, the experiments were repeated in presence of a high concentration (250 nM) of peptide containing a scrambled version (HRTSKINIYRDA) of the binding site (Figure 3.4 A). The binding of MAP-1B to ρ_1 was determined by Western blotting and probing with a MAP-1B antibody. The binding-site peptide prevented binding of MAP-1B to ρ_1 in a dose-dependent manner (Figure 3.4 B, lanes 4, 5, 6), whereas even a high concentration of the scrambled control peptide did not interfere with binding (Figure 3.4 B, lane 3). This confirmed that the last 12 amino acids of the large intracellular loop are sufficient to bind MAP-1B, and allowed me to use the peptide in electrophysiological recordings to study the effect of MAP-1B binding on $GABA_C$ receptor properties.

Figure 3.4: Competitive inhibition of MAP-1B binding to ρ_1 by peptides

The binding site peptide containing the motif RINTHAIDKYSR competes with ρ_1 for binding to MAP-1B in retinal pull-down assays. **(A)** Cartoon illustrating the pull-down assay performed in B. Immobilized GST (small circles on bead) was incubated with retinal extract to control for unspecific binding (1st panel). GST-$\rho_1^{355-454}$ (small circles with cresent shape) was incubated with retinal extract, followed by a peptide. With a scrambled control peptide (containing the sequence X–HRTSKINIYRDA, where X was the antennapedia sequence RQIKIWFQNRRMKWKK, biotinylated at the N-terminus; X promotes peptide entry into cells, but this property was not used in the experiments reported here), MAP-1B binds to the ρ_1 bead as usual (2nd panel). With binding site peptides present (with sequence X–RINTHAIDKYSR) some MAP-1B binds to the peptide instead of the ρ_1 bead (3rd panel). With an excess of binding site peptide present (4th panel), no MAP-1B binds to the ρ_1 bead. **(B)** Results of the experiments. MAP-1B binding was assessed by Western blotting probed with a MAP-1B antibody. MAP-1B binds to the ρ_1 beads in the presence of the scrambled control peptide (250 nM, lane 3), but 50-250 nM of the binding site peptide progressively block the binding (lanes 4-6). "GST" shows no binding of MAP-1B to GST alone (lane 2), and "in" represents MAP-1B present in 1% of input (lane 1).

This work was carried out by my collaborator Jonathan Hanley.

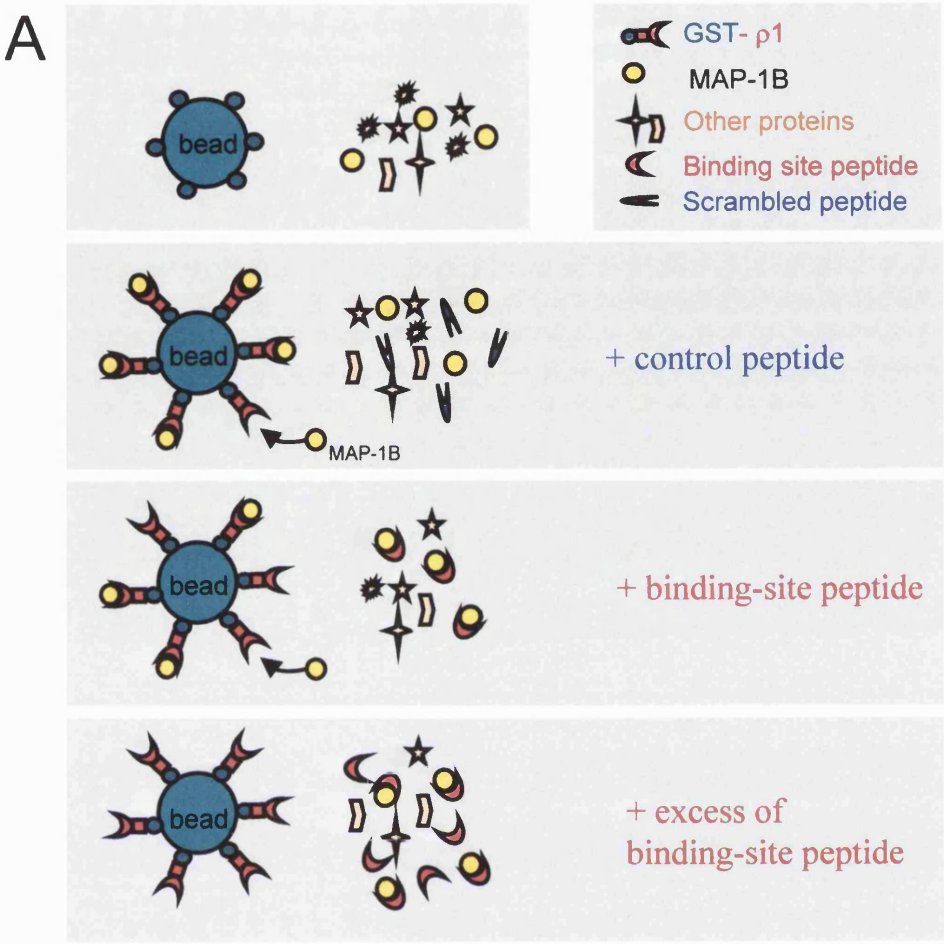
A
bead
GST- ρ1
MAP-1B
Other proteins
Binding site peptide
Scrambled peptide
bead
MAP-1B
+ control peptide
bead
+ binding-site peptide
bead
+ excess of
binding-site peptide

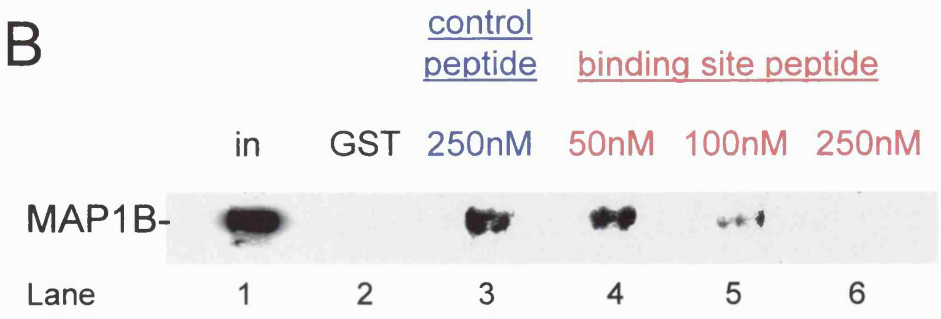
B
control
peptide
binding site peptide
in
GST
250nM
50nM
100nM
250nM
MAP1B-
Lane
1
2
3
4
5
6

3.4. $GABA_C$ receptors in bipolar cells

To investigate the properties of $GABA_C$ receptor mediated currents and their possible modulation by MAP-1B, I carried out electrophysiological recordings on rat retinal bipolar cells. These express $GABA_C$ receptors on their synaptic terminals, where they mediate feedback inhibition in the inner retina. The vast majority of my recordings were done on rod bipolar cells (RBC), both in retinal slices (see below) and isolated from the retina. Isolated RBCs can be easily identified by their morphology (Karschin and Wassle, 1990), comprising a relatively small soma (diameter around 7 μm), short dendritic branches and a long axon (around 40-80 μm long), which *in vivo* spans most of the inner plexiform layer, with a bulbous, unbranched axon terminal (Figure 3.5).

To confirm the presence of the $GABA_C$ receptor subunit ρ_1 on the type of bipolar cell that I recorded from, I performed antibody staining for ρ on isolated bipolar cells. As previously shown (Enz et al., 1996; Hanley et al., 1999), the antibodies labelled the axon terminal, axon, soma and dendrites of the bipolar cell (Figure 3.6 A). Omitting the primary antibody and incubating the cells only with the secondary antibody gave no labelling (Figure 3.6 B).

3.5. The electrophysiological experimental design

To determine whether the interaction of ρ_1 with MAP-1B affects the properties of $GABA_C$ receptors, I whole-cell patch-clamped the soma of rat retinal bipolar cells (Figure 3.7). Included in the patch-pipette, and thus dialyzed into the cell, was either the "binding site peptide" (containing ρ_1's MAP-1B binding sequence RINTHAIDKYSR, see above, section 3.3), or a "control peptide", containing a scrambled version of the binding site peptide, HRTSKINIYRDA. The aim, as in the *in vitro* experiments described in section 3.3 (Figure 3.4), was for the

Figure 3.5: Picture of a dissociated rod bipolar cell

Isolated rod bipolar cells are easily identified by their morphology: a medium sized soma, short dendritic branches and a long axon ending in a single, relatively large, bulbous axon terminal. The scale bar is 10 μm.

Dissociated Bipolar Cell

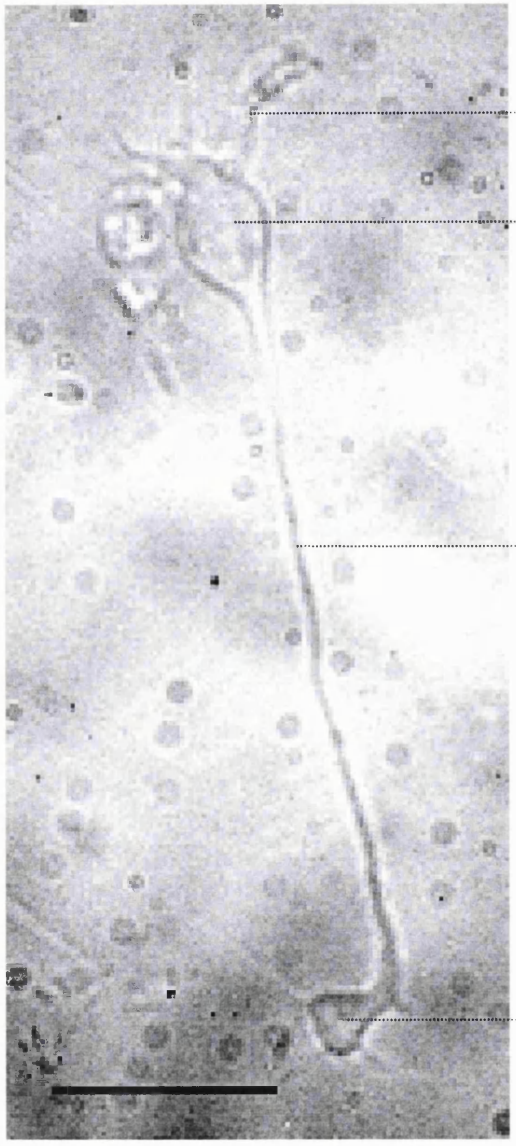

Figure 3.6: ρ_1 is present in rod retinal bipolar cells

Antibody labelling for the ρ_1 subunit in isolated rat rod bipolar cells. (A) Left panel: transmission light image of an isolated bipolar cell. Right panel: the antibody against ρ_1 reveals localization of the $GABA_C$ receptor subunit in rod bipolar cells in the axon terminal, the axon and soma of the cell. The primary antibody was raised in rabbit against the extracellular N-terminus of ρ_1. The secondary antibody was anti-rabbit with the fluorophore Texas-Red fused onto it. (B) As in A but omitting the primary antibody in the right panel. This negative control shows no staining.

A

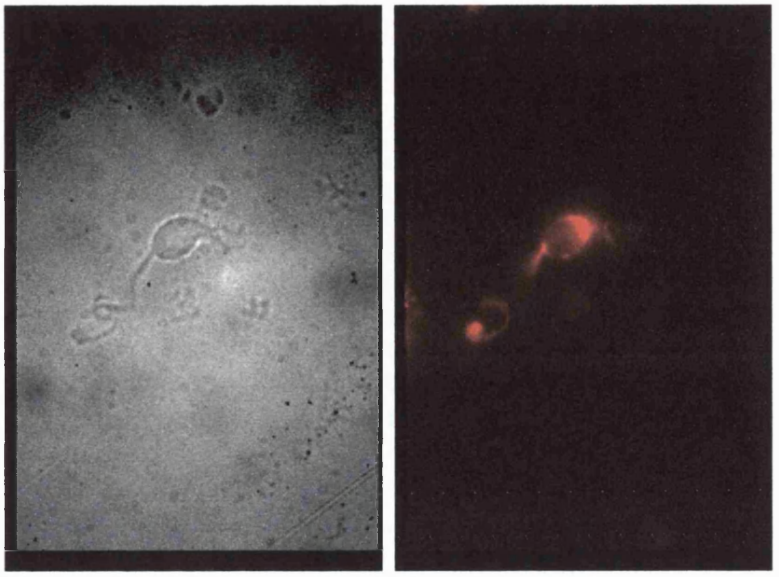

ρ1

B

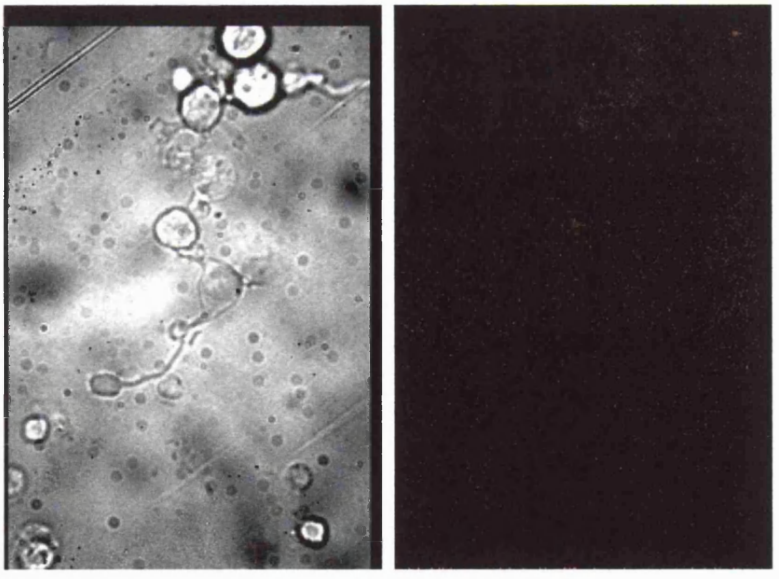

Omitting primary antibody

Figure 3.7: Experimental design for electrophysiological recordings

To investigate the effect of disrupting the ρ_1 – MAP-1B interaction on $GABA_C$ receptor mediated currents, the somata of bipolar cells in retinal slices were whole-cell patch-clamped, as shown in this cartoon. Included in the pipette solution, and thus dialyzed into the cell, was either the binding-site peptide (indicated in red) or a scrambled version of it. Whereas the scrambled control peptide (blue) does not compete with the $GABA_C$ receptor subunit for binding to MAP-1B (left side of inset), the binding-site peptide (red) competes with ρ_1 for binding MAP-1B (indicated in brown) and displaces MAP-1B from the $GABA_C$ receptor subunit (right site of inset). Possible changes of $GABA_C$ receptor properties (e.g. EC_{50} and I_{max}) were investigated by recording GABA dose-response curves for $GABA_C$ receptor mediated currents over a 30 minute recording period.

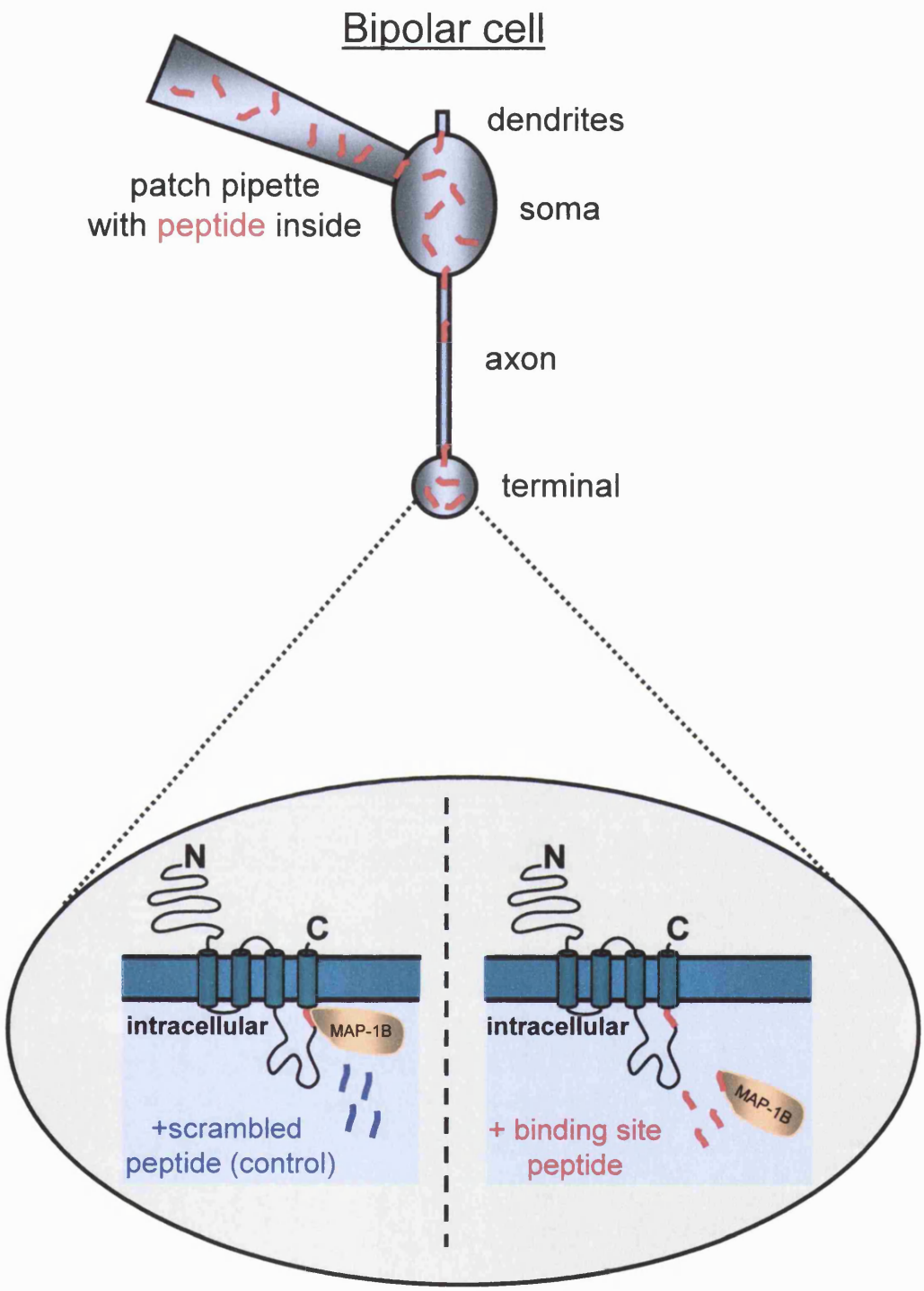
Bipolar cell
dendrites
patch pipette
with peptide inside
soma
axon
terminal
N
C
intracellular
MAP-1B
+scrambled
peptide (control)
N
C
intracellular
MAP-1B
+ binding site
peptide

binding –site peptide to compete with endogenous ρ_1 for binding to MAP-1B, and to thus displace MAP-1B from ρ_1. The scrambled peptide is not expected to do this, and serves as a control (Figure 3.7). The peptides were estimated to equilibrate throughout the cytoplasm with a time-constant of around 250 seconds (see section 3.8). Thus, to allow for the peptide to equilibrate inside the cell and disrupt the ρ_1 – MAP-1B interaction, the properties of $GABA_C$ receptor mediated currents needed to be observed over a period of time (up to 30 minutes seemed sufficient). Such a strategy has been used successfully by others to disrupt the interaction of endogenous proteins with AMPA receptors and with glutamate transporters (Nishimune et al., 1998; Marie and Attwell, 1999).

$GABA_C$ receptor mediated currents were activated by bath application of GABA, and recorded in the presence of bicuculline to block $GABA_A$ receptor mediated currents. The intra- and extracellular solutions contained equimolar chloride concentrations, resulting in a chloride reversal potential (from the Nernst equation) of around 0mV. Since the recordings described in this chapter were all done at –60 mV, GABA-evoked chloride currents are inward.

The aim of the experiments was to determine whether the ρ_1 – MAP-1B interaction altered either the EC_{50} of the $GABA_C$ receptors for GABA, or the maximum current they can generate at a saturating GABA concentration (I_{max}). Preliminary experiments therefore established that it was possible to isolate $GABA_C$ receptor currents, and defined the EC_{50} for GABA in control conditions with the ρ_1 – MAP-1B interaction functioning.

3.6. TPMPA blocks the bicuculline resistant GABA-evoked current in isolated bipolar cells

Initially I recorded GABA-evoked currents in dissociated bipolar cells (Figure 3.8 A). Application of GABA (10 μM) evoked inward currents, which were reduced by 20.7 ± 3.1 % (n=4) by the $GABA_A$ antagonist bicuculline (100 μM),

Figure 3.8: Isolated bipolar cells contain functional $GABA_A$ and $GABA_C$ receptors

(A) Specimen trace recorded from an isolated rod bipolar cell of a 35 day old rat. GABA evoked an inward current, which was partially blocked by 100 μM bicuculline (a $GABA_A$ receptor antagonist). The remaining current was abolished by 200 μM TPMPA (a $GABA_C$ receptor antagonist). These effects were reversible. The cell was voltage-clamped at –60 mV. **(B)** Averaged data from 4 isolated bipolar cells. The bicuculline resistant current (left bar) was blocked by TPMPA (right bar), revealing it as $GABA_C$ receptor mediated.

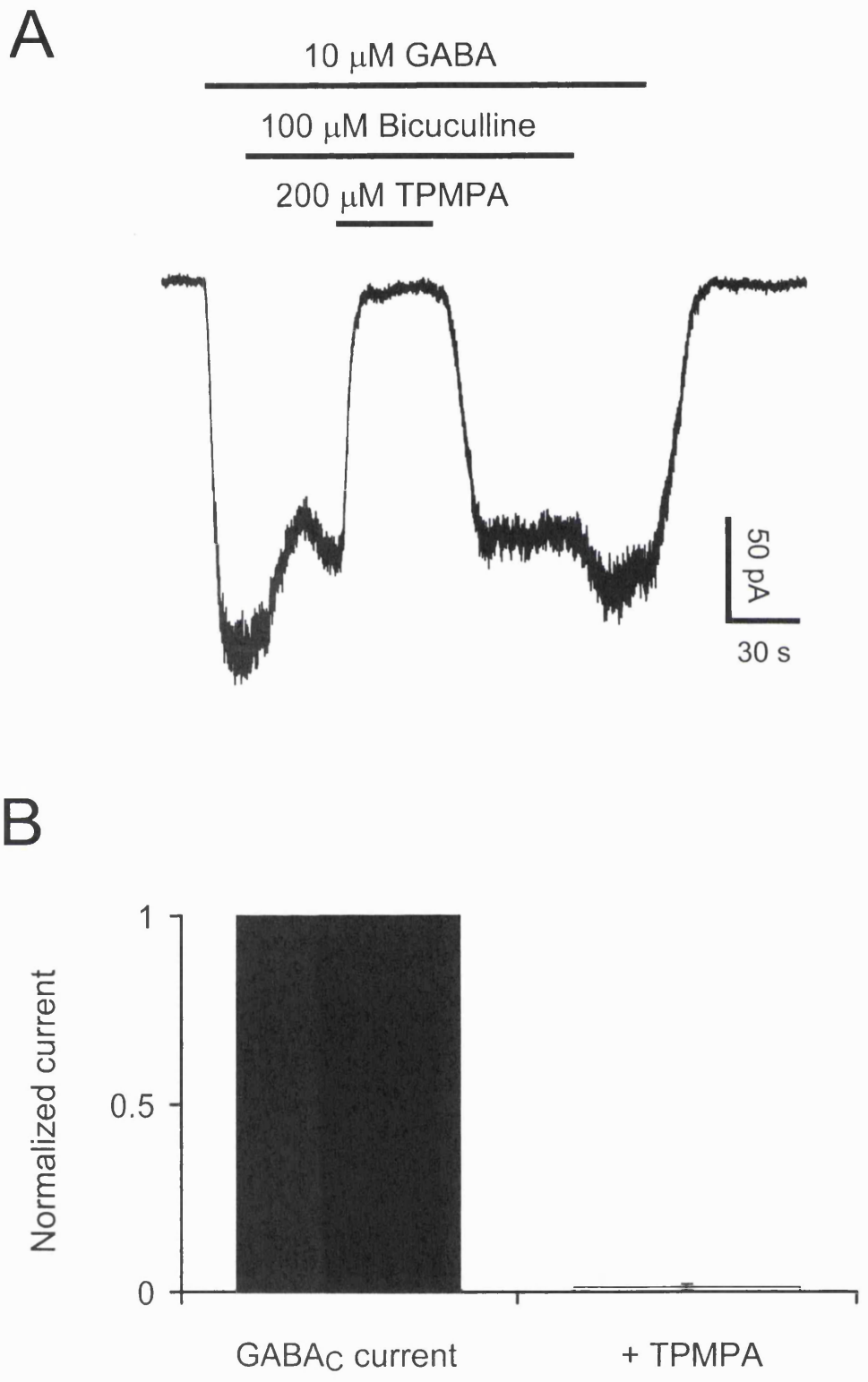
A
10 μM GABA
100 μM Bicuculline
200 μM TPMPA
50 pA
30 s
B
Normalized current
1
0.5
0
GABAC current
+ TPMPA

which is expected to block 99% of the current generated by $GABA_A$ receptors (assuming activation of $GABA_A$ receptors obeys a Hill equation with an EC_{50} of 10 μM, a Hill coefficient of 1 and that the K_i for bicuculline is 1 μM (Woodward et al., 1993; Krishek et al., 1996). The remaining current was blocked by co-application of the $GABA_C$ receptor inhibitor TPMPA (200 μM) (Ragozzino et al., 1996), which did not generate a current on its own (as shown later for slice bipolar cells in Figure 3.12). The bicuculline resistant current, i.e. the $GABA_C$ receptor mediated current, was reduced by 98.4 ± 0.9% (n=4) by TPMPA (Figure 3.8 B). These results confirm that dissociated bipolar cells contain functional $GABA_A$ and $GABA_C$ receptors. On average the $GABA_C$ current is about 79.3 ± 3.1 % of the total current evoked by 10 μM GABA, and can be isolated by application of bicuculline.

3.7. The EC_{50} for GABA of $GABA_C$ receptors in isolated bipolar cells

To obtain the apparent affinity of the $GABA_C$ receptor for GABA, different concentrations (1, 3, 10, 30 μM) of GABA were applied to isolated rod bipolar cells in the presence of 300 μM bicuculline (Figure 3.9 A). The evoked currents in each cell were normalized to the value evoked by 10 μM GABA in that cell, and fitted to the Hill equation:

$$I = \frac{I_{max} \cdot [GABA]^N}{EC_{50}{}^N + [GABA]^N} \qquad (3.1)$$

where I_{max} is the maximum current at saturating [GABA], and N is the Hill coefficient. Best fits were obtained using N = 1.6, and this value was fixed for all subsequent curve fitting using this equation. The averaged EC_{50} of 7 cells was 3.0 ± 0.2 μM (Figure 3.9 B), a value similar to the 4.2 μM obtained for the same cell type by Feigenspan and Bormann (1994).

Figure 3.9: GABA dose-response curve recorded from isolated bipolar cells in calcium containing solution

(A) Specimen trace recorded from an isolated rod bipolar cell at –60 mV. Different concentrations of GABA were bath applied in the presence of 300 μM bicuculline to block $GABA_A$ receptors and isolate $GABA_C$ receptor currents. **(B)** Dose-response curve for the GABA evoked $GABA_C$ responses recorded from 7 isolated bipolar cells. In each cell the responses were normalized to the response evoked by 10 μM GABA, and then rescaled to a saturating response of 1. The curve is a fit to the Hill equation (equation 3.1) with N = 1.6 and a mean EC_{50} of 3 μM.

A

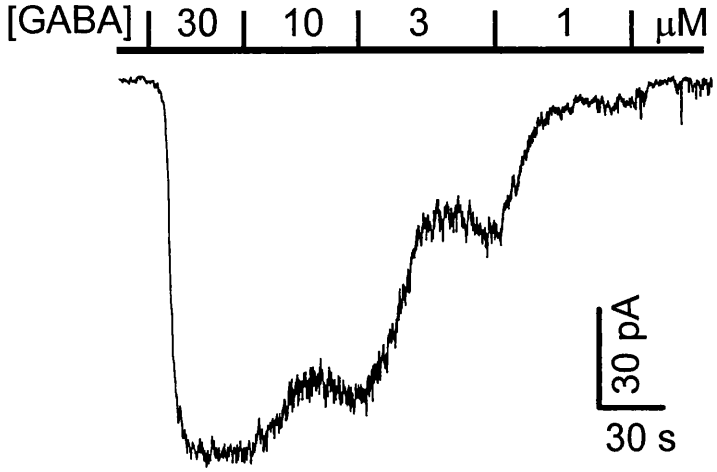
[GABA]
30
10
3
1
μM
30 pA
30 s

B

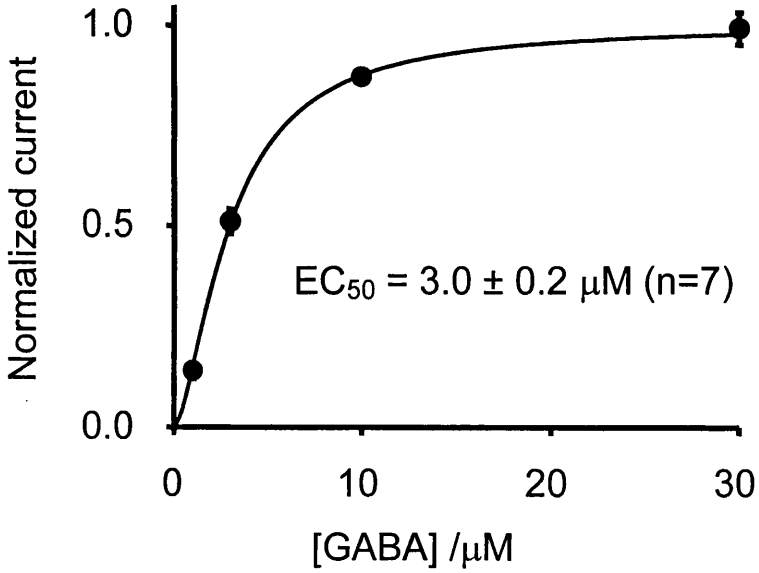
1.0
0.5
0.0
Normalized current
EC50 = 3.0 ± 0.2 μM (n=7)
0
10
20
30
[GABA] /μM

Figure 3.10: GABA dose-response curve recorded from isolated bipolar cells in zero calcium/cobalt containing solution

(A) Specimen trace recorded from an isolated rod bipolar cell at –60 mV in zero calcium / 4 mM cobalt solution. Different concentrations of GABA were bath applied in the presence of 300 μM bicuculline to block $GABA_A$ receptors and isolate currents mediated by $GABA_C$ receptors. Occasionally, as shown here, the current desensitized, but this may by an artefact of the cell isolation procedure as it was not observed in recordings made from bipolar cells in retinal slices. **(B)** Dose-response curve for the GABA evoked $GABA_C$ responses recorded from 5 isolated bipolar cells. In each cell the responses were normalized to the response evoked by 30 μM GABA, and then rescaled to a saturating response of 1. The curve is a fit to the Hill equation (equation 3.1) with N = 1.6 and a mean EC_{50} of 11 μM.

A

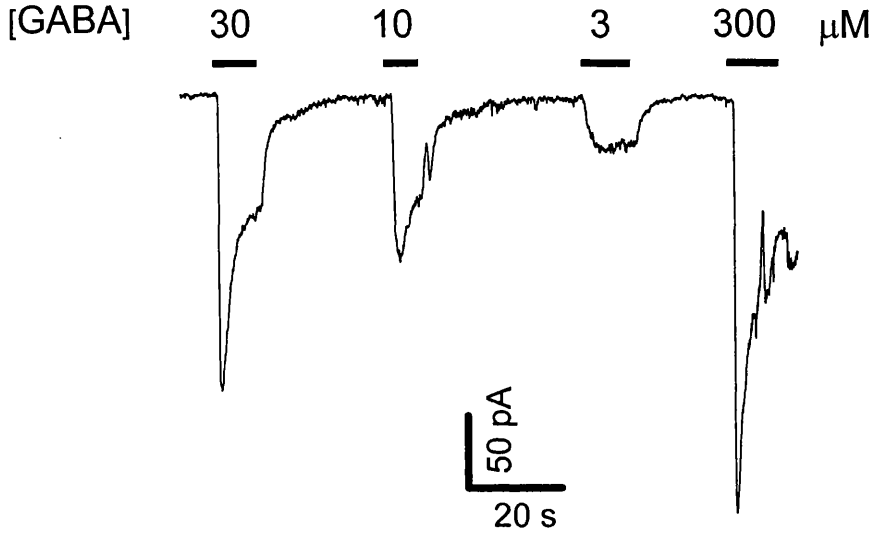
[GABA]
30
10
3
300
μM
50 pA
20 s

B

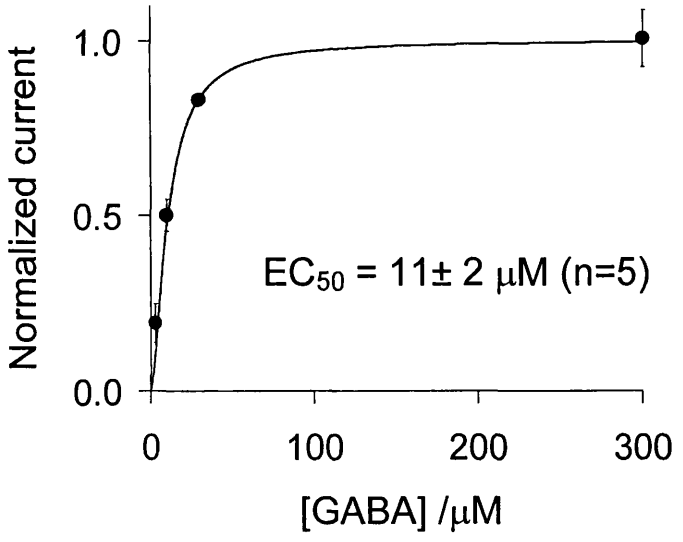
Normalized current
1.0
0.5
0.0
EC50 = 11± 2 μM (n=5)
0
100
200
300
[GABA] /μM

Repeating these experiments in solution containing no calcium and with 4 mM added cobalt chloride, as used to block synaptic transmission in experiments on slices described below, gave a higher EC_{50} of 11 ± 2 μM in 5 isolated bipolar cells (Figure 3.10 A, B). Cobalt is routinely used to synaptically isolate bipolar cells in retinal slices (Euler et al., 1996; Euler and Wassle, 1998), but this result shows that it also modifies the properties of the $GABA_C$ receptors, as has been reported previously for ρ_1 transfected cells (*Xenopus* oocytes) and horizontal cells isolated from the catfish retina (Calvo et al., 1994; Kaneda et al., 1997).

3.8. Peptide diffusion time to bipolar cell axon terminal

As has been reported by others (Karschin and Wassle, 1990), dissociated bipolar cells stayed healthy for only a few minutes, after which their membrane resistance dropped, and the current became too noisy to measure the dose-response curve accurately. To allow the peptide to equilibrate throughout the cytoplasm and to disrupt the ρ_1 – MAP-1B interaction, the $GABA_C$ receptor mediated currents needed to be monitored for longer than the few minutes possible with dissociated bipolar cells. One can calculate the time constant for the peptide diffusing into the cytoplasm and equilibrating inside the cell as follows. The diffusion constant of the peptides was estimated as $D = 1.07 \times 10^{-10}$ m^2/sec by scaling the value for somatostatin in proportion to the square root of the ratio of its molecular weight (1638) to that of the peptides used here (3945). For an axon of length L = 50 μm, the diffusion time from the soma to the axon terminal is $\sim \frac{L^2}{2 \cdot D} = 12$ sec. Thus, once inside the cell soma, the peptides used should equilibrate through the cell relatively quickly. The time constant for the peptide to equilibrate between the patch pipette and the cell volume is given by (see Chapter 2.7, equation 2.20)

$$\tau = \frac{V \cdot R_S}{D \cdot \rho}$$

where the cell volume V is ~850 μm^3 (for a 10 μm diameter soma, 100 μm total length of axon plus dendrites of diameter 2 μm, and a synaptic terminal of diameter 3 μm), the series resistance R_s is 25 MΩ, and the resistivity of the pipette solution ρ is 0.8 Ωm. With these numbers, τ = 248 sec (~ 4 minutes).

Since isolated bipolar cells only stayed healthy for a few minutes, I switched to patch-clamping bipolar cells in retinal slices, which could be recorded from for 30 minutes without any deterioration in health. Slice bipolar cells were also preferred because the cytoskeleton with which the $GABA_C$ receptors are thought to interact via MAP-1B is likely to be less disrupted than in isolated cells that have been enzyme treated and triturated through a Pasteur pipette.

3.9. Bipolar cells in retinal slices

The type of bipolar cells recorded from in retinal slices were identified by filling with the fluorescent dye Lucifer Yellow from the patch pipette (Figure 3.11 and 4.1; Chapter 2). Rod bipolar cells were identified by the presence of a soma in the outermost part of the inner nuclear layer, and a long axon terminating in the inner part of the inner plexiform layer (Figure 3.11). The majority of cells with this morphology are rod bipolar cells. A small fraction are ON cone bipolar cells (of classes 8 and 9: see (Euler and Wassle, 1995; Euler et al., 1996; Hartveit, 1997; Euler and Wassle, 1998) for the morphological characterization of rat bipolar cells).

3.10. TPMPA blocks the bicuculline resistant GABA-evoked current in slice bipolar cells

In retinal slices (Figure 3.12 A), as in isolated cells, bath application of 30 μM GABA in the presence of the $GABA_A$ receptor antagonist bicuculline (300 μM) evoked an inward current in bipolar cells (with E_{Cl} set at 0mV), which was blocked by co-application of the $GABA_C$ receptor antagonist TPMPA (200 μM). This block

Figure 3.11: Rat retinal slice

Transmitted light pictures of a retinal slice taken with an **(A)** 10X and a **(B)** 60X lens. In (A) all layers of the retina are clearly visible: photoreceptor outer segments (OSL), outer nuclear layer (ONL), outer plexiform layer (OPL), inner nuclear layer (INL), inner plexiform layer (IPL) with sublamina a and b, and ganglion cell layer (GCL). The black strip at the bottom is the millipore filter paper to which the slice was attached. (B) shows the inner nuclear layer in higher magnification. The star indicates the soma of a rod ON bipolar cell (a fluorescence picture of this cell is shown in Figure 4.1); the arrow heads point to a cell process (possibly a bipolar cell axon) which penetrates the IPL.

A

B

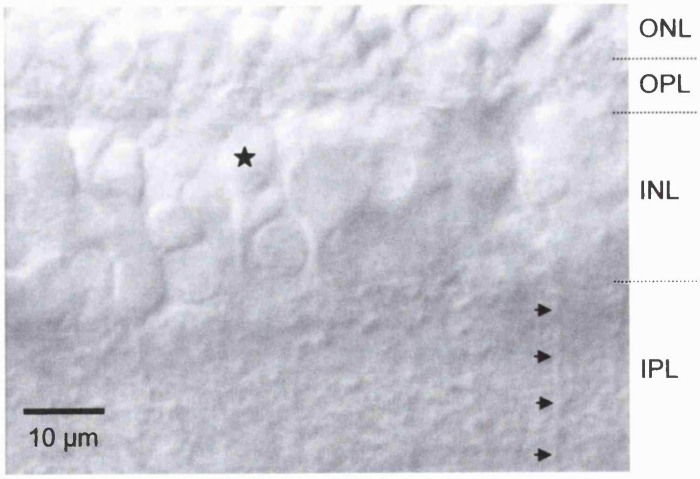

Figure 3.12: $GABA_C$ receptor mediated currents in slice bipolar cells

(A) Specimen trace recorded from a slice bipolar cell of a 35 day old rat. GABA evoked an inward current, which was almost completely inhibited by 200 μM TPMPA (the $GABA_C$ receptor antagonist). The blocking effect was slowly reversible. TPMPA itself did not affect the membrane current. The cell was voltage-clamped at –60 mV and recorded from in the presence of 300 μM bicuculline and in 0 mM calcium / 4 mM cobalt solution. **(B)** Averaged data from 4 slice bipolar cells. The GABA evoked current (left bar) was blocked by 97% by TPMPA (right bar), revealing it as $GABA_C$ receptor mediated.

A

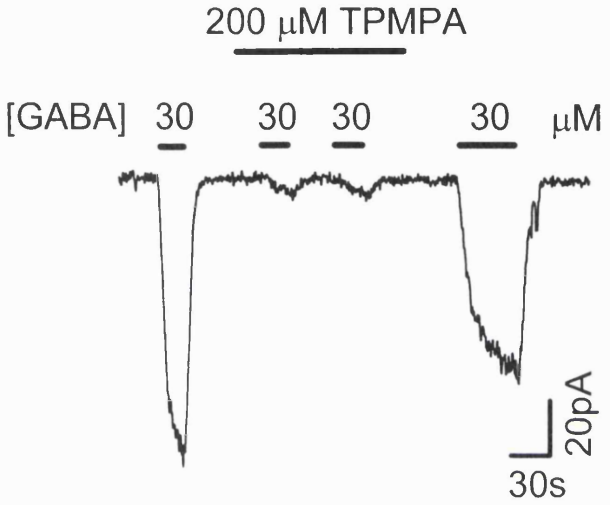
200 μM TPMPA
[GABA] 30 30 30 30 μM
20pA
30s

B

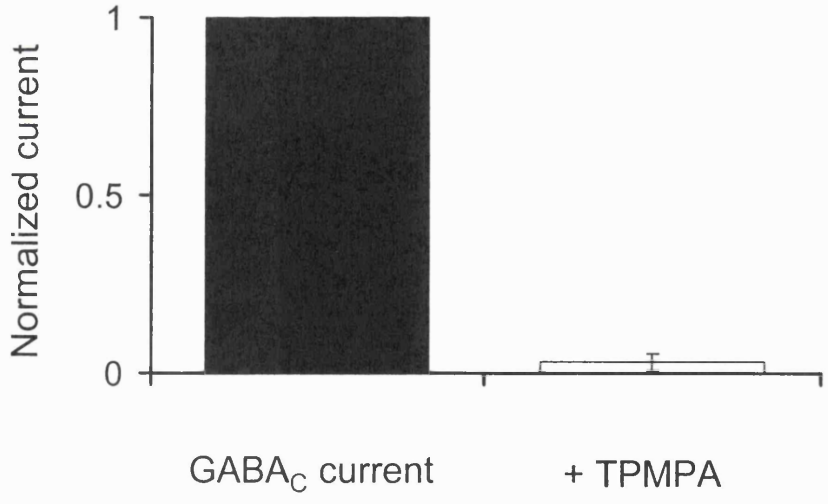
Normalized current
1
0.5
0
GABA$_C$ current
+ TPMPA

was only slowly reversible. TPMPA did not evoke a current on its own (Figure 3.12 A). The $GABA_C$ receptor mediated current evoked by 30 μM GABA was reduced by 97 ± 2 % (n = 4) by 200 μM TPMPA (Figure 3.12 B), whereas 2 mM TPMPA reduced the current generated by 300 μM GABA by 93 ± 3 % (n=2). These results confirm that the GABA-evoked current in the presence of bicuculline is mediated by $GABA_C$ receptors.

3.11. The EC_{50} for GABA of $GABA_C$ receptors recorded in slices

To obtain the EC_{50} of the $GABA_C$ receptors in bipolar cells *in situ* in retinal slices, different concentrations (3, 10, 30, 100, 300 μM) of GABA were bath applied in the presence of 300 μM bicuculline, with external Ca^{2+} removed and 4 mM Co^{2+} added to block synaptic transmission (see Chapter 2; this was done to prevent GABA evoking a response in e.g. horizontal or amacrine cells and thus producing a synaptic response in the bipolar cell). Whereas low GABA doses evoked a sustained current, high doses evoked a slightly desensitizing current (Figure 3.13 A). The currents (I) evoked by different GABA concentrations were normalized to the value evoked by 300 μM in the same cell, and fit by the Hill equation (equation 3.1; N was set to 1.6 as for isolated cells). The averaged EC_{50} of 14 cells was 40.4 ± 1.9 μM (ranging from 26 to 80 μM in individual cells), i.e. much higher than the 3 μM or 11 μM obtained in isolated cells in the absence or presence, respectively, of cobalt (section 3.7).

3.12. GABA transporters increase the apparent EC_{50} for GABA of $GABA_C$ receptors in slice bipolar cells

A possible reason for why the apparent EC_{50} for GABA is so much higher for $GABA_C$ receptors in slice bipolar cells, compared to in isolated cells, is the presence of prominent GABA uptake mechanisms in the slice. GABA transporters (see section

Figure 3.13: Effect of SKF-98776A on the GABA dose response curve in retinal slice bipolar cells

(A) and (B) Specimen GABA evoked currents, at –60 mV, recorded from a slice bipolar cell in zero calcium / 4 mM cobalt solution containing 300 μM bicuculline. To obtain the dose-response curve of $GABA_C$ receptors in control solution **(A)**, and with GABA uptake inhibited **(B)**, different concentrations of GABA were bath applied in the absence (A) or presence (B) of the GAT-1 blocker SKF-89976A (100 μM). The data shown in A and B are from the same cell and have been scaled to have the same peak at 300 μM GABA (slight run down with time resulted in the maximum current being smaller when the measurements in SKF-89976A were made). **(C)** Dose-response curve for $GABA_C$ responses recorded as in A and B from 5 slice bipolar cells in control or in the presence of 100 μM SKF-89976A. In each cell the responses were normalized to the response evoked by 300 μM GABA. **(D)** Hill curves fitted through the data in C, with N = 1.6, had an EC_{50} of 51 μM in control conditions and 13 μM with GAT-1 blocked.

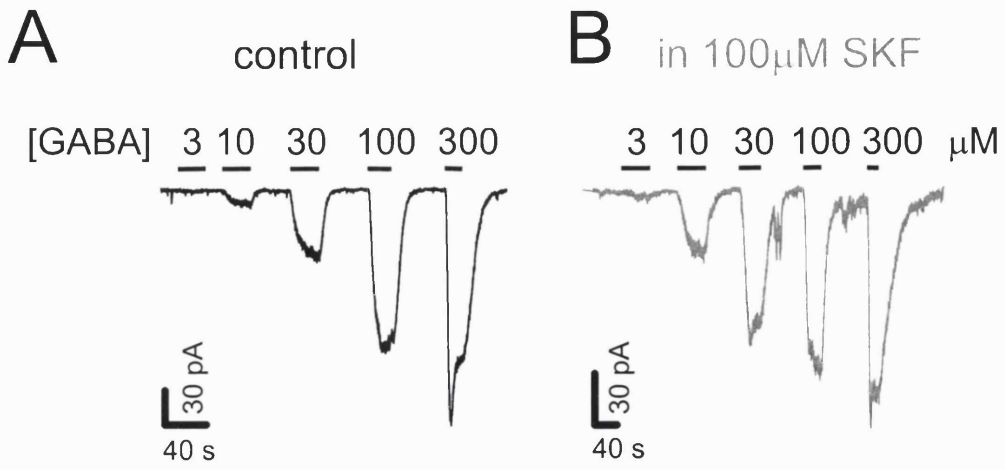
A
control
B
in 100μM SKF
[GABA] 3 10 30 100 300
3 10 30 100 300 μM
30 pA
40 s
30 pA
40 s

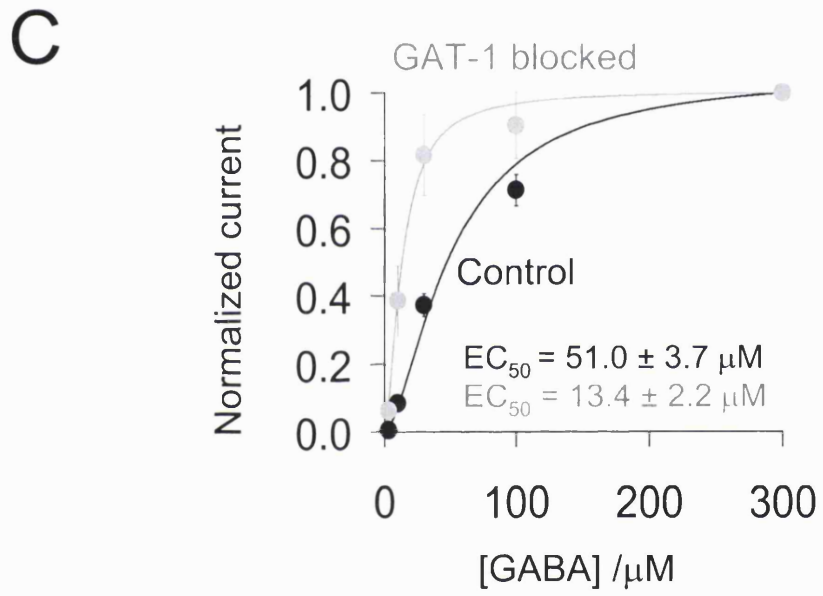
C
GAT-1 blocked
Normalized current
1.0
0.8
0.6
0.4
0.2
0.0
Control
EC50 = 51.0 ± 3.7 μM
EC50 = 13.4 ± 2.2 μM
0
100
200
300
[GABA] /μM

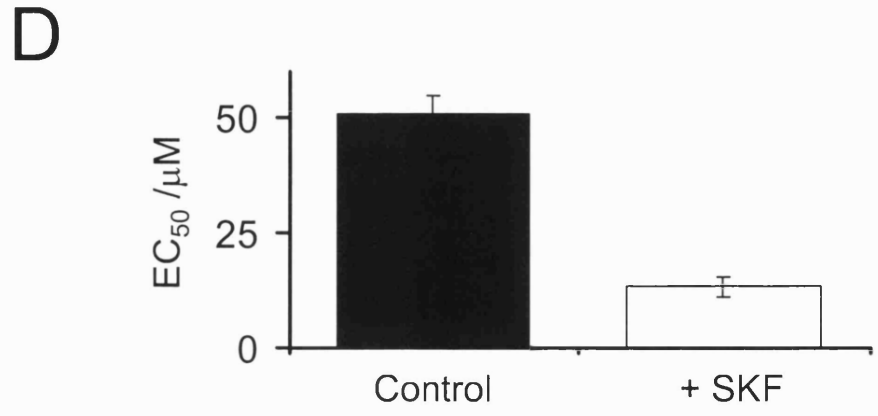
D
EC50 /μM
50
25
0
Control
+ SKF

1.5), mainly GAT-1 in neurones and GAT-3 in glial cells, remove GABA from the extracellular space and lower the [GABA] around the cells within the slice below the concentration which is applied in the bulk solution. This will result in a higher apparent EC_{50} (measured as the GABA concentration in the superfusion solution) for $GABA_C$ receptors in slice bipolar cells. To try to reduce this effect, I applied the GAT-1 inhibitor SKF-89976A (100 μM) (Borden et al., 1994; Takahashi et al., 1995a), which decreased the EC_{50} of $GABA_C$ receptors recorded in slice bipolar cells by a factor of four (Figure 3.13 A, B). The average EC_{50} for GABA in 5 cells decreased from 51.0 ± 3.7 μM to 13.4 ± 2.2 μM when GAT-1 was blocked ($p=0.00002$) (Figure 3.13 C, D). Thus, GABA uptake into surrounding cells in the slice seems to be a major reason for the higher EC_{50} of $GABA_C$ receptors when recorded in slice bipolar cells. As stated above, the recorded EC_{50} values in the absence of the GAT-1 blocker were found to vary substantially, i.e. between 26 and 80 μM. This huge variation is likely to depend on how influential the uptake mechanisms are, for example how deep within the slice the recorded cell is.

Although GAT-3 transporters may also lower the GABA concentration around bipolar cells, there are no specific non-transported GAT-3 blockers to test this: the GAT-3 blocker β-alanine also activates $GABA_C$ receptors (Calvo and Miledi, 1995), and in addition is transported by GAT-3 (Clark and Amara, 1994) so it will tend to raise the extracellular GABA concentration by heteroexchange on GAT-3 with intracellular GABA.

Figure 3.14 summarizes EC_{50} values measured in the different conditions. Isolated bipolar cells recorded in zero cobalt solution show an EC_{50} of around 3 μM (first bar). This value increases to around 11 μM when cobalt is present and calcium is removed (second bar). Slice bipolar cells recorded in cobalt containing zero Ca^{2+} solution with GABA uptake functioning, show an EC_{50} of around 40 μM (fourth bar), and the GAT-1 uptake inhibitor decreases the EC_{50} to around 13 μM (third bar), a level which is not significantly different ($p=0.44$) from the 11 μM recorded in

Figure 3.14: EC_{50} for GABA of $GABA_C$ receptors recorded in different conditions

First bar: Isolated bipolar cells recorded in normal calcium containing solution have an EC_{50} of around 3 μM (see Section 3.7; Figure 3.9). **2nd bar**: Isolated bipolar cells in the presence of 4 mM cobalt and zero calcium have an EC_{50} of around 11 μM (see section 3.7; figure 3.10). **3rd bar**: Slice bipolar cells recorded in zero calcium / 4 mM cobalt solution, with GAT-1 blocked (100 μM SKF-89976A) have an EC_{50} of around 13 μM (see section 3.11; figure 3.13), not significantly different p=0.44 from isolated cells in zero calcium / 4 mM cobalt solution (2nd bar). **4th bar**: Slice bipolar cells recorded in zero calcium / 4 mM cobalt solution have an EC_{50} of around 40 μM (see section 3.11).

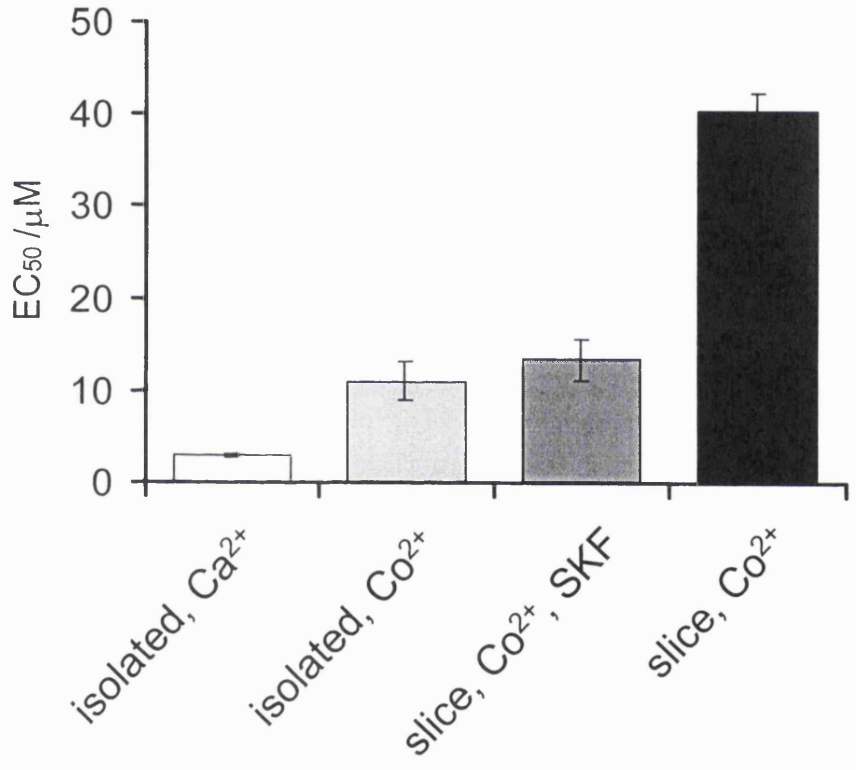
50
40
30
20
10
0
EC50 /µM
isolated, Ca2+
isolated, Co2+
slice, Co2+ , SKF
slice, Co2+

isolated cells in the presence of cobalt (second bar). These data suggest that uptake by GAT-1 is the main cause of the high EC_{50} measured in slices.

Experiments (described below) disrupting the ρ_1 – MAP-1B interaction were done without blocking GABA uptake. Mathematical analysis (section 3.13) shows this does not affect my conclusions about the effect of the ρ_1 – MAP-1B interaction on the EC_{50}.

3.13. Disrupting the ρ – MAP-1B interaction decreases the EC_{50} of $GABA_C$ receptors

When the peptide mimicking the MAP-1B binding site ("binding site peptide") was present in the solution in the whole cell patch pipette, $GABA_C$ receptor mediated current responses changed with time after starting whole cell clamping (Figure 3.15 A, B). After 25 minutes (Figure 3.15 B), low doses of GABA produced a larger current than before (at 5 minutes, Figure 3.15 A), whereas the response to a high dose of GABA changed little (although it often desensitized more than when recorded just after going to whole-cell mode, as in Figure 3.15 B). This is equivalent to a decrease in the EC_{50} with time, as illustrated by the corresponding dose-response curves in Figure 3.15 C, in which the data were fit with the Hill equation with the Hill coefficient N fixed at 1.6. In this example, the EC_{50} decreased from 79 μM at 5 minutes to 31 μM at 25 minutes of whole-cell clamping. In contrast, introducing the scrambled version of the peptide into the cell resulted either in no time dependent change of the $GABA_C$ receptor currents, or a slight reduction of the fractional response to low [GABA] (Figure 3.15 D). The EC_{50} in this example increased from 37 μM at 5 minutes to 53 μM at 25 minutes.

To quantify these changes of $GABA_C$ receptor properties, the dose-response data obtained at different times after starting whole-cell clamping, i.e. 5, 15 and 25 minutes after going to whole-cell mode, were each normalized to their value at 300 μM GABA and fitted with the Hill equation. The resulting EC_{50} and I_{max} in each cell

Figure 3.15: Effect of dialysis with MAP-1B binding site peptide on the dose response curve of $GABA_C$ receptors in retinal slice bipolar cells

Specimen current responses to different GABA concentrations of a slice bipolar cell with the binding-site peptide included in the pipette, recorded at 5 minutes **(A)** or 25 minutes **(B)** after going to whole cell mode (in 300 μM bicuculline; at –60 mV). Responses from A and B are from the same cell and have been scaled to be the same at 300 μM GABA, to compensate for a slight decline with time and to facilitate comparison of the dose-dependence of the responses. The fractional responses at low doses of GABA are much larger in B than in A. **(C)** Dose-response curves from the data shown in A and B. The currents were normalized to the current evoked by 300 μM GABA and fit with the Hill equation (with N = 1.6). At 5 minutes the EC_{50} was 79 μM, but this decreased to 31 μM at 25 minutes. **(D)** $GABA_C$ receptor dose-response curves from a cell with the scrambled peptide included in the pipette. The currents were normalized to the current evoked by 300 μM GABA and fit with the Hill equation (with N = 1.6). At 5 minutes the EC_{50} was 37 μM, and this increased to 53 μM at 25 minutes.

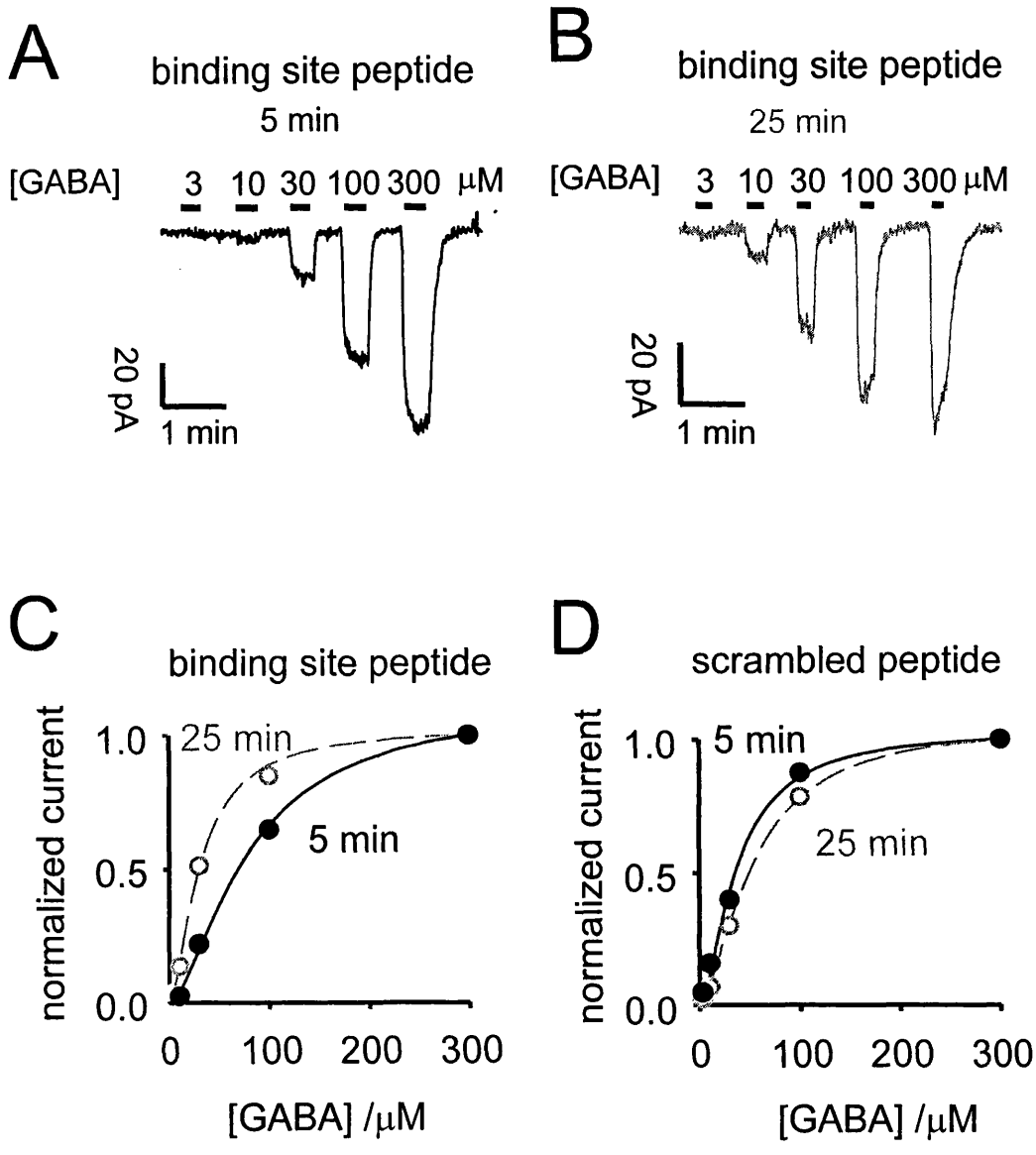
A
binding site peptide
5 min
[GABA]
3 10 30 100 300 μM
20 pA
1 min
B
binding site peptide
25 min
[GABA]
3 10 30 100 300 μM
20 pA
1 min
C
binding site peptide
normalized current
1.0
0.5
0.0
25 min
5 min
0 100 200 300
[GABA] /μM
D
scrambled peptide
normalized current
1.0
0.5
0.0
5 min
25 min
0 100 200 300
[GABA] /μM

Figure 3.16: Time-dependent changes in the properties of $GABA_C$ receptors induced by competitive removal of MAP-1B binding

Maximum current (I_{max}) **(A)** and EC_{50} **(B)** derived from fitting the Hill equation to $GABA_C$ receptor mediated GABA dose-response data (as in figure 3.15) measured at different times after starting whole-cell clamping. The pipette solution contained either the binding site peptide (hollow circles) or a scrambled version of it (filled circles). Data from each cell were normalized to their values measured 5 minutes after starting whole cell clamping, before averaging for these graphs. Data in A are not significantly different for the two peptides. The p values in B are from two-tailed t-tests. 8-13 cells contribute to each data point.

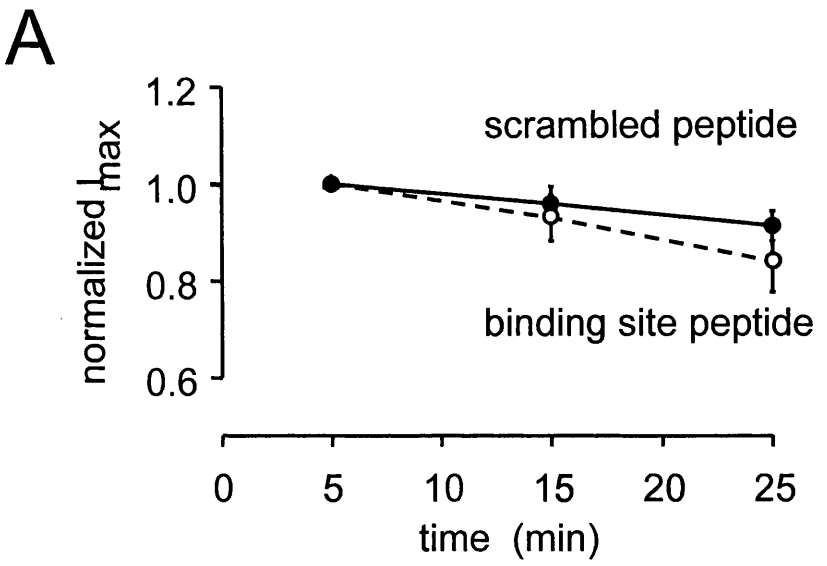
A
normalized I_{max}
1.2
1.0
0.8
0.6
scrambled peptide
binding site peptide
0
5
10
15
20
25
time (min)

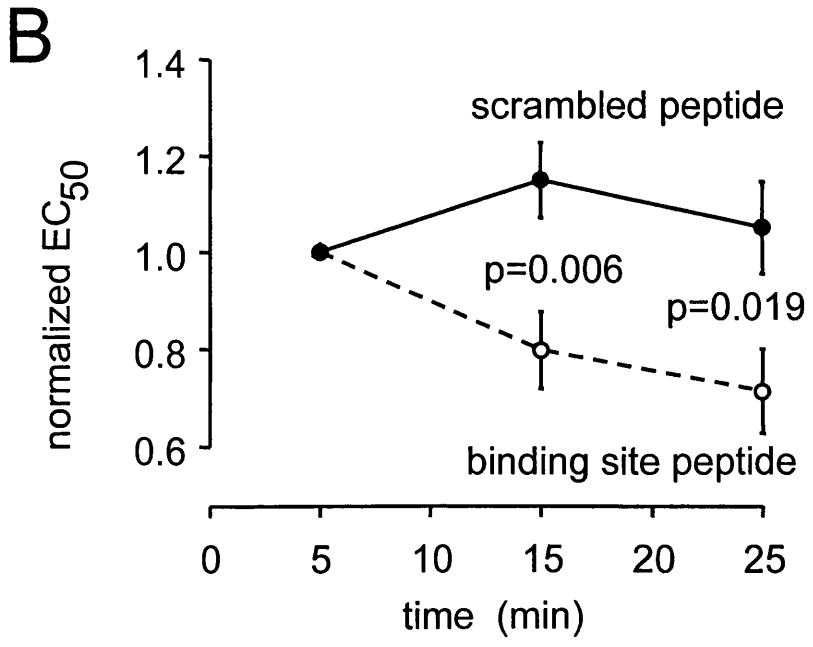
B
normalized EC_{50}
1.4
1.2
1.0
0.8
0.6
scrambled peptide
p=0.006
p=0.019
binding site peptide
0
5
10
15
20
25
time (min)

were normalized to the EC_{50} and I_{max} obtained in the same cell at the start of the recording (i.e. after 5 minutes). This procedure was adopted to remove variability in the initial value of the EC_{50} (probably resulting from differing degrees of influence of uptake, as explained in section 3.12), and to allow monitoring of just the time-dependent changes of EC_{50} and I_{max}.

The maximum evoked current decreased slightly within the 25 minutes of recording. However, this run-down occurred whether the binding site or the scrambled peptide was introduced into the cells (Figure 3.16 A), and might simply reflect an alteration of internal milieu by the non-peptide components of the pipette solution, as reported before (Feigenspan and Bormann, 1994b).

The EC_{50} decreased to around 70% of its initial value within the 25 minute recording period when the binding site peptide was included in the pipette solution. In contrast, the scrambled peptide produced no significant change of the EC_{50} within this time frame. The data for the two peptides differed significantly after 15 and 25 minutes of recording. (Figure 3.16 B). These differences are likely to be underestimated by my data, because the "initial" value of EC_{50} by which the subsequent data were normalized was measured 5 minutes after starting whole-cell clamping, by which time the binding site peptide might have had some effect already. The time constant for filling the cell by the dialyzed peptides is estimated to be around 4 minutes (see section 3.8 above), so the time course of the changes seen with the binding site peptide in Figure 3.16 B may reflect both the filling time and the time needed for competitive displacement of endogenous ρ_1 from MAP-1B by the peptide.

The mean data in Figure 3.16 B show that the binding site peptide reduces the EC_{50} at 25 minutes after starting whole-cell clamping to 68% of its value with the scrambled peptide. Using the Hill equation, where I is the current, I_{max} is the maximal evoked current, [GABA] is the GABA concentration, N is the Hill coefficient and EC_{50} is the GABA concentration which produces a half maximal

current:

$$I = \frac{I_{max} \cdot [GABA]^N}{EC_{50}{}^N + [GABA]^N} \tag{3.1}$$

one can calculate how changes in the EC_{50} will change the magnitude of the GABA-evoked currents. The current produced by receptors before the change, i.e. with the "old" EC_{50}, is given as

$$I_{(old)} = \frac{I_{max} \cdot [GABA]^N}{EC_{50(old)}{}^N + [GABA]^N}$$

and the current produced by receptors after the change, i.e. with the "new" EC_{50}, is given as

$$I_{(new)} = \frac{I_{max} \cdot [GABA]^N}{EC_{50(new)}{}^N + [GABA]^N}$$

since the value of I_{max} was not affected by the binding site peptide (Figure 3.16 A). The ratio of the current with the ρ_1 – MAP-1B interaction disrupted or not disrupted is thus

$$\frac{I_{(new)}}{I_{(old)}} = \frac{EC_{50(old)}{}^N + [GABA]^N}{EC_{50(new)}{}^N + [GABA]^N}$$

For low GABA concentrations, when [GABA] << EC_{50}

$$\frac{I_{(new)}}{I_{(old)}} = \frac{1}{\left(\frac{EC_{50(new)}}{EC_{50(old)}}\right)^N} \tag{3.2}$$

Thus, with my experimental value of $\frac{EC_{50(new)}}{EC_{50(old)}} = 0.68$ and N = 1.6, we get

$$\frac{I_{(new)}}{I_{(old)}} = 1.9$$

The decrease of the EC_{50} evoked by disrupting the MAP-1B – ρ interaction (to 68%) will thus result in a 1.9 fold increase of the current evoked by low doses of GABA,

and a large change of this order can indeed be seen in the specimen traces in Figure 3.15. Normally therefore, in the absence of the binding-site peptide, the interaction of MAP-1B with ρ_1 roughly halves the size of the current that low doses of GABA generate.

3.14. Effect of GABA uptake on EC_{50} changes

The results described above and their possible implications for retinal physiology are intriguing. However, as mentioned before (section 3.12), GABA uptake influences the value of the EC_{50} in slices significantly (Figure 3.13), and one has to think about the possibility that changes of EC_{50} defined by the bulk solution GABA concentration do not necessarily reflect accurately the changes which occur of the real EC_{50}. To quantify how uptake reduces the GABA concentration outside bipolar cells in retinal slices, below the concentration applied in the bulk solution, and how this affects the EC_{50}, one can consider a simplified 3 compartment model of the slice, where the bulk solution, with GABA concentration $[GABA]_B$, is separated from the extracellular space, with GABA concentration $[GABA]_O$, by a diffusion barrier of permeability P (Figure 3.17). GABA enters the extracellular space from the bulk solution at a rate:

$$P \cdot ([GABA]_B - [GABA]_O)$$

and GABA is removed from the extracellular space by transporters into cells at a rate of:

$$\frac{U \cdot [GABA]_O}{[GABA]_O + K_U}$$

where U and K_U are the maximum rate and Michaelis-Menten constant of uptake. The GABA transporters GAT-1 and GAT-3 show a first order Michaelis-Menten dependence of uptake on GABA concentration (Risso et al., 1996). At equilibrium

Figure 3.17: Three compartment model of GABA diffusion into slice

The bulk solution (with GABA concentration $[GABA]_B$) is separated from the extracellular space in the slice (with GABA concentration $[GABA]_O$) by a diffusion barrier of permeability P. GABA enters the extracellular space from the bulk solution at a rate $P \cdot ([GABA]_B - [GABA]_O)$ and is removed from the extracellular space by uptake into cells at a rate of $\frac{U \cdot [GABA]_O}{[GABA]_O + K_U}$ (U and K_U are the maximum rate and Michaelis-Menten constant of uptake).

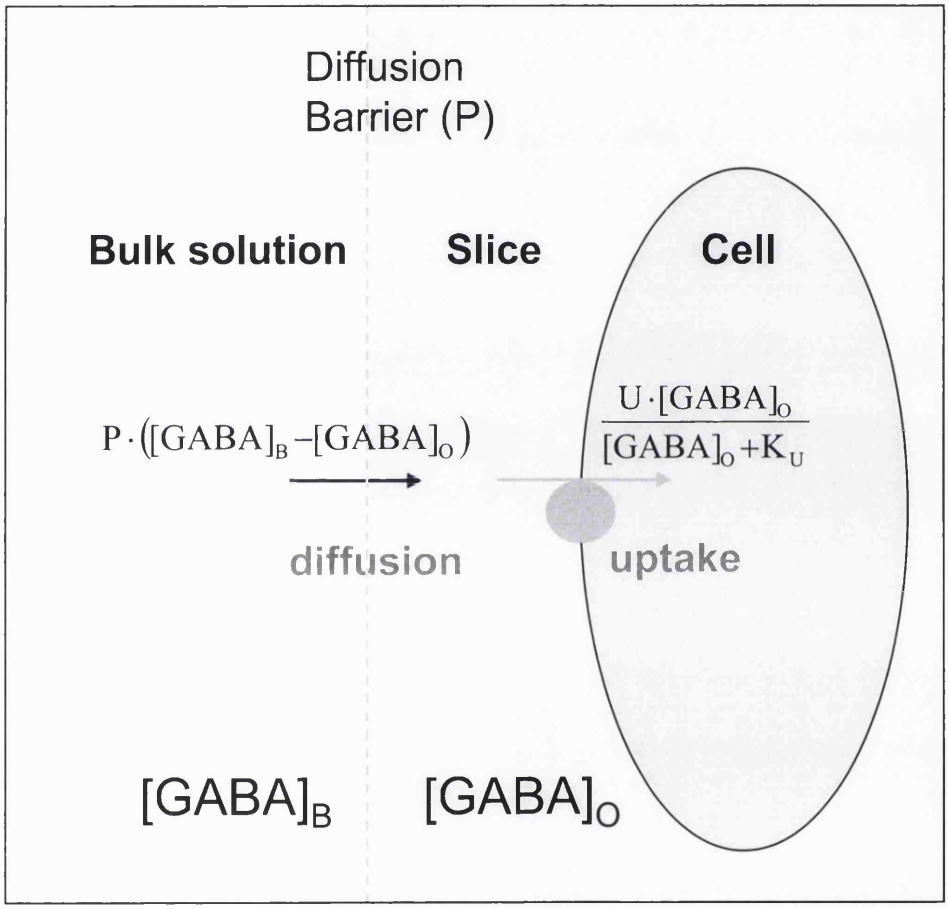
Diffusion
Barrier (P)
Bulk solution
Slice
Cell
$P \cdot ([GABA]_B - [GABA]_O)$
$\frac{U \cdot [GABA]_O}{[GABA]_O + K_U}$
diffusion
uptake
$[GABA]_B$
$[GABA]_O$

the rate of entry into the extracellular space and the rate of uptake from the extracellular space must be equal, so

$$P \cdot ([GABA]_B - [GABA]_O) = \frac{U \cdot [GABA]_O}{[GABA]_O + K_U}$$

Solving this equation for $[GABA]_B$ results in:

$$[GABA]_B = [GABA]_O + \frac{\frac{U}{P}}{1 + \frac{K_U}{[GABA]_O}}$$

When the bulk solution $[GABA]_B$ is at a value that makes $[GABA]_O$ equal the EC_{50}, so a half maximal current is generated:

$$[GABA]_B = EC_{50} + \frac{\frac{U}{P}}{1 + \frac{K_U}{EC_{50}}} \qquad (3.3)$$

Because $[GABA]_O = EC_{50} = 11$ μM (measured in isolated cells in the cobalt/zero calcium solution used for slice experiments: Figures 3.10 and 3.14), when the applied $[GABA]_B = 40.4$ μM (mean EC_{50} measured when recorded in slices: Figure 3.14), and $K_U \sim 30$ μM for GAT-1 and GAT-3 in rat (Borden et al., 1994), equation 3.3 gives $\frac{U}{P} = 109.6$ μM.

For a 32% reduction of the $[GABA]_B$ generating a half-maximal current (i.e. from 40.4 μM to 27.2 μM), as seen experimentally with the peptide disrupting the MAP-1B – ρ_1 interaction (Figure 3.16 B), solving equation 3.3 for the EC_{50} gives

$$EC_{50} = -\frac{p}{2} + \sqrt{\left(\frac{p}{2}\right)^2 - q}$$

with

$$p = K_U + \frac{U}{P} - [GABA]_B = 30\mu M + 109\mu M - 27.2\mu M = 111.8\mu M$$

and

$$q = -K_U[GABA]_B = -30\mu M \cdot 27.2\mu M = -816\mu M^2$$

resulting in an EC_{50} value of 6.9 μM, i.e. reduced from 11 μM by 37 %. Thus, fractional changes in the bulk solution EC_{50} underestimate fractional changes of the real EC_{50} by a factor of 32/37 = 0.86, i.e. a 14% underestimate. The presence of uptake therefore has no significant effect on the conclusion that disrupting the ρ_1 – MAP-1B interaction approximately doubles the current at low GABA concentrations, since using an EC_{50} ratio of $\frac{EC_{50(new)}}{EC_{50(old)}}$ = 0.63 (instead of 0.68) in equation 3.2 leads to a produces current ratio of 2.1 (instead of 1.9).

3.15. The glycine transporter GLYT-1E/F and MAP-1B bind to different regions of ρ_1

As described in section 3.1, the glycine transporter GLYT-1E/F also binds to ρ_1. To determine whether it binds to the same region of ρ_1 as MAP-1B or has a separate binding site, my collaborator Jon Hanley performed pull-down assays (Figure 3.18 A). He used beads to which either GST-MAP-1B (containing the amino acid residues 460-585 of MAP-1B which bind to ρ_1 (Hanley et al., 1999): Figure 3.18 A, lanes 3 and 4) or GST-GLYT-1E/F (containing the 58 most C-terminal amino acids of the transporter which bind ρ_1 (Hanley et al., 2000): Figure 3.18 A, lanes 5 and 6) were attached, to pull down *myc*-tagged ρ_1 (full length ρ_1) from transfected COS cell extract. As described in section 3.3 (Figure 3.4), each of the two reactions were treated with 250nM of the peptide including ρ_1's MAP-1B binding site (Figure 3.18 A, lanes 4 and 6, " + "), or of the scrambled control peptide (Figure 3.18 A, lanes 3 and 5, " – "). Binding of ρ_1 to GST-MAP-1B and GST-GLYT-1E/F was determined by Western blotting and probing with a *myc* antibody. The binding site peptide competed with ρ_1^{myc} for binding to GST-MAP-1B, confirming that this ρ_1 amino acid sequence is the site of interaction with MAP-1B as shown above.

However, the peptide did not compete for binding to GST-GLYT-1E/F, indicating that the transporter binds to a different region of ρ_1.

To confirm this result, the MAP-1B binding site mutants of ρ_1^{myc} (described in section 3.2, Figure 3.3) were tested for binding to GST-GLYT-1E/F in pull-down assays from transfected COS cell lysate (Figure 3.18 B). All four mutants showed a similar level of binding compared with the input to the assay, indicating that they bind equally well to GST-GLYT-1E/F and implying that the GLYT-1E/F binding site differs from that for MAP-1B (as schematized in Figure 3.22).

3.16. Glycine does not alter $GABA_C$ responses

The cellular location of GLYT-1E/F transporters is not known, but their mRNA has been shown to be expressed in the (bovine) retina (Hanley et al., 2000). Their interaction *in vitro* with ρ_1 suggests that, if these transporters are present in bipolar cells, the rate of glycine uptake could alter $GABA_C$ receptor properties or vice versa. To test this, I whole cell patch clamped bipolar cells in retinal slices and recorded GABA-evoked $GABA_C$ receptor mediated currents in the absence and presence of glycine. Applying 300 μM glycine (in the presence of 10 μM strychnine to block glycine receptors, and 300 μM bicuculline to block $GABA_A$ receptors) had no effect on the $GABA_C$ receptor response of retinal bipolar cells to 30 μM GABA, a dose which was chosen to be sub-saturating (the mean EC_{50} in slices is around 40 μM; see Figure 3.14) so that I might observe changes in either the EC_{50} or the maximum current (Figure 3.19 A). In five cells, the current in the presence of glycine was 101.8 ± 2.4 % of the control current in the absence of glycine (Figure 3.19 B). No glycine uptake current was detectable in the bipolar cells, so I could not test the effect of $GABA_C$ receptor activation on the rate of glycine uptake.

Figure 3.18: GLYT-1E/F and MAP-1B interact with different regions of the ρ_1 intracellular loop

(A) Immobilized GST-GLYT-1E/F (lanes 5 and 6) or GST-MAP-1B$^{460\text{-}585}$ (lanes 3 and 4) were incubated first with extract of COS cells transfected with ρ_1^{myc}, followed by 250 nM of the MAP-1B binding site peptide (+) containing RINTHAIDKYSR, or of the peptide containing a scrambled version (–) of the binding site peptide. ρ_1^{myc} bound to beads after this treatment was determined by Western blotting and probing against *myc*. "GST" shows lack of binding of ρ_1^{myc} to GST alone, and "in" represents the ρ_1^{myc} present in 5% of the input. **(B) Upper panel**: Alignment of the extreme C-terminal regions of the intracellular TM3-TM4 loop of the ρ_1 and α_1 subunits. The amino acid substitutions made are shown in boxes; identical amino acids were not mutated. **Lower panel**: Immobilized GST-GLYT-1E/F was incubated with extracts of COS cells transfected with mutants of ρ_1^{myc} in pull-down assays. Groups of residues in ρ_1 were mutated to the equivalent sequence of the α_1 subunit of $GABA_A$ receptors (see Figure 3.3). For each construct, "in" represents the ρ_1^{myc} present in 5% of the input, and "bd" represents protein bound to GST-GLYT-1E/F; "GST" shows lack of binding of ρ_1^{myc} to GST alone.

This work was carried out by my collaborator Jonathan Hanley.

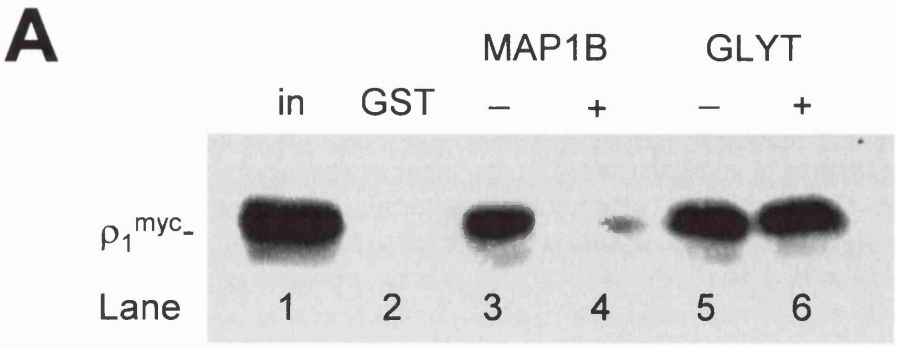
A
MAP1B
GLYT
in
GST
–
+
–
+
ρ1myc-
Lane
1
2
3
4
5
6

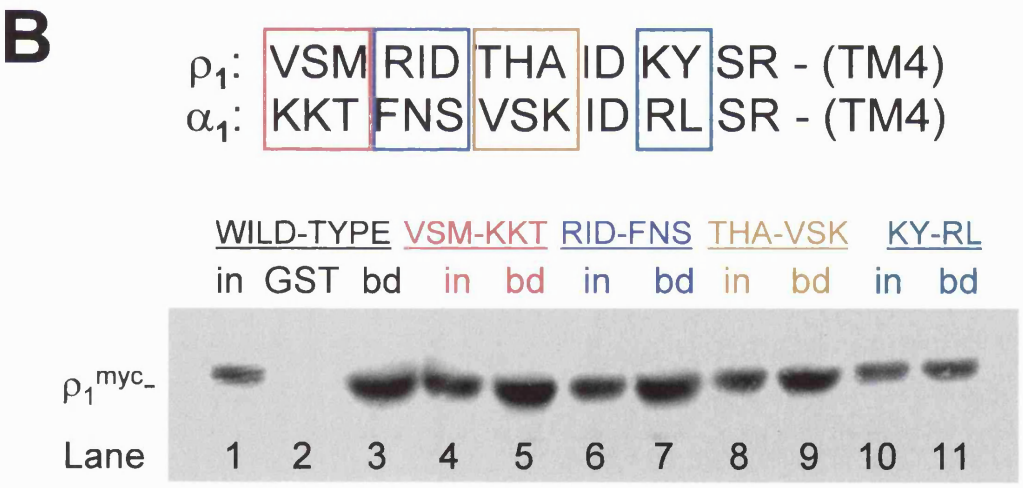
B
ρ1: VSM RID THA ID KY SR - (TM4)
α1: KKT FNS VSK ID RL SR - (TM4)
WILD-TYPE
VSM-KKT
RID-FNS
THA-VSK
KY-RL
in GST bd in bd in bd in bd in bd
ρ1myc-
Lane
1 2 3 4 5 6 7 8 9 10 11

Figure 3.19: Effect of glycine on $GABA_C$ receptor mediated currents in slice bipolar cells

(A) Specimen currents recorded from a slice bipolar cell voltage clamped at -60 mV. GABA (30 μM) was applied in the presence of 300 μM bicuculline and 10 μM strychnine either in the absence (1st and 3rd trace) or presence (2nd trace) of 300 μM glycine. **(B)** Averaged data from 5 slice bipolar cells recorded as described in A. The $GABA_C$ receptor mediated response to GABA (black bar) remains unchanged when 300 μM glycine is co-applied.

A

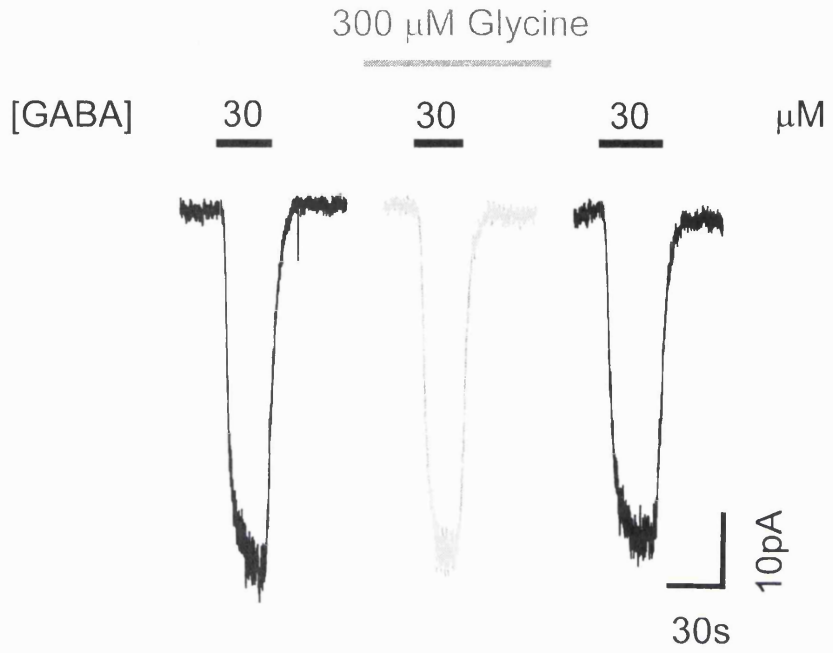
300 μM Glycine
[GABA]
30
30
30
μM
10pA
30s

B

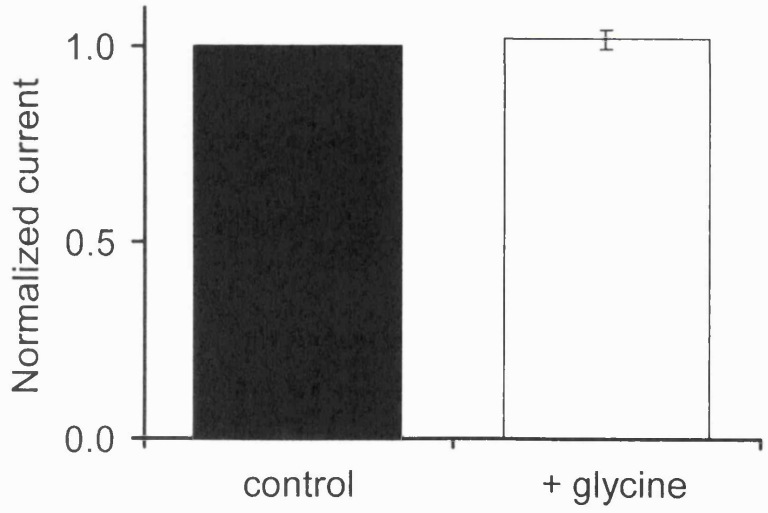
Normalized current
1.0
0.5
0.0
control
+ glycine

3.17. Discussion

The experiments described in this chapter were carried out to (1) narrow down the MAP-1B binding site on ρ_1 and create peptides which could be used in the electrophysiological experiments (sections 3.1 to 3.3), (2) investigate whether MAP-1B influences $GABA_C$ receptor properties (sections 3.4 to 3.13), (3) see if GLYT-1E/F and MAP-1B share the same binding site on ρ_1 (section 3.15), and (4) see if glycine alters $GABA_C$ receptor mediated responses (section 3.16).

3.17.1 The binding site of MAP-1B on ρ_1

Analysis of the binding site for MAP-1B on the ρ_1 subunits of $GABA_C$ receptors suggested that MAP-1B binds to the last 12, most C-terminal amino acids of the large intracellular loop joining TM3-TM4 with the sequence R^{443} I $(D/N)^{445}$ T H A I^{449} D K Y S R^{454} (where D/N denotes the human/rat sequence). Of this sequence, K^{451} Y^{452} seems crucial, as mutating these two amino acids prevents binding (Figure 3.3). The other C-terminal residues I^{449} D^{450} and S^{453} R^{454} may contribute to binding, but are preserved in the $GABA_A$ receptor α and β subunits, which do not interact with MAP-1B. Mutating the more N-terminal amino acids $T^{446}H^{447}A^{448}$ or $R^{443}I^{444}D^{445}$ to the homologous amino acids in α_1 subunits also reduced binding, indicating that these amino acids contribute to binding as well (Figure 3.3). The rat sequence peptide, containing N^{445}, competes well with human ρ_1, which contains D at the D/N position, indicating that binding occurs whether N or D is present at this site (Figure 3.4). Mutating the even more N-terminal amino acids $V^{440}S^{441}M^{442}$ to KKT did not affect binding, suggesting that the binding site does not extend N-terminally beyond R^{443}. Competition assays using synthesized peptides representing this amino acid stretch indicate that these 12 residues are sufficient for binding (Figure 3.4). Thus, the 12 most C-terminal amino acids of the large

intracellular loop of ρ_1 form a binding site for MAP-1B.

The question arises as to whether this amino acid stretch is present in other proteins also, since if it were, the peptide I used in my electrophysiological experiments might have non-specific actions. Comparison to other proteins in the NCBI database show that the motif **R I (N/D) T H A I D K Y S R** in its entirety is unique to ρ_1. However, another $GABA_C$ receptor subunit, ρ_2, has an equivalent 12 amino acid motif of F Q **N T H A I D K Y S R**, i.e. only the two most N-terminal amino acids differ from those in ρ_1. ρ_2 also has been shown to bind MAP-1B in pull down assays (Billups et al., 2000). This suggests a minimal binding motif of N T H A I D K Y S R. The other $GABA_C$ receptor subunit, ρ_3, contains the sequence L E **N N H V I D** T **Y S R**, but was not tested for pull-down of MAP-1B in that study. The major $GABA_A$ receptor subunits do not show high homology with ρ in this region, the most similar being the β subunit region (e.g. β_3: L T **D** V N **A I D** R W **S R**). Consistent with these differing sequences are results from pull-down assays and immunoprecipitation from retina, which demonstrate that MAP-1B does not bind to $GABA_A$ receptors (Hanley et al., 1999; Billups et al., 2000).

Whereas $GABA_C$ receptors seem to be anchored to the cytoskeleton via the microtubule associated protein MAP-1B (Hanley et al., 1999), $GABA_A$ receptors may be anchored by interaction with an as yet unknown protein linking them to the tubulin binding protein gephyrin (Moss and Smart, 2001), or through gephyrin-independent mechanisms which are as yet not fully understood (Fischer et al., 2000; Kneussel et al., 2001). The existence of the different tethering molecules for $GABA_A$ and $GABA_C$ receptors may help to explain their specific localization at different synapses and their lack of co-localization in bipolar cells (Enz et al., 1996; Koulen et al., 1998a).

It is interesting that the microtubule-binding protein GABARAP, which was first suggested to anchor $GABA_A$ receptors to the cytoskeleton (Wang et al., 1999; Wang and Olsen, 2000), but is now thought to be involved in the intracellular

trafficking, targeting and clustering of the receptors (Chen et al., 2000a; Kneussel et al., 2000), shows 31% identity to the light-chain-3 of MAP-1A and MAP-1B, and it binds to γ_2 subunits in a C-terminal region of their TM3-TM4 loop at an equivalent position to the MAP-1B binding site on ρ_1/ρ_2. Moreover, co-expressing GABARAP and $GABA_A$ receptors ($\alpha_1\beta_2\gamma_2L$) in cultured QT-6 quail fibroblasts not only promotes $GABA_A$ receptor clustering, but produces a decreased apparent affinity for GABA, faster deactivation and slower desensitization kinetics than cells displaying diffuse receptor localization (Chen et al., 2000a). Thus, the (1) molecular similarity between GABARAP and the light chain-3 (LC3) of MAP-1B, (2) similar binding region for both proteins on the intracellular loop of the respective receptor, and (3) decreased sensitivities of both receptors to GABA when the respective protein is bound, indicates a similar function for both proteins. However, there are differences. $GABA_C$ receptors bind to the heavy chain of MAP-1B, not the light chain to which GABARAP is similar. Furthermore, whereas MAP-1B and $GABA_C$ receptors have been shown to be co-localized in the retina, especially on bipolar cell axon terminals (Hanley et al., 1999), GABARAP has been shown **not** to co-localize with $GABA_A$ receptors in the retina (Kneussel et al., 2000), suggesting that GABARAP is important for cellular functions other than receptor anchoring.

3.17.2. Disrupting the MAP-1B – ρ_1 interaction alters $GABA_C$ receptor properties

Dialyzing retinal bipolar cells with a peptide mimicking the MAP-1B binding motif, which competitively disrupts MAP-1B – ρ_1 binding (Figure 3.4), led to a 32 % decrease in the EC_{50} of the cells $GABA_C$ receptors (Figure 3.16 B), which is sufficient to approximately double the GABA-evoked current at low GABA concentrations (section 3.13, Figure 3.15 A, B, C). At the same time, there was no change of the maximum GABA-evoked current, suggesting that binding of MAP-1B to ρ_1 does not alter the number of functional receptors in the plasma membrane or

their maximum open probability.

3.17.2.1. Comparison to other work studying protein-protein interactions

How do the results obtained in this chapter compare to other studies investigating the effect of interacting proteins on receptor or transporter function?

Nishimune et al. (1998) used a similar approach of dialyzing binding site peptides (10 amino acids of the AMPA receptor gluR2 subunit) into the cell via the patch pipette to disrupt the interaction of AMPA receptors with NSF (see section 1.7.1): disrupting this interaction in CA1 neurones of hippocampal slices or in cultured hippocampal neurones had profound effects on the amplitude of the current generated by the receptors, suggesting a decrease of the number of functional channels in the membrane. Thus, the interaction of NSF with the AMPA receptor seems to aid the insertion of functional receptor channels into the membrane rather than having a modulatory role on the receptor's properties.

Similarly, Bedford et al (2000), dialysed peptides (10 amino acids of the $GABA_A$ receptor α_1 subunit intracellular loop) via the whole cell patch pipette into HEK293 cells transfected with $GABA_A$ receptors, to disrupt the interaction of the α_1 subunit with the interacting protein GRUB1, and altered the number of GABA receptors on the cell surface, but not receptor properties such as the EC_{50} for GABA or the single channel conductance. They concluded that GRUB1 modulates receptor insertion into the plasma membrane and not receptor properties.

As a final example Marie and Attwell (1999) investigated the interaction of the glutamate transporter GLAST and an unknown intracellular protein in salamander Müller cells. Again, the approach taken was to dialyse peptides, in this case the last 8 amino acids of the C-terminus of GLAST, into the cell via the whole cell patch pipette, on the assumption that this peptide would compete with the transporter C-terminus for binding to an interacting protein. Similar to the results obtained in this chapter, disrupting the interaction of GLAST with this hypothetical

protein increased the apparent affinity of the transporter without affecting the maximal evoked current. Thus, the unknown intracellular protein appears to modulate transporter properties, but does not seem to be involved in insertion of the transporter into the membrane or its stabilization there.

The above examples demonstrate that some interacting proteins affect receptor trafficking and insertion or stabilization of proteins in the plasma membrane, while others modulate receptor functioning, as shown in this chapter. How can a cytoskeletal interacting protein such as MAP-1B affect the $GABA_C$ receptor agonist sensitivity, considering that the agonist (e.g. GABA) binds from outside the cell. One possible mechanism is that MAP-1B could alter the energetics of the conformation changes that occur when the receptor binds GABA and opens its channel, and in this way shift the EC_{50}. The rate constants which may be altered to achieve this are analyzed below (section 3.17.3).

3.17.2.2. How could the ρ_1 – MAP1B interaction be regulated?

For the alteration of $GABA_C$ receptor EC_{50} shown in Figure 3.16 to be of physiological relevance, the MAP-1B – $GABA_C$ receptor interaction would need to be modulated *in vivo*. Since the interaction was disrupted quite easily by dialyzing the binding-site peptide into the cell, it seems that this interaction could be modulatable on a reasonable time-scale. The intracellular loop of the $GABA_C$ receptor subunit contains several putative phosphorylation sites, and phosphorylation of any of these might influence MAP-1B binding. Two of these sites (serine residues) are of particular interest, as they are within, or flanking the MAP-1B binding site: S^{441} and S^{453}, with S^{441} being a consensus site for PKC phosphorylation. Interestingly, PKC has been shown to reduce $GABA_C$ receptor mediated currents in patch-clamped rat retinal bipolar cells (Feigenspan and Bormann, 1994b), although it is unclear from their experiments whether PKC decreases the maximum evoked current (e.g. due to receptor internalization: (Kusama et al., 1995; Filippova et al.,

1999)) or increases the EC_{50}. Thus, $GABA_C$ receptor functioning in retinal bipolar cells is modulatable by PKC, and this might be due, at least in part, to a modulation of MAP-1B binding.

Alternatively, the MAP-1B – $GABA_C$ receptor interaction could be modulated by phosphorylation of MAP-1B, which contains several consensus sites for phosphorylation by different kinases. Some of these phosphorylation sites, such as PKC and PKA sites (Kennelly and Krebs, 1991), are located within the binding domain for ρ_1 (amino acids 460-565 of MAP-1B (Hanley et al., 1999)), and phosphorylation at any of these sites might modulate the interaction with ρ_1.

3.17.3. Estimating the effect of increasing the EC_{50} on the IPSC duration

The above data show that MAP-1B binding increases the $GABA_C$ receptors' EC_{50} for GABA. But what is the physiological relevance of this EC_{50} change - how would a change in agonist EC_{50} affect the duration of the inhibitory post-synaptic current?

As outlined in Chapter 1, neurotransmitter gets released during synaptic transmission from the presynaptic terminal, diffuses across the synaptic cleft and binds to post-synaptic receptors. These open their channels in response to agonist binding and conduct ions. The time course of the postsynaptic current depends on (a) the receptor channel kinetics and (b) the time course of the transmitter concentration in the synaptic cleft. Lowering the EC_{50} of the $GABA_C$ receptors, e.g. when MAP-1B unbinds from the receptor, is expected to increase the duration of the synaptic current (IPSC) in the following circumstances. First, if after the peak of the IPSC the extracellular GABA concentration falls slowly compared to the receptor and channel gating kinetics, then if the EC_{50} is lower the GABA concentration will have to fall to a lower level before the receptors can deactivate, which will take longer. Alternatively, if the GABA concentration falls to zero rapidly (compared with the

GABA unbinding and channel gating kinetics), then a lower EC_{50} is predicted to prolong the IPSC decay provided that the effect of MAP-1B on the EC_{50} is mediated by an alteration of the rate constant for GABA unbinding (k_2) or for channel opening (β) or channel closing (α). However, there will be no effect on the IPSC decay if the EC_{50} is lowered by increasing the GABA binding rate (k_1) (Jones et al., 1998). To illustrate quantitatively the latter situation (rapid fall of $[GABA]_O$), I calculated how a change of EC_{50} (produced by a change in either of the rate constants k_2, β or α) would affect the time course of the IPSC.

The first step in this analyzis was to determine the change of rate constant needed to produce the observed change of EC_{50}. A recent paper (Chang and Weiss, 1999) describes experiments investigating the binding and gating properties of $GABA_C$ receptors expressed in *Xenopus* oocytes (homomeric human ρ_1). The authors proposed a kinetic scheme for the $GABA_C$ receptor in which there are five GABA binding sites, but channel opening occurs when three GABA molecules are bound.

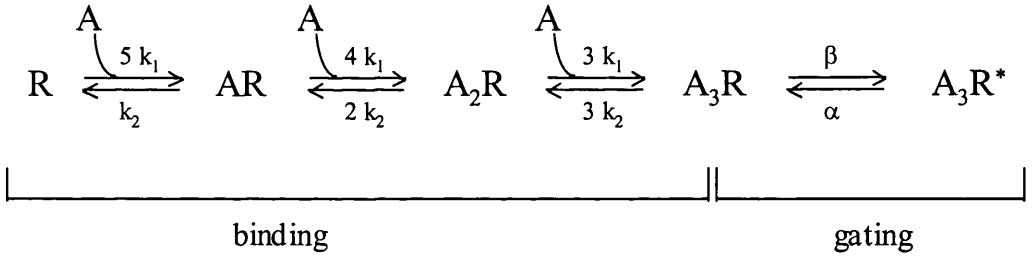

A - agonist
R – receptor, closed channel
R* - receptor, open channel
k_1 - binding rate constant
k_2 - unbinding rate cnstant
α - closing rate constant
β - opening rate constant

Chang and Weiss determined the rate constants for such a kinetic scheme from their experimental data, which I will use for the calculations below.

To work out by how much the rate constants need to change to produce the observed change in EC_{50} (when MAP-1B binding is altered), one needs to analyze

the full reaction scheme to work out the EC_{50}. The fraction of receptors in each state will be abbreviated as:

A_3R^* – **x** (fraction of receptors in state A_3R^* - channel open)

A_3R – **y** (fraction of receptors in state A_3R)

A_2R – **z** (fraction of receptors in state A_2R)

AR – **w** (fraction of receptors in state AR)

R – **1-x-y-z-w** (fraction of receptors in state R – no GABA bound)

In equilibrium:

(a) $\beta \cdot y = \alpha \cdot x$

(b) $3 \cdot k_1 \cdot A \cdot z = 3 \cdot k_2 \cdot y$

(c) $4 \cdot k_1 \cdot A \cdot w = 2 \cdot k_2 \cdot z$

(d) $5 \cdot k_1 \cdot A \cdot (1 - x - y - z - w) = k_2 \cdot w$

with (a), (b) and (c) put into (d):

$$x = \frac{1}{1 + \frac{\alpha}{\beta} + \frac{\alpha}{\beta} \cdot \frac{k_2}{k_1 \cdot A} + \frac{1}{2} \cdot \frac{\alpha}{\beta} \cdot \left(\frac{k_2}{k_1 \cdot A} \right)^2 + \frac{1}{10} \cdot \frac{\alpha}{\beta} \cdot \left(\frac{k_2}{k_1 \cdot A} \right)^3} \tag{3.4}$$

The maximum channel opening is produced when the GABA concentration is saturating, i.e. $A \rightarrow \infty$. Then the maximum open probability is:

$$x_{max} = \frac{1}{1 + \frac{\alpha}{\beta}} \tag{3.5}$$

At the EC_{50} ($A=A_{1/2}$) the fraction of open channels (x) is $x_{max}/2$, so

$$1 + \frac{\alpha}{\beta} = \frac{\alpha}{\beta} \cdot \frac{k_2}{k_1 \cdot A_{1/2}} + \frac{1}{2} \cdot \frac{\alpha}{\beta} \cdot \left(\frac{k_2}{k_1 \cdot A_{1/2}} \right)^2 + \frac{1}{10} \cdot \frac{\alpha}{\beta} \cdot \left(\frac{k_2}{k_1 \cdot A_{1/2}} \right)^3 \tag{3.6}$$

With the rate constants obtained by Chang and Weiss:

$k_1 = 0.96 \cdot 10^5 /Ms$

$k_2 = 0.18/s$

$\alpha = 0.31/s$

$\beta = 3.6/s$

solving equation 3.6 iteratively gives $A_{1/2}$ = 0.562 μM, which is similar to the 0.6 μM predicted and observed by Chang and Weiss.

The data in Figure 3.16 B show that disrupting the MAP-1B – ρ_1 interaction decreases the EC_{50} to around 68%. That means that binding of MAP-1B increases the EC_{50} of the receptor by 47% (1/0.68 = 1.47), i.e. from 0.526 to 0.826 μM (assuming that MAP-1B is not binding in the oocytes used by Chang & Weiss (1999)). This change of EC_{50} ($A_{1/2}$) could be produced by the following changes in the rate constants.

(I) Changing k_1: equation 3.6 shows that k_1 is reciprocally proportional to $A_{1/2}$, so if

k_1 changes from	$0.96 \cdot 10^5$	to	$0.65 \cdot 10^5 /Ms$
$A_{1/2}$ changes from	0.562	to	0.826 μM

(II) Changing k_2: equation 3.6 shows that k_2 is directly proportional to $A_{1/2}$, so if

k_2 changes from	0.18	to	0.265 /s
$A_{1/2}$ changes from	0.562	to	0.826 μM

(III) Changing α: solving equation 3.6 for α shows that if

α changes from	0.31	to	0.718 /s
$A_{1/2}$ changes from	0.562	to	0.826 μM

(IV) Changing β: solving equation 3.6 for β shows that if

β changes from	3.6	to	1.555 /s
$A_{1/2}$ changes from	0.562	to	0.826 μM

The 47% increase in EC_{50} that occurs when MAP-1B binds to the $GABA_C$ receptor could be produced by MAP-1B changing any of the four rate constants to the extent just described. But how does changing the $GABA_C$ receptor rate constants affect the time course of the IPSC? When the extracellular GABA concentration drops rapidly to zero after GABA has been present for some time, the kinetic scheme above simplifies to:

$$A_2R \underset{3\,k_2}{\longleftarrow} A_3R \underset{\alpha}{\overset{\beta}{\rightleftarrows}} A_3R^*$$

since there is no rebinding of GABA when [GABA] = A = 0. The fraction of receptors in each state will now be abbreviated as:

A_3R^* - **x** (fraction of receptors in state A_3R^* - channel open)

A_3R - **y** (fraction of receptors in state A_3R)

A_2R - **1-x-y** (fraction of receptors in state A_2R)

Ions can only permeate when the $GABA_C$ receptor channels are open, i.e. in state A_3R^*. So in order to understand how the time-course of the IPSC is altered by changes in channel kinetics, we need to consider how the fraction of open channels (x) change with time.

Initially at t=0:

$$\beta \cdot y_0 = \alpha \cdot x_0 \tag{3.7}$$

Generally:

$$\frac{dx}{dt} = \beta \cdot y - \alpha \cdot x \tag{3.8}$$

and

$$\frac{dy}{dt} = \alpha \cdot x - \beta \cdot y - 3 \cdot k_2 \cdot y \tag{3.9}$$

Differentiating equation 3.8 gives:

$$\frac{d^2x}{dt^2} = \beta \cdot \frac{dy}{dt} - \alpha \cdot \frac{dx}{dt} \tag{3.10}$$

merging 3.8 and 3.9 into 3.10 gives:

$$\frac{d^2x}{dt^2} + \frac{dx}{dt} \cdot (\beta + \alpha + 3 \cdot k_2) + 3 \cdot k_2 \cdot \alpha \cdot x = 0 \tag{3.11}$$

Equation 3.11 has the solution:

$$x(t) = x_1 \cdot e^{-\lambda_1 \cdot t} + x_2 \cdot e^{-\lambda_2 \cdot t} \tag{3.12}$$

where

$$\lambda_{1/2} = \frac{\beta + \alpha + 3 \cdot k_2}{2} \pm \sqrt{\left(\frac{\beta + \alpha + 3 \cdot k_2}{2}\right)^2 - 3 \cdot k_2 \cdot \alpha} \tag{3.13}$$

and x_1 and x_2 are the constants set by the initial conditions.

Using the values for the rate constants from Chang & Weiss (see above) gives:

$\lambda_1 = 4.412$ /s

$\lambda_2 = 0.038$ /s

That means that the fraction of open channels (x) decays with two exponential components - one fast (λ_1) and one slow (λ_2) one. To obtain the values of x_1 and x_2 I proceed as follows. Rearranging equation 3.8 to:

$$y = \frac{1}{\beta} \cdot \frac{dx}{dt} + \frac{\alpha}{\beta} \cdot x \tag{3.14}$$

and substituting x and dx/dt from equation 3.12 and its derivative gives:

$$y(t) = x_1 \cdot e^{-\lambda_1 \cdot t} \cdot \left(\frac{\alpha - \lambda_1}{\beta}\right) + x_2 \cdot e^{-\lambda_2 \cdot t} \cdot \left(\frac{\alpha - \lambda_2}{\beta}\right) \tag{3.15}$$

At t = 0 (when the GABA concentration jumps to zero) equation 3.12 gives:

$$x(0) = x_1 + x_2 \tag{3.16}$$

and equation 3.15 gives:

$$y(0) = x_1 \cdot \left(\frac{\alpha - \lambda_1}{\beta} \right) + x_2 \cdot \left(\frac{\alpha - \lambda_2}{\beta} \right) \tag{3.17}$$

Rearranging equation 3.7 gives:

$$y(0) = \frac{\alpha}{\beta} \cdot x(0) . \tag{3.18}$$

From (3.17) and (3.18), eliminating y(0) gives:

$$x_1 = -\frac{\lambda_2}{\lambda_1} \cdot x_2 . \tag{3.19}$$

Merging equation 3.19 with equation 3.12 gives:

$$x(t) = x_2 \cdot e^{-\lambda_2 \cdot t} \cdot \left(1 - \frac{\lambda_2}{\lambda_1} \cdot e^{(-\lambda_1 + \lambda_2) \cdot t} \right) \tag{3.20}$$

With $\lambda_1 = 4.412$ /s and $\lambda_2 = 0.038$ /s (from equation 3.13) the second component in brackets is very small (tiny amplitude and fast decay) and equation 3.20 reduces thus to:

$$x(t) = x_2 \cdot e^{-\lambda_2 \cdot t} \tag{3.21}$$

The fraction of open channels x, and the IPSC, therefore decays with a time constant of

$$\tau_{decay} = \frac{1}{\lambda_2} \tag{3.22}$$

where λ_2 is given by equation 3.13. Using equations 3.13 and 3.22 one can now calculate the time constant of the IPSC when either of the rate constants is altered to

produce the increase of EC_{50} which is produced by MAP-1B binding. The results of these calculations are summarized in this table:

τ_{decay}	k_1 (/Ms)	k_2 (/s)	α (/s)	β (/s)	$A_{1/2}$ (μM)	λ_2 (/s)	τ_{decay} (s)	% change of τ when MAP-1B unbinds
Control (MAP-1B not bound)	96000	0.18	0.31	3.6	0.562	0.038	**26.4**	
Changing k_1	**65000**	0.18	0.31	3.6	0.826	0.038	**26.4**	0
Changing k_2	96000	**0.265**	0.31	3.6	0.826	0.053	**18.9**	40% up
Changing α	96000	0.18	**0.718**	3.6	0.826	0.081	**12.3**	114% up
Changing β	96000	0.18	0.31	**1.555**	0.826	0.072	**13.9**	89% up

Table 3.1: Predictions of the IPSC time course

As expected, changing the binding rate (k_1) does not affect the IPSC time course when GABA concentration drops rapidly compared to the channel kinetics, because if $[GABA]_O$ has fallen to zero there can be no binding of GABA. However, producing the observed 32% decrease in EC_{50} (when MAP-1B unbinds from the $GABA_C$ receptor) by either decreasing the unbinding rate (k_2), increasing the channel opening rate (β) or decreasing the channel closing rate (α) leads to the IPSC decay time constant being increased by 40, 89 or 114%, respectively. The prolongation of deactivation, and hence of the IPSC, by changes in any of the rate constants are shown in Figure 3.20. These predicted changes in the $GABA_C$ receptor mediated IPSC time course are likely to have profound effects on retinal signal processing, as discussed in more detail in Section 3.17.4.

Figure 3.20: Estimating the effect of increasing the EC_{50} on the IPSC duration

(A) Schematic drawing of a GABAergic synapse. $GABA_C$ receptors, which are located in the postsynaptic membrane, interact with the microtubule associated protein MAP-1B, which binds to microtubules and actin. $GABA_C$ receptors also interact with the glycine transporter GLYT-1E/F. When $GABA_C$ receptors open they conduct anions, such as chloride. In this example (model, no real data) GABA evokes an inward current, which is predicted to decay (deactivate) with a time constant of 26.4 seconds when GABA is removed (the time constant is calculated with equation 3.13 and 3.22, as described in the text and table 3.1).

(B) Same as in A, but with MAP-1B unbound from the $GABA_C$ receptor. The observed decrease in EC_{50} when the $GABA_C$ receptor – MAP-1B interaction is disrupted could be due to a change in either of the rate constants, as explained in the text. A change of k2, alpha or beta is predicted to speed up the deactivation time constant (see text and table 3.1 for calculations and explanations). Control is with no rate constant changed (same as in (A) when MAP-1B is bound), k2 is the unbinding rate constant, alpha is the closing rate constant and beta is the opening rate constant. The lines are single exponentials with time constants of 26.4 seconds (control), 18.9 seconds (k2 changed), 12.3 seconds (alpha changed) and 13.9 seconds (beta changed).

A

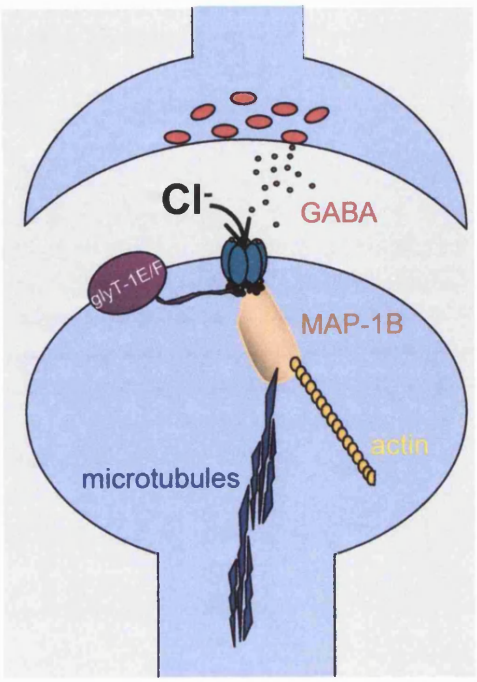
Cl-
GABA
glyT-1E/F
MAP-1B
actin
microtubules

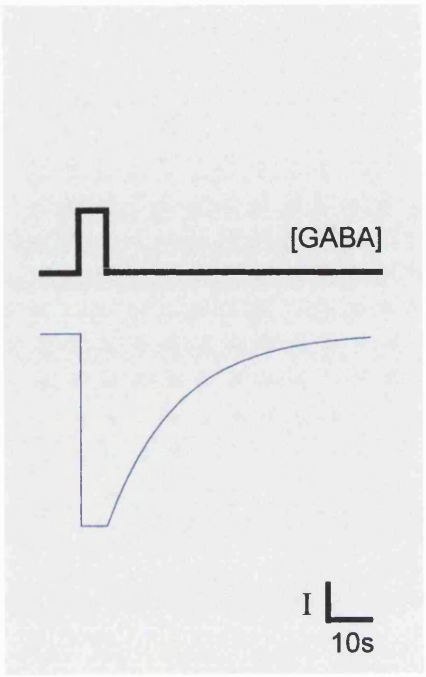
[GABA]
I
10s

B

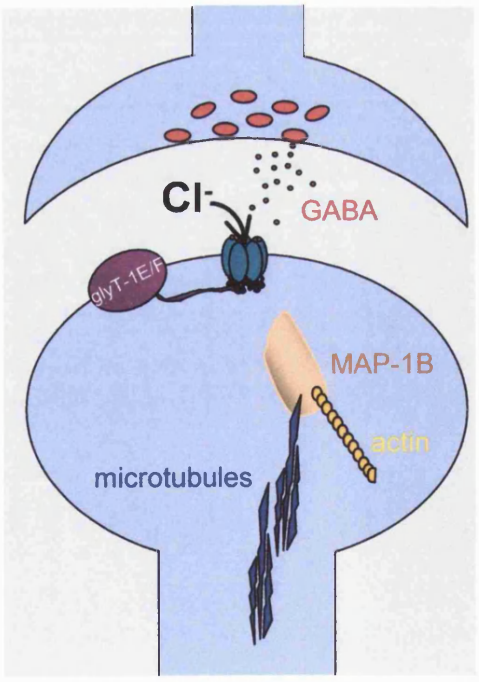
Cl-
GABA
glyT-1E/F
MAP-1B
actin
microtubules

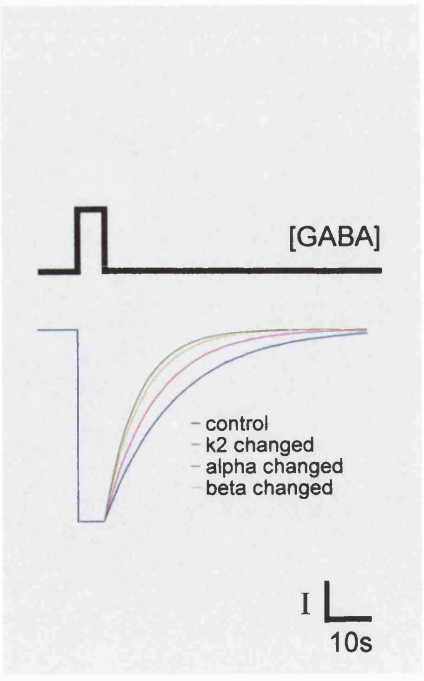
[GABA]
control
k2 changed
alpha changed
beta changed
I
10s

It is not clear which of the four rate constants is in fact affected by MAP-1B binding. To try to determine this, I used equation 3.5 to calculate the expected changes in the maximum evoked current when each of the rate constants is changed as described above. The results are summarized in this table:

$\mathbf{I_{max}}$	k_1 (/Ms)	k_2 (/s)	α (/s)	β (/s)	$A_{1/2}$ (μM)	I_{max}	% change of τ when MAP-1B unbinds
Control (MAP-1B not bound)	96000	0.18	0.31	3.6	0.562	**0.921**	
Changing k_1	**65000**	0.18	0.31	3.6	0.826	**0.921**	0
Changing k_2	96000	**0.265**	0.31	3.6	0.826	**0.921**	0
Changing α	96000	0.18	**0.718**	3.6	0.826	**0.834**	10.4% up
Changing β	96000	0.18	0.31	**1.555**	0.826	**0.834**	10.4% up

Table 3.2: Calculation of I_{max}

Whereas changing k_1 or k_2 does not affect I_{max}, decreasing the closing rate (α) or increasing the opening rate (β) when MAP-1B unbinds from the receptor increases the I_{max} by around 10%. This change of I_{max} is small and might not have been detected in my recordings. It is therefore not possible to use measurements of I_{max} to determine which rate constant MAP-1B alters to produce the shift in EC_{50}.

Figure 3.21: Wiring diagram showing the role of $GABA_C$ receptors in the retina

Photoreceptor layer is at the top, ganglion cell layer (GCL) is at the bottom. Synapses from the photoreceptors and bipolar cells release glutamate as a transmitter. Horizontal cells, interplexiform cells and Müller cells are not shown in this diagram.

ONL = outer nuclear layer
OPL = outer plexiform layer
INL = inner nuclear layer
IPL = inner plexiform layer
a, b = sublamina in IPL

Inset shows a cartoon of a reciprocal synapse formed between bipolar cells and amacrine cells in the inner plexiform layer. $GABA_C$ receptors are located on the bipolar cell terminal where they mediate negative feedback inhibition when bipolar cells excite A17 or AII amacrine cells. AII amacrine cells also send gap junctional synapses (black vertical bar in main picture) to cone bipolar cells.

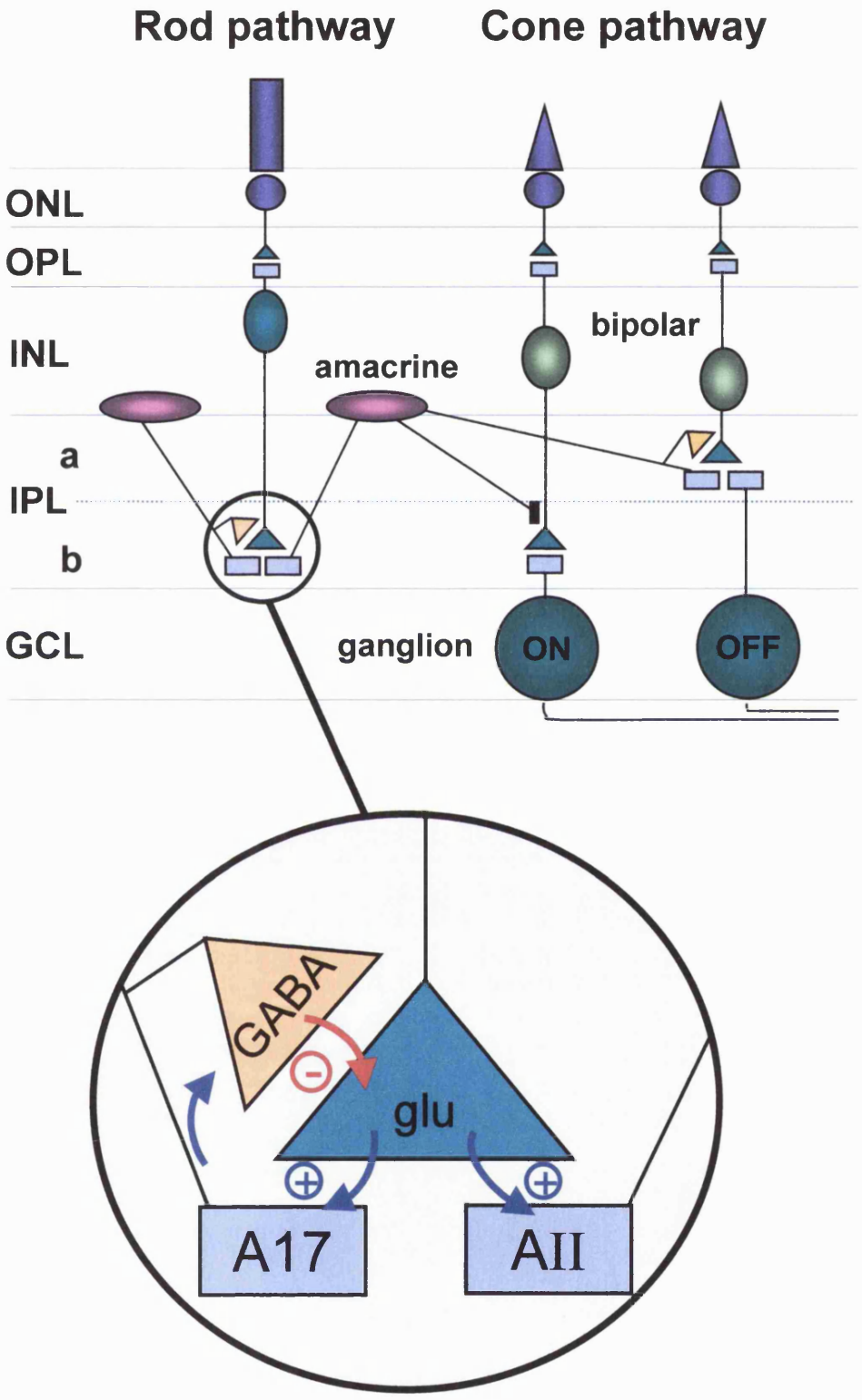
Rod pathway
Cone pathway
ONL
OPL
INL
bipolar
amacrine
a
IPL
b
GCL
ganglion
ON
OFF
GABA
glu
A17
AII

3.17.4. Physiological relevance of the MAP-1B – ρ_1 interaction in the retina

As shown in Figure 3.21, and described in section 1.8, bipolar cells transmit information from the outer to the inner retina, where they release glutamate onto ganglion and amacrine cells. Glutamate release is modulated by the activity of GABAergic synapses from amacrine cells to the bipolar cell synaptic terminal, where GABA acts on $GABA_A$ and $GABA_C$ receptors. The contribution of $GABA_C$ receptors, which desensitize much less than $GABA_A$ receptors, is particularly important because of the long graded depolarizations occurring in retinal cells and the fact that in the retina low levels of GABA are likely to be present at all times, since they desensitize much less than $GABA_A$ receptors. Decreasing the EC_{50} of $GABA_C$ receptors by 32% (by unbinding of MAP-1B) roughly doubles the current that these receptors carry at low GABA concentrations (see section 3.13), which will increase tonic inhibition of glutamate release from the bipolar cell axon terminal, decrease ganglion cell firing and thus affect the output of the retina. Temporal aspects of the alteration by MAP-1B of $GABA_C$ inhibition are considered below.

MAP-1B may affect not only the $GABA_C$ receptor sensitivity, but also the anchoring and localization of $GABA_C$ receptors in the plasma membrane. Although both $GABA_A$ and $GABA_C$ receptor mediated currents can be recorded from one cell (Figures 3.8, 3.12), immunohistochemistry and immuno-gold labelling showed no co-localization of $GABA_A$ and $GABA_C$ receptors (see section 1.4), suggesting that the two receptor types do (a) not co-assemble in these cells (but see (Qian and Ripps, 1999; Pan et al., 2000) for co-assembly of $GABA_A$ and $GABA_C$ subunits co-expressed in oocytes), and (b) are present at different synapses in the cell (Koulen et al., 1998a). Since $GABA_A$ and $GABA_C$ receptors mediate currents of very different kinetics (see section 1.4), the presence of both receptor types in one axon terminal suggests that the time course of the GABAergic inhibition received from amacrine

cells, and thus the cell's membrane potential and the time course of glutamate release onto ganglion and amacrine cells, will depend strongly on the relative contribution of $GABA_A$ and $GABA_C$ receptor mediated currents in the terminal (Shields et al., 2000). Disrupting the MAP-1B – $GABA_C$ receptor interaction could shift the ratio of the $GABA_A$: $GABA_C$ receptor mediated currents in the cell and thus influence the kinetics of the cell's glutamate release by (a) causing the $GABA_C$ receptors to move to a more extrasynaptic location, and (b) changing the duration of the $GABA_C$ receptor mediated IPSC.

When bipolar cells are depolarized, they release glutamate onto postsynaptic cells; in turn they receive GABAergic input from the amacrine cells they just excited (Figure 3.21, inset), which shortens their synaptic output. It has been shown that this feedback inhibition increases the dynamic range of the bipolar cell (Euler and Masland, 2000) and produces temporal and spatial shaping of the visual signal, making signals more transient and enhancing edge detection (Dong and Werblin, 1998; Jacobs and Werblin, 1998; Roska et al., 2000). All of these studies emphasize the importance of $GABA_C$ receptors located on bipolar cells in this feedback loop, which produce long lasting IPSCs in bipolar cells when amacrine cells release GABA (Lukasiewicz and Shields, 1998; Shields et al., 2000). A prolongation of the IPSC, as expected when the EC_{50} for GABA is lowered if MAP-1B unbinds from the receptor, see section 3.17.3), would be expected to alter the spatio-temporal filtering mediated by this feedback synapse.

Interestingly, a novel mechanism in retinal processing has been described in mammals recently (Roska and Werblin, 2001), which the authors coined "vertical inhibition", by analogy with the well described "lateral inhibition" which occurs in the OPL by means of inhibitory horizontal cells. Vertical inhibition takes place in the IPL, and $GABA_C$ receptors located on bipolar cells play a crucial role in this mechanism. From the branching pattern and stratification level of the bipolar cell axon terminals and ganglion cell dendrites, one can distinguish ten different layers

(strata) within the IPL (Euler and Wassle, 1995). The processes of inhibitory amacrine cells are ideally positioned to carry information and mediate vertical inhibition between these strata. Roska & Werbin (2001) showed that the different strata receive unique and distinct excitatory and inhibitory inputs, which are integrated to form at least ten different, parallel space-time spiking outputs from the different ganglion cell types. As a result, the information about the visual signal is transmitted to higher centres in a set of parallel channels. This division into strata was shown to be mediated by $GABA_C$ receptors – for example, blocking $GABA_C$ receptors transformed the response to light in a class of ON ganglion cell to show an additional OFF response when the light was turned off. Any change in $GABA_C$ receptor properties, e.g. modulation of their GABA sensitivity by interaction with MAP-1B, would thus be expected to interfere with the mechanism of vertical inhibition, altering the ganglion cell output and changing the way visual signals are transmitted to higher centres.

3.17.4.1. Properties of $GABA_C$ receptor knock-out and MAP-1B knock-out mice

Knock-out mice can yield valuable information about the functional importance of the knocked-out protein, but since this protein is absent all through the development of the animal, one has also to be aware that other proteins can and probably will be up- or down-regulated in response to the knock-out. It is nevertheless of interest to study the phenotype and physiology of these mice to try to gain further insight into the functional role of the protein. Of most interest for the project described in this chapter are mice lacking $GABA_C$ receptors and mice lacking MAP-1B, so I will briefly describe the results obtained on these mice by others.

One group has generated a $GABA_C$ receptor ρ_1 knock-out mouse (Miller et al., 2000). The mice had a normal phenotype. Preliminary experiments recording electroretinograms (ERGs) from these mice revealed subtle abnormalities in the knock-out mice, e.g. an increase in the number and amplitude of the oscillatory

potentials preceding the b-wave, suggesting that $GABA_C$ receptors play a role in the retinal circuitry that mediates these oscillations. However, these data were only preliminary, and one awaits a more thorough characterization of these mice.

Several groups have generated MAP-1B knock-out mice (Edelmann et al., 1996; Takei et al., 1997; Takei et al., 2000), but their results are contradictory, and might be explained by the different gene disruption strategies the groups employed. Edelmann et al (1996) did not delete the entire MAP-1B gene, but disrupted it in a position corresponding to amino acid 571, that is just before the putative microtubule binding region, which should theoretically result in a truncated version of MAP-1B, i.e. the first 571 amino acids of MAP-1B, being synthesized (the authors claim not to detect this truncated polypeptide, but see Takei et al (1997) for discussion on this issue). The homozygotes of these "MAP1B571" mice died during embryogenesis, whereas the heterozygotes survived, but displayed severe phenotypic abnormalities, such as slower growth rates, motor system defects and loss of visual acuity. Furthermore, histological analysis of the heterozygote animals revealed abnormalities most notably in the cerebellum and the retina. Takei and co-workers generated two different mouse strains – one disrupting the entire gene for MAP-1B (resulting theoretically in expression of only 11 amino acids of MAP-1B), known as the "R21" mouse (Takei et al., 1997), and another one with a double mutation lacking another microtubule associated protein, tau, as well as MAP-1B (Takei et al., 2000). In contrast to Edelmann's MAP1B571 mouse, the homozygotes of the R21 mouse survived to adulthood and showed only slight decreases in brain weight and delayed nervous system development. Moreover, the R21 heterozygotes did not show any abnormalities in their development or behaviour. However, the presence of tau might have compensated for the loss of MAP-1B in the R21 mice, and the properties of the double-knock out mice, lacking both MAP-1B and tau, indicated that these two proteins act in a synergistic fashion. These mice survived to adulthood, but with increased incidents of postnatal death, and displayed most

notably defects in axonal elongation and neuronal migration. Unfortunately, the authors have not investigated any possible changes of visual function or retinal morphology.

In terms of my project, the defects in retinal morphology and the loss of visual acuity of the MAP1B571 mice described by Edelmann et al (1996) are of most interest and support a role of MAP-1B in retinal physiology, possibly involving the interaction with $GABA_C$ receptors.

3.17.5. Interaction of the glycine transporter GLYT-1E/F and the $GABA_C$ receptor ρ_1 subunit

The MAP-1B binding site peptide did not compete for binding of ρ_1 to the C-terminal tail of the glycine transporter GLYT-1E/F (Figure 3.18 A), and none of the MAP-1B binding site mutants in ρ_1^{myc} affected binding to GST-GLYT1-E/F (Figure 3.18 B), indicating that the transporter binds to a region on ρ_1 distinct from the MAP-1B binding site (Figure 3.22). This suggests that MAP1B and GLYT-1E/F may be able to interact with ρ_1 simultaneously, perhaps allowing ρ_1 and GLYT-1E/F to be anchored to the cytoskeleton as a complex. The location of GLYT-1E/F in the retina has not yet been determined: previous studies of glycine transporter location have used antibodies raised against transporter C and N termini which are not present in GLYT-1E/F. Because some bipolar cells accumulate glycine, but not via GLYT-1A or -1B (Pow and Hendrickson, 1999), it is possible that GLYT-1E/F is colocalized in bipolar cell synaptic terminals with ρ_1 subunits. Application of glycine had no effect on $GABA_C$ receptor-mediated currents (Figure 3.19), implying that if GLYT-1E/F transporters are present, their linkage to ρ_1 subunits does not result in transporter activity modulating $GABA_C$ receptor properties. It also shows that the potentiation of homomeric ρ_1 receptor activity by glycine seen in oocyte expression experiments (Calvo and Miledi, 1995) does not occur for the rat bipolar cell $GABA_C$ receptors, which are most likely heteromeric receptors containing the rat ρ_1 and ρ_2 subunits. I

have been unable to test whether activation of $GABA_C$ receptors modulates glycine uptake into bipolar cells, because the glycine uptake present in these cells is too small to generate a detectable transporter current.

Figure 3.22: Schematic diagram of ρ_1 and its interacting proteins

The large intracellular loop of the $GABA_C$ receptor subunit could interact with the glycine transporter GLYT-1E/F and possibly simultaneously with MAP-1B, which is linked to the cytoskeleton via actin and microtubules.

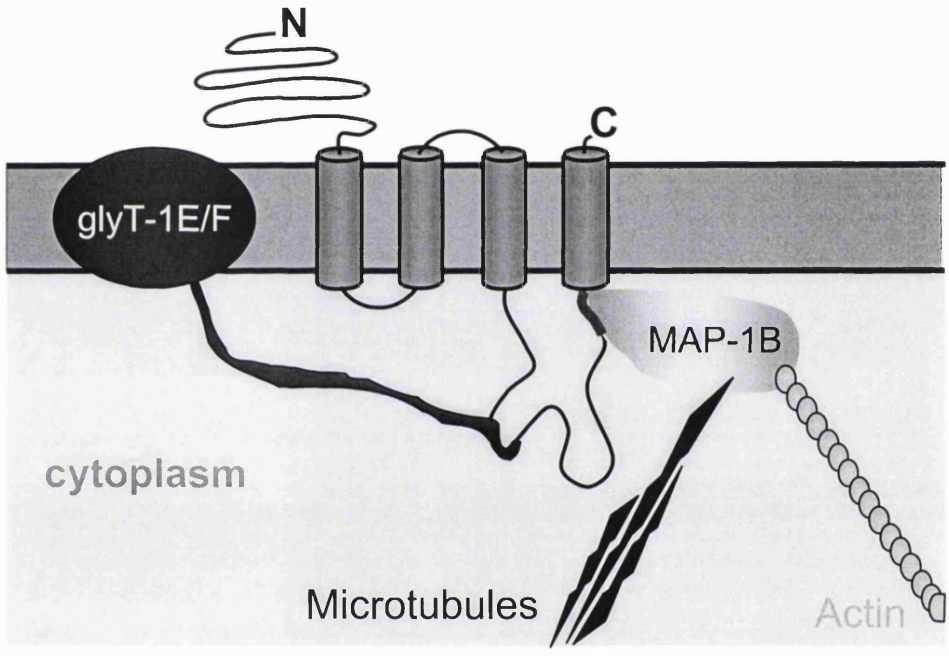
N
C
glyT-1E/F
MAP-1B
cytoplasm
Microtubules
Actin

CHAPTER 4

Control of $[Cl^-]_i$ and GABA response polarity in retinal ON bipolar cells

4.1 Introduction

The two classes of retinal bipolar cell, the ON and OFF cells, are depolarized and hyperpolarized respectively when photoreceptors in the centre of their receptive field absorb light (see section 1.8). Bipolar cells also receive lateral inhibition at their dendrites: light falling in the bipolar cell receptive field surround hyperpolarizes horizontal cells, decreasing release of their transmitter GABA, and thus hyperpolarizing ON bipolars and depolarizing OFF bipolars. Lateral inhibition plays an important role in early visual processing by removing low spatial frequencies from the visual signal, thereby enhancing the detection of edges and spots (Kuffler, 1953; Marr and Hildreth, 1980; Roska et al., 2000). It is mediated in part by a feedback synapse to photoreceptors, and in part by a feedforward signal from horizontal cells to bipolar cells, which may employ GABA release by reversed uptake as a release mechanism (Schwartz, 1982; Kondo and Toyoda, 1983; Yang and Wu, 1991; Vardi and Sterling, 1994). In addition, both ON and OFF bipolars are hyperpolarized at their synaptic terminals by GABA released from amacrine cells (see Figure 3.21 for a wiring diagram of the retina). This generates transience in the bipolar cell response, with temporal tuning characteristics that depend on the mix of $GABA_A$ and $GABA_C$ receptors expressed (Kondo and Toyoda, 1983; Tachibana and Kaneko, 1987; Euler and Wassle, 1998; Lukasiewicz and Shields, 1998; Euler and Masland, 2000; Roska et al., 2000; Shields et al., 2000).

For the feedforward signal at the dendrites to generate an antagonistic surround (i.e. hyperpolarizing in ON bipolar cells and depolarizing in OFF bipolar

cells) when GABA release from horizontal cells is decreased by light, the reversal potential of GABA-gated Cl^- channels must be more positive than the resting potential in ON cells and more negative in OFF cells. However, for GABA released from amacrine cells to hyperpolarize bipolar cells, the reversal potential of GABA-gated Cl^- channels must be more negative than the resting potential. Thus, for ON bipolar cells, there should be a gradient of intracellular chloride concentration, $[Cl^-]_i$, along the bipolar cell, being higher in the dendrites and lower in the synaptic terminals. The observed distribution of chloride transporters in bipolar cells is consistent with this prediction. Two transporters contributing to the regulation of $[Cl^-]_i$ in neurones are a Na-K-2Cl co-transporter (NKCC-1) which normally accumulates chloride, and a K-Cl co-transporter (KCC-2) that normally extrudes Cl^- (Delpire, 2000). NKCC-1 is expressed in ON bipolar dendrites where $[Cl^-]_i$ is expected to be high, while KCC-2 is expressed in OFF bipolar dendrites and ON and OFF synaptic terminals where $[Cl^-]_i$ is expected to be low (Vardi et al., 2000a; Vu et al., 2000).

This chapter describes experiments to test the functional significance of this apparent congruence between transporter location and the $[Cl^-]_i$ needed for GABAergic modulation of bipolar cell voltage. I examined how $[Cl^-]_i$ varies along the ON bipolar cell, using the response to local application of GABA (puffed on) to measure the reversal potential of the GABA-evoked current (E_{Cl}) and thus (via the Nernst equation below, equation 4.1) the value of $[Cl^-]_i$ (a possible contribution of bicarbonate to the reversal potential is considered in section 4.8). In addition I examined how $[Cl^-]_i$ is affected by the extracellular potassium concentration which is known to change during illumination (Steinberg et al., 1980), and by the membrane potential of the bipolar cell.

Figure 4.1: Identification of ON bipolar cells

Pictures of two ON bipolar cells in a retinal slice, filled with Lucifer Yellow via the whole-cell patch-pipette. The picture in (A) shows the transmitted light image (see also picture 3.11) merged with the fluorescence image taken with a CCD camera. The pictures in (B) shows the same cells as in (A) imaged with a confocal microscope. ON bipolar cells have their soma in the outermost part of the inner nuclear layer (INL), their dendrites branch in the outer plexiform layer (OPL), their axon spans the entire inner plexiform layer (IPL) before terminating as a large, bulbous axon-terminal in the inner part of the IPL. The cell on the left is a rod ON bipolar cell, whereas the cell on the right is a cone ON bipolar cell type 8 or 9 (Euler and Wassle, 1995; Euler et al., 1996; Hartveit, 1997; Euler and Wassle, 1998).

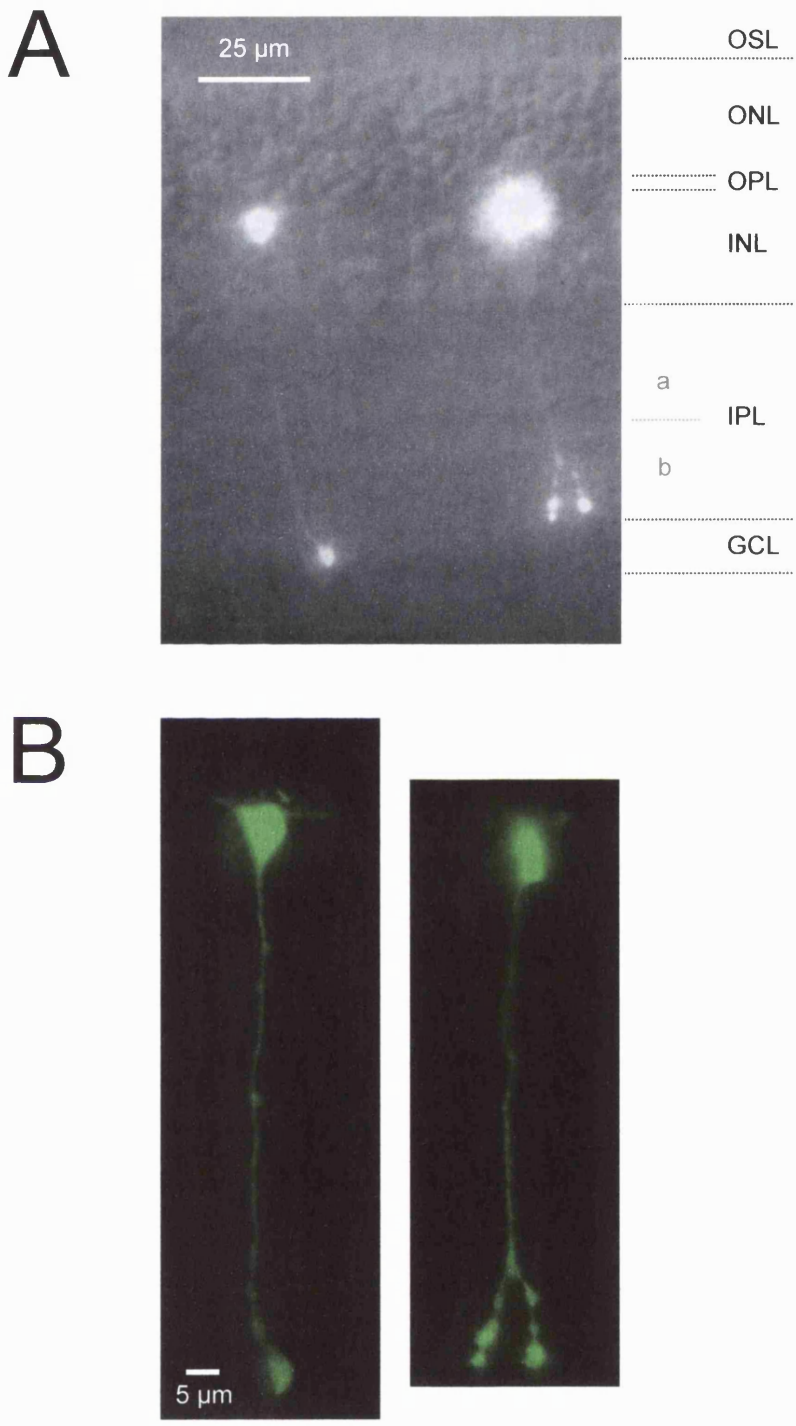
A
25 µm
OSL
ONL
OPL
INL
a
IPL
b
GCL
B
5 µm

4.2 Identification of bipolar cells

After recording GABA-evoked currents using the perforated patch technique (as described below) to avoid altering the intracellular chloride concentration, I then went to whole-cell mode and filled the recorded bipolar cells with Lucifer yellow to identify the type of bipolar cell. Figure 4.1 shows that I was able to select ON bipolar cells, defined by the position of their soma being close against the outer plexiform layer, into which their dendrites run, and by the fact that their axon terminated in the ON lamina of the inner plexiform layer close to the ganglion cells (see section 1.8). Comparing the morphology of the two filled cells in Figure 4.1 (which were typical of all the cells I filled), with the catalogue of different bipolar cell classes in rat retina (Euler and Wassle, 1995; Euler et al., 1996; Hartveit, 1997; Euler and Wassle, 1998), reveals that the bipolar cells I recorded from were either ON rod bipolars or class 8 or 9 ON cone bipolars. I was not confident that I could distinguish these 3 different types of ON bipolar cell (for example, although the left cell in Figure 4.1 looks like a rod ON bipolar and the right cell looks like a class 8 or 9 cone ON bipolar, if the right cell happened to lose part of its synaptic terminal during the retinal slicing procedure it would be identified falsely as a rod ON bipolar). Since both rod and cone ON bipolars are predicted to have the same non-uniformity of $[Cl]_i$ based on their transporter distribution, and since all of the cells I recorded gave similar results, I pooled all my data from ON bipolars.

4.3 GABA activates a current at the dendrites and at the synaptic terminals of ON bipolar cells

As described in chapter 2, I studied GABA-evoked currents using the perforated patch clamp technique, employing gramicidin as the perforant. Gramicidin forms cation channels in the membrane under the electrode, but does not alter the

intracellular chloride concentration (Ebihara et al., 1995; Kyrozis and Reichling, 1995; Akaike, 1996). When recording responses to GABA, synaptic transmission was blocked by replacing calcium with magnesium (Table 2 solution B or C), adding 5 mM Na_2EGTA to chelate trace calcium, and adding 20 μM NBQX and 50 μM AP-5 to block ionotropic glutamate receptors. I did not use the glutamate analogue aminophosphorobutyrate (APB) to block the mGluR6 metabotropic glutamate receptors on ON bipolar cells (Neal et al., 1981; Tian and Slaughter, 1994), because APB has been reported to activate a chloride flux through glycine-gated channels in retinal ganglion cells (Chiba and Saito, 1994) and might do the same in bipolar cells, perturbing the normal $[Cl^-]_i$. To obtain GABA responses, 100 μM GABA was pressure applied (puffed) from a pipette (Figure 4.2). The flow rate of the external solution was around 5 ml/min, and the flow was oriented across the retinal slice, parallel to the plexiform layers, so that GABA puffed onto the OPL would not be swept over the IPL and vice versa. The GABA puffs were only 100 ms in duration to restrict the time of ejection and minimize the chance of GABA diffusing laterally far from the site of ejection. For a diffusion coefficient of $D = 7.5 \times 10^{-10}$ m^2/s, as measured for glutamate (Barbour, 2001), the distance, x, which GABA will diffuse laterally in the time t = 100 ms is given by $x \sim \sqrt{2 \cdot D \cdot t} = 12\,\mu m$. Proof of the spatially restricted flow pattern was obtained from the observation that in some cells no response was obtained when GABA was puffed onto the inner plexiform layer (IPL) because the axon and synaptic terminals had been cut in the slicing procedure, despite the occurrence of a robust response when GABA was puffed onto the outer plexiform layer (OPL): thus GABA does not diffuse laterally sufficiently to activate receptors at one plexiform layer when it is applied at the other plexiform layer. Puffing 100 μM GABA under such conditions produced a current that lasted about 0.5–1 sec (Figure 4.2). GABA evoked a qualitatively similar response at the dendrites and the synaptic terminals, as expected from the presence of $GABA_A$ and

Figure 4.2: Experimental design and GABA evoked currents

To investigate the chloride reversal potential in the dendrites (OPL) and the axon terminal (IPL) of ON bipolar cells, the somata of ON bipolar cells in retinal slices were perforated patch-clamped using the chloride-impermeable pore-forming antibiotic gramicidin as the perforating agent. GABA was pressure-applied to either the dendrites or the axon terminal via a small patch-pipette ("puff"). The flow of the bath solution was oriented at 90^{O} to the layers to avoid GABA puffed at one plexiform layer being swept to the other plexiform layer, and thus to spatially restrict the GABA application.

The insets on the right show specimen traces of the responses to such GABA puff applications (100 ms duration, 100 μM GABA) to either the OPL (upper circle) or the IPL (lower circle). The responses lasted about 0.5–1 seconds. The cell was voltage clamped at –42 mV and in this cell the reversal potential of the response was negative to –42 mV at both the OPL and the IPL. To determine the chloride reversal potential a voltage ramp from +8 to –92 mV (200 ms duration) was applied 100 ms after the GABA puff started (i.e. about at the peak of the GABA evoked current). Examples of such ramps are shown in Figure 4.4 and described in section 4.4.

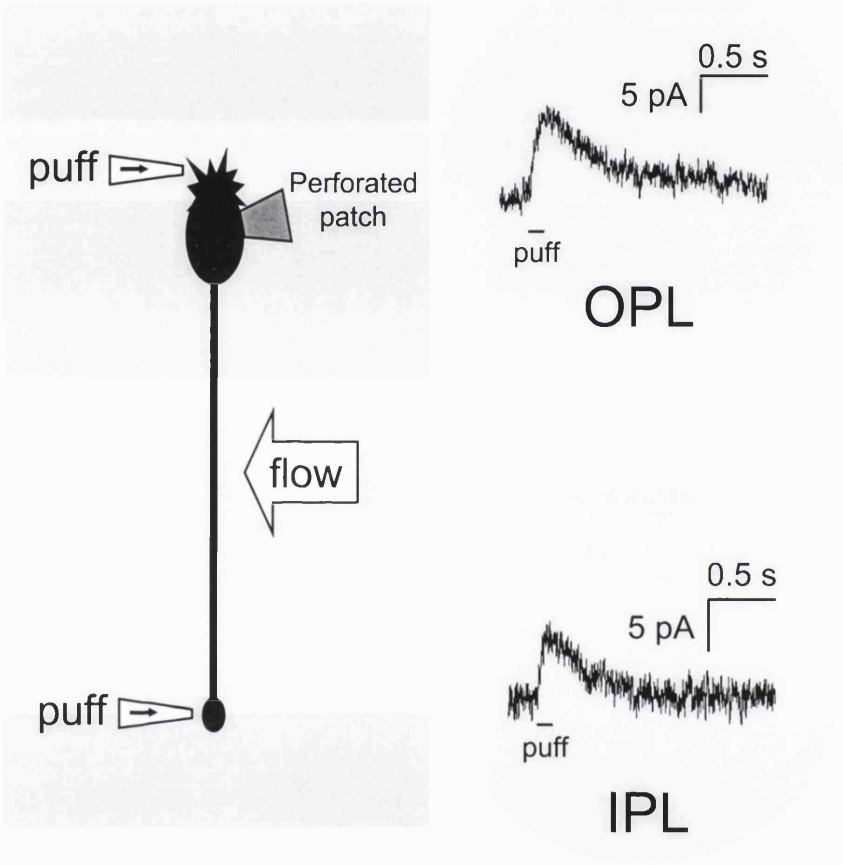
puff
Perforated
patch
flow
puff
0.5 s
5 pA
puff
OPL
0.5 s
5 pA
puff
IPL

Figure 4.3: Properties of the GABA-evoked current

(A) Plot of the GABA-evoked conductance (g_{GABA}) in the dendrites (OPL) and the axon terminal (IPL) of ON bipolar cells (measurements made at both ends of 7 cells). The value of the conductance was obtained by measuring the slope of the GABA-evoked current-voltage relation, which was obtained by subtracting the current responses to voltage ramps applied in the absence and presence of the puff of GABA.

(B) Specimen traces of currents evoked by bath application of 30 μM GABA or 100 μM baclofen. The ON bipolar cell was voltage clamped at –42 mV (upper panel) or –22 mV (lower panel). Baclofen did not evoke a significant current at either potential, confirming that the GABA evoked current is not mediated by $GABA_B$ receptors, but by ionotropic $GABA_A$ and $GABA_C$ receptors.

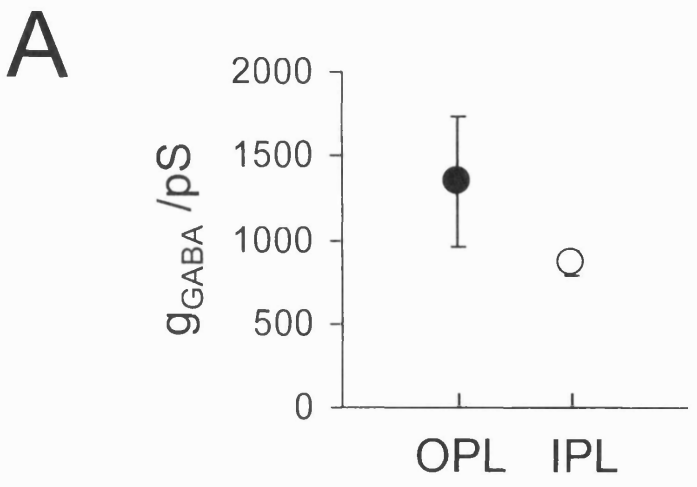
A
2000
1500
1000
500
0
g_{GABA} /pS
OPL
IPL

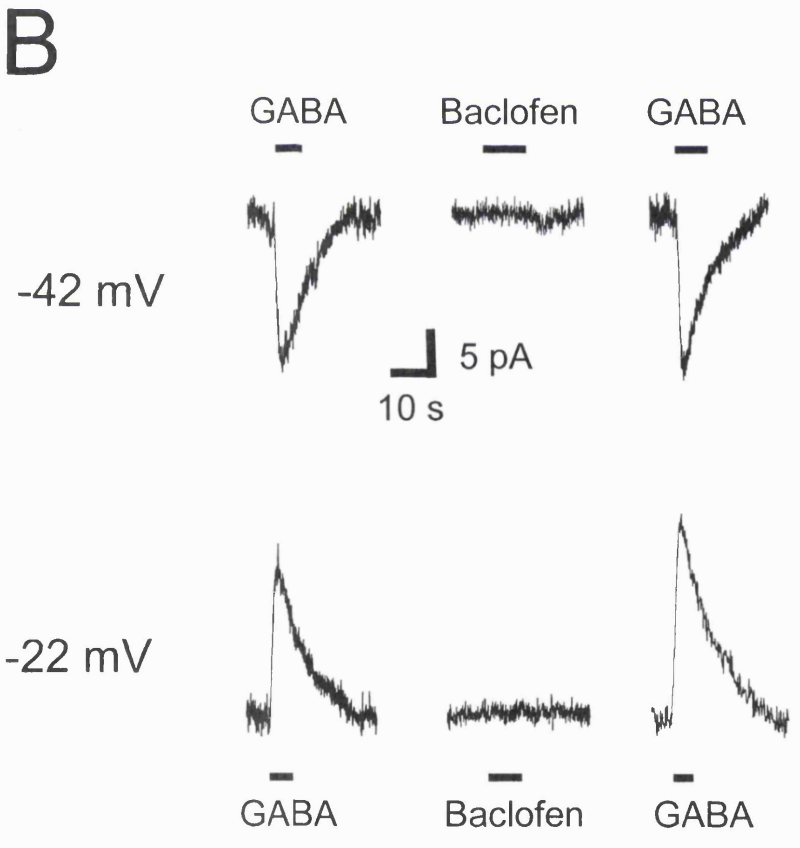
B
GABA
Baclofen
GABA
-42 mV
5 pA
10 s
-22 mV
GABA
Baclofen
GABA

$GABA_C$ receptors at both locations (Qian and Dowling, 1995; Haverkamp et al., 2000). The conductance activated (deduced using the reversa potential measurements described below) was somewhat higher on average at the dendrites (OPL) than at the synaptic terminals (IPL) (Figure 4.3 A), although this difference was not significant ($p = 0.21$).

Essentially all of the GABA-evoked current in whole-cell clamped bipolar cells was abolished by a combination of $GABA_A$ and $GABA_C$ blockers (see section 3.6 and Figure 3.12). To confirm that there was no significant contribution of $GABA_B$ receptors to the current in these cells recorded with the less intrusive perforated patch technique, I compared the response to bath-applied GABA and baclofen, a $GABA_B$ receptor agonist, at –42 and –22 mV. In all 3 cells tested baclofen (100 μM) generated no current (Figure 4.3 B), confirming that the GABA response was generated by $GABA_A$ and $GABA_C$ receptors.

4.4 The $[Cl^-]_i$ is higher at the dendrites than at the synaptic terminals of ON bipolar cells

Since the GABA-evoked current is generated by $GABA_A$ and $GABA_C$ receptors, and there is no bicarbonate in my solutions (which permeates GABA-gated Cl^- channels: (Bormann et al., 1987)), I used the reversal potential of the GABA-evoked current to determine the value of $[Cl^-]_i$ in the dendrites and synaptic terminals of the cell. Figure 4.4 shows the protocol used to determine the reversal potential. From a holding potential of –42 mV (nominally –40 mV but with –2 mV added from the electrode junction potential, see chapter 2), a voltage ramp from +8 mV to –92 mV was applied (over 200 ms), initially in the absence of GABA (grey traces). It was important that the holding potential should be the same for all cells since, as described below, the resting $[Cl^-]_i$ adapts to the holding potential used. The voltage ramp was then repeated during a puff of GABA applied to the outer plexiform layer (black traces). At the point where the current traces, obtained in the

Figure 4.4: Chloride reversal potential measurements in bipolar cells

The chloride reversal potential in ON bipolar cells was measured as described in section 4.4. The cell was voltage clamped at –42 mV and a voltage ramp from +8 to –92 mV (200 ms duration) applied in control solution (grey traces) or 100 ms after the start of the puff (100 ms duration) of 100 μM GABA to **(A)** the OPL or **(B)** the IPL. The reversal potential of the GABA-evoked current is at the voltage where the current in control and in GABA cross (arrows). Current traces have been clipped at the positive voltages to show data near the reversal potential at a higher gain.

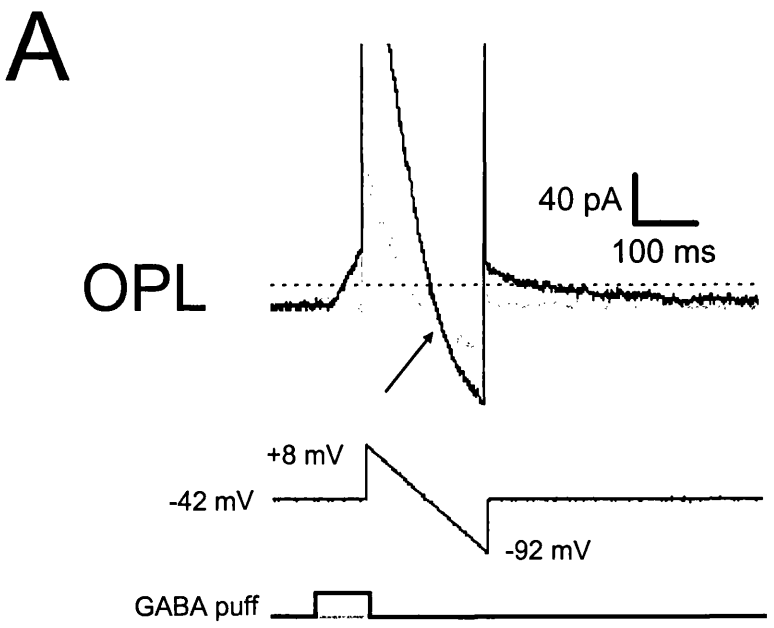
A
OPL
40 pA
100 ms
+8 mV
-42 mV
-92 mV
GABA puff

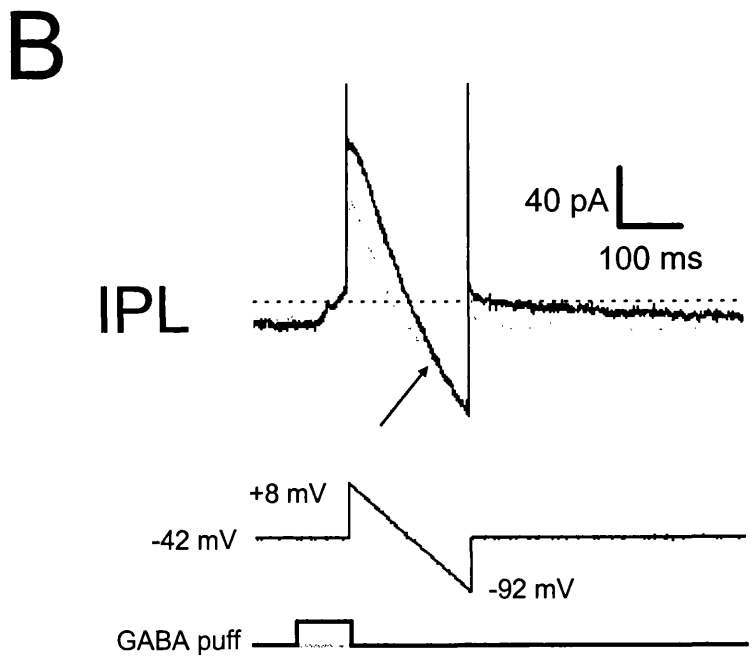
B
IPL
40 pA
100 ms
+8 mV
-42 mV
-92 mV
GABA puff

presence and absence of GABA, cross in Figure 4.4 (arrows) is the apparent reversal potential of the GABA-evoked current (E_{Cl}), which was –56 mV (including the electrode junction potential) in the case of Figure 4.4 A. Using the net membrane current flowing at this point (–32 pA for Figure 4.4 A), and the measured series resistance of the perforated patch plus electrode (45 MΩ in this example), this value was then corrected for the series resistance voltage error (1.4 mV in this case) to obtain the final reversal potential of –54.6 mV. From the Nernst potential for Cl^-:

$$E_{rev} = \frac{R \cdot T}{z \cdot F} \cdot \ln_e \left(\frac{[Cl^-]_O}{[Cl^-]_i} \right) \tag{4.1}$$

with $[Cl^-]_O$ = 145.5 mM, a temperature of T = 24^{O}C (297 K), F = 96485 C/mol, R = 8.3 J/K.mol and z = –1, this gives a value of $[Cl^-]_i$ = 17.2 mM at the bipolar cell dendrites (OPL). The value of the reversal potential varied quite significantly between different cells, ranging from –35 to –67 mV, corresponding to $[Cl^-]_i$ ranging from 37 to 11 mM. This variability between cells made it essential to compare the values of $[Cl^-]_i$ at the dendrites and synaptic terminal of the same cell, rather than comparing between cells.

The whole procedure was then repeated in the same cell while puffing GABA at the inner plexiform layer (Figure 4.4 B), which gave a reversal potential of –62 mV, 7.4 mV more negative than at the OPL, and corresponding to a value of $[Cl^-]_i$ = 12.9 mM at the bipolar cell synaptic terminals. Out of 7 cells to which GABA was applied at the OPL and the IPL, 6 had a reversal potential that was more negative at the IPL (in the 7th cell there was no difference at the two locations). The mean difference between the two ends of the cell was 4.2 ± 1.5 mV in 7 cells (significantly different with p = 0.033): the mean reversal potential was –46.2 ± 4.0 mV at the OPL and –50.4 ± 3.9 mV at the IPL (Figure 4.5 A). The corresponding mean values for $[Cl^-]_i$ were 25.4 ± 3.1 mM at the OPL and 21.5 ± 2.8 mM at the IPL (Figure 4.5 B).

Figure 4.5: The E_{Cl} is more negative in the axon terminal than in the dendrites

(A) Plot of the chloride reversal potential (E_{Cl}) obtained as described in section 4.4 and shown in Figure 4.4 (n = 7). E_{Cl} slightly is more negative at the axon terminals (IPL) than in the dendrites (OPL) of the same cell.

(B) Plot of the internal chloride concentration ($[Cl^-]_i$) calculated from the Nernst equation (equation 4.1) using the E_{Cl} measurements from (A). $[Cl^-]_i$ is lower in the axon terminals (IPL) than in the dendrites (OPL) of the same cell.

A

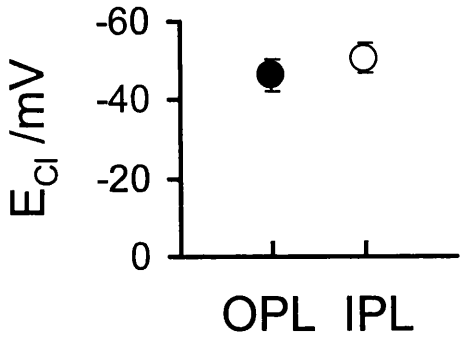

B

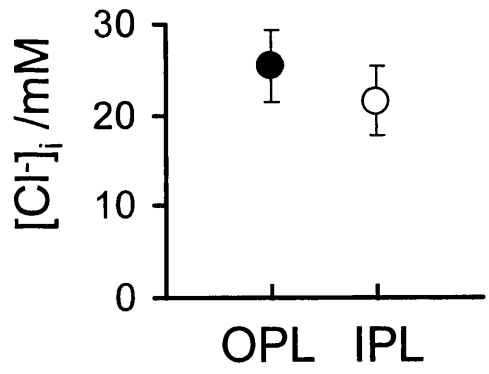

4.5 $[Cl^-]_i$ is strongly affected by membrane potential

If the ON bipolar cell has a significant membrane permeability to Cl^- ions then, when central light depolarizes the cell, entry of Cl^- is expected to displace E_{Cl} in the positive direction, unless membrane Cl^- transporters confer a stronger control of $[Cl]_i$ than do membrane channels. To test the effect of membrane potential on $[Cl^-]_i$ in ON bipolars cells, I stepped the membrane potential from –42 mV to a test membrane potential for 1-2 minutes, and then applied a puff of GABA to either the dendrites or the synaptic terminals of the cell, and used voltage ramps to measure the reversal potential of the GABA-evoked current, as described above.

Figure 4.6 A shows a remarkable adaptation of the steady state value of E_{Cl} to the prevailing membrane potential. At both the dendrites and the synaptic terminal, the steady state E_{Cl} varies roughly linearly with holding potential. This relationship has a slope of about 0.5, and E_{Cl} is approximately equal to the membrane potential at around –40 to –45 mV. Although these data, like those in Figure 4.5 B, show $[Cl^-]_i$ to be slightly higher in the dendrites than in the synaptic terminal, at both locations the steady state E_{Cl} is positive to the membrane potential for membrane potentials more negative than about –50 mV, while E_{Cl} is negative to the membrane potential for membrane potentials positive to about –40 mV. This remains the case even after correcting the derived values of E_{Cl} for a possible contribution of intracellular bicarbonate to the reversal potential of the GABA-evoked current, as described in detail below (section 4.8).

These results imply that at positive potentials there is an active extrusion of Cl^- from the cell, while at negative potentials there is active accumulation of Cl^-. Although in principle the extrusion and accumulation could be done by a single mechanism (e.g. KCC-2) operating in different directions as $[Cl^-]_i$ alters, considering the extent to which $[Cl^-]_i$ alters at positive and negative extremes of potential suggests that two separate mechanisms (presumably KCC-2 and NKCC-1) must

Figure 4.6: Voltage dependence of the E_{Cl}

(A) Plot of the chloride reversal potential (E_{Cl}) as a function of the membrane potential (V). The membrane potential was changed from –42 mV to a different value for 1-2 minutes before obtaining the E_{Cl} in the OPL (filled circles) or the IPL (hollow circles) by applying a brief voltage ramp, as described in section 4.3 and shown in Figure 4.4 (number of cells per point is 1-4 for the OPL and 2-5 for the IPL). The lines are linear regressions with slope 0.56 (OPL) and 0.51 (IPL).

(B) The energy needed to move a chloride ion inwards across the membrane when transported by KCC-2 (black line) or NKCC-1 (grey line), as a function of the internal chloride concentration ($[Cl^-]_i$). Positive values indicate energy values favouring efflux, negative values indicate energy values favouring influx of chloride. The curves are plots of equations (4.2) and (4.3). The dotted bar indicates the internal chloride changes observed during the voltage change measured in (A) – over this range of $[Cl^-]_i$ neither transporter reverses, so that KCC-2 always extrudes, whereas NKCC-1 always accumulates chloride.

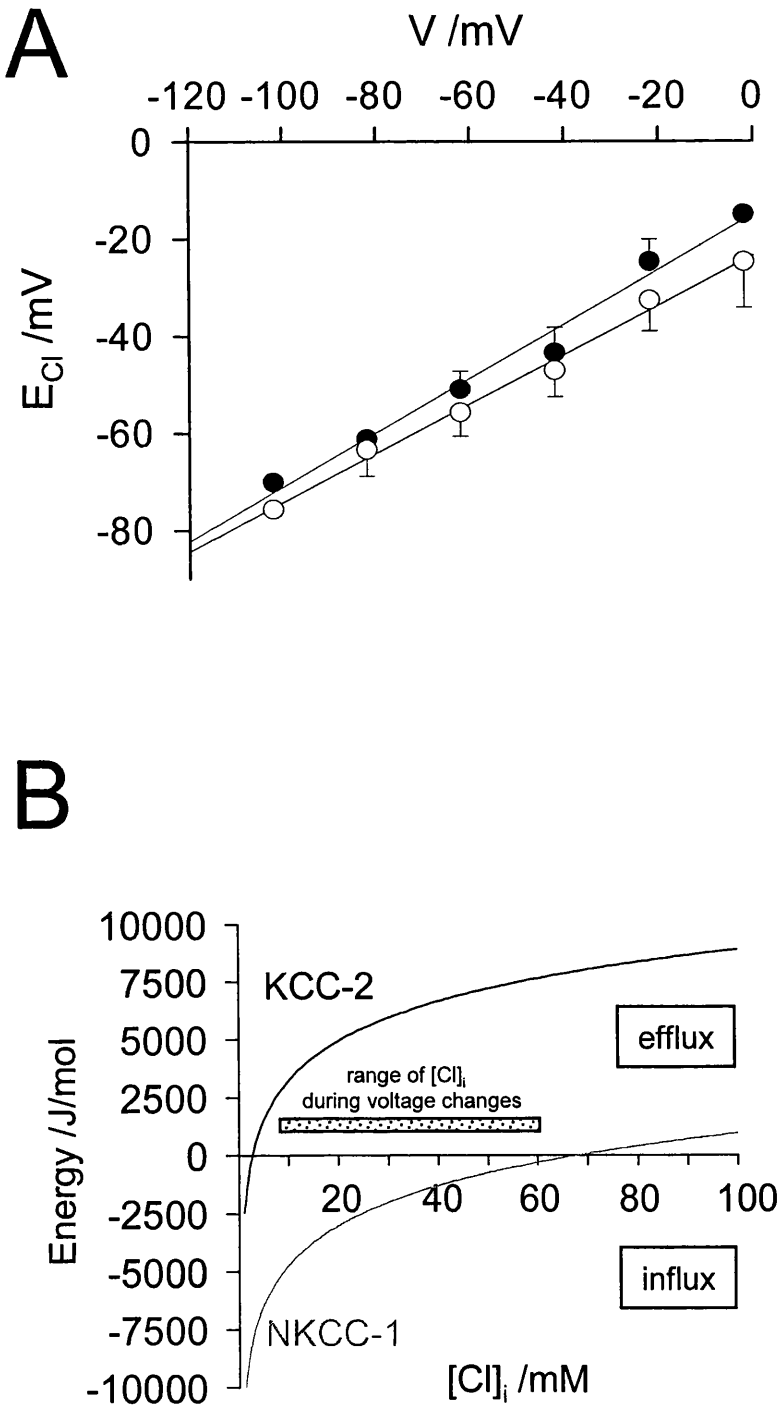
A
V /mV
-120 -100 -80 -60 -40 -20 0
0
-20
-40
-60
-80
E_{Cl} /mV
B
10000
7500
5000
2500
0
-2500
-5000
-7500
-10000
Energy /J/mol
KCC-2
efflux
range of $[Cl]_i$
during voltage changes
20 40 60 80 100
influx
NKCC-1
$[Cl]_i$ /mM

mediate the extrusion and accumulation. Figure 4.6 B shows the energy needed to move a Cl^- inwards across the membrane using either KCC-2 (with a stoichiometry such that one K^+ moves with each Cl^- (Payne, 1997); black trace) or NKCC-1 (with a stoichiometry such that one Na^+, one K^+ and 2 Cl^- move together: (Russell, 2000); grey trace), as a function of $[Cl^-]_i$, which allows prediction of the direction of operation of each transporter. The free energy needed to transport a Cl^- with the KCC-2 transporter is given by:

$$E_{KCC\text{-}2} = R \cdot T \cdot \ln_e \left(\frac{[K^+]_i}{[K^+]_O} \cdot \frac{[Cl^-]_i}{[Cl^-]_O} \right) \tag{4.2}$$

while that for the NKCC-1 transporter is given by:

$$E_{NKCC\text{-}1} = \frac{R \cdot T}{2} \cdot \ln_e \left(\frac{[K^+]_i}{[K^+]_O} \cdot \frac{[Na^+]_i}{[Na^+]_O} \cdot \frac{[Cl^-]_i^{\,2}}{[Cl^-]_O^{\,2}} \right) \tag{4.3}$$

The factor 2 in the denominator of equation (4.3) appears because I am calculating the energy needed to move <u>one</u> Cl^- rather than two. In the steady state at a holding potential of –102 mV, the most negative value of E_{Cl} at the synaptic terminals is around –76 mV (Figure 4.6 A), corresponding to a $[Cl^-]_i$ of 7.5 mM. From Figure 4.6 B when $[Cl^-]_i$ =7.5 mM, KCC-2 still extrudes Cl^-, so the Cl^- accumulation needed to maintain E_{Cl} positive to the membrane potential is assumed to be produced by NKCC-1. Conversely, at –22 mV the most positive value of E_{Cl} at the dendrites is around –24 mV, corresponding to a $[Cl^-]_i$ of 56.9 mM. From Figure 4.6 B when $[Cl^-]_i$ = 56.9 mM NKCC-1 still accumulates Cl^-, so the Cl^- extrusion needed to maintain E_{Cl} negative to the membrane potential is presumably mediated by KCC-2.

The data in Figure 4.6 A show the tendency of E_{Cl} to be more positive in the dendrites than in the synaptic terminal which was shown in Figure 4.5 A, but the differences between the OPL and IPL data at each voltage are not statistically significant. This is because the prolonged duration experiment required for these

steady state measurements meant that the OPL and IPL data could not be obtained in the same cells (unlike in Figure 4.5), so that cell-cell variability contributes a great deal to the error bars.

I investigated the kinetics of the adaptation of $[Cl^-]_i$ to the prevailing membrane potential, by clamping a cell to a potential of –62 mV for different durations (from a holding potential of –42 mV), and then returning to –42 mV, applying a GABA puff and using voltage ramps to determine the reversal potential of the GABA evoked current. An example of such a recording is shown in Figure 4.7 A. In this example E_{Cl} was –37.5 mV when no voltage step was applied (a; 0 sec; black dot in Figure 4.7B), –40.2 mV when the cell was hyperpolarized to –62 mV for 2 seconds before giving the GABA puff (b; dark grey dot in Figure 4.7B), –42.2 mV when the cell was hyperpolarized to –62 mV for 6 seconds (c; light grey dot in Figure 4.7B) and –46.9 mV when the cell was hyperpolarized to –62 mV for 20 seconds (d; white dot in Figure 4.7B). The approximately 10 mV shift in E_{Cl} that occurred on stepping the membrane potential from –42 to –62 mV (Figure 4.7 A) took place with a time constant of 11.0 seconds (single exponential fit to the data in Figure 4.7B). Averaged results from 6 cells are shown in Figure 4.7C, in which the value of E_{Cl} after each voltage step was normalized to the value of E_{Cl} when no voltage step was applied (i.e. 0 sec at –62 mV), and the data were fit with a single exponential. The time constant of the averaged E_{Cl} change after stepping the membrane potential to -62 mV was 10.9 seconds.

Both NKCC-1 and KCC-2 are electroneutral, so their direction (and, for NKCC-1 at least, the rate) of operation is not affected by changes of membrane potential (Payne, 1997; Russell, 2000). Consequently the tendency of E_{Cl} to track membrane potential changes is most simply explained by there being a significant resting permeability to Cl^-. In section 4.8 I attempt to model the voltage-dependence of $[Cl^-]_i$ based on the assumption that $[Cl^-]_i$ is determined by a combination of a chloride conductance, NKCC-1 and KCC-2.

Figure 4.7: Kinetics of the voltage-dependent change of E_{Cl}

(A) Specimen voltage ramp data for a cell held at –42 mV, before (grey traces) or 100 ms after the start of a GABA puff (black traces). When the cell was hyperpolarized to –62 mV for 0 (a), 2 (b), 6 (c) or 20 (d) seconds 300 ms before the ramp was obtained. The vertical dotted lines indicate the E_{Cl} when the cell was not hyperpolarized (*) or hyperpolarized for 20 seconds (^{V}). A larger gain of the data are shown in the insets in the middle. The voltage protocol is shown at the right.

(B) The graph shows the measured E_{Cl} of the specimen traces during the course of the experiment – each value of E_{Cl} (i.e. each dot) was obtained at intervals of 2-4 minutes to allow $[Cl^-]_i$ to return to control levels.

(C) Averaged data for the change of E_{Cl}, measured as in (A). In each cell the values of E_{Cl} were normalized to the control value of E_{Cl} (i.e. when the membrane was not hyperpolarized before the ramp). The mean ± s.e.m., of data from 1-6 cells per duration, are plotted as a function of the durations of the voltage step to –62 mV. The line shows the fit of the data with a single exponential.

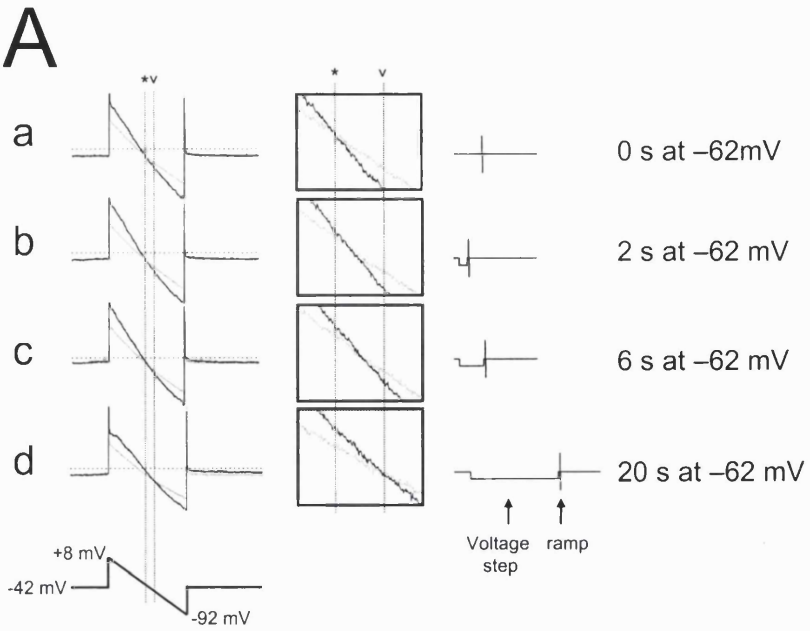
A
a
b
c
d
*v
*
v
0 s at –62mV
2 s at –62 mV
6 s at –62 mV
20 s at –62 mV
Voltage step
ramp
+8 mV
-42 mV
-92 mV

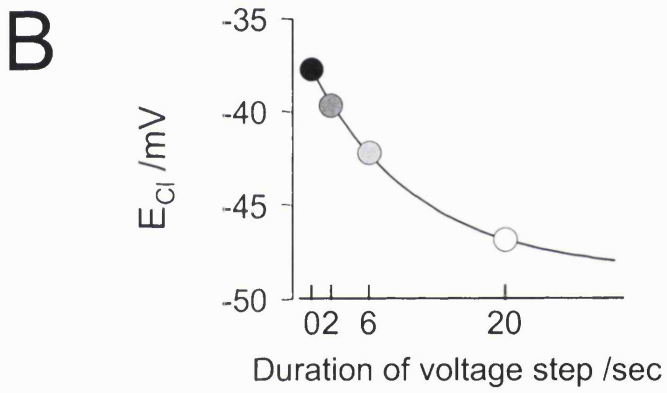
B
-35
-40
-45
-50
E_{Cl} /mV
02 6
20
Duration of voltage step /sec

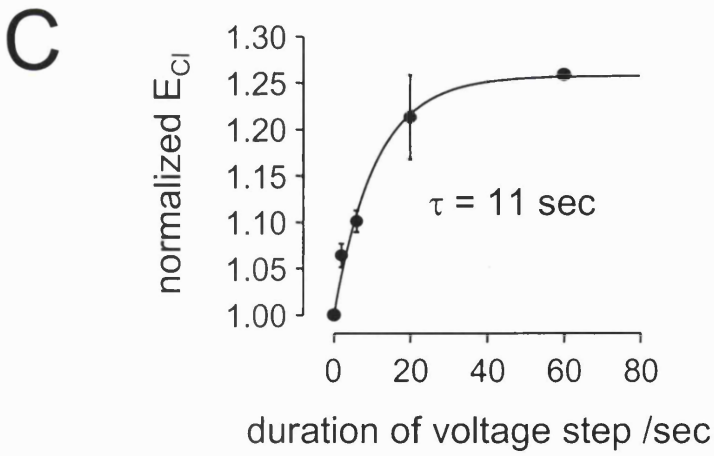
C
normalized E_{Cl}
1.30
1.25
1.20
1.15
1.10
1.05
1.00
τ = 11 sec
0
20
40
60
80
duration of voltage step /sec

4.6 Furosemide raises $[Cl]_i$ at the OPL

The loop diuretic furosemide inhibits KCC-1 and NKCC-2 with an IC_{50} of ~25 μM (Payne, 1997). If NKCC-1 was the dominant transporter controlling $[Cl^-]_i$ at the ON bipolar dendrites, as suggested by Vardi et al. (2000a), then furosemide, by blocking the Cl^- influx mediated by NKCC-1, would be expected to shift negative the reversal potential of currents evoked by GABA puffed at the bipolar cell dendrites. Figure 4.8 shows that, in fact, furosemide (100 μM) displaced the reversal potential in the positive direction (done in only 1 cell at a holding potential of –42 mV) suggesting that (at least at –42 mV) KCC-2 is the main transporter controlling E_{Cl} at the dendrites. The shift of E_{Cl} could be approximated by an exponential with a time constant of 132 seconds, greater than the time constant of the change produced by a change of membrane potential (when E_{Cl} changed with a time constant of 11 seconds, section 4.4). This might suggest that the passive chloride conductance of the cell can move chloride across the membrane substantially faster than furosemide-sensitive transporters, but could also be explained if Cl^- efflux by KCC-2 is only slightly greater than Cl^- influx by NKCC-1, so that when furosemide blocks both transporters there is only a slow rise of $[Cl^-]_i$. Further experiments using bumetanide, a specific inhibitor of NKCC-1, are needed to assess the relative importance of NKCC-1, KCC-2 and the passive chloride conductance of the cell in controlling $[Cl^-]_i$.

Figure 4.8: The effect of furosemide on E_{Cl} in the bipolar cell dendrites

(A) Specimen data showing the response to the voltage ramps before (grey traces) and 100 ms after a GABA puff (black traces) in the absence (larger current; ramp at the right; a) or presence (smaller outward current before and after the ramp; ramp at the left; b) of 100 μM furosemide. The chloride reversal potential is at the voltage where the current in control and in GABA cross (arrows).

(B) The measured E_{Cl}, obtained about every 2 minutes, during the course of an experiment. The lower case letters indicate the E_{Cl} values of the specimens traces shown above.

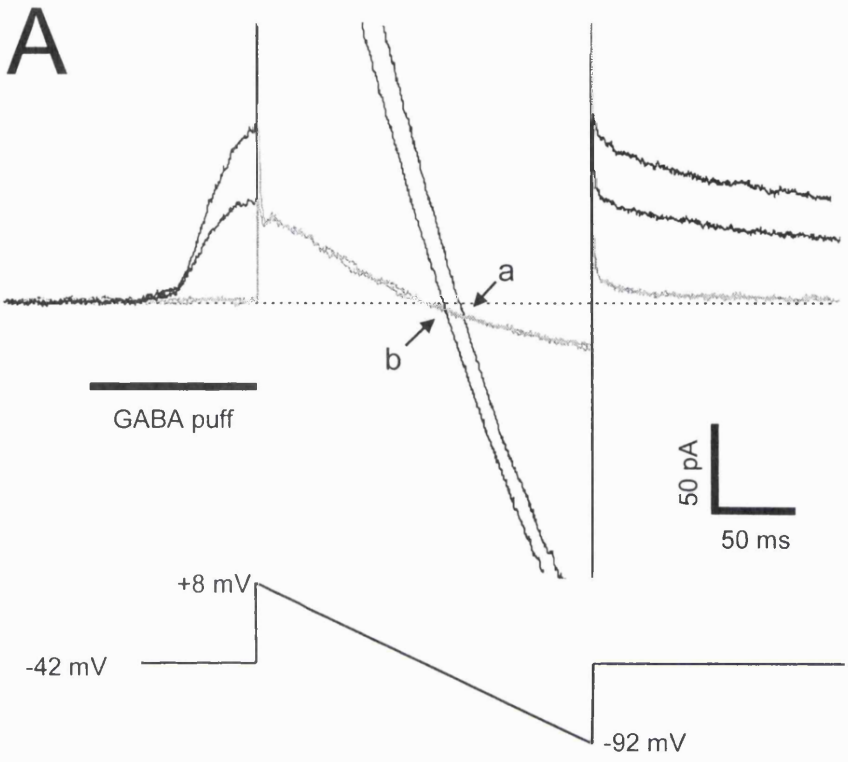
A
a
b
GABA puff
50 pA
50 ms
+8 mV
-42 mV
-92 mV

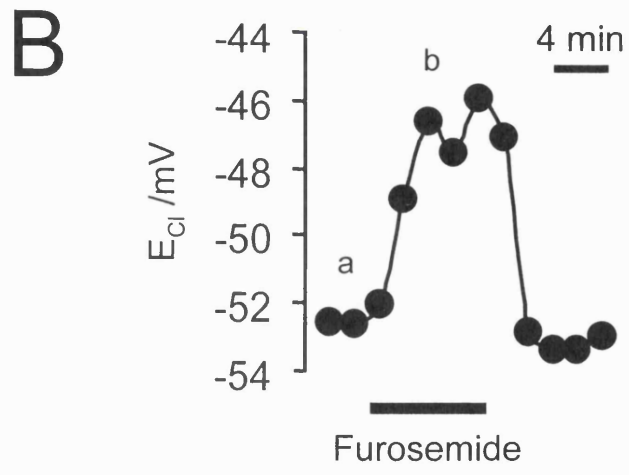
B
-44
-46
-48
-50
-52
-54
E_{Cl} /mV
4 min
a
b
Furosemide

4.7 E_{Cl} is more positive when $[K^+]_o$ is higher

From the thermodynamics of their carrier cycle, both the NKCC-1 and the KCC-2 transporters are expected to produce a higher equilibrium level of $[Cl^-]_i$ when the extracellular potassium concentration rises. For KCC-2 the equilibrium $[Cl^-]_i$ is given by $\frac{[K^+]_o \cdot [Cl^-]_o}{[K^+]_i}$ (from equation (4.2)), and for NKCC-1 it is given by $\sqrt{\frac{[K^+]_o \cdot [Na^+]_o \cdot [Cl^-]_o^2}{[K^+]_i \cdot [Na^+]_i}}$ (from equation (4.3)). Since light results in changes of $[K^+]_o$ in the outer and the inner retina (Steinberg et al., 1980; Frishman et al., 1992; Dmitriev et al., 1999), I examined the effect of changing $[K^+]_o$ on $[Cl^-]_i$.

Raising $[K^+]_o$ from 2.5 to 6 mM at a holding potential of –42 mV shifted E_{Cl} positive by about 7 mV for the cell of Figure 4.9 A/B (mean value 7.4 ± 1.6 mV in 5 cells to which GABA was applied at the dendrites; from –49.2 ± 5.1 to –41.8 ± 3.8 mV ($p = 0.0097$); Figure 4.9 C), corresponding to an increase of $[Cl^-]_i$ by about 6 mM (mean value 6.7 ± 1.0 mM in 5 cells to which GABA was applied at the dendrites; from 22.8 ± 3.8 to 29.5 ± 4.0 mM ($p = 0.0028$); Figure 4.9 D). Similarly, E_{Cl} shifted positive by 9 mV when $[K^+]_o$ was raised from 2.5 to 6 mM in 1 cell to which GABA was applied at the synaptic terminals (from –67 to –58 mV). The shift of E_{Cl} in the dendrites could be approximated by an exponential with a time constant of 271 ± 47 seconds in 5 cells, greater than the time constant of the change produced by a change of membrane (see section 4.5), but similar to the time needed for E_{Cl} to change when furosemide was applied (section 4.6). In a non-voltage-clamped cell *in vivo*, if $[K^+]_o$ rose uniformly around the cell the resulting depolarization of the membrane potential would produce an extra positive shift of E_C, due to the voltage-dependence of $[Cl^-]_i$ characterized in section 4.5.

Figure 4.9: The effect of elevated $[K^+]_O$ on E_{Cl}

(A) Specimen current responses to voltage ramps before (grey traces) and 100 ms after a GABA puff (black traces) in 6 mM $[K^+]_O$ (smaller outward current, ramp at the left; a) or in 2.5 mM $[K^+]_O$ (larger outward current, ramp at the right; b). The chloride reversal potential is at the voltage where the current in control and in GABA cross (arrows).

(B) The measured E_{Cl}, obtained about every 2 minutes, during the course of the experiment in (A). The lower case letters indicate the E_{Cl} of the specimens traces shown above.

(C) Plot of the average chloride reversal potential (E_{Cl}) for 5 cells bathed in 6 mM $[K^+]_O$ (black circles) or in 2.5 mM $[K^+]_O$ (white circles). For each of the cells the E_{Cl} was more negative when the cell was in 2.5 mM $[K^+]_O$ than when it was in 6 mM $[K^+]_O$.

(D) The averaged internal chloride concentration ($[Cl^-]_i$) calculated from the Nernst equation (equation 4.1) using the data in (C). The $[Cl^-]_i$ was lower in 2.5 mM $[K^+]_O$ (white circles) than in 6 mM $[K^+]_O$ (black circles).

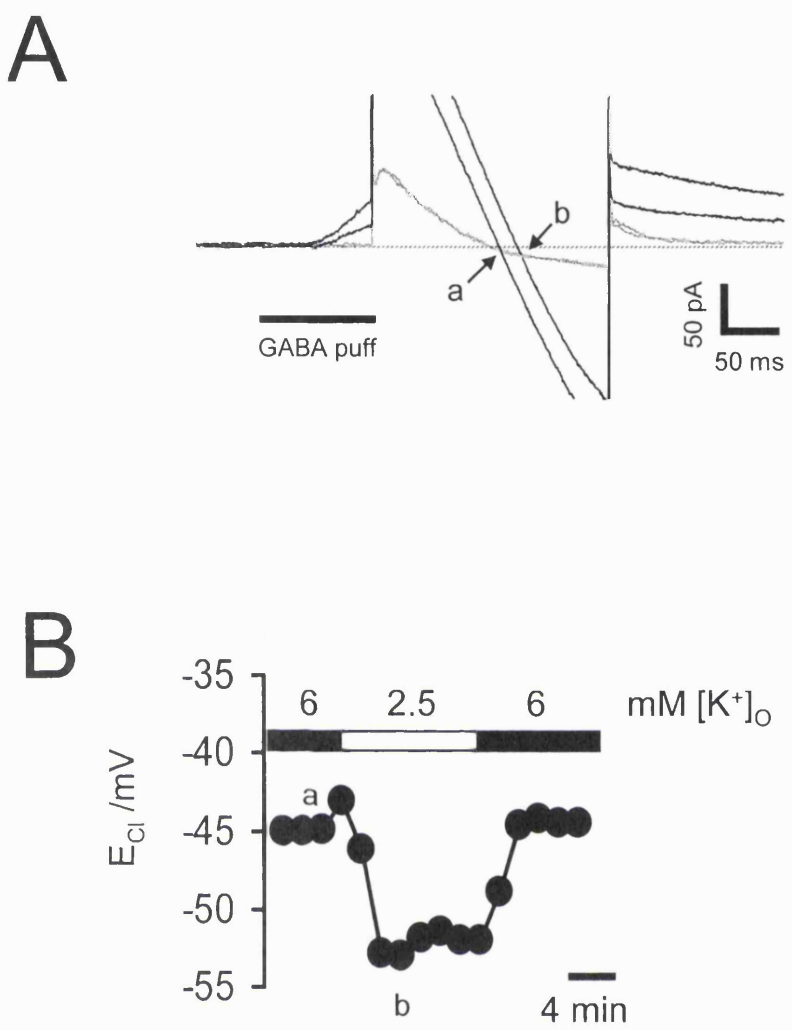
A
b
a
GABA puff
50 pA
50 ms
B
-35
-40
-45
-50
-55
6
2.5
6
mM [K+]O
ECl /mV
a
b
4 min
C
-60
-40
-20
0
ECl /mV
6K
2.5K
D
40
30
20
10
0
[Cl-]i /mM
6K
2.5K

4.8 Modelling of the control of $[Cl^-]_i$

To gain a more quantitative understanding of how Cl^- transporters control $[Cl^-]_i$ in bipolar cells, I analysed a simplified model in which I ignored the small difference in $[Cl^-]_i$ between the two ends of the cell, treated the cell as a single well-mixed compartment, and tried to fit the data in Figure 4.6 A. Chloride fluxes across the cell membrane were assumed to reflect current flow through an ohmic Cl^- conductance G_{Cl} (note that although bipolar cells express hyperpolarization-activated CLC-2 chloride channels, these are only significantly activated at voltages negative to –80 mV (Enz et al., 1999)). Extrusion of Cl^- by KCC-2 was assumed to be at a rate $k.[Cl^-]_i$, since KCC-2 has a low affinity for Cl^- (at least for external Cl^-: K_M=101 mM, (Payne, 1997)) and a Michaelis Menten dependence of rate on $[Cl^-]_i$ predicts a linear dependence for $[Cl^-]_i << K_m$. Pumping of Cl^- into the cell by NKCC-1 was assumed to occur at a constant rate n. Inhibition of NKCC-1 when $[Cl^-]_i$ rises was ignored for simplicity (see below). Both n and k were assumed to be voltage-independent, since both NKCC-1 and KCC-2 are electroneutral, and the rate of operation of NKCC-1 has been suggested to be voltage-independent (see discussion in Russell et al. (2000)). With U being the cell volume, the amount of chloride in the cell is $[Cl^-]_i.U$. The rate of change of $[Cl^-]_i$ is then given as:

$$U \cdot \frac{d[Cl^-]_i}{dt} = \frac{G_{Cl} \cdot (V - E_{Cl})}{F} + n - k \cdot [Cl^-]_i \qquad (4.4)$$

where F is the Faraday constant. In the steady state $d[Cl^-]_i/dt = 0$, so:

$$E_{Cl} = V + \frac{F}{G_{Cl}} \cdot (n - k \cdot [Cl^-]_i) \qquad (4.5)$$

In Figure 4.6A, V is approximately equal to the mean of the E_{Cl} values at the dendrites and synaptic terminals when $V = E_{Cl} = -40$ mV and hence $[Cl^-]_i = 30.4$ mM (from the Nernst equation: 4.1), so

$$k = \frac{n}{30.4\,\text{mM}} \tag{4.6}$$

and thus, from (4.5),

$$E_{Cl} = V + \frac{n \cdot F}{G_{Cl}} \cdot \left(1 - \frac{[Cl^-]_i}{30.4\text{mM}} \right) \tag{4.7}$$

The value of $[Cl^-]_i$ is related to the value of the reversal potential for chloride and can be calculated from the Nernst equation (equation (4.1)). Inserting this into equation (4.7) and rearranging leads to

$$V = E_{Cl} - \frac{n \cdot F}{G_{Cl}} \cdot \left(1 - \frac{[Cl^-]_O}{30.4\text{mM} \cdot e^{\left(\frac{z \cdot F}{R \cdot T} \cdot E_{Cl} \right)}} \right) \tag{4.8}$$

In this equation the membrane potential, V, is a function of the reversal potential for chloride, E_{Cl}, with the only unknown parameters being in $n.F/G_{Cl}$. I thus set the value of $n.F/G_{Cl}$, which sets the ratio of Cl^- fluxes mediated by pumping to those mediated by the conductance, so that the relationship between V and E_{Cl} predicted by equation (4.8) gave as good a fit as possible to the data of Figure 4.6 A. The dashed line in Figure 4.10 A, which is superimposed on the data replotted from Figure 4.6 A, shows a plot of equation (4.8) using $n.F/G_{Cl} = 30$ mV, which gives a reasonable fit to the data over the range of membrane potentials between -30 and -80 mV, but predicts values of E_{Cl} which are too negative at extremes of potential. Including inhibition of NKCC-1 by $[Cl^-]_i$, by making the rate of operation of NKCC-1 be given by

Figure 4.10: Modelling the voltage dependence of the E_{Cl}

(A) Data points are the OPL and IPL values of E_{Cl} from Figure 4.6. The dashed line is a fit to the data, i.e. equation (4.8) with $nF/G_{Cl} = 30$ mV.

(B) Points show the data in (A) corrected for the presence of internal bicarbonate and its contribution to the reversal potential of the GABA evoked current (see section 4.8, equation 4.11). The dashed line is a fit to the corrected data, i.e. equation (4.8) with $nF/G_{Cl} = 10$ mV.

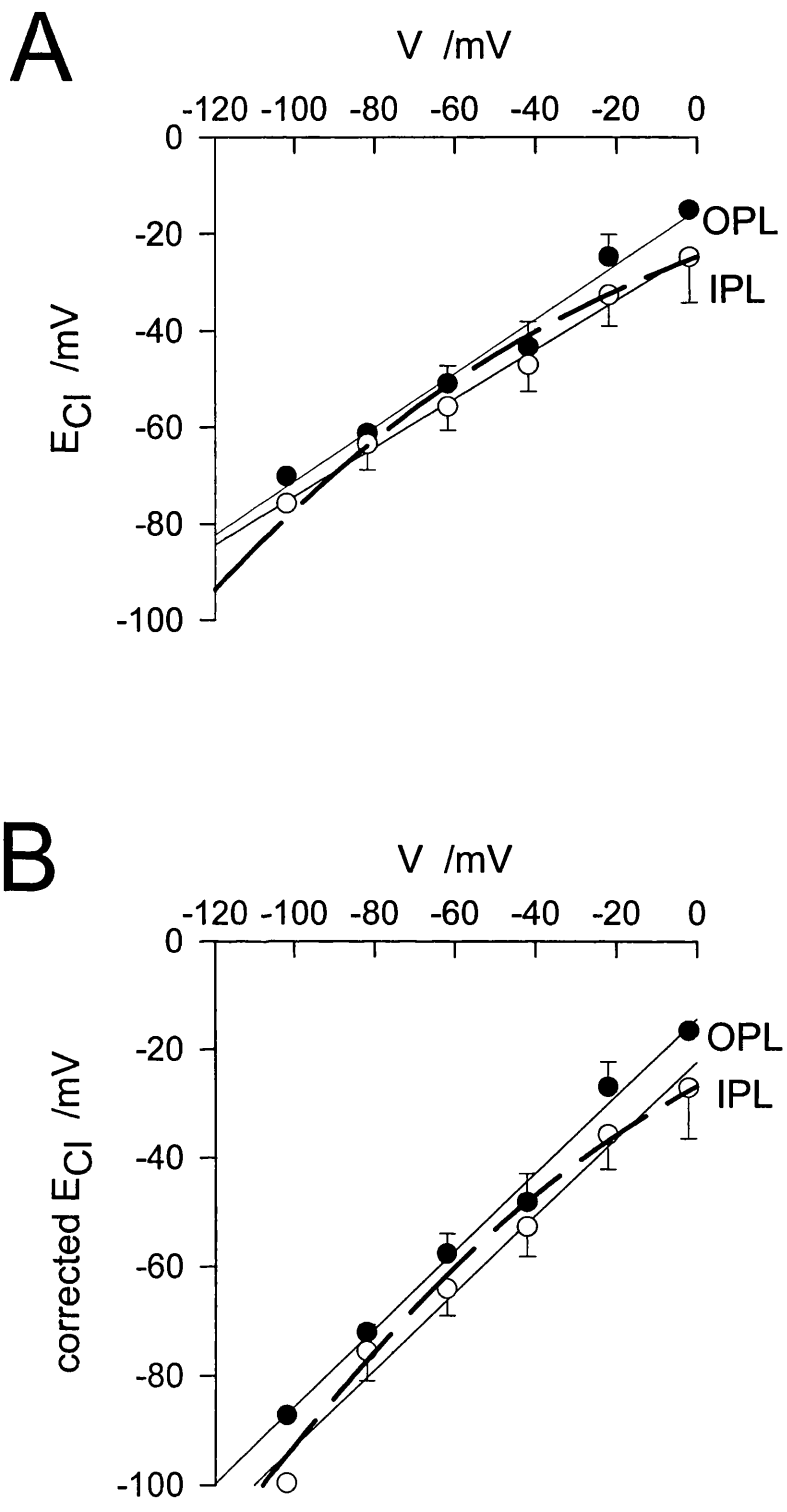
A
V /mV
-120 -100 -80 -60 -40 -20 0
0
-20
-40
-60
-80
-100
E_{Cl} /mV
OPL
IPL
B
V /mV
-120 -100 -80 -60 -40 -20 0
0
-20
-40
-60
-80
-100
corrected E_{Cl} /mV
OPL
IPL

$n(1-\lambda[Cl^-]_i)$, with λ constant, led to an equation that was formally equivalent to equation (4.8) and so did not improve the fit. I then considered the possible contribution of bicarbonate to the reversal potential of the GABA-evoked currents. Although there is no bicarbonate in my HEPES-buffered superfusing solution (see Methods), HCO_3^- might be present inside the cell at a maximum concentration that can be calculated using the Henderson-Hasselbalch equation:

$$pH_i = pK + \log_{10}\left(\frac{[HCO_3^-]_i}{[CO_2]_i}\right) \tag{4.9}$$

With a pK for bicarbonate of 6.1, an internal pH of 7.2 and 1.2 mM (40 mm Hg) CO_2 produced by metabolism, this predicts an internal bicarbonate concentration of 15.2 mM. HCO_3^- passes through $GABA_A$ receptor channels with a permeability that is about 0.3 of that for Cl^- (Kaila et al., 1989; Wotring et al., 1999). Thus, the reversal potential of the GABA-gated current, E_{rev}, could be displaced positive from the value of E_{Cl} by the presence of intracellular HCO_3^-, according to the Goldman-Hodgkin-Katz equation:

$$E_{rev} = \frac{R \cdot T}{F} \cdot \ln_e\left(\frac{[Cl^-]_i + b \cdot [HCO_3^-]_i}{[Cl^-]_O + b \cdot [HCO_3^-]_O}\right) \tag{4.10}$$

where the permeability ratio $b = P_{HCO3}/P_{Cl} = 0.3$. Assuming $[HCO_3^-]_O = 0$ mM, as in my superfusion solution, and $[HCO_3^-]_i = 15.2$ mM, this gives:

$$E_{rev} = \frac{R \cdot T}{F} \cdot \ln_e\left(\frac{[Cl^-]_i + 4.6\,mM}{[Cl^-]_O}\right) \tag{4.11}$$

From equation (4.11) I calculated, for the data in Figure 4.6 A, the corrected value of $[Cl^-]_i$ and thus a corrected value of E_{Cl} from equation (4.1), and plotted this against the membrane potential (V). As shown in Figure 4.10 B, the main effect of correcting

for the possible presence of intracellular HCO_3^- is that at more negative membrane potentials the values of E_{Cl} become more negative. Fitting equation (4.8) to the points in Figure 4.10 B, with E_{Cl} equal to V at –60 mV, i.e. when $[Cl^-]_i$ = 13.9 mM, and $n.F/G_{Cl}$ = 10 mV, gave the dashed curve shown. This curve fits reasonably well over most of the voltage range.

To determine whether this model (not including the possible presence of bicarbonate) could account for the shift of E_{Cl} seen when $[K^+]_o$ was raised from 2.5 to 6 mM, I assumed for simplicity that raising $[K^+]_o$ stimulates Cl^- influx mediated by NKCC-1 (i.e. alters the value of *n*) but has no effect on the Cl^- efflux mediated by KCC-2 (in fact raising $[K^+]_o$ shifts E_{Cl} positive even in neurones which have had NKCC-1 knocked out (Sung et al., 2000), presumably by slowing KCC-2 extrusion, so this is an oversimplification). The shift of E_{Cl} predicted by equation (4.5) at constant voltage (–42 mV), when the rise of $[K^+]_o$ elevates $[Cl^-]_i$ from $[Cl^-]_{i(2.5K)}$ to $[Cl^-]_{i(6K)}$, is given by

$$E_{Cl(6K)} - E_{Cl(2.5K)} = \Delta E_{Cl} = \frac{F}{G_{Cl}} \cdot \left(n_{6K} - n_{2.5K} - k \cdot \left([Cl^-]_{i(6K)} - [Cl^-]_{i(2.5K)}\right)\right) \qquad (4.12)$$

or

$$\frac{\Delta E_{Cl}}{\frac{F \cdot n_{2.5K}}{G_{Cl}}} = \frac{n_{6K} - n_{2.5K}}{n_{2.5K}} - \frac{k \cdot \left([Cl^-]_{i(6K)} - [Cl^-]_{i(2.5K)}\right)}{n_{2.5K}} \qquad (4.13)$$

Using $n_{2.5K}.F/G_{Cl}$ = 30 mV, $n_{2.5K} = k.[Cl^-]_{i(2.5K)}$ from eqn. (4.6), and ΔE_{Cl} from the Nernst equation (4.1) this becomes

$$\frac{R \cdot T}{F \cdot 30\,mV} \cdot \ln_e\left(\frac{[Cl^-]_{i(6K)}}{[Cl^-]_{i(2.5K)}}\right) = \frac{n_{6K}}{n_{2.5K}} - \frac{[Cl^-]_{i(6K)}}{[Cl^-]_{i(2.5K)}} \qquad (4.14)$$

To give a 7 mV shift of E_{Cl} as observed experimentally, $[Cl^-]_{i(6K)}/[Cl^-]_{i(2.5K)} = 1.315$; inserting this into (4.14) and rearranging gives

$$\frac{n_{6K}}{n_{2.5K}} = 1.55 \tag{4.15}$$

i.e. a 2.4-fold increase of $[K^+]_o$ from 2.5 to 6 mM is predicted to increase the rate of NKCC-1 by a factor of 1.55. If the rate of NKCC-1 is assumed to depend in a Michaelis-Menten fashion on $[K^+]_o$, that is:

$$\frac{n_K}{n_{Kmax}} = \frac{[K^+]_O}{[K^+]_O + EC_{50}} \tag{4.16}$$

then to produce a 1.81-fold rise in the rate when $[K^+]_o$ is raised from 2.5 to 6 mM:

$$\frac{n_{6K}}{n_{2.5K}} = 1.55 = \frac{\frac{6mM}{6mM + EC_{50}}}{\frac{2.5mM}{2.5mM + EC_{50}}} \tag{4.17}$$

so the EC_{50} for activation by $[K^+]_o$ must be

$$EC_{50} = \frac{6mM \cdot \left(1 - \frac{n_{6K}}{n_{2.5K}}\right)}{\frac{n_{6K}}{n_{2.5K}} - \frac{6mM}{2.5mM}} = 3.9\,mM \tag{4.18}$$

This predicted value is in reasonable agreement with the EC_{50} of 2 mM measured for activation of human and mouse NKCC-1 by external Rb^+ and K^+ (Isenring et al., 1998; Glanville et al., 2001). A value of 2 mM (rather than 3.9 mM) for the EC_{50} would allow some of the effect of external K^+ on E_{Cl} to be mediated by a slowing of KCC-2.

4.9 Discussion

4.9.1 Factors controlling $[Cl^-]_i$ in ON bipolar cells

The experiments in this chapter show that the intracellular chloride concentration in retinal ON bipolar cells is neither constant, nor in equilibrium with the membrane potential, but is controlled actively by the membrane potential, by the extracellular potassium concentration, and by two separate Cl^- transporters, probably KCC-2 which extrudes K^+ and Cl^-, and NKCC-1 which pumps Na^+, K^+ and $2Cl^-$ into the cell. Around a membrane potential of –40 to –50 mV, in the steady state E_{Cl} is approximately equal to the membrane potential. Altering the membrane potential leads to a time-dependent alteration of the chloride reversal potential in the same direction, as expected if there is a passive membrane conductance to Cl^-, but in the steady state the shift of E_{Cl} is only about half that of the membrane potential change (Figure 4.6A). Consequently, at more positive potentials E_{Cl} is more negative than the membrane potential, probably because KCC-2 actively lowers $[Cl^-]_i$, and at more negative potentials E_{Cl} is more positive than the membrane potential, probably because NKCC-1 raises $[Cl^-]_i$. Raising the extracellular $[K^+]$ leads to a positive shift of E_{Cl}, presumably because the raised $[K^+]_o$ stimulates Cl^- entry by NKCC-1 and inhibits Cl^- efflux on KCC-2. A simple mathematical model, incorporating a membrane chloride conductance and KCC-2 and NKCC-1 transporters could account approximately for the voltage- and $[K^+]_o$-dependence of E_{Cl} (see Figure 4.10 and section 4.8). Future experiments (which I did not have time to do for this thesis) comparing the effects of bumetanide, which at low doses specifically blocks NKCC-1, with furosemide, which blocks NKCC-1 and KCC-2, may allow the relative importance of NKCC-1 and KCC-2 to be assessed.

These data are consistent with demonstrations of a role for NKCC-1 and KCC-2 in controlling $[Cl^-]_i$ in other neurones (hippocampal pyramidal cells: Rivera

et al. (1999); superior olive neurones: Kakazu et al. (1999); neocortical pyramidal cells: DeFazio et al. (2000); dorsal root ganglion cells: Sung et al. (2000); amygdala and neocortical cells: Martina et al. (2001); spinal motoneurones: Hübner et al. (2001b)). Indeed, these transporters have the power to change the sign of GABA-evoked signalling, since an increase in the expression of KCC-2 during development can lead to a shift of E_{Cl} from above to below the resting potential of central neurones, so that GABA or glycine changes from being initially excitatory during development to being inhibitory in the adult animal (Ben-Ari et al., 1994; Ehrlich et al., 1999; Rivera et al., 1999; Ganguly et al., 2001).

4.9.2 Non-uniformity of $[Cl^-]_i$ along the ON bipolar cell

The observed distribution of Cl^- transporters in ON bipolar cells, with NKCC-1 at the dendrites and KCC-2 at the synaptic terminals, suggested that the intracellular chloride concentration should be higher at the dendrites than at the synaptic terminals (Vardi et al., 2000a; Vu et al., 2000). If this difference were sufficiently large, so that E_{Cl} were significantly more depolarized than the resting potential at the dendrites, and significantly more hyperpolarized than the resting potential at the synaptic terminals, then it would allow GABA released by horizontal cells to produce a depolarization at the dendrites and GABA released by amacrine cells to produce a hyperpolarization at the synaptic terminals. As discussed below, this would fit in with current ideas about the sign of inhibition at the two plexiform layers.

Experimentally, although E_{Cl} was consistently more positive at the dendrites than at the synaptic terminal, i.e. in the direction predicted by the asymmetrical transporter distribution in ON bipolar cells, the difference was only 4 mV, corresponding to $[Cl^-]_i$ being approximately 4 mM higher (25 mM versus 21 mM). My experiments were carried out in HEPES buffered solution, with the aim of eliminating any contribution of Cl^-/HCO_3^- and Na^+-dependent Cl^-/HCO_3^- exchange to

the control of $[Cl^-]_i$ (which may in fact be relatively unimportant (Ballanyi and Grafe, 1985; Thompson et al., 1988)), and thus maximizing any difference of $[Cl^-]_i$ which could be produced between the dendrites and synaptic terminal of the cell. Even in this optimal situation, however, the difference in reversal potential for GABA-evoked currents at the two ends of the cell does not seem large enough to produce a significant functional difference between the effects of GABA at the two ends of the cell. In the intact retina, in the dark, the extracellular $[K^+]$ is around 0.5 mM higher around the bipolar cell dendrites than around the synaptic terminals (Steinberg et al., 1980) because of K^+ efflux from the photoreceptors (which are depolarized in the dark). Data of Steinberg et al. (1980) show that during prolonged illumination, as was present in my experiments, this difference is abolished. The data in Figure 4.9 (where a 3.5 mM increase of $[K^+]_o$ produces a 7 mV positive shift of E_{Cl}) suggest that the 0.5 mM higher $[K^+]_o$ at the dendrites in the dark might increase the difference in E_{Cl} between the two ends of the cell to approximately 5 mV in the dark (this difference will be reduced when illumination initially lowers $[K^+]_o$ around the dendrites by around 2 mM (reducing the E_{Cl} at the OPL by around –4 mV) and initially raises $[K^+]_o$ around the synaptic terminals by around 0.5 mM (increasing the E_{Cl} by around +1 mV): Steinberg et al. (1980)). If the dark resting potential of the bipolar cell (around –45 mV: Euler & Masland (2000)) were exactly half way between the values of E_{Cl} at the two ends of the cell in the dark, it would result in only 2.5 mV of driving force for GABA-evoked chloride currents to produce a depolarization at the dendrites and a hyperpolarization at the synaptic terminals, and the driving force for depolarization at the dendrites would disappear as soon as the bipolar cell were depolarized by central illumination (see below). Furthermore, despite being consistently slightly more positive than the value of E_{Cl} in the synaptic terminal, there was great variability in the absolute value of E_{Cl} in the dendrites of ON bipolar cells, ranging from –35 to –67 mV. Although I did not systematically measure the resting potential of the cells (because the seal conductance leads to the

apparent resting potential being significantly more positive than the actual resting potential (Tessier-Lavigne et al., 1988)), the more negative E_{Cl} values I measured would require an extremely negative resting potential for E_{Cl} to be more positive than the resting potential. Thus, the average E_{Cl} is not sufficiently positive for GABA to reliably produce a depolarization at the dendrites of ON bipolar cells.

My data differ from those of Satoh et al. (2001) who measured the reversal potential of GABA-evoked currents in mouse retinal bipolar cells. Satoh et al. (2001) reported no difference between the reversal potential at the dendrites and at the synaptic terminals of ON bipolar cells. The reason for this is unclear, although their long (5 second) pressure applications of GABA, which may allow more GABA to diffuse between the dendrites and synaptic terminal than is the case for my brief GABA puffs (which lasted only 100 msec), may contribute to their not observing a more positive E_{Cl} at the dendrites. Satoh et al. (2001) also reported that E_{Cl} was more positive in rod bipolar cells than in cone ON or OFF bipolars (which had a similar E_{Cl}). I was not as confident as Satoh et al. (2001) that I could distinguish dye-filled rod and cone ON bipolar cells, and my grouping of them together may account for some of the variability in the values of E_{Cl} that I measured (although Satoh et al. reported a similar variability, -23 to -61mV, even in rod ON bipolars).

4.9.3 Implications for visual processing: lateral inhibition in ON bipolar cells

Early visual processing depends on lateral interactions mediated by changes in the activation of $GABA_A$ and $GABA_C$ receptors at the dendrites and synaptic terminals of retinal bipolar cells. The effect of these receptors is determined by the value of the chloride reversal potential relative to the membrane potential. I had expected that there would be a gradient of intracellular chloride concentration, $[Cl^-]_i$, along ON bipolar cells, being higher in the dendrites and lower in the synaptic terminals. This distribution is predicted, not only from the non-uniform expression of

NKCC-1 and KCC-2 transporters (Vardi et al., 2000a; Vu et al., 2000), but also from current ideas on how bipolar cells integrate lateral inhibitory signals arriving from horizontal and amacrine cells with the direct synaptic input they receive from photoreceptors (see section 4.1 and references therein). ON bipolar cells are depolarized when light falling on the centre of their receptive field suppresses glutamate release from photoreceptors, and to produce an antagonistic surround to their receptive field the suppression of GABA release from horizontal cells, which is produced by peripheral light, must lead to a hyperpolarization. This can only occur if E_{Cl} in the dendrites is more positive than the resting potential (around –45 mV in the dark: Euler & Masland (2000)). At the same time, release of GABA from amacrine cells onto the synaptic terminal needs to produce a hyperpolarization to induce transience into the voltage response of the bipolar cell to central light. The data in this chapter show that E_{Cl} in the dendrites is unlikely to be more than a few mV more positive than the resting potential in the dark and as soon as central light has depolarized the cell (by up to ~20 mV: Euler & Masland (2000); also in discussion of Karschin & Waessle (1990)) the membrane potential will be positive to E_{Cl} so that suppression of GABA release by surround light will lead to further depolarization. By contrast, inhibition at the synaptic terminal will still be able to function, since depolarization by central light will increase the amount by which the membrane potential is more positive than E_{Cl} (at least initially: see below).

The generation of a centre-surround receptive field for bipolar cells by lateral inhibitory signals from horizontal cells is well established for amphibian retinae (Werblin and Dowling, 1969; Kaneko, 1970; Stone and Schutte, 1991; Hare and Owen, 1996), but less so for mammalian retinae particularly for rod bipolar cells. Anatomically-defined synapses from horizontal cells to bipolar cells are reported to be rare in mammals (Kolb, 1979), but have been reported for rod (ON) bipolar cells (Linberg and Fisher, 1988), and it is also possible that GABA is released at this synapse by reversed uptake (Schwartz, 1982) rather than by exocytosis of

anatomically observable vesicles. Cone bipolar cells (ON and OFF) show an antagonistic surround to their receptive field (Dacheux & Miller, 1981; Dacey et al., 2000), but rod (ON) bipolar cells have been reported to show no antagonistic surround (Bloomfield and Xin, 2000). My observation that E_{Cl} in the dendrites of ON bipolar cells is similar to the dark potential of the cells would explain why rod bipolar cells can show no antagonistic surround mediated by suppression of GABA release from horizontal cells. It is possible that most of the bipolar cells that I recorded were rod bipolars, but if cone ON bipolar cells were included in my sample (implying that they also do not have a dendritic E_{Cl} very positive to the dark potential) then the receptive field antagonistic surround that they exhibit (Dacey et al., 2000) presumably is generated by feedback from horizontal cells to cones or by inhibitory input from amacrine cells.

4.9.4 Implications for visual processing: time-dependent adaptation of $[Cl^-]_i$ and inhibitory signals

A striking result of my study is that $[Cl^-]_i$ in ON bipolar cells, and thus the driving force for inhibitory signals generated by $GABA_A$ and $GABA_C$ receptors, adapts on a time scale of ~10 seconds following a change of the bipolar cell membrane potential. This has important implications for the time course of inhibition following membrane potential changes produced either by central illumination or by GABAergic input. When central light depolarizes the cell, initially the membrane potential will be substantially more positive than the value of E_{Cl} at the synaptic terminal, and GABA released from amacrine cells will have a large hyperpolarizing effect on the bipolar cell. However, during a maintained depolarization induced by central light, E_{Cl} will move positive (over ~10sec) by about half the depolarization produced by the central light (Figure 4.6 and 4.7), resulting in a halving of the driving force for the inhibitory input. Similarly, if GABA receptors in the bipolar cell membrane are activated by a change of input from horizontal or amacrine cells (e.g.

due to a change of illumination in the receptive field surround) then after an initial hyperpolarization the resulting adaptation of E_{Cl} towards the new membrane potential will result in a decrease of the strength of the inhibitory signal, inducing an inherent transience to the inhibitory signal. It appears, therefore, that the time-dependent adaptation of $[Cl^-]_i$ in ON bipolar cells may add another layer of temporal processing to signals as they pass through the retina.

CHAPTER 5

The effect of Ajuba on the properties of GLT-1

5.1 Introduction

As described in section 1.7, although much is known about proteins interacting with neurotransmitter receptors and ion channels, little is known about proteins interacting with glutamate transporters. So far only two groups have addressed this issue. They investigated the interactions of cytoplasmic proteins with (1) the C-terminus of the neuronal glutamate transporter EAAC-1 (Lin et al., 2001), which is expressed ubiquitously in the brain, (2) the C-terminus (Jackson et al., 2001) and (3) the N-terminus (Law & Rothstein, 2000) of the neuronal glutamate transporter EAAT-4, which is mainly expressed by Purkinje cells in the cerebellum, and (4) the C-terminus of the glial glutamate transporter GLAST (Marie and Attwell, 1999), which is heavily expressed in retinal Müller cells and cerebellar Bergmann glia. Interestingly, all of these four studies report modulation of the glutamate transporter activity by intracellular proteins, as described in detail in section 1.7. Since all of this other work was on relatively minor glutamate transporters, which in most of the CNS contribute only a small fraction of the glutamate uptake present, our lab set out to identify and characterize proteins interacting with the glial glutamate transporter GLT-1, which in most parts of the brain provides the great majority of glutamate uptake. I shall briefly summarize the main findings of this work (Marie et al., 2002) to provide the background to the electrophysiological work that I performed.

The LIM protein Ajuba, which is described in more detail in section 1.7, was identified by Helene Marie as a binding partner for the N-terminal part of the

glutamate transporter GLT-1 (Figure 5.1), using the yeast-two hybrid method. Pull-down assays confirmed that these two proteins interact *in vitro*, and the binding region on GLT-1 was narrowed down to be between amino acids 9 and 23 ($GLT\text{-}1^{9\text{-}23}$). This 15 amino acid stretch is identical in the rat transporter GLT-1 and its human homologue EAAT-2, but is not present in any of the other glutamate transporters, and is less than 54% identical to other proteins in GenBank, suggesting that Ajuba binds specifically to the GLT-1 (EAAT-2) subtype of glutamate transporters. Antibodies against Ajuba co-immunoprecipitated GLT-1 from rat brain, and antibody labelling of rat brain slices for GLT-1 and Ajuba showed co-localization in glial cells of the cerebellum and hippocampus, and neurones of the retina, suggesting that these two proteins interact *in vivo*. When expressed alone in COS-7 cells, Ajuba showed a mainly cytoplasmic localization, whereas when GLT-1 was expressed alone it was concentrated in the cell's plasma membrane. While co-expression of Ajuba with GLT-1 in these cells did not significantly alter the localization of GLT-1, Ajuba was recruited from the cytoplasm to the plasma membrane, where the two proteins co-localized, suggesting that the binding of Ajuba to GLT-1 influences the distribution of Ajuba within the cell.

This biochemical and histological work did not reveal the functional significance of the interaction between Ajuba and GLT-1. In the work described in this chapter I investigated whether Ajuba modulates the properties of GLT-1 when both proteins are transiently expressed in a mammalian cell line. Briefly, I patch-clamped COS-7 cells, expressing either GLT-1 alone, or GLT-1 and Ajuba, to see if co-expression of Ajuba alters the functional properties of the transporter (such as glutamate affinity, maximum uptake rate, surface expression of GLT-1, voltage-dependence of uptake, or anion channel behaviour).

Figure 5.1: Schematic drawing of GLT-1 with Ajuba bound

Membrane topology of GLT-1 as suggested by (Grunewald et al., 1998): GLT-1 is thought to have eight transmembrane spanning α-helices (indicated by the Arabic numbering (1-8)). A structure reminiscent of a pore-loop (indicated by the Roman numbering (I and II)), and a hydrophobic linker (indicated as "linker") are positioned between the 7^{th} and the 8^{th} domains. With this topology the C- as well as the N-terminus of the transporter are intracellular. Ajuba binds to amino acids 9-23 of the N-terminus of GLT-1.

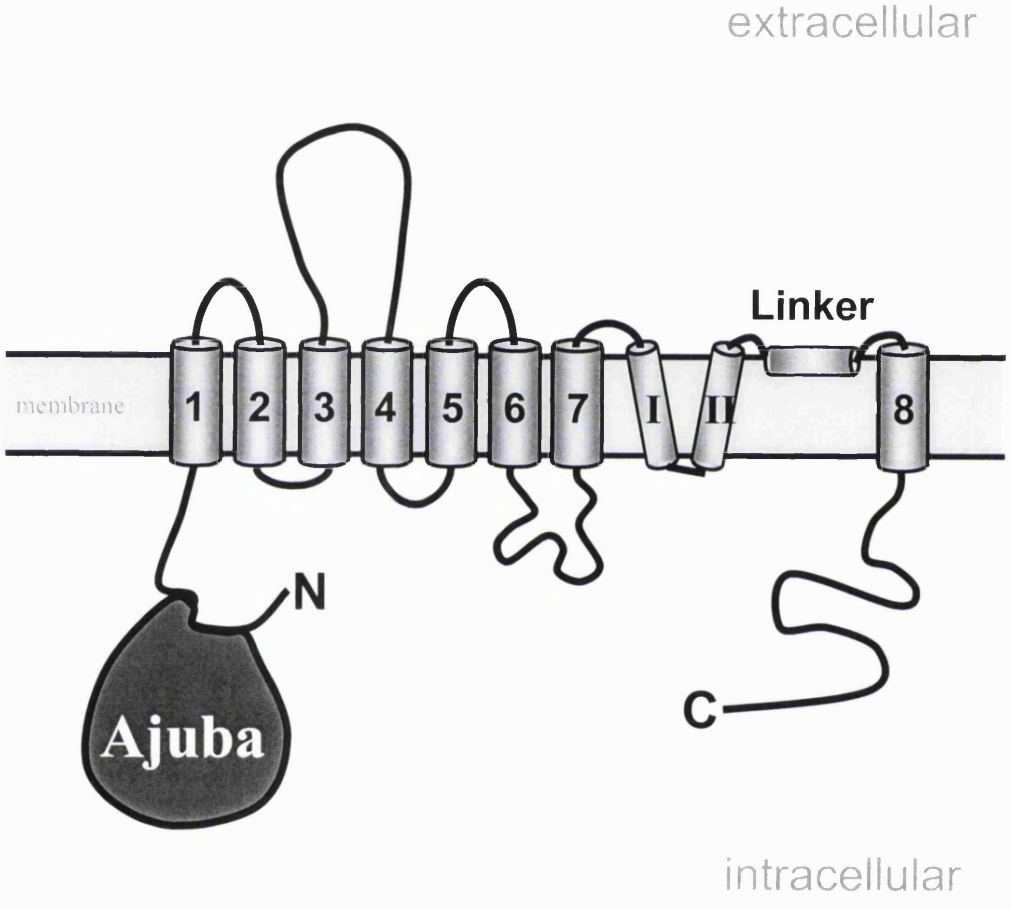
extracellular
Linker
membrane
1
2
3
4
5
6
7
I
II
8
N
Ajuba
C
intracellular

5.2 Co-expression of Ajuba and GLT in micro-injected COS-7 cells

COS-7 cells do not express GLT-1 or Ajuba endogenously (personal communication, Helene Marie). To study the potential effects of Ajuba on GLT-1, I micro-injected the cDNA for GLT-1 alone, or the cDNAs for GLT-1 and Ajuba, into the nucleus of these cells. About 95% of the injected cells co-expressed GLT-1 and Ajuba when both cDNAs were injected, as shown in the confocal images of Figure 5.2, in which antibody staining for GLT-1 (1^{st} panel) is shown in green and antibody labelling for Ajuba (2^{nd} panel) is shown in red. The co-localization of both proteins can be seen as yellow in the 3^{rd} panel, which is the superimposition of the double-labelling.

To identify successfully injected cells for electrophysiological experiments, I also co-injected the cDNA for green fluorescent protein (GFP). The cells were identified from their GFP fluorescence and used for patch-clamp experiments 24 hours after injection. It was assumed that if a cell expressed GFP it would also express the other products of the injected cDNAs, i.e. GLT-1 or GLT-1 and Ajuba. Indeed, most cells (n = 73/78) that were identified by GFP expression also produced an uptake current in response to glutamate (see below), whereas cells lacking GFP fluorescence never produced a glutamate-evoked current (n = 7).

5.3 Recording glutamate-evoked currents in COS-7 cells expressing GLT-1

Glutamate transporters use the electrochemical gradients for sodium, protons and potassium to power the uptake of glutamate. As described in section 1.3, it is thought that for each glutamate, three sodium ions and one proton are co-transported, whereas one potassium ion is counter-transported (Figure 5.3 A). This results in two

Figure 5.2: Co-localization of GLT-1 and Ajuba in micro-injected COS-7 cells

Confocal images and antibody labelling of two COS-7 cells co-injected with GLT-1 and *myc*-tagged-Ajuba cDNA. The antibody (B12) against GLT-1 (green, 1st column) reveals localization of the transporter mainly in the plasma membrane. The primary antibody was raised in rabbit, and the secondary antibody was anti-rabbit with the fluorophore FITC fused onto it. The antibody against *myc* (9E10) (red, 2nd column) reveals localization of *myc*-tagged Ajuba in the cytoplasm and the plasma membrane. The primary antibody was raised in mouse, and the secondary antibody was anti-mouse and had the fluorophore TexasRed fused onto it. Co-localization of the proteins is shown as yellow in the 3rd column, which is the superimposition of the 1st and 2nd columns.

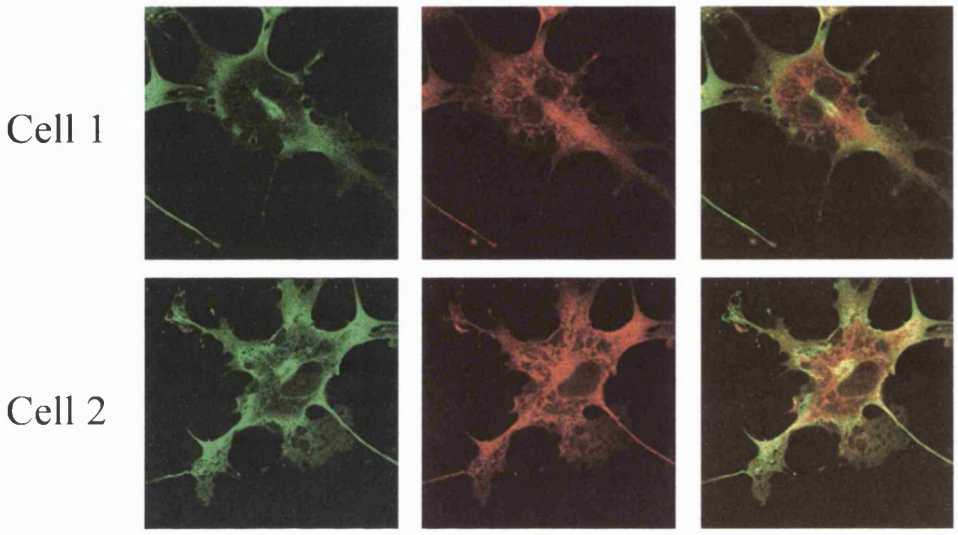
Cell 1
Cell 2
GLT-1
Ajuba
Super-
imposition

Figure 5.3: Recording glutamate uptake currents in COS-7 cells

(A) GLT-1 localized in the membrane of transfected COS-7 cells transports glutamate into the cell. For each glutamate$^-$, 3 Na^+ and 1 H^+ are co-transported and 1 K^+ is counter-transported (Levy et al., 1998). That results in two net positive charges being translocated during each cycle, which can be recorded as a membrane current (I).

(B) Examples of currents recorded from a COS-7 cell expressing GLT-1 and from a non-injected COS-7 cell, using the whole-cell patch clamp technique. The cells were voltage clamped at –60 mV. Whereas glutamate (100 μM) evokes an inward current in the GLT-1 expressing cell, the non-injected cell does not respond to glutamate.

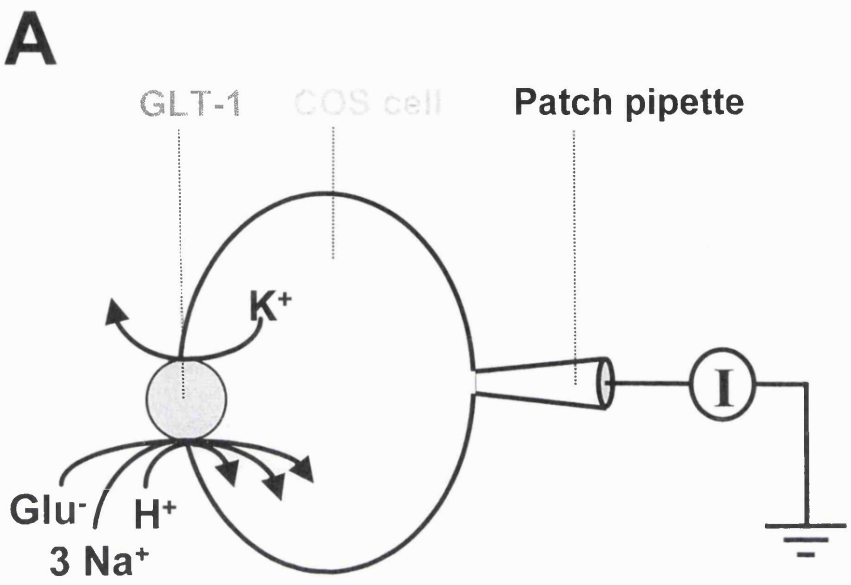
A
GLT-1
COS cell
Patch pipette
K+
I
Glu-
H+
3 Na+

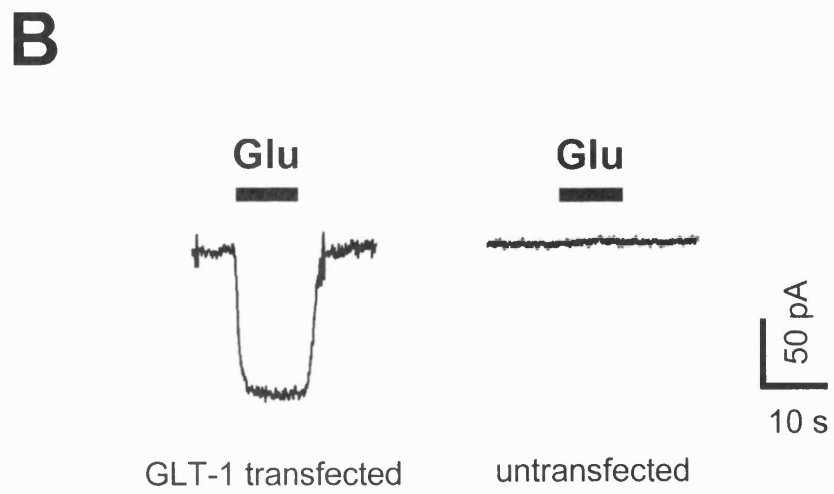
B
Glu
Glu
50 pA
10 s
GLT-1 transfected
untransfected

net positive charges being translocated with each glutamate, which can be recorded as a current across the cell membrane. The size of the recorded glutamate uptake current (when keeping the intra- and extracellular ion concentrations constant) depends on (1) the glutamate concentration (relative to the K_M), (2) the membrane potential (the transporter is electrogenic, being inhibited at positive potentials), (3) the number of functional transporters in the cell membrane (more transporters produce a larger current), and (4) the cycling time of the transporter (the shorter the cycle time, the larger the current). As well as the current generated by the co-transport of ions with glutamate, these transporters can also generate an anion current, because cycling of the carrier leads to an anion conductance being activated (see section 1.3). However, this anion current is negligible for GLT-1 unless highly permeant anions are present (Levy et al., 1998), as used in section 5.8 below.

An example of a glutamate transporter current in a whole-cell patch-clamped COS-7 cell expressing GLT-1 is shown in Figure 5.3 B. Bath application of 100 μM glutamate generated an inward current of mean amplitude 183 ± 20 pA (n = 20). Non-injected cells did not show such a current (n = 7), indicating that COS-7 cells do not express functional ionotropic glutamate receptors or glutamate transporters endogenously (Figure 5.3 B). To see whether Ajuba modulates the properties of GLT-1, I compared transporter-mediated currents in cells expressing either GLT-1 alone or GLT-1 and Ajuba. Unless otherwise stated, the cells were voltage clamped at –60 mV and transporter mediated currents were evoked by bath application of glutamate. All recordings were at room temperature (22-25°C).

5.4 Effect of co-expressing Ajuba on GLT-1's K_M for glutamate

The glutamate affinity of the glutamate transporter EAAC-1 is modulated by interaction with the glutamate transporter interacting protein GTRAP3-18 (Lin et al., 2001). Similarly, the glutamate affinity of GLAST is modulated by an unknown

intracellular protein in salamander Müller cells. To see whether co-expressing Ajuba alters the GLT-1 transporter's apparent affinity for glutamate, I applied different concentrations (5, 20, 100 μM) of glutamate to cells expressing GLT-1 alone or GLT-1 and Ajuba, and recorded the current responses. To obtain the K_M, the data from each cell were normalized to the current evoked by 100 μM glutamate in that cell, and were fit with the Michaelis-Menten equation:

$$I = \frac{I_{max} \cdot [glutamate]}{K_M + [glutamate]} \quad (5.1)$$

where I is the recorded current, I_{max} is the maximum evoked current at high [glutamate], and K_M, the Michaelis-Menten constant, is the glutamate concentration generating a half-maximal current (the reciprocal of the apparent affinity). An example of a recording from a COS-7 cell expressing only GLT-1 is shown in Figure 5.4 A, in which the amplitude of the glutamate transporter mediated currents increased in a dose-dependent manner. The dose-response curve of this cell is shown in Figure 5.4 B, and the line shows the fit of the data by the Michaelis-Menten equation (eqn 5.1). In this cell, the K_M was 18.2 μM and the I_{max} was –255 pA. For comparison, Figure 5.5 A shows an example of a recording from a COS-7 cell expressing GLT-1 and Ajuba. Again, the amplitude of the glutamate transporter mediated currents increased in a dose-dependent manner. The dose-response curve of this cell and the fit of the data by the Michaelis-Menten equation (eqn 5.1) are shown in Figure 5.5 B. In this cell, the K_m was 17.4 μM and the I_{max} was -446 pA.

Figure 5.6 A shows the averaged dose-response data obtained when either GLT-1 was expressed (filled circles, n=15) or when GLT-1 and Ajuba were co-expressed (open circles, n=10). The lines are Michaelis-Menten curves with K_M values equal to the means of the K_M values obtained in each condition. These did not differ significantly (p=0.13) and were 23.1 ± 2.7 μM when GLT-1 was expressed alone and 17.2 ± 2.4 μM when GLT-1 and Ajuba were co-expressed (Figure 5.6 B). This indicates that Ajuba does not modulate the apparent affinity of GLT-1 when co-expressed in COS-7 cells.

Figure 5.4: Specimen glutamate dose-response data from a GLT-1 expressing COS-7 cell

(A) Current responses at –60 mV to different concentrations of bath applied glutamate, recorded (using the whole-cell patch-clamp configuration) from a GLT-1 expressing COS-7 cell. **(B)** The data were normalized to the response evoked by 100 μM glutamate, plotted as a dose-response curve and fit by the Michaelis-Menten equation (smooth line). The K_M in this cell was 18.2 μm, and the I_{max} was 1.182 normalized to the current at 100 μM glutamate, or –255 pA in absolute units.

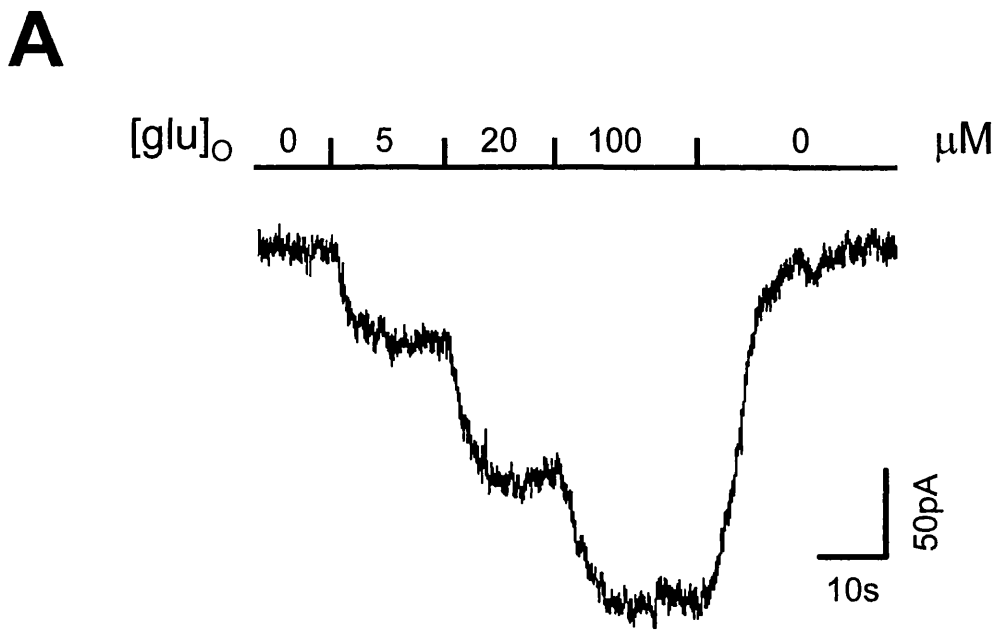
A
[glu]O
0
5
20
100
0
μM
50pA
10s

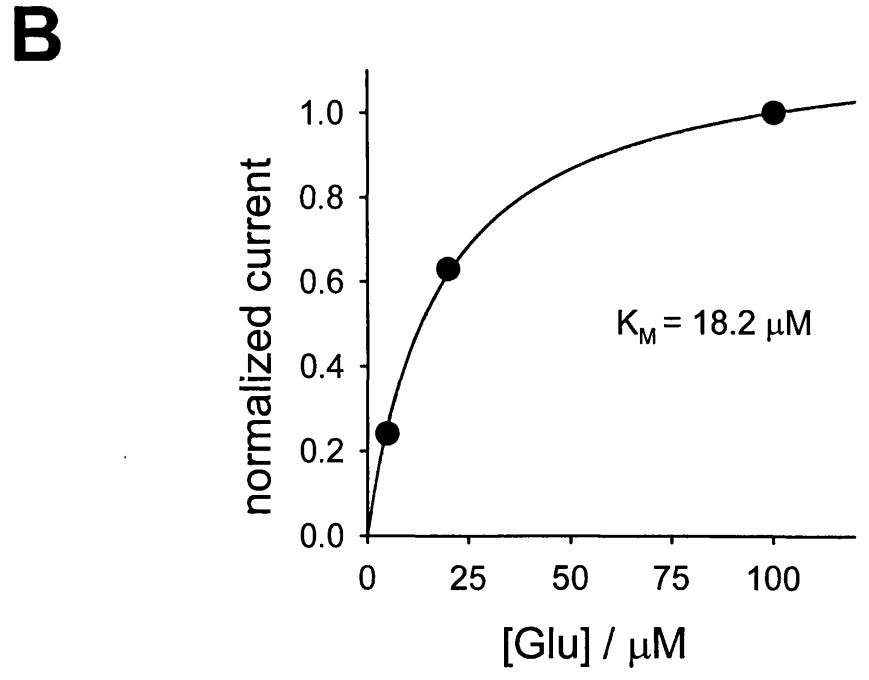
B
normalized current
1.0
0.8
0.6
0.4
0.2
0.0
0
25
50
75
100
[Glu] / μM
KM = 18.2 μM

Figure 5.5: Specimen glutamate dose-response data from a COS-7 cell co-expressing GLT-1 and Ajuba

(A) Current responses at –60 mV to different concentrations of bath applied glutamate, recorded (using the whole-cell patch-clamp configuration) from a COS-7 cell expressing GLT-1 and Ajuba. **(B)** The data were normalized to the response evoked by 100 μM glutamate, plotted as a dose-response curve and fit by the Michaelis-Menten equation (smooth line). The K_M in this cell was 17.4 μM, and the I_{max} was 1.174 normalized to the current with 100 μM glutamate, or –446 pA in absolute units.

A

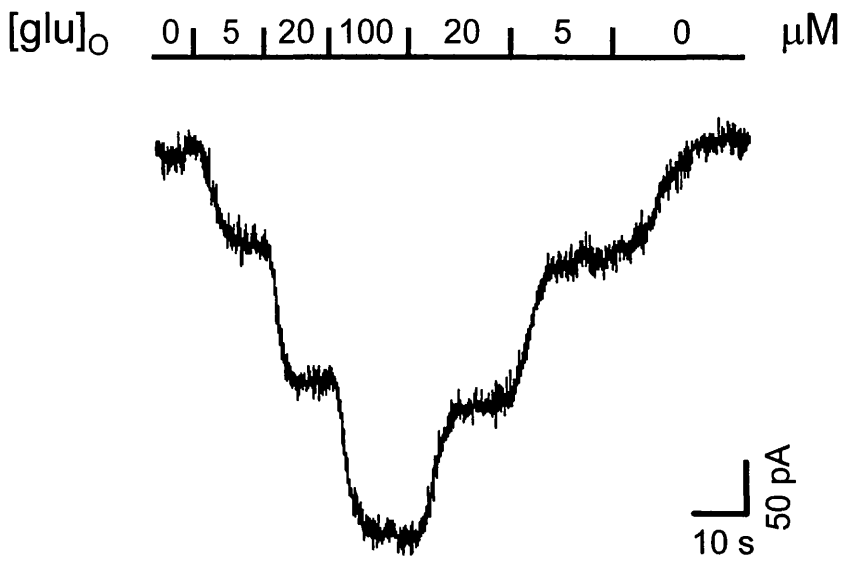
[glu]O
0
5
20
100
20
5
0
μM
50 pA
10 s

B

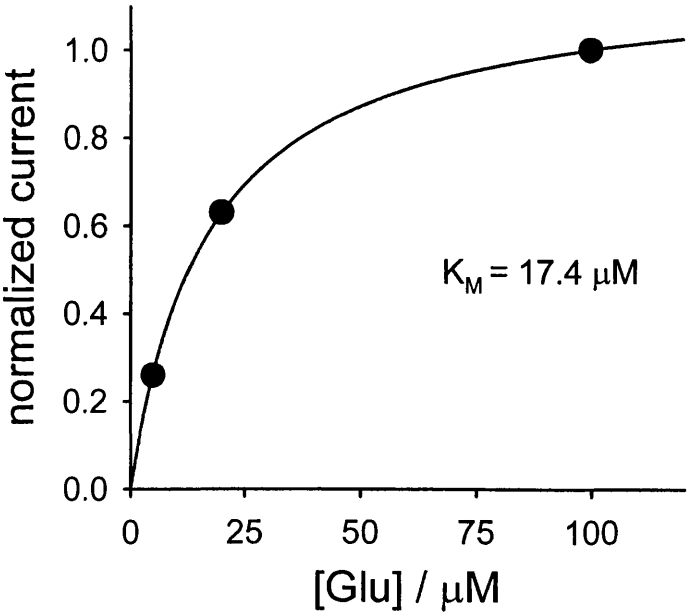
normalized current
1.0
0.8
0.6
0.4
0.2
0.0
0
25
50
75
100
[Glu] / μM
KM = 17.4 μM

Figure 5.6: The K_M for glutamate of GLT-1 is not changed when Ajuba is co-expressed

(A) Dose-response curves for glutamate-evoked GLT-1 mediated currents recorded from 15 COS-7 cells expressing only GLT-1 (filled circles, mean ± s.e.m), and 10 COS-7 cells expressing GLT-1 and Ajuba (open circles, mean ± s.e.m.), using the whole-cell patch-clamp technique (-60 mV). In each cell the responses were normalized to the response evoked by 100 μM glutamate, and fit by the Michaelis-Menten equation. The resulting K_Ms were averaged **(B)** and were 23.1 ± 2.7 μM when GLT-1 was expressed alone (n=15) and 17.2 ± 2.4 μM when GLT-1 and Ajuba were co-expressed (n=10). The smooth lines in (A) are the Michaelis-Menten curves using K_M values equal to the means of the averaged K_Ms.

A

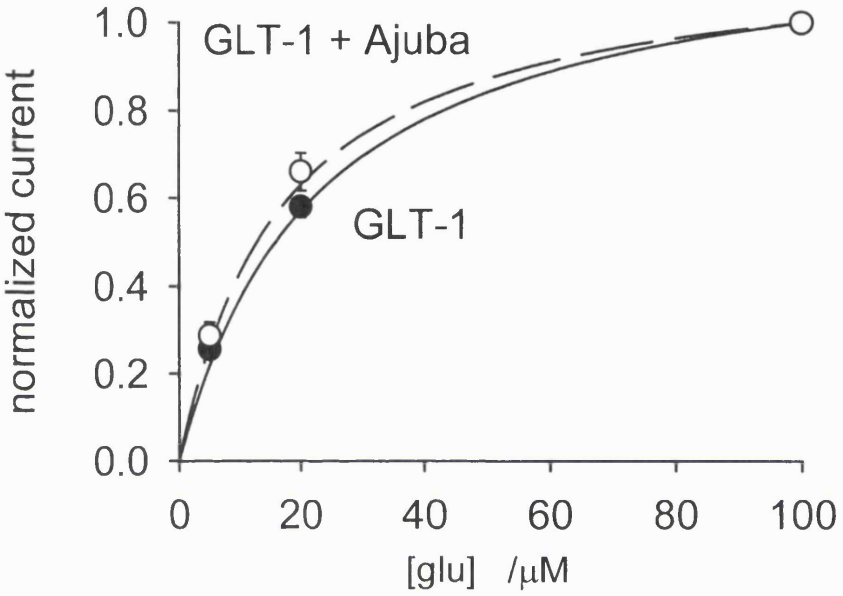
normalized current
1.0
0.8
0.6
0.4
0.2
0.0
GLT-1 + Ajuba
GLT-1
0
20
40
60
80
100
[glu] /μM

B

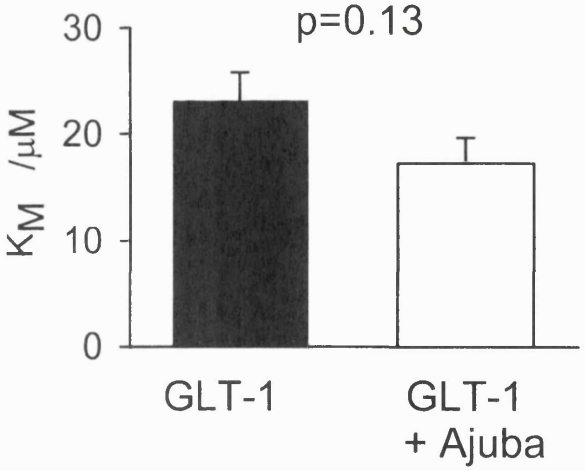
p=0.13
30
20
10
0
K_M /μM
GLT-1
GLT-1
+ Ajuba

Similarly, the maximum uptake current (I_{max}) at high glutamate concentrations (extrapolated from the fitted curve in each cell) did not differ significantly (p=0.97) and was -212.3 ± 26.5 pA when GLT-1 was expressed alone (n=15) and -210.4 ± 42.9 μM when GLT-1 and Ajuba were co-expressed (n=10). However, both this calculated value for I_{max} and also the size of the currents evoked by a near saturating (100 μM) dose of glutamate differed substantially between cells. The current response to 100 μM glutamate (at –60 mV) ranged from as low as -26 pA to as large as -416 pA, and was on average -182.8 ± 20.1 pA (n=20) when GLT-1 was expressed alone; it ranged from as low as –30 pA to as large as -380 pA, and was on average -195.0 ± 27.8 pA (n=15) when GLT-1 + Ajuba were expressed (p=0.72 compared with GLT-1 alone).

Theoretically, the size of the glutamate-evoked steady state uptake current produced by a near saturating dose of glutamate (e.g. 100 μM), at a given membrane potential (e.g. –60 mV), and with a fixed stoichiometry (i.e. 2 net positive charges moving with each glutamate), depends on the number of transporters operating and the rate at which they transport glutamate (their cycling rate). Since, within each transfection group, the stoichiometry and the cycling rate of GLT-1 are presumably constant, the variability of the recorded currents indicates that the number of functional transporters in the plasma membrane varies hugely between cells. This variation probably reflects differences in cell size (membrane area), as well as differences in the expression level of GLT-1 and/or differences of protein insertion into the membrane. To remove this variability and thereby try to get a better estimate of the maximum uptake rate per glutamate transporter in COS-7 cells expressing GLT-1 alone or GLT-1 and Ajuba, I took the approach described in the following section.

5.5 Effect of co-expressing Ajuba on GLT-1's maximum uptake rate

To obtain a measure of the maximum uptake current per transporter independent of the number of transporters on the cell surface, I normalized the current produced by 100 μM glutamate (a near saturating dose) in each cell by the cell's kainate-suppressible capacitance, which is (as explained below) proportional to the number of transporters in the membrane. Transporters have been shown to produce a rapid charge movement in response to a voltage change, equivalent to an extra membrane capacitance (Mager et al., 1993; Wadiche et al., 1995b). As illustrated in Figure 5.7, the Na^+ ions which drive glutamate uptake are thought to bind to the transporter within the membrane field. When a positive voltage step is applied, the Na^+ are forced out of the membrane, generating a transient outward component of capacity current. For EAAT-2, which is the human homologue of the rat GLT-1, this charge movement can be prevented by application of the competitive non-transported glutamate analogue kainate (Wadiche et al., 1995b). Kainate is thought to lock the transporter in a state so that the sodium ions are trapped and cannot move out of the membrane electric field (Figure 5.7). This occurs because the binding of substrates to the transporter is ordered, with glutamate/kainate binding occurring after binding of the Na^+ which generate the charge movement: once glutamate/kainate has bound the transporter conformation is changed so that the Na^+ cannot unbind. The size of the kainate-suppressible capacity current is, therefore, directly proportional to the number of transporters in the membrane, and also depends on the membrane potential and the size of the voltage step (Wadiche et al., 1995b). Thus, to investigate whether Ajuba affects the maximum uptake current per transporter (i.e. the cycling rate), I used the transporter charge movement, measured as the difference of capacity current in the absence and presence of kainate, as a measure of the transporter number. If the ratio of the maximum glutamate uptake current to the kainate-suppressible capacitance (loosely speaking the ratio of the total

Figure 5.7: Scheme of the kainate suppressible charge movements

Each glutamate transporter (indicated as large round structure) contains three sodium binding sites. In resting, steady state conditions, sodium ions will be bound to these sites, resulting in three positive charges (Na^+; indicated as small circles with a "+") being localized within the membrane electric field. When the membrane potential is stepped to a positive potential, the three positive charges (Na^+) will move outwards (dashed arrows) through the membrane field, generating a small capacity current. The size of the charge movement in the whole cell depends on the number of transporters (number of sodium binding sites), the initial membrane potential (which determines what fraction of Na^+ binding sites are occupied before the positive voltage step) and the voltage step (which determines what fraction of the Na^+ are displaced from their binding sites). **(B)** Kainate blocks the charge movement, restraining the sodium ions to their binding site within the membrane. This abolishes the transporter component of the capacity transient. The difference of the capacitance between when kainate is absent (i.e. the Na^+ are free to move) and present (i.e. the Na^+ are locked in the membrane), that is the kainate-suppressible capacitance, is proportional to the number of transporters in the membrane.

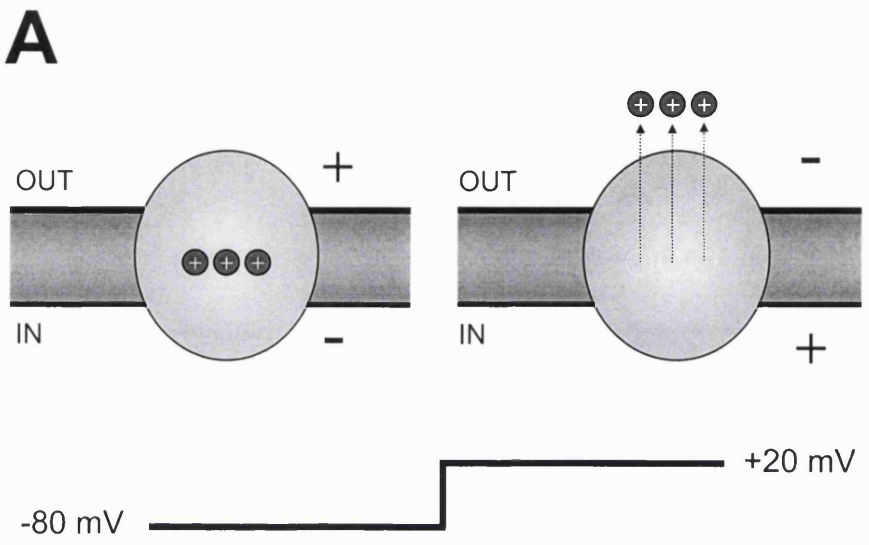
A
OUT
IN
+
-
OUT
IN
-
+
+20 mV
-80 mV

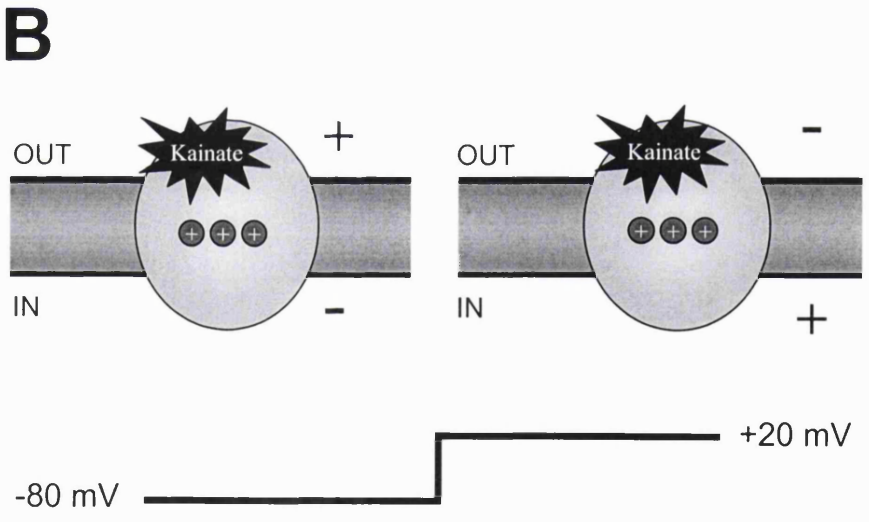
B
OUT
Kainate
IN
+
-
OUT
Kainate
IN
-
+
+20 mV
-80 mV

glutamate taken up per unit time to the number of transporters present) is larger in the presence of Ajuba, the cycling rate must be faster; if it is smaller, the cycling rate must be slower.

I recorded the response of COS-7 cells expressing either GLT-1 alone, GLT-1 and Ajuba, or neither GLT-1 nor Ajuba, to voltage steps from –80 mV to +20 mV, in the presence (to inhibit the charge movements) and absence (to permit the charge movements) of 300 μM kainate. The current transients were fitted with a mono-exponentially decaying function to obtain a value of the capacitance (see Chapter 2), and the difference of the capacitance in the absence and the presence of kainate (ΔC_{KA}), which is proportional to the number of transporters in the membrane. I also recorded the steady state glutamate uptake current in each cell (I_{glu}) by applying 100 μM glutamate at a holding potential of –80 mV. Examples of such recordings are shown in Figure 5.8 (when GLT-1 was expressed alone) and Figure 5.9 (when GLT-1 and Ajuba, or neither, were co-expressed). This approach assumes that Ajuba does not affect (1) the binding of sodium ions to the transporter, and (2) the blocking effect of kainate. The glutamate transporter current in the presence of kainate compared to the current when kainate was absent ($I_{glu,inKA} / I_{glu,noKA}$) was 0.34 ± 0.02 (n = 10) when GLT-1 was expressed alone and 0.45 ± 0.10 (n = 5, not significantly different, p = 0.16) when GLT-1 and Ajuba were co-expressed, suggesting that Ajuba does not interfere with the kainate block. These values are similar to the 0.38 ± 0.02 (n = 6) observed by (Otis and Kavanaugh, 2000) in HEK-293 cells expressing GLT-1.

Figure 5.10 A shows results obtained from 15 different COS-7 cells expressing either GLT-1 (filled circles, n=10) or GLT-1 and Ajuba (open circles, n=5), as described above. The uptake current is plotted as a function of the kainate-suppressible capacitance. The resulting graphs are expected to be a straight line with a slope proportional to the cycling rate of a single transporter. The lines shown on the graph are the mean ± s.e.m. of the slopes ($I_{glu} / \Delta C_{KA}$) when GLT-1 alone (dashed

Figure 5.8: Kainate-suppressible capacitance in a cell expressing GLT-1 alone

Specimen capacity currents of a cell expressing GLT-1 alone, when the membrane potential was stepped from –80 to +20 mV, in the absence ("control") and presence ("kainate") of 300 μM kainate. The ΔC_{KA} in this cell was 1.83 pF, the cell capacitance was 63 pF, and the inward current evoked by 100 μM glutamate was -87 pA (at –80 mV).

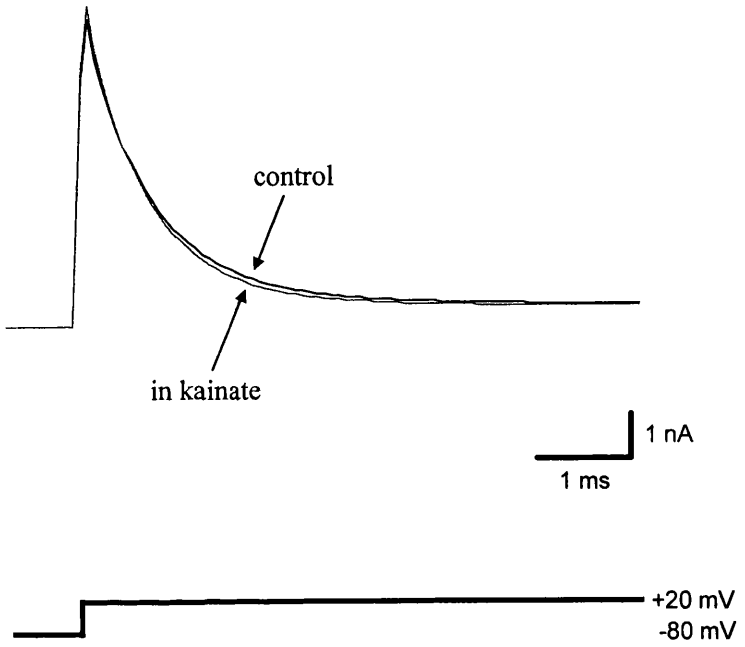
control
in kainate
1 nA
1 ms
+20 mV
-80 mV

Figure 5.9: Kainate-suppressible capacitance in a cell expressing GLT-1 and Ajuba

(A) Specimen capacity currents of a cell expressing GLT-1 and Ajuba, when the membrane potential was stepped from –80 to +20 mV, in the absence ("control") and presence ("kainate") of 300 μM kainate. The ΔC_{KA} in this cell was 2.22 pF, the capacitance in kainate was 76 pF, and the inward current evoked by 100 μM glutamate was -73 pA (at –80 mV).

(B) Specimen capacity currents of a non-transfected cell, when the membrane potential was stepped from –80 to +20 mV, in the absence ("control") and presence ("kainate") of 300 μM kainate. Note that kainate does not affect the capacity current.

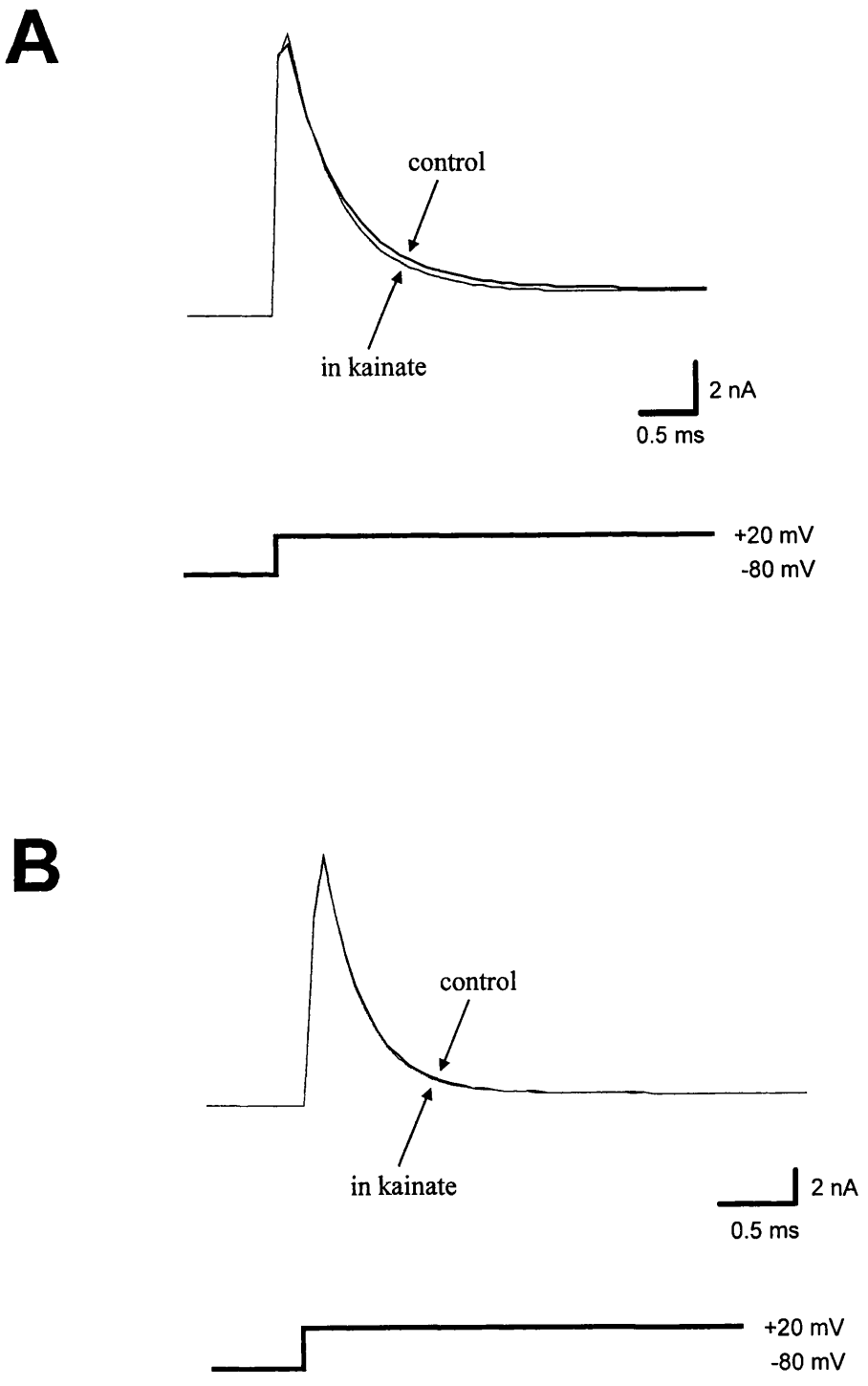
A
control
in kainate
2 nA
0.5 ms
+20 mV
-80 mV
B
control
in kainate
2 nA
0.5 ms
+20 mV
-80 mV

Figure 5.10: The maximum uptake rate of GLT-1 is not changed when Ajuba is co-expressed in COS-7 cells

(A) Scatter plot of the current evoked by 100 μM glutamate (I_{glu}) as a function of the kainate-suppressible capacitance ($\Delta C_{KA} = C_{noKA} - C_{inKA}$). The filled circles are data from 10 COS-7 cells expressing GLT-1 alone, the open circles are data from 5 COS-7 cells expressing GLT-1 and Ajuba. The lines (dashed for GLT-1; dotted for GLT-1 and Ajuba) are the mean ± s.e.m. of the averaged $I_{glu}/\Delta C_{KA}$ ratio. **(B)** Bar graph of the mean ± s.e.m. of the $I_{glu}/\Delta C_{KA}$ ratio (n=10 for GLT-1; n=5 for GLT-1 and Ajuba).

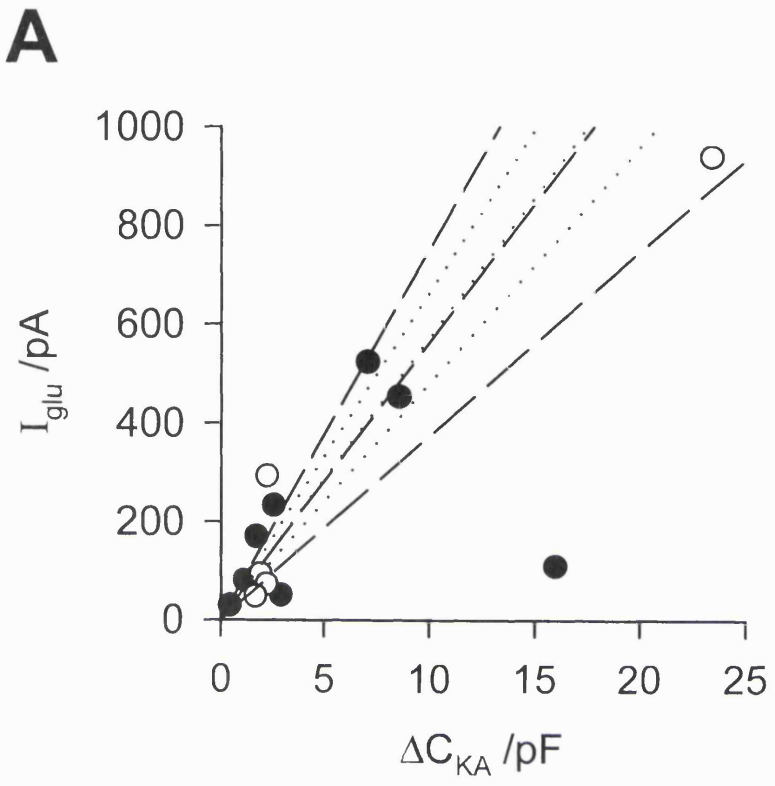
A
1000
800
600
400
200
0
I_{glu} /pA
0
5
10
15
20
25
ΔC_{KA} /pF

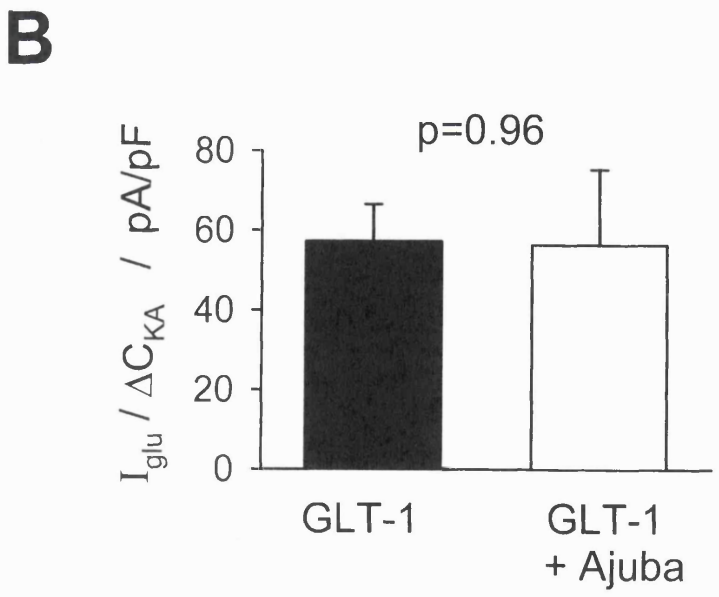
B
p=0.96
80
60
40
20
0
I_{glu} / ΔC_{KA} / pA/pF
GLT-1
GLT-1
+ Ajuba

lines) or GLT-1 and Ajuba (dotted lines) was expressed. The slopes were not significantly different (p=0.96) between cells expressing GLT-1 alone (57.3 ± 9.2 pA/pF, n=10) and cells expressing GLT-1 and Ajuba (56.3 ± 18.9 pA/pF, n=5). This indicates that the maximum uptake rate of GLT-1 is not different when Ajuba is co-expressed in COS-7 cells. However, the kainate-suppressible capacitance is tiny (Figure 5.8 B and 5.9 B), the variability is large (Figure 5.10 A) and it is hard to rule out the possibility that Ajuba does alter the I_{max} per transporter but I have, by chance, failed to detect it.

5.6 Effect of co-expressing Ajuba on the surface expression of GLT

The surface expression of the glutamate transporter EAAT-4 has been shown to be regulated by the glutamate transporter interacting proteins GTRAP41 and GTRAP48 (Jackson et al., 2001). To see if Ajuba regulates the surface expression of GLT-1 in COS-7 cells, that is the number of transporters per plasma membrane area, I normalized the kainate-suppressible capacitance (ΔC_{KA}), which is proportional to the number of transporters, by the cell membrane capacitance (C_m), which is proportional to the surface area of the cell, in each cell. The kainate-suppressible capacitance was on average 3.8 ± 0.6 % of the total cell capacitance when GLT-1 was expressed alone (n=10), and 4.3 ± 0.9 % of the total cell capacitance when GLT-1 and Ajuba were co-expressed (n=5), indicating that the surface expression of GLT-1 in COS-7 cells was not significantly changed by Ajuba (p=0.66, Figure 5.11).

Figure 5.11: Co-expression of Ajuba does not change the surface expression of GLT-1

Bar graph showing the ratio of the kainate-suppressible capacitance to the total cell capacitance($\Delta C_{KA}/C_m$) when GLT-1 alone, or GLT-1 and Ajuba, are expressed in COS-7 cells.

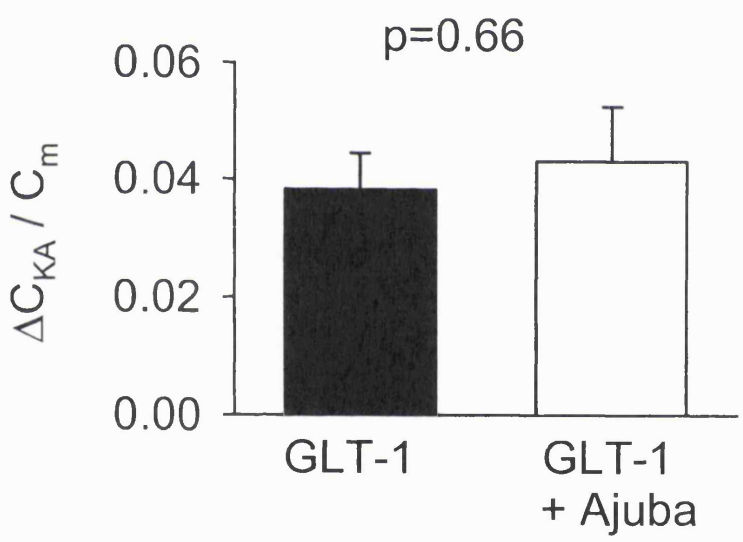
p=0.66
0.06
0.04
0.02
0.00
$\Delta C_{KA} / C_m$
GLT-1
GLT-1
+ Ajuba

5.7 Effect of co-expressing Ajuba on the voltage dependence of the GLT-1 transporter current

As mentioned in section 5.4 and section 1.3, glutamate uptake is electrogenic, transporting 2 net positive charges across the plasma membrane with each glutamate. This results in the transport of glutamate being inhibited at depolarized membrane potentials. To see whether Ajuba affects the voltage-dependence of glutamate uptake mediated by GLT-1, I recorded the current response to 100 μM glutamate at different membrane potentials. Examples of such recordings are shown for a COS-7 cell expressing GLT-1 alone in Figure 5.12, and for a COS-7 cell expressing GLT-1 and Ajuba in Figure 5.13. The currents in each cell were normalized to the current produced at –60 mV in that cell. The averaged glutamate-evoked current-voltage relation (I-V) for cells expressing GLT-1 alone (filled circles, n=6) and for cells expressing GLT-1 and Ajuba (open circles, n=9) were not significantly different from each other (Figure 5.14), and, as expected, neither I-V relation reversed at positive potentials (since applying external glutamate can only make the transporter run more in the inward direction or less in the outward direction, both of which give an inward current). The ratio of the currents produced at 0 mV (I_{0mV}) and at –60 mV (I_{-60mV}) was 0.219 ± 0.070 in cells expressing GLT-1 (n=6) and 0.180 ± 0.024 in cells expressing GLT-1 and Ajuba (n=9, p=0.56). This suggests that co-expressing Ajuba in COS-7 cells does not affect the rate limiting charge-moving steps in the carrier cycle of GLT-1.

Figure 5.12: Voltage-dependence of the transporter current generated by GLT-1 expressed in COS-7 cells

(A) Specimen traces showing the response to 100 μM glutamate of a COS-7 cell expressing GLT-1. The cell was voltage clamped at different membrane potentials. **(B)** I-V curve of the specimen data shown in (A). As expected for this electrogenic transporter, the current is reduced at depolarized potentials and does not reverse.

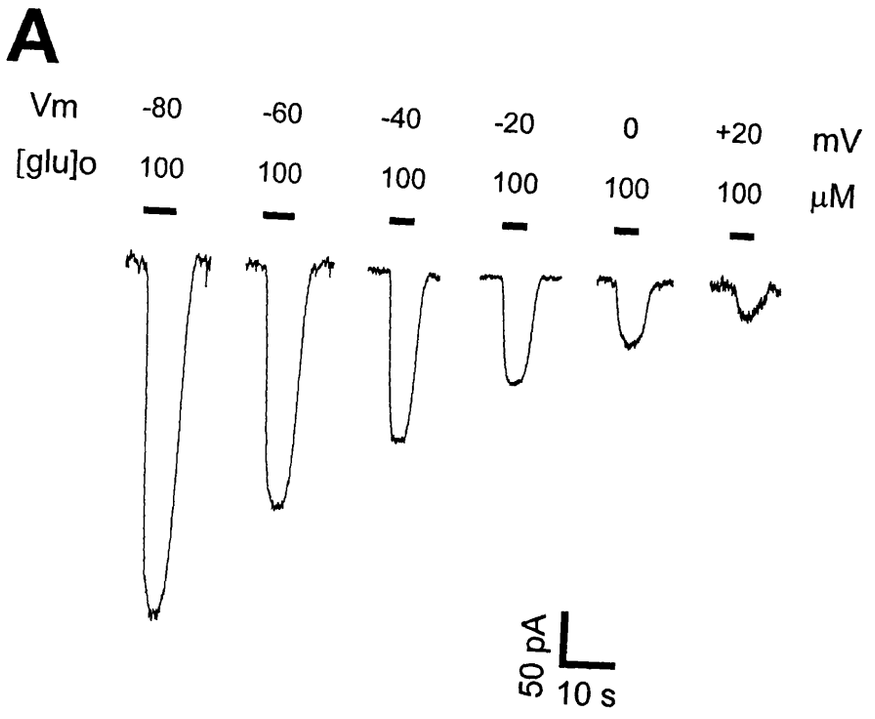
A
Vm
-80
-60
-40
-20
0
+20
mV
[glu]o
100
100
100
100
100
100
µM
50 pA
10 s

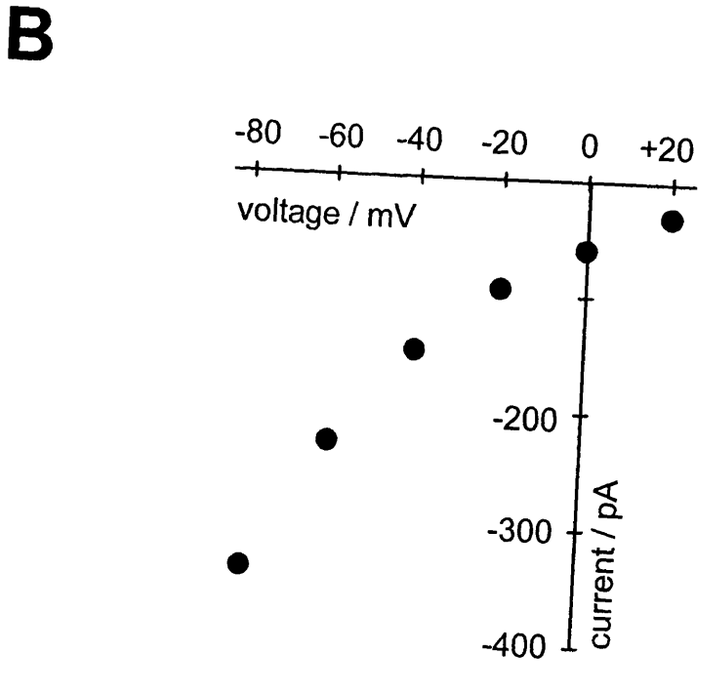
B
-80
-60
-40
-20
0
+20
voltage / mV
-200
-300
-400
current / pA

Figure 5.13: Voltage-dependence of the transporter current generated by GLT-1 when Ajuba was co-expressed in COS-7 cells

(A) Specimen traces showing the response to 100 μM glutamate of a COS-7 cell expressing GLT-1 and Ajuba. The cell was voltage clamped at different membrane potentials. **(B)** I-V curve of the specimen data shown in (A).

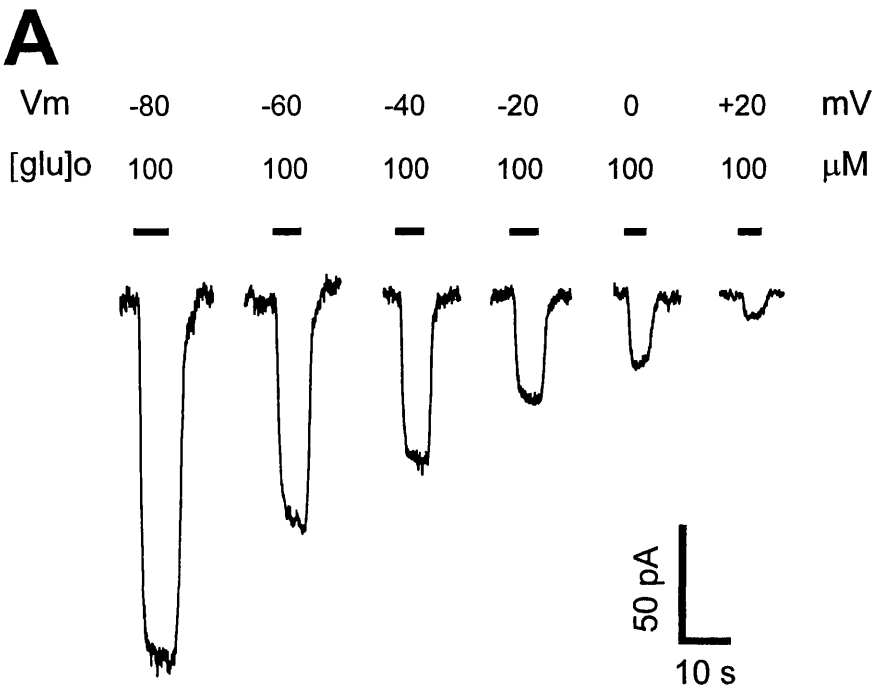
A
Vm
-80
-60
-40
-20
0
+20
mV
[glu]o
100
100
100
100
100
100
µM
50 pA
10 s

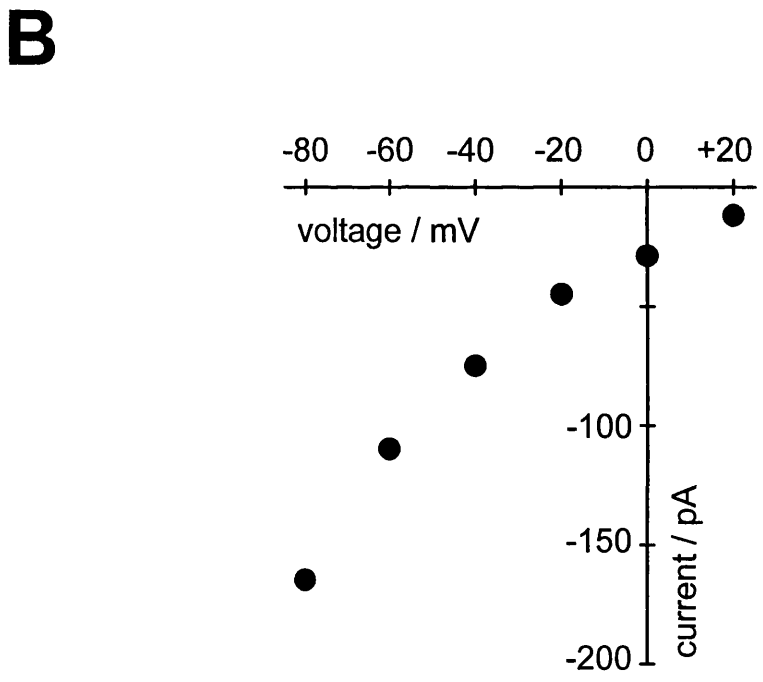
B
-80
-60
-40
-20
0
+20
voltage / mV
-100
-150
-200
current / pA

Figure 5.14: The voltage-dependence of the GLT-1 transporter current is not changed when Ajuba is co-expressed in COS-7 cells

Current-voltage relation of 6 COS-7 cells expressing GLT-1 alone (filled circles) and 9 COS-7 cells expressing GLT-1 and Ajuba (open circles; mean ± s.e.m.). The currents were evoked by bath application of 100 μM glutamate, and recorded at different membrane potentials. In each cell, the currents were normalized to the current recorded at –60 mV to compensate for differences between cells in the number of transporters expressed.

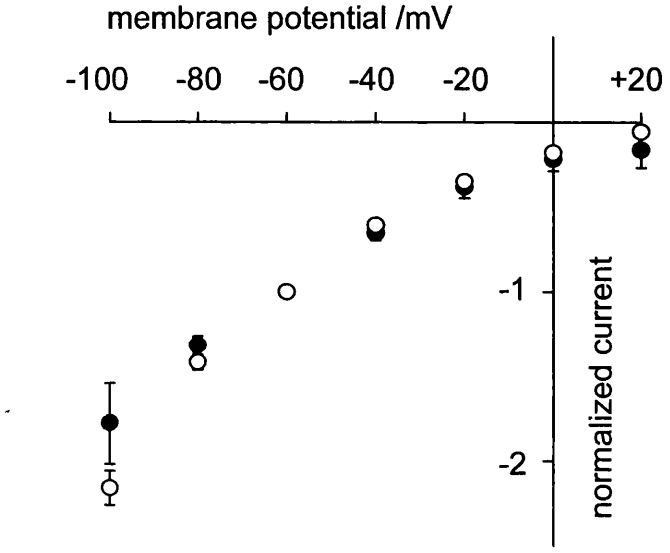
membrane potential /mV
-100
-80
-60
-40
-20
+20
-1
-2
normalized current

5.8 Effect of co-expressing Ajuba on GLT-1's anion conductance

In addition to transporting glutamate, glutamate transporters also possess an anion channel (see section 1.3 for more detail and Figure 1.2). Under approximately physiological conditions (i.e. with chloride as the major extracellular anion) the glutamate-evoked current mediated by GLT-1 is mainly due to the uptake of glutamate accompanied by the net entry of two positive charges. Less of this inward transporter current flows at depolarized potentials where the charge movement is opposed by the voltage (Figures 5.12 - 5.14). Other external anions, such as nitrate, have been shown to permeate the glutamate transporter's anion conductance much more readily than chloride, resulting in a more linear I-V relation for the glutamate-evoked current, which reverses at depolarized potentials due to anion influx through the anion conductance (Fairman et al., 1995; Billups et al., 1996; Levy et al., 1998). The glutamate transporter mediated current is thus composed of two underlying mechanisms: the uptake of glutamate generating an inward current, and the anion flux through the transporter which can generate an inward or outward current depending on the anion gradient and the voltage. These two current components can be recorded and investigated in isolation by providing conditions favouring either of the two. The glutamate uptake current can be studied in isolation by using chloride as the major intra- and extracellular anion (which hardly permeates the transporter) and recording the current at hyperpolarized potentials where the uptake current is large (Figure 5.15 A). The anion conductance of the transporter can be studied in isolation by using nitrate as the major extracellular anion (which permeates the transporter well) and recording the current at depolarized potentials, where uptake is inhibited and where glutamate will evoke an outward current which is predominantly due to the influx of nitrate through the transporter's anion channel (Figure 5.15 B).

Figure 5.15: Conditions for recording the GLT-1 glutamate uptake or anion channel currents

Glutamate transporter mediated currents are a mixture of the current produced by glutamate uptake and the current produced by the anion channel of the transporter. Certain conditions favour one or the other component. **(A)** If the major external anion is chloride and the membrane potential is hyperpolarized, the current mediated by the transporter will predominantly be due to the uptake of glutamate with 2 net positive charges (inward current). **(B)** If the major extracellular anion is nitrate and the membrane potential is depolarized, the current mediated by the transporter will predominantly be due to the influx of nitrate through the transporter's anion channel (outward current).

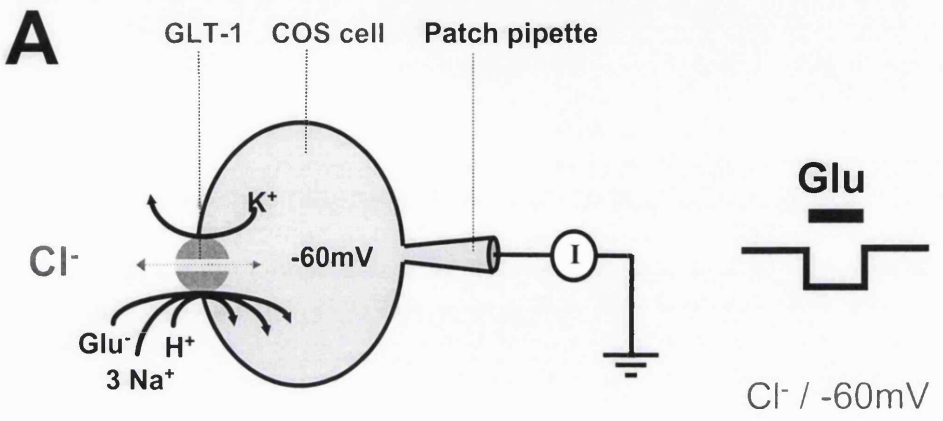

Conditions favouring the glutamate uptake current

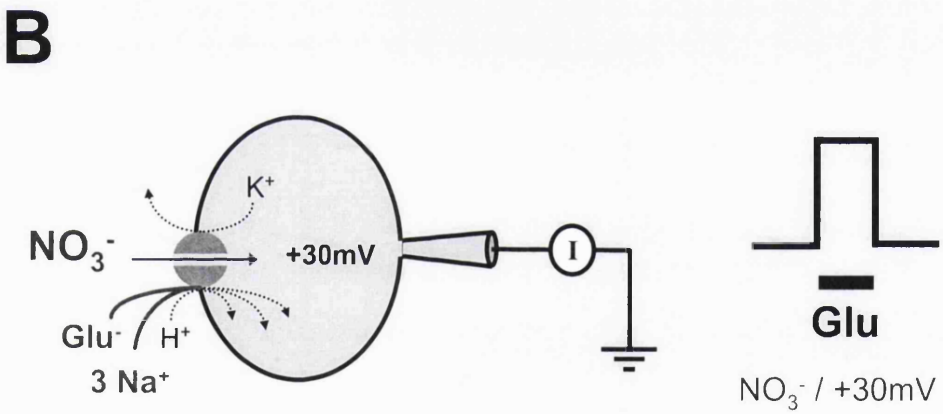

Conditions favouring the anion channel current

To see whether Ajuba modulates the anion conductance of GLT-1, I recorded currents evoked by 100 μM glutamate in COS-7 cells expressing either GLT-1 alone or GLT-1 and Ajuba, either at –60 mV in chloride containing solution (to measure the size of the glutamate uptake component ($I_{-60mV, Cl}$)) or at +30 mV in nitrate containing solution (to measure the size of the anion channel component ($I_{+30mV, NO3-}$)). I normalized the anion channel current ($I_{+30mV, NO3-}$) to the uptake current ($I_{-60mV, Cl}$) in each cell to correct for differences in expression levels and cell sizes.

An example of a recording from a COS-7 cell expressing GLT-1 alone is shown in Figure 5.16, for which the current ratio was 2.69. For comparison, an example of a recording from a COS-7 cell expressing GLT-1 and Ajuba is shown in Figure 5.17, for which the current ratio was 2.07. On average (Figure 5.18), the ratio was 2.68 ± 0.56 when GLT-1 was expressed alone (n=5) and 2.00 ± 0.32 when GLT-1 and Ajuba were co-expressed (n=5, not significantly different, p=0.32). This results indicate that Ajuba does not significantly alter activation of the anion conductance of GLT-1 when co-expressed in COS-7 cells.

5.9 Effect of co-expressing Ajuba on GLT-1's K_M when using the perforated patch configuration

The data in Section 5.4 to 5.8 were obtained using the conventional whole-cell patch-clamp technique. This technique allows one to control the membrane potential and to record currents through the cell membrane, and has the advantage of controlling the intracellular milieu by dialyzing the solution of the patch pipette into the cell. Conversely, however, it also means that anything present in the cytoplasm can be dialyzed out of the cell into the patch-pipette, perhaps even large proteins such as Ajuba (molecular weight 58 kDa). The perforated patch-clamp configuration (see Chapter 2) also allows one to control the membrane potential and to record current through the cell membrane, but prevents the dialysis out of the cell of large molecules, including proteins, and certain ions. To see if co-expression of Ajuba had

Figure 5.16: Uptake and anion current of GLT-1 expressed in COS-7 cells

(A) Specimen traces of the glutamate uptake current (1st trace, -60 mV, extracellular solution contained chloride) and anion channel current (2nd trace, +30 mV, extracellular solution contained nitrate) of GLT-1 expressed in COS-7 cells, evoked by bath application of 100 μM glutamate. The ratio of the anion channel current compared to the uptake current for this specimen cell is shown in **(B)**.

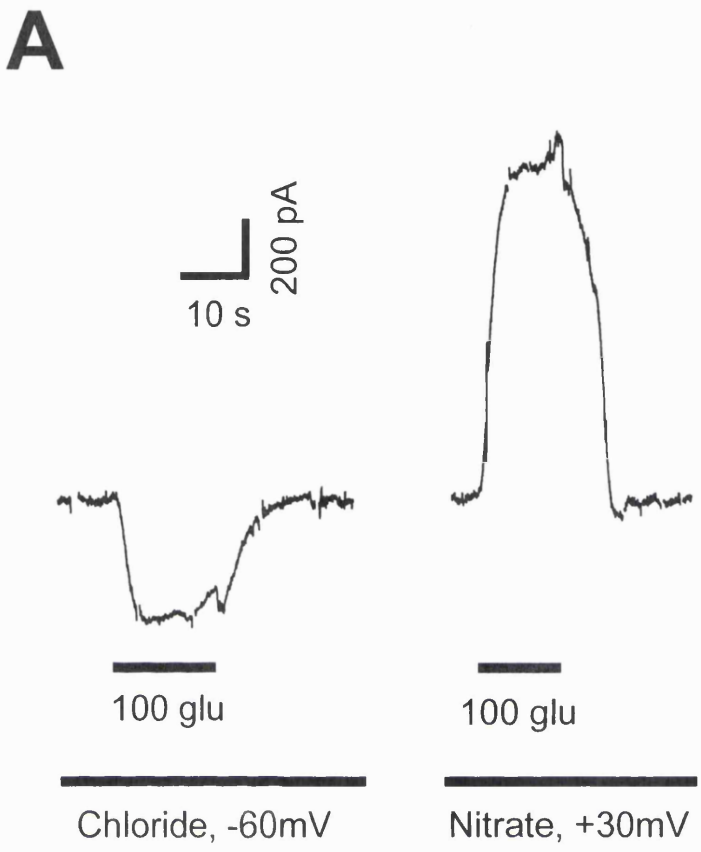
A
200 pA
10 s
100 glu
100 glu
Chloride, -60mV
Nitrate, +30mV

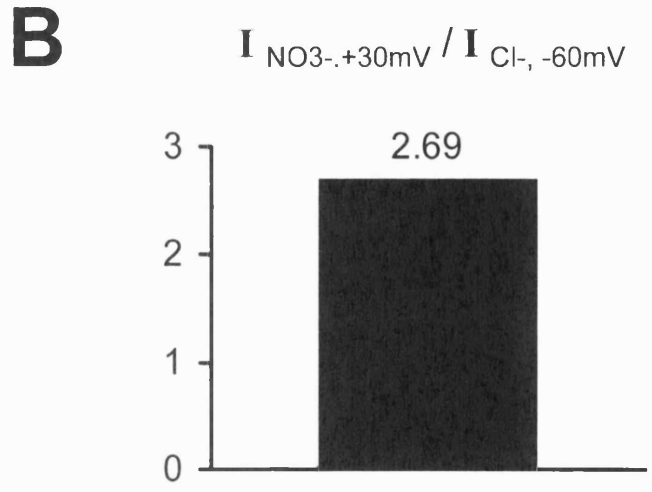
B
I NO3-.+30mV / I Cl-, -60mV
2.69
3
2
1
0

Figure 5.17: Uptake and anion current of GLT-1 when Ajuba was co-expressed in COS-7 cells

(A) Specimen traces of the glutamate uptake current (1st trace, -60 mV, extracellular solution contained chloride) and anion channel current (2nd trace, +30 mV, extracellular solution contained nitrate) of GLT-1 when Ajuba was co-expressed in COS-7 cells, evoked by bath application of 100 μM glutamate. The ratio of the anion channel current to the uptake current for this specimen cell is shown in **(B)**

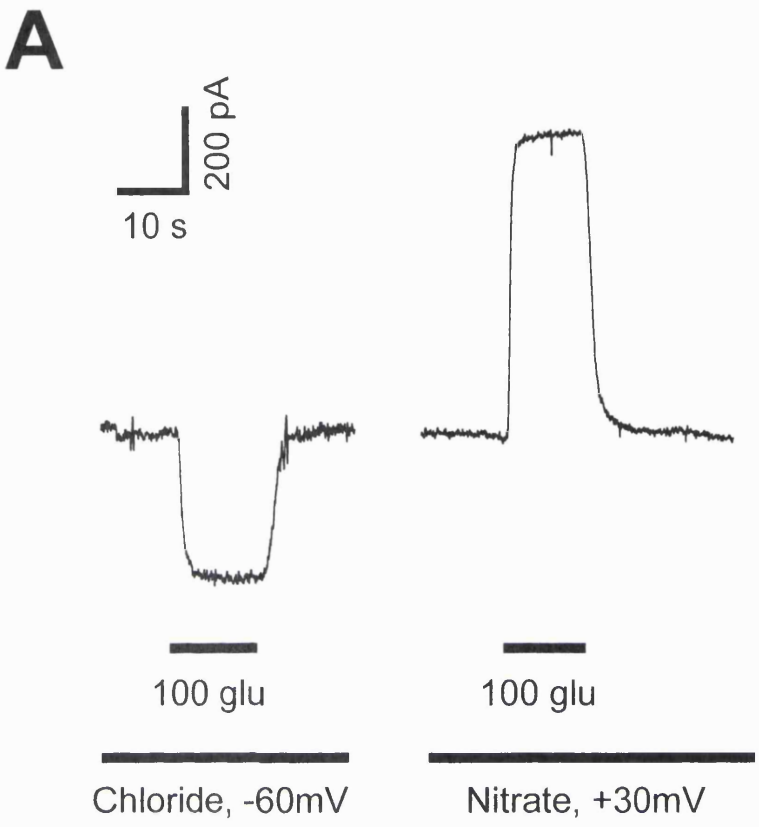
A
200 pA
10 s
100 glu
100 glu
Chloride, -60mV
Nitrate, +30mV

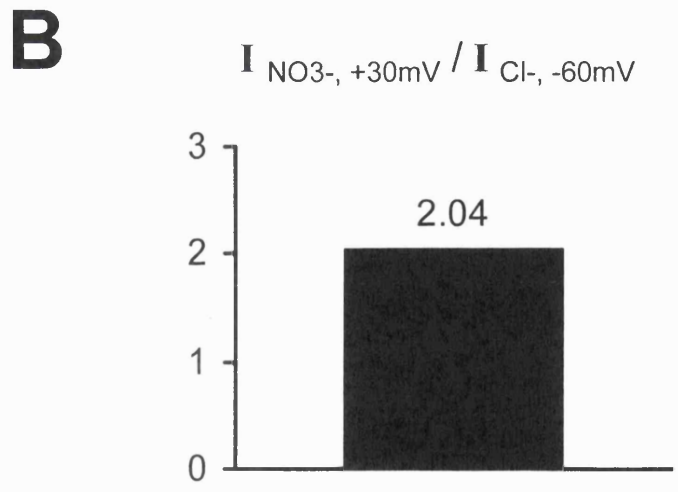
B
I NO3-, +30mV / I Cl-, -60mV
3
2
1
0
2.04

Figure 5.18: The anion conductance of GLT-1 is not changed when Ajuba is co-expressed in COS-7 cells

Mean (± s.e.m.) ratio of the anion channel current ($I_{+30mV,\ NO3-}$) to the glutamate uptake current ($I_{-60mV,\ Cl-}$), in 5 COS-7 cells expressing GLT-1 alone and 5 COS-7 cells expressing GLT-1 and Ajuba. The transporter currents were evoked by bath application of 100 μM glutamate.

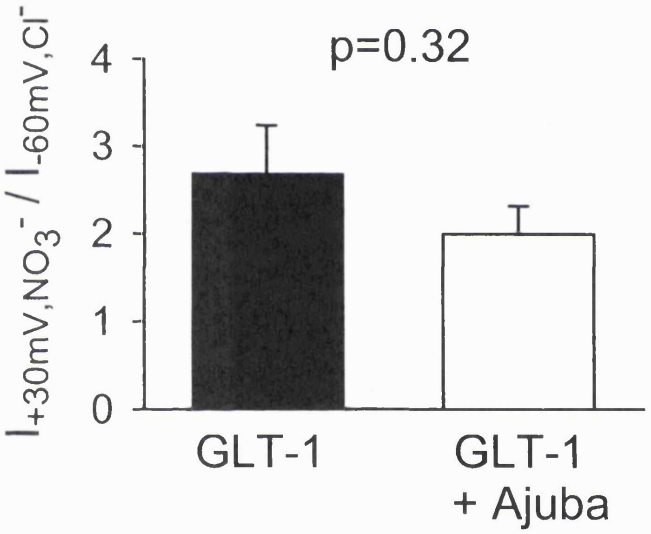
p=0.32
$I_{+30mV,NO_3^-} / I_{-60mV,Cl^-}$
4
3
2
1
0
GLT-1
GLT-1
+ Ajuba

an effect on GLT-1's K_M for glutamate when recorded in the perforated patch clamp configuration, i.e. when Ajuba cannot be dialysed out of the cytoplasm, I patch-clamped COS-7 cells expressing either GLT-1 alone or GLT-1 and Ajuba using the antibiotic amphotericin B in the patch-pipette as the perforating agent (Chapter 2). The recordings were started when the series resistance had stabilized (typically around 20 MΩ after 15-30 minutes). As for the whole-cell patch-clamp experiments in section 5.4, I bath applied different concentrations of glutamate at a membrane potential of –60 mV. The data in each cell were normalized to the current evoked by 100 μM glutamate in that cell and fitted with the Michaelis-Menten equation (eqn 5.1) to obtain the K_M.

An example of a recording from a COS-7 cell expressing only GLT-1 is shown in Figure 5.19 A, in which the amplitude of the glutamate transporter mediated currents increased in a dose-dependent manner. The dose-response curve of this cell is shown in Figure 5.19 B, and the line shows the fit of the data by the Michaelis-Menten equation (eqn 5.1). In this cell, the K_m was 19.8 μM and the I_{max} was –110 pA. For comparison, Figure 5.20A shows an example of a recording from a COS-7 cell expressing GLT-1 and Ajuba. Again, the amplitude of the glutamate transporter mediated currents increased in a dose-dependent manner. The dose-response curve of this cell and the fit of the data by the Michaelis-Menten equation (eqn 5.1) are shown in Figure 5.20 B. In this cell, the K_m was 16.3 μM and the I_{max} was -112 pA.

Figure 5.21 A shows the averaged dose-response data when either GLT-1 was expressed (filled circles, n=5) or when GLT-1 and Ajuba were co-expressed (open circles, n=3). The lines are Michaelis-Menten curves using the mean of the K_M values obtained in each condition. The averaged K_M derived from fitting a Michaelis-Menten curve to the data from each cell group did not differ significantly (p=0.97) and was 22.6 ± 9.2 μM when GLT-1 was expressed alone (n=5) and 22.1 ± 6.6 μM when GLT-1 and Ajuba were co-expressed (n=3) (Figure 5.6 B). This indicates that

Figure 5.19: Glutamate dose-response data from a GLT-1 expressing COS-7 cell

(A) Current responses to different concentrations of bath applied glutamate recorded (using the perforated patch-clamp configuration) from a GLT-1 expressing COS-7 cell at –60mV. **(B)** The data were normalized to the response evoked by 100 μM glutamate, plotted as a dose-response curve and fit by the Michaelis-Menten equation (smooth line). The K_M in this cell was 19.8 μM and the normalized I_{max} was 1.198, or –110 pA in absolute units.

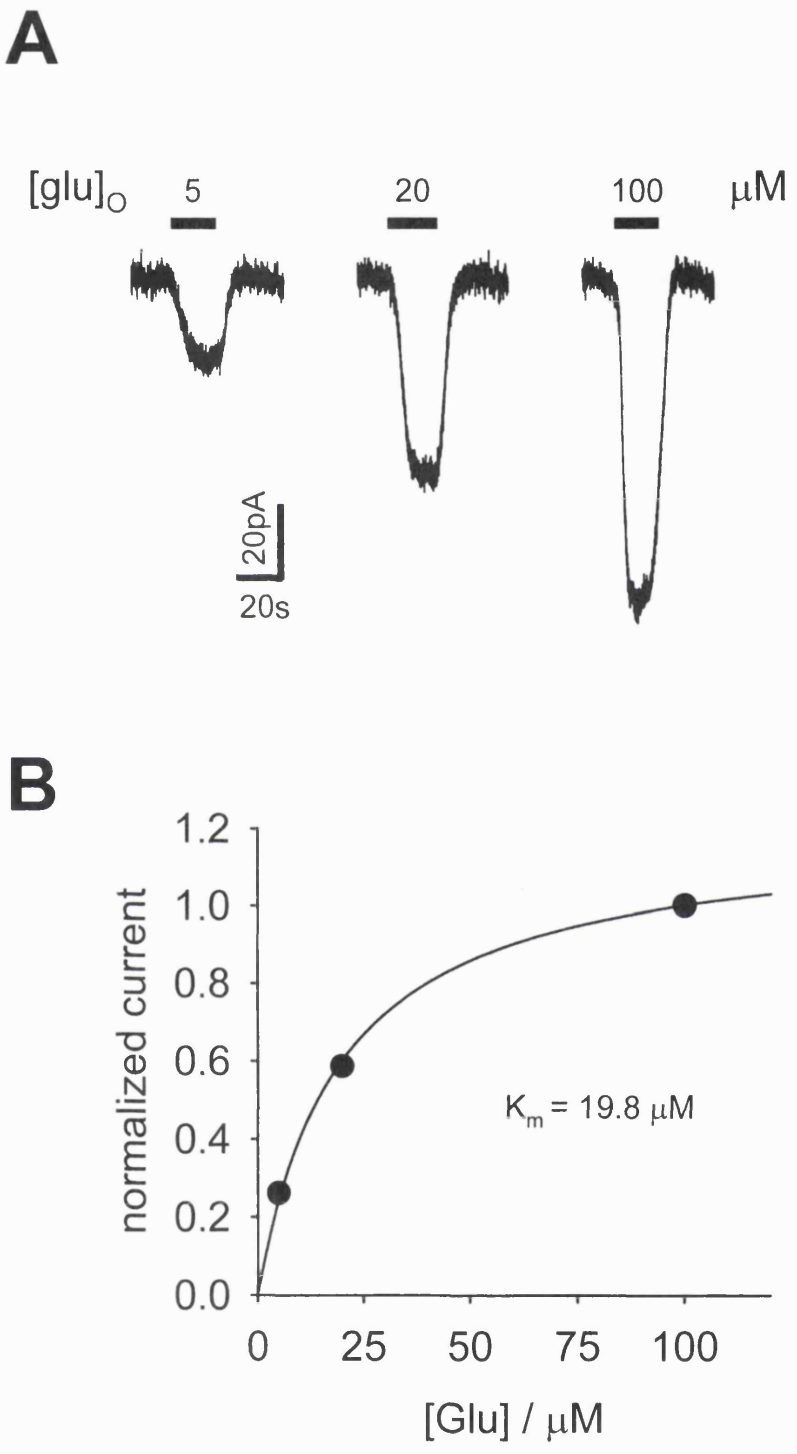
A
[glu]O
5
20
100
μM
20pA
20s
B
normalized current
1.2
1.0
0.8
0.6
0.4
0.2
0.0
0
25
50
75
100
[Glu] / μM
Km = 19.8 μM

Figure 5.20: Glutamate dose-response data from a COS-7 cell co-expressing GLT-1 and Ajuba

(A) Current responses to different concentrations of bath applied glutamate recorded (using the perforated patch-clamp configuration) from a COS-7 cell expressing GLT-1 and Ajuba at –60 mV. **(B)** The data were normalized to the response evoked by 100 μM glutamate, plotted as a dose-response curve and fit by the Michaelis-Menten equation (smooth line). The K_M in this cell was 16.3 μM and the normalized I_{max} was 1.163, or –112 pA in absolute units.

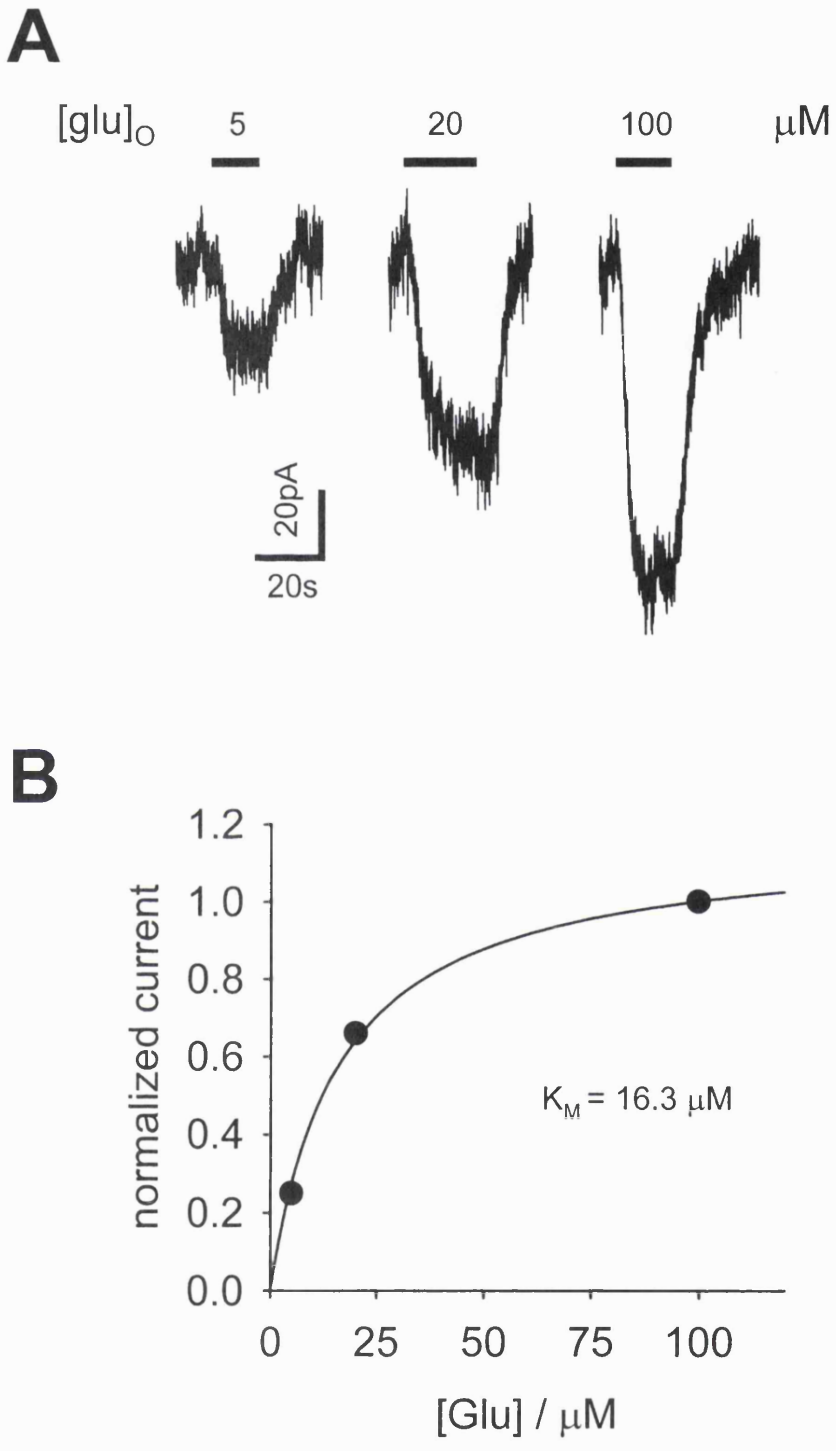
A
[glu]O
5
20
100
μM
20pA
20s
B
normalized current
1.2
1.0
0.8
0.6
0.4
0.2
0.0
0
25
50
75
100
[Glu] / μM
KM = 16.3 μM

Figure 5.21: GLT-1's K_M for glutamate is not changed when Ajuba is co-expressed (recorded in the perforated patch-clamp configuration)

(A) Dose-response curves for the glutamate-evoked GLT-1 mediated currents recorded from 5 COS-7 cells expressing only GLT-1 (filled circles, mean ± s.e.m.), and 3 COS-7 cells expressing GLT-1 and Ajuba (open circles, mean ± s.e.m.), using the perforated patch-clamp technique (-60 mV). In each cell the responses were normalized to the response evoked by 100 μM glutamate, and fit by the Michaelis-Menten equation. The resulting K_Ms for each expression type were averaged and were 23 ± 9 μM when GLT-1 was expressed (n=5) and 22 ± 7 μM when GLT-1 and Ajuba were co-expressed (n=3) **(B)**. The smooth lines in (A) are the Michaelis-Menten curves using the mean of the averaged K_Ms.

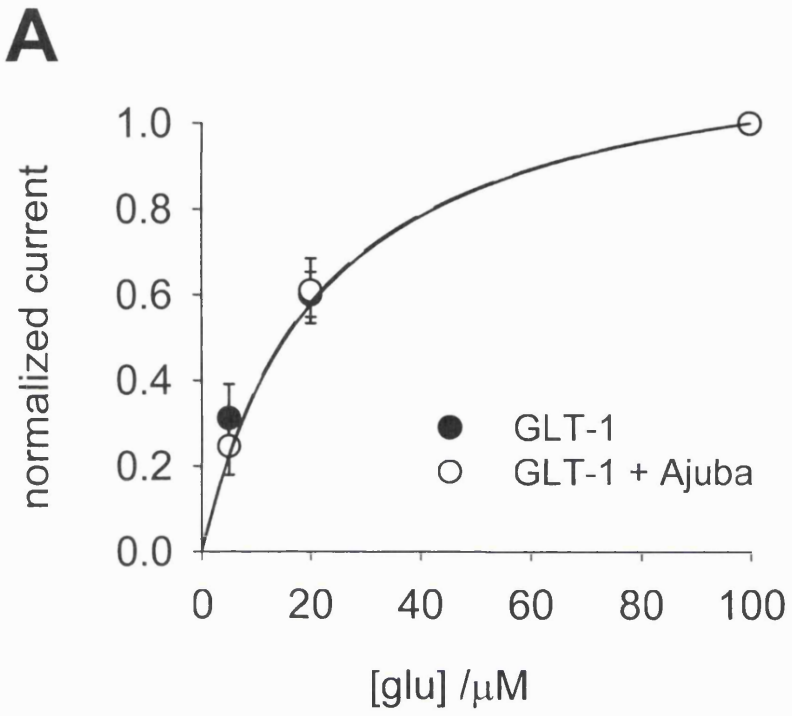
A
normalized current
1.0
0.8
0.6
0.4
0.2
0.0
0
20
40
60
80
100
[glu] /μM
GLT-1
GLT-1 + Ajuba

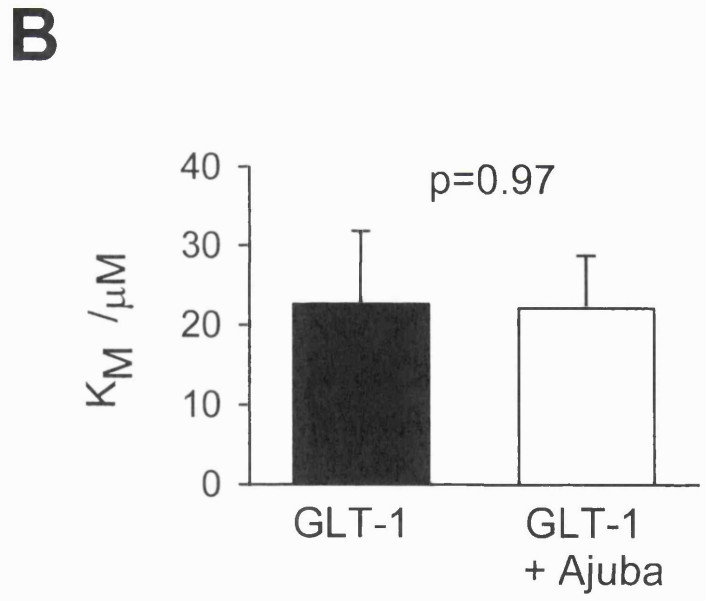
B
p=0.97
K_M /μM
40
30
20
10
0
GLT-1
GLT-1
+ Ajuba

Ajuba does not modulate the apparent affinity of GLT-1 when co-expressed in COS-7 cells, even when recorded with the perforated patch-clamp technique.

The maximum uptake current (I_{max}) at high glutamate concentrations (extrapolated from the fitted curve in each cell) did not differ significantly either ($p=0.31$), and was -116 ± 14 pA when GLT-1 was expressed alone ($n=5$) and -204 ± 105 pA when GLT-1 and Ajuba were co-expressed ($n=3$). However, as was mentioned in section 5.4, the expression levels varied greatly between cells, introducing great variability into the I_{max} values.

5.10 Discussion

The experiments described in this chapter were carried out to investigate whether Ajuba modulates the (1) K_M (sections 5.4, 5.5), (2) maximum uptake rate (section 5.6), (3) surface expression (section 5.7), (4) voltage-dependence (section 5.8), or (5) anion conductance (section 5.9) of the glutamate transporter GLT-1. None of the investigated properties of GLT-1 appear to be altered by co-expression of Ajuba.

Marie at al. (2002) have shown that Ajuba interacts with the glutamate transporter GLT-1 in vitro and in vivo. However, Ajuba has a more widespread distribution than GLT-1, being present in many tissues of the body, so it is likely to fulfil some functions independent of its interaction with the glutamate transporter. So what is the function of the GLT-1 – Ajuba interaction? The interaction between the two proteins could serve several purposes:

(1) Ajuba could modulate the properties of GLT-1. However, in this chapter I present data showing the Ajuba does not modulate the functional properties of GLT-1 when expressed in COS-7 cells. Using expression systems, the worry always remains that under native conditions the properties might be modulated, for example requiring the presence of other proteins or molecules, which were not expressed in the cell type studied. I therefore tried to record glutamate transporter currents in a

cell type that endogenously expresses GLT-1 and Ajuba, i.e. retinal bipolar cells (Marie et al., 2002). The idea was to introduce peptides mimicking the transporter's binding sequence for Ajuba via the patch-pipette into the cytoplasm, as in chapter 3 for the $GABA_C$ receptor – MAP-1B interaction, to see if disrupting the GLT-1 – Ajuba interaction would alter the transporters properties. There were several problems, however, which ultimately made these experiments not feasible. Only a subset of cone bipolar cells express GLT-1 (Rauen and Kanner, 1994; Euler and Wassle, 1995; Rauen et al., 1996; Rauen, 2000), and bipolar cells also express other glutamate transporters, such as EAAT-5 (Pow and Barnett, 2000). There are no specific EAAT-5 antagonists, so the glutamate-evoked current, recorded in a cocktail of glutamate receptor antagonists, is mediated by both GLT-1 and EAAT-5 in a unknown and probably quite variable ratio. Additionally the glutamate-evoked transporter current (with glutamate receptors blocked) turned out to be very small (low signal to noise ratio), making it practically impossible to record glutamate dose-response curves, let alone compare them and detect small differences occurring over time. This set of experiments had thus to be abandoned.

(2) Ajuba could serve to anchor GLT-1 to the cytoskeleton or localize it to certain parts of the cell. Many LIM proteins are cytoskeletal proteins and Ajuba can associate with actin in keratinocytes (personal communication, Helene Marie), opening up the possibility of Ajuba anchoring GLT-1 to the cytoskeleton. However, co-expression of Ajuba and GLT-1 in COS-7 cells did not change the distribution of GLT-1 in the cell membrane (Marie at al., 2002), suggesting that GLT-1 does not require Ajuba to be present in order to be transported to, inserted and stabilized in the plasma membrane. Since GLT-1 binds to a part of the pre-LIM domain of Ajuba (177-340) different from the SH3 recognition sites, Ajuba could theoretically bind to other proteins (via its LIM domains (347-399, 413-463 and 472-532) and/or its SH3 recognition motifs (70-75 and 100-108)) at the same time as interacting with GLT-1. This could result in the formation of large protein complexes, linking the transporter

closely to other proteins, which may modulate its function (or vice versa). Huge protein complexes have been shown to be present, for example, at the postsynaptic density of glutamatergic synapses (see section 1.7), where membrane proteins are linked to intracellular signalling pathways.

(3) Rather than Ajuba modulating the function of GLT-1, GLT-1 could equally well modulate the function of Ajuba. When co-expressed in COS-7 cells, GLT-1 recruited Ajuba to the plasma membrane, suggesting that GLT-1 can influence the location of Ajuba. It is not known if and how the interaction of GLT-1 and Ajuba is modulated, but one could speculate that the transporter serves to sense the level of extracellular glutamate and transmit this information to Ajuba, which in turn could dissociate from the transporter and shuttle to the nucleus to modulate gene transcription or activate the MAP kinase pathway, two processes that Ajuba has been shown to influence (Goyal et al., 1999; Kanungo et al., 2000). In this way GLT-1 could convey extracellular signals (i.e. glutamate levels) to activate intracellular processes. Interestingly, activation of glutamate transporters in cultured astrocytes has recently been shown to activate MAP kinase (Abe and Saito, 2001).

CHAPTER 6

Synaptic transmission in the cerebellum of mice lacking either the GLT-1 or the GLAST glial glutamate transporter

6.1 Introduction

As described in more detail in section 1.2, the time-course of the postsynaptic response at a glutamatergic synapse depends on the kinetics of postsynaptic glutamate receptors (activation, deactivation and desensitization), and on the duration of the glutamate concentration in the synaptic cleft, which is determined by the rate at which glutamate is removed by glutamate transporters and diffusion. Several groups have investigated whether blocking glutamate transporters, pharmacologically or by the use of glutamate transporter knock-out mice, alters the postsynaptic response at different synapses in the brain. The varied results of their studies are reviewed in section 1.3.

This chapter describes experiments to determine whether the glial glutamate transporters GLT-1 and GLAST shape synaptic currents at the cerebellar mossy fibre to granule cell and parallel fibre to Purkinje cell synapses. These two synapses have been shown to have a prolonged postsynaptic response, due to slower glutamate removal and a prolonged glutamate transient in the synaptic cleft, when glutamate transporters are inhibited with the glutamate uptake inhibitor PDC (see section 1.3 and section 6.5). Interpretation of experiments using PDC to study the role of glutamate transporters is complicated by the fact that PDC is a glutamate analogue that competitively blocks glutamate transporters while being taken up by them into the cell. As a result, bath application of PDC results in glutamate release via hetero-exchange with intracellular glutamate (because the entry of PDC on the transporter is followed rapidly by exit of glutamate on the transporter: Volterra et al. (1996)),

raising the extracellular glutamate concentration in the slice. This elevated extracellular glutamate level will result in a less steep concentration gradient between the synaptic cleft and the extrasynaptic space, which could slow diffusion out of the synaptic cleft and thus prolong the time course of the EPSC, even if diffusion rather than uptake were the main means of glutamate clearance from the cleft. The elevated extracellular glutamate level could also desensitize receptors, changing the shape of the postsynaptic response. Another disadvantage of using PDC is that it acts on *all* the different types of plasma membrane glutamate transporter, making it impossible to isolate the function of the different transporter subtypes.

To overcome these problems, I used specific glutamate transporter knock-out mice. GLT-1 and GLAST, expressed in astrocytes, are both present in the granule cell layer, whereas GLAST in Bergmann glia is the dominant glutamate transporter in the molecular layer (Chaudhry et al., 1995; Lehre et al., 1995; Furuta et al., 1997a; Ullensvang et al., 1997; Lehre and Danbolt, 1998). By recording mossy fibre to granule cell and parallel fibre to Purkinje cell EPSCs in mice lacking GLT-1 or GLAST, I therefore investigated the role of GLT-1 and GLAST at the mossy fibre to granule cell synapse and the role of GLAST at the parallel fibre – Purkinje cell synapse. The expectation was that deleting a glutamate transporter would slow glutamate removal, leading to a prolonged glutamate transient in the synaptic cleft and a longer EPSC. Another reason to study mossy fibre to granule cell transmission in mice lacking GLAST, is that knocking it out may alter the granule cell properties as a result of their being exposed to an altered extracellular glutamate concentration as they migrate across the molecular layer during development (Komuro and Rakic, 1993; Rossi and Slater, 1993).

As will be seen, deleting the glutamate transporters had no effect on mossy fibre to granule cell transmission (sections 6.2 – 6.3), but slowed the decay of the EPSC at the parallel fibre to Purkinje cell synapse (section 6.4).

6.2 Synaptic transmission at the mossy fibre – granule cell synapse in mice lacking the glutamate transporter GLT-1

The following three sections describe experiments to investigate the role of the glial glutamate transporter GLT-1 in shaping synaptic transmission at the mossy fibre – granule cell synapse. These experiments were carried out on P11-P15 day old mice, at a holding potential of –60 mV. In rats, which mature more slowly than mice, at P11-P15 GLT-1 is expressed at only around 5–40% of its adult level (Furuta et al., 1997a; Ullensvang et al., 1997). However, for Home Office reasons we were not allowed to use these mice after P15.

6.2.1. Mossy fibre EPSCs evoked by a single stimulus, recorded at room temperature in external solution lacking magnesium

To see whether the most abundant glial glutamate transporter in the granule cell layer, GLT-1, shapes synaptic transmission at the mossy fibre – granule cell synapse, I recorded mossy fibre EPSCs in granule cells of wild-type (+/+) and GLT-1 knock-out (-/-) mice. I did the experiments initially in a solution lacking extracellular magnesium, to reveal any effect on the NMDA component of the EPSC, as observed by Overstreet et al. (1999) when blocking transporters pharmacologically at this synapse in the rat (see section 1.3).

Figure 6.1 shows specimen traces of such recordings, obtained at room temperature. The shape of the EPSC, with a rapidly decaying AMPA component and a slowly decaying NMDA component as reported previously by Silver et al. (1992) and Overstreet et al. (1999), was not systematically different in mice lacking GLT-1. The EPSCs could be fully blocked (grey traces) by the AMPA receptor antagonist NBQX (25 μM) and the NMDA receptor antagonist AP-5 (50 μM), confirming that only these receptors mediate the EPSC. To quantify the properties of the EPSC and make it possible to compare the two genotypes, I measured (1) the peak amplitude of

Figure 6.1: The shape of the mossy fibre to granule cell EPSC evoked by a single stimulus is not altered in mice lacking GLT-1 (in zero magnesium, at room temperature)

A and B: Specimen traces of mossy fibre synaptic currents recorded in cerebellar granule cells of (A) a wild type and (B) a GLT-1 knock-out mouse, in the absence (black) or presence (grey) of the glutamate receptor antagonists NBQX (25 μM) and D-AP-5 (50 μM), in response to a single stimulus delivered to the mossy fibres. The dashed box corresponds to the region of the current which is shown at a faster time-scale below. The recordings were at room temperature, in magnesium-free external solution containing 20 μM bicuculline and 10 μM glycine (Table 4, solution D), at a holding potential of –60 mV.

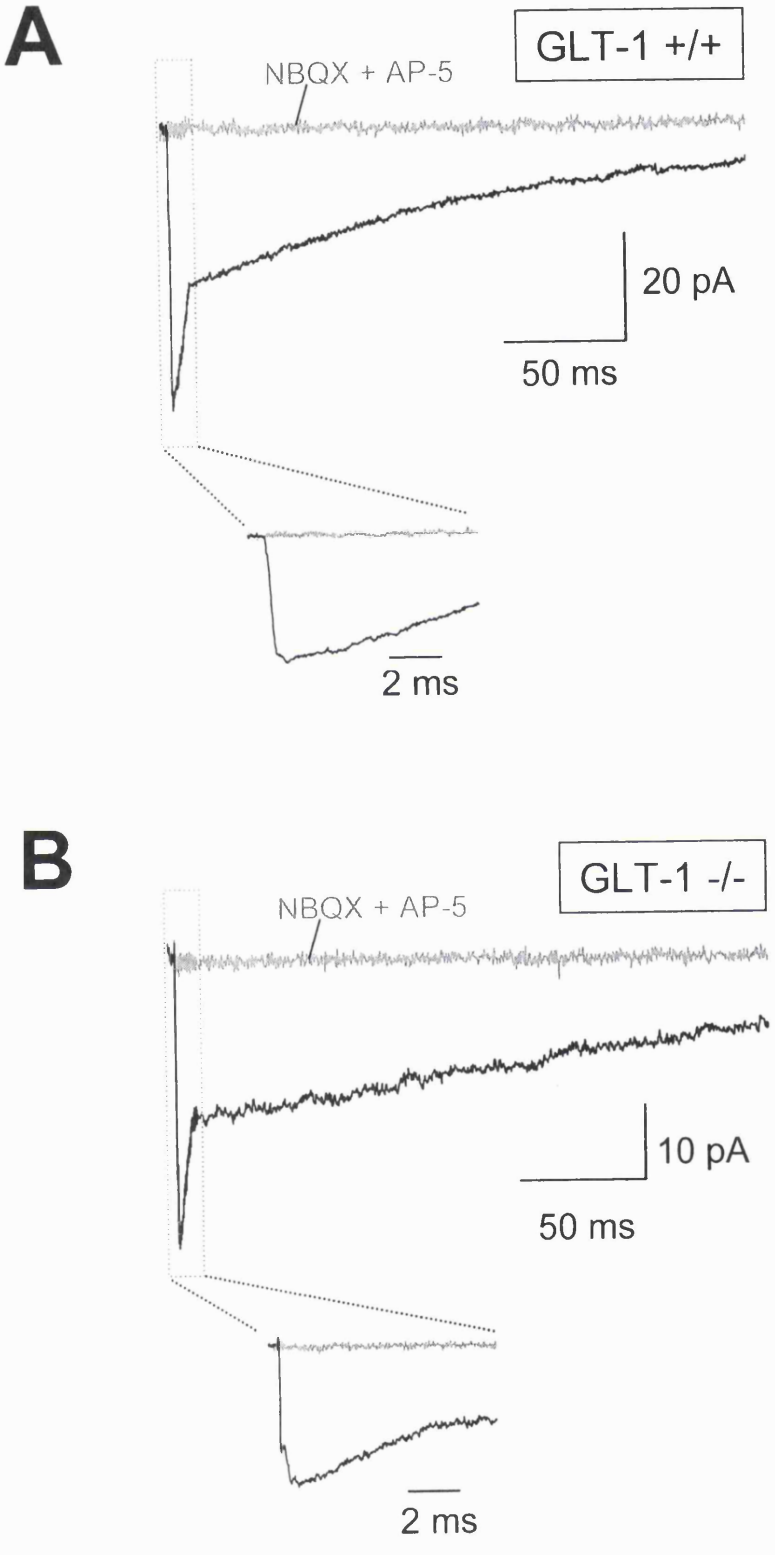
A
GLT-1 +/+
NBQX + AP-5
20 pA
50 ms
2 ms
B
GLT-1 -/-
NBQX + AP-5
10 pA
50 ms
2 ms

Figure 6.2: Comparison of mossy fibre EPSC properties in wild type and GLT-1 knock-out mice (single stimulus, in zero magnesium, at room temperature)

Bar graphs of (A) the peak current amplitude (I_{peak}), (B) the current amplitude measured 50 ms after the peak (I_{50ms}), (C) the ratio of I_{50ms} to I_{peak}, and (D) the total area of the EPSC, in wild type (black; n = 8 cells) and GLT-1 knock-out (white; n = 11 cells) mice. Specimen traces and recording conditions are in Figure 6.1.

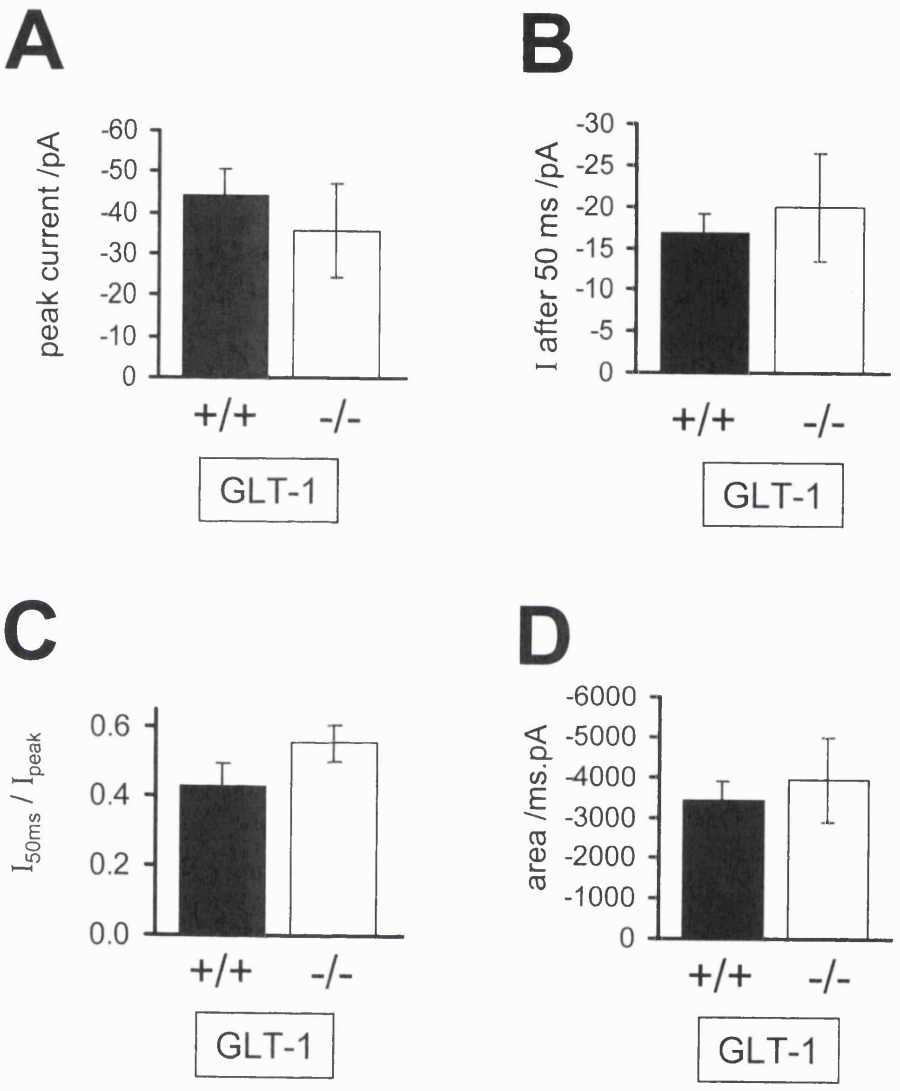
A
peak current /pA
-60
-50
-40
-30
-20
-10
0
+/+
-/-
GLT-1
B
I after 50 ms /pA
-30
-25
-20
-15
-10
-5
0
+/+
-/-
GLT-1
C
I_{50ms} / I_{peak}
0.6
0.4
0.2
0.0
+/+
-/-
GLT-1
D
area /ms.pA
-6000
-5000
-4000
-3000
-2000
-1000
0
+/+
-/-
GLT-1

the EPSC at approximately 0.5 msec after the stimulus, reflecting the AMPA component of the current, as the NMDA component at this synapse in the rat rises over about 9-10 ms (Silver et al., 1992), quantified in Figure 6.2 A), (2) the current amplitude 50 ms after the peak, as a measure of the NMDA component of the EPSC, as the AMPA component at this synapse in the rat decays within about 1-2 ms (Silver et al., 1992), quantified in Figure 6.2 B, and (3) the total area of the EPSC (charge transfer) shown in Figure 6.2 D. To test whether knocking-out GLT-1 altered the contribution of the NMDA component to the EPSC, I normalized the NMDA component to the peak EPSC amplitude, i.e. I took the ratio of the current measured at 50 ms after the peak to that of the current amplitude at the peak (Figure 6.2 C). The bar graphs in Figure 6.2 show the averaged data for such an analysis, with the data from the wild-type mice (+/+) shown as black bars (n = 8 cells) and the data from the knock-out mice (-/-) shown as white bars (n = 11 cells). None of these measured parameters showed a significant difference between the wild-type and the knock-out mice. P values for unpaired t-tests comparing the peak amplitude (I_{peak}; Figure 6.2 A), the amplitude of the EPSC 50 ms after the peak (I_{50ms}; Figure 6.2 B), the ratio I_{50ms}/I_{peak} (Figure 6.2 C) and the total area (Figure 6.2 D) were 0.57, 0.69, 0.15 and 0.68 respectively.

These data suggest that the glial glutamate transporter GLT-1 does not shape the EPSC at the mossy fibre granule cell under these recording conditions.

6.2.2. Mossy fibre EPSCs evoked by single stimulation, recorded at 37^{O}C in external solution containing magnesium

To see whether the absence of GLT-1 would influence synaptic transmission at the mossy fibre to granule cell synapse when investigated under more physiological conditions, I recorded EPSCs in wild-type (+/+) or GLT-1 knock-out (-/-) mice at 37^{O}C. The higher temperature will speed up transporters and influence also the function of other proteins (for example presynaptic calcium channels), which

are important during synaptic transmission (Sabatini and Regehr, 1996). In addition, to make the conditions as physiological as possible, for these experiments the external solution contained 1.2 mM magnesium, which will not only influence the charge passed through (postsynaptic) NMDA receptors but also reduce the calcium flux though (presynaptic) calcium channels, thus influencing transmitter release. Figure 6.3 shows specimen traces of such recordings for a wild-type (A) and a knock-out (B) mouse. I analysed these data as described in the previous section to obtain the peak current amplitude (Figure 6.4 A), the amplitude 10 ms after the peak (Figure 6.4 B), the ratio I_{10ms}/I_{peak} (Figure 6.4 C) and the total charge transfer (Figure 6.4 D). I measured the current 10 ms after the peak (rather than 50 ms after the peak as in the previous section) as an estimate of the NMDA component, because the AMPA and NMDA current components decay much more rapidly at higher temperature. The bar graphs in Figure 6.4 show the averaged data for such an analysis, with the data from the wild-type mice (+/+) shown as black bars (n = 9 cells) and the data from the knock-out mice (-/-) shown as white bars (n = 5 cells). None of the measured parameters showed a significant difference between the wild-type and the knock-out mice. P values for unpaired t-tests comparing the peak amplitude (I_{peak}), the amplitude of the EPSC 10 ms after the peak (I_{10ms}), the ratio I_{10ms}/I_{peak} and the total area were 0.49, 0.98, 0.72 and 0.53 respectively. I also recorded EPSCs from a few cells for each genotype at –30 mV (n = 3 (+/+) and 2 (-/-) cells) and +30 mV (n = 3 (+/+) and 1 (-/-) cells), to relieve the voltage dependent magnesium block of the NMDA receptor channel, but again the data were not significantly different between the +/+ and the -/- mice (data not shown).

These data suggest that the glial glutamate transporter GLT-1 does not contribute to shaping the EPSC at the mossy fibre granule cell even under these more physiological recording conditions.

Figure 6.3: The shape of the mossy fibre to granule cell EPSC at 37^{O}C is not altered in mice lacking GLT-1 (single stimulus, 1.2 mM magnesium)

A and B: Specimen traces of mossy fibre synaptic currents recorded in cerebellar granule cells of (A) a wild type and (B) a GLT-1 knock-out mouse, in response to a single stimulus delivered to the mossy fibres. The dashed box corresponds to the region of the current, which is shown at a faster time-scale below. The recordings were at 37^{O}C, in 1.2 mM magnesium external solution containing 20 μM bicuculline and 10 μM glycine (Table 4, solution C), at a holding potential of -60 mV.

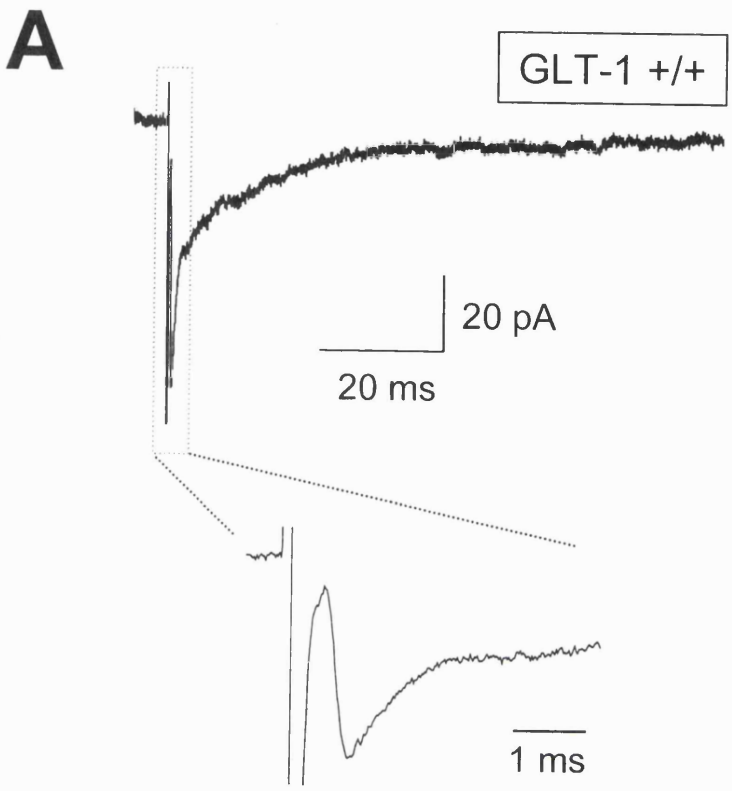
A
GLT-1 +/+
20 pA
20 ms
1 ms

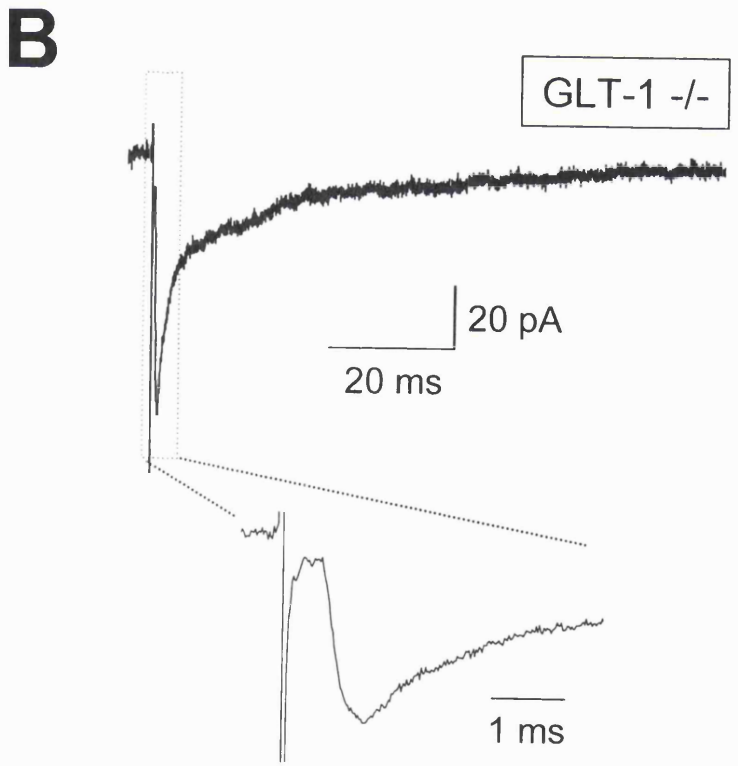
B
GLT-1 -/-
20 pA
20 ms
1 ms

Figure 6.4: Comparison of mossy fibre EPSC properties in wild type and GLT-1 knock-out mice at 37^{o}C (single stimulus, 1.2 mM magnesium)

Bar graphs of (A) the peak current amplitude (I_{peak}), (B) the current amplitude measured 10 ms after the peak (I_{10ms}), (C) the ratio of I_{10ms} to I_{peak}, and (D) the total area of the EPSC, in wild type (black; n = 9 cells) and GLT-1 knock-out (white; n = 5 cells) mice. Specimen traces and recording conditions are in Figure 6.3.

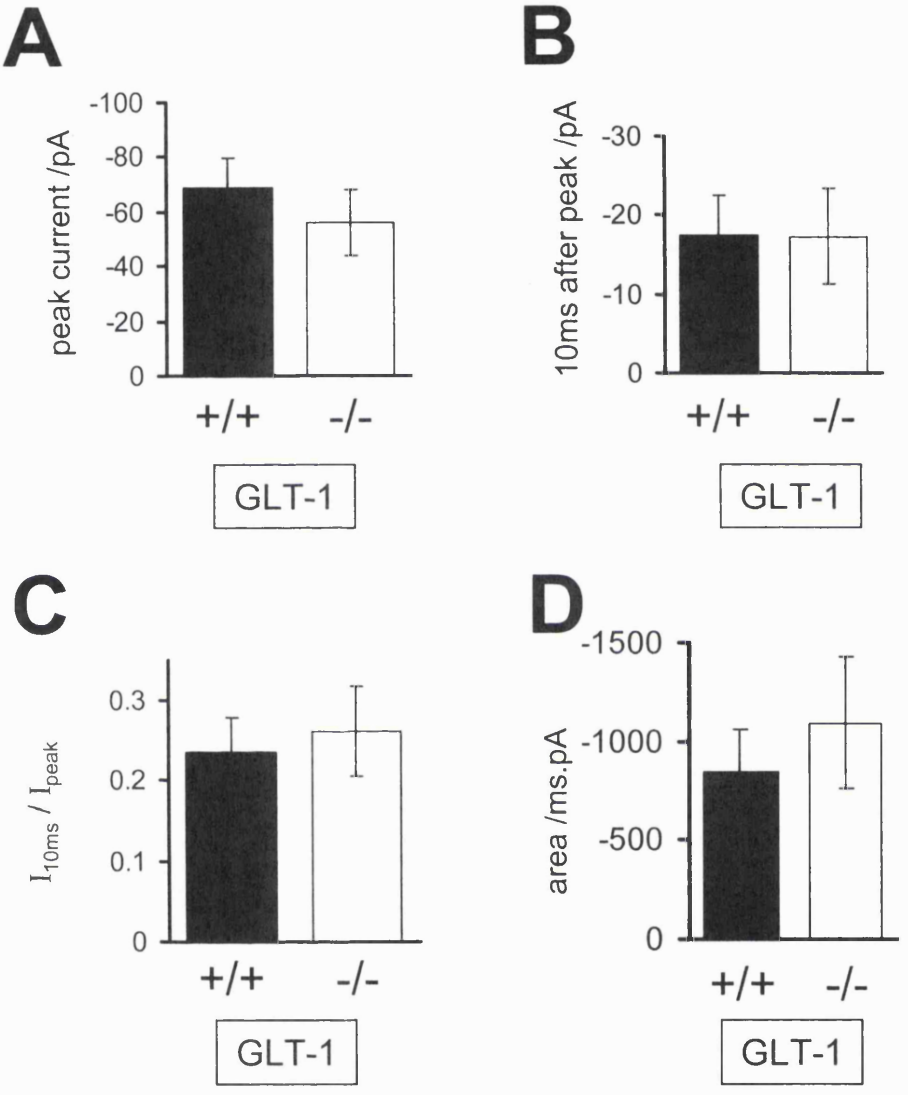
A
peak current /pA
-100
-80
-60
-40
-20
0
+/+
-/-
GLT-1
B
10ms after peak /pA
-30
-20
-10
0
+/+
-/-
GLT-1
C
I_{10ms} / I_{peak}
0.3
0.2
0.1
0
+/+
-/-
GLT-1
D
area /ms.pA
-1500
-1000
-500
0
+/+
-/-
GLT-1

6.2.3. Mossy fibre EPSCs evoked by repetitive stimulation, recorded at 37°C in external solution containing magnesium

Mossy fibres can fire at frequencies up to several hundred hertz (Goldberg and Fernandez, 1971). In such conditions of repetitive glutamate release, the extracellular glutamate concentration could rise, especially in a glial-wrapped structure such as the cerebellar glomerulus, making the functioning of glutamate transporters more important. Indeed, in experiments blocking glutamate uptake pharmacologically, I have suggested that glutamate transporters play a crucial role in shaping the time-course of the mossy fibre EPSC and the resulting action potential firing pattern of granule cells during single and repetitive stimulation (Overstreet et al., 1999).

To see whether knocking-out GLT-1 would influence synaptic transmission at the mossy fibre – granule cell synapse during repetitive stimulation, I recorded EPSCs in wild-type (+/+) and GLT-1 knock-out (-/-) mice in response to 10 stimuli at 100 Hz at 37°C in a solution containing 1.2 mM magnesium. Figure 6.5 shows specimen traces of such recordings for a wild-type (A) and a knock-out (B) mouse. For the last (10^{th}) EPSC in the train I measured the peak amplitude (Figure 6.6 A), the amplitude 10 ms after the peak (Figure 6.6 B), the ratio I_{10ms}/I_{peak} (Figure 6.6 C) and the total charge transfer after the 10^{th} stimulus (Figure 6.6 D), which lasted several hundred milliseconds (Figure 6.5) presumably reflecting glutamate accumulation during the stimulus train which took time to be cleared after glutamate release stopped. The bar graphs in Figure 6.6 show the averaged data for such an analysis, with the data from the wild-type mice (+/+) shown as black bars (n = 7 cells) and the data from the knock-out mice (-/-) shown as white bars (n = 3 cells). None of these parameters showed a significant difference between the wild-type and the knock-out mice. P values for unpaired t-tests comparing the amplitude of the 10^{th}

Figure 6.5: The shape of the mossy fibre to granule cell EPSC evoked by repetitive stimulation at 37^{O}C is not altered in mice lacking GLT-1 (in 1.2 mM magnesium)

A and B: Specimen traces of synaptic currents recorded in cerebellar granule cells of (A) a wild type and (B) a GLT-1 knock-out mouse, in response to repetitive stimulation (10 stimuli at 100 Hz) delivered to the mossy fibres. The recordings were at 37^{O}C, in 1.2 mM magnesium external solution containing 20 μM bicuculline and 10 μM glycine (Table 4, solution C), at a holding potential of –60 mV. Large vertical lines are stimulus artefacts.

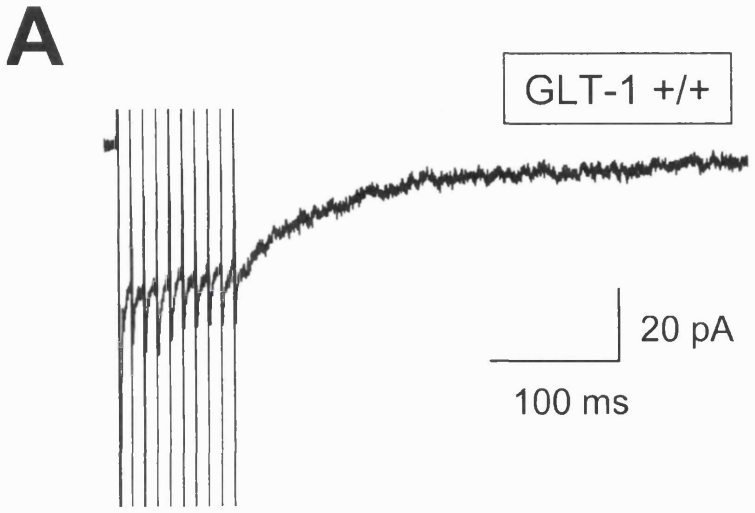
A
GLT-1 +/+
20 pA
100 ms

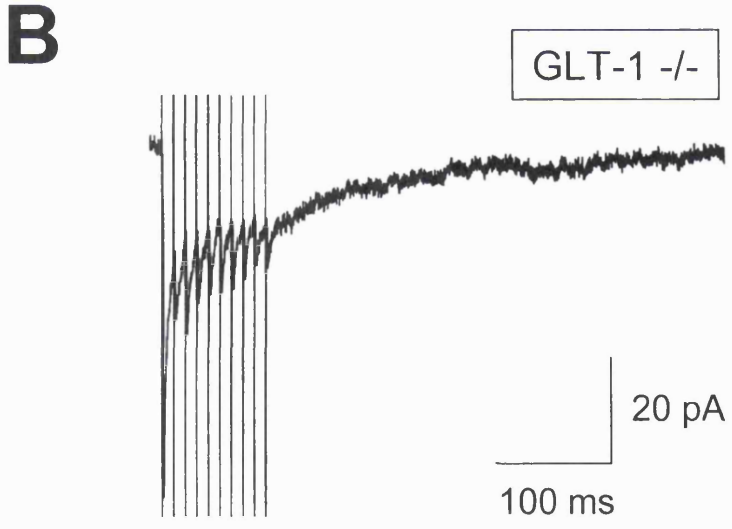
B
GLT-1 -/-
20 pA
100 ms

Figure 6.6: Comparison of the properties of the EPSC evoked by repetitive stimulation in wild type and GLT-1 knock-out mice (1.2 mM magnesium, at 37^{O}C)

Bar graphs of (A) the amplitude of the peak of the 10th EPSC (I_{peak}) of a 100 Hz train, (B) the amplitude measured 10 ms after the 10th peak (I_{10ms}), (C) the ratio of I_{10ms} and I_{peak}, and (D) the area of the EPSC after the 10th peak (i.e. the last peak of the train) in wild type (black; n = 7 cells) and GLT-1 knock-out (white; n = 3 cells) mice. Specimen traces and recording conditions are in Figure 6.5.

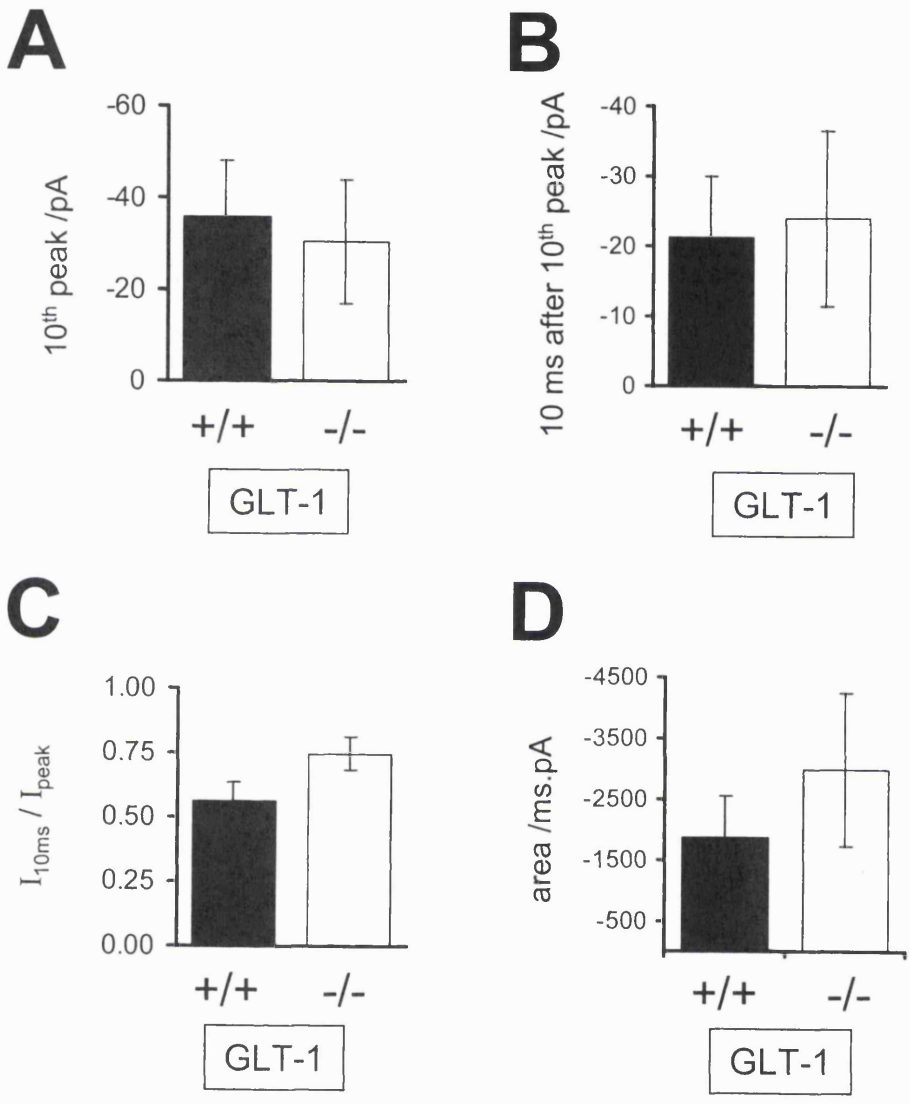
A
-60
-40
-20
0
10th peak /pA
+/+
-/-
GLT-1
B
-40
-30
-20
-10
0
10 ms after 10th peak /pA
+/+
-/-
GLT-1
C
1.00
0.75
0.50
0.25
0.00
I10ms / Ipeak
+/+
-/-
GLT-1
D
-4500
-3500
-2500
-1500
-500
area /ms.pA
+/+
-/-
GLT-1

peak (I_{peak}), the amplitude of the EPSC 10 ms after the 10th peak (I_{10ms}), the ratio I_{10ms}/I_{peak} and the total area after the 10th peak were 0.81, 0.86, 0.16 and 0.43 respectively. I also recorded EPSCs from a few cells for each genotype at –30 mV (n = 4 (+/+) and 2 (-/-) cells) and +30 mV (n = 2 (+/+) and 1 (-/-) cells), but as before the data were not significantly different between the +/+ and the -/- mice (data not shown).

These data suggest that the glial glutamate transporter GLT-1 does not contribute to shaping the EPSC at the mossy fibre granule cell synapse even during repetitive stimulation. A lack of effect of inhibiting GLT-1, using the non-transported GLT-1 blocker DHK, on the mossy fibre – granule cell EPSC has also been shown by Overstreet et al. (1999).

6.3 Synaptic transmission at the mossy fibre – granule cell synapse in mice lacking the glutamate transporter GLAST

The following two sections describe experiments to investigate whether knocking-out the glial glutamate transporter GLAST alters synaptic transmission at the mossy fibre – granule cell synapse. These experiments were carried out on P29-P31 day old mice at a holding potential of –60 mV. At this age GLAST is expressed at around 80% of its adult level, at least in rats (Furuta et al., 1997a; Ullensvang et al., 1997).

6.3.1. Mossy fibre EPSCs evoked by single stimulation, recorded at 37^{O}C in external solution containing magnesium

I recorded EPSCs in wild-type (+/+) or GLAST knock-out (-/-) mice at 37^{O}C in a solution containing 1.2 mM magnesium, as in the experiments described in section 6.2.2 for mice lacking GLT-1. Figure 6.7 shows specimen traces of such recordings for a wild-type (A) and a knock-out (B) mouse. I analysed these data as

Figure 6.7: The shape of the mossy fibre to granule cell EPSC evoked by single stimulus is not altered in mice lacking GLAST (1.2 mM magnesium, at 37^{O}C)

A and B: Specimen traces of synaptic currents recorded in cerebellar granule cells of (A) a wild type and (B) a GLAST knock-out mouse, in response to a single stimulus delivered to the mossy fibres. The dashed box corresponds to the region of the current that is shown at a faster time-scale below. The recordings were at 37^{O}C, in 1.2 mM magnesium external solution containing 20 μM bicuculline and 10 μM glycine (Table 4, solution C), at a holding potential of –60 mV.

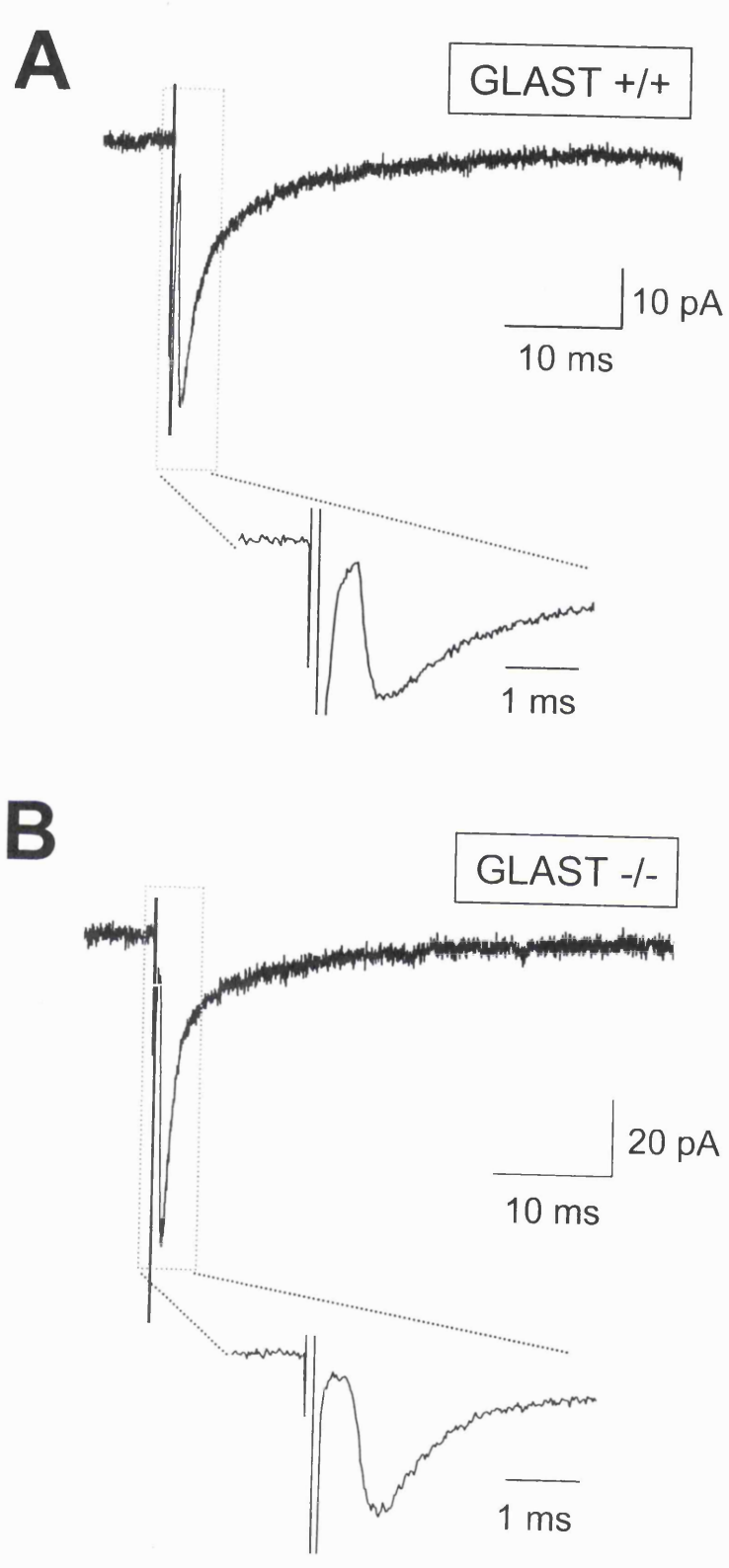
A
GLAST +/+
10 pA
10 ms
1 ms
B
GLAST -/-
20 pA
10 ms
1 ms

Figure 6.8: Comparison of the properties of the EPSC evoked by a single stimulus in wild type and GLAST knock-out mice (1.2 mM magnesium, at 37^{O}C)

Bar graphs of (A) the peak amplitude (I_{peak}), (B) the amplitude measured 10 ms after the peak (I_{10ms}), (C) the ratio of I_{10ms} and I_{peak} and (D) the total area of the EPSCs in wild type (black; n = 5 cells) and GLAST knock-out (white; n = 7 cells) mice. Specimen traces and recording conditions are in Figure 6.7.

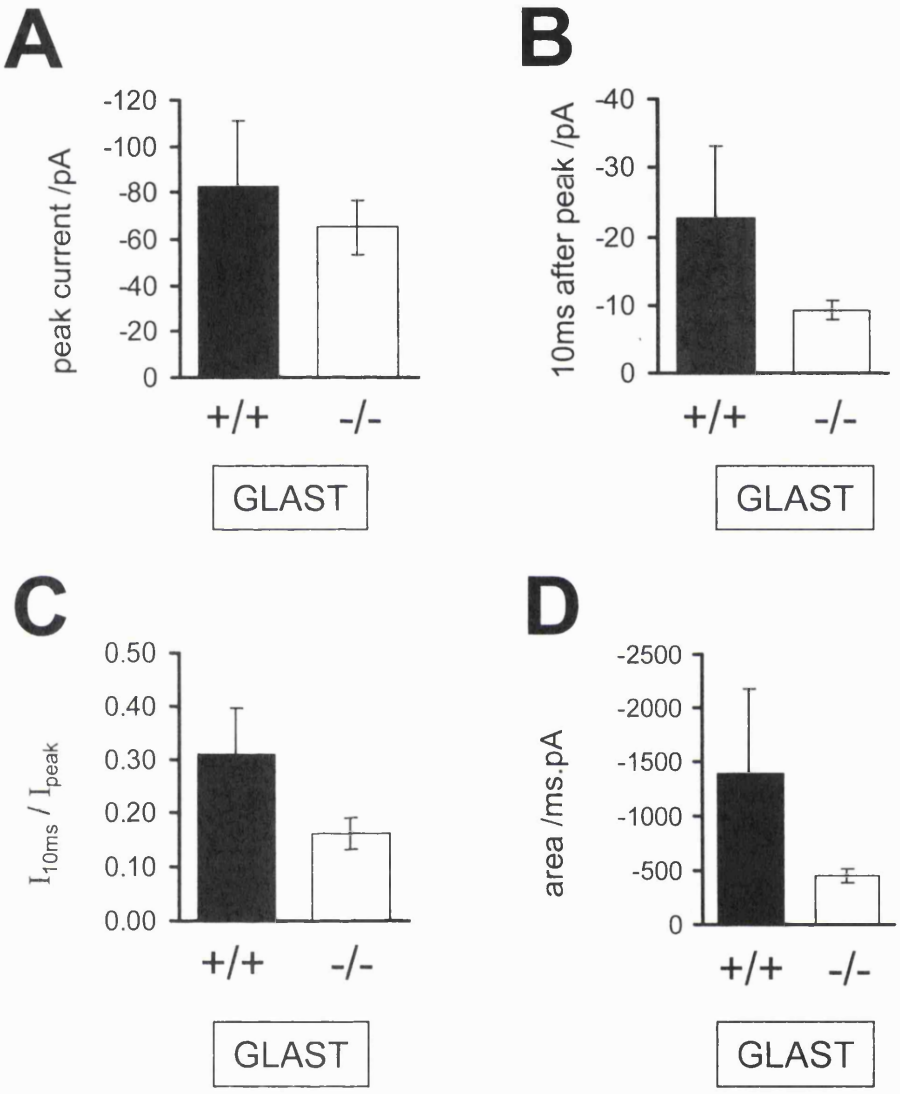
A
peak current /pA
-120
-100
-80
-60
-40
-20
0
+/+
-/-
GLAST
B
10ms after peak /pA
-40
-30
-20
-10
0
+/+
-/-
GLAST
C
I_{10ms} / I_{peak}
0.50
0.40
0.30
0.20
0.10
0.00
+/+
-/-
GLAST
D
area /ms.pA
-2500
-2000
-1500
-1000
-500
0
+/+
-/-
GLAST

described in section 6.2.2 for the peak current (Figure 6.8 A), the amplitude 10 ms after the peak (Figure 6.8 B), the ratio I_{10ms}/I_{peak} (Figure 6.8 C), and the total charge transfer (Figure 6.8 D). The bar graphs in Figure 6.8 show the averaged data for such an analysis, with the data from the wild-type mice (+/+) shown as black bars (n = 5 cells) and the data from the knock-out mice (-/-) shown as white bars (n = 7 cells). None of these parameters showed a significant difference between the wild-type and the knock-out mice. P values for unpaired t-tests comparing the peak amplitude (I_{peak}), the amplitude of the EPSC 10 ms after the peak (I_{10ms}), the ratio I_{10ms}/I_{peak} and the total area were 0.52, 0.18, 0.16 and 0.10 respectively. I also recorded EPSCs from a few cells for each genotype at –30 mV (n = 3 (+/+) and 3 (-/-) cells) and +30 mV (n = 2 (+/+) and 2 (-/-) cells), to relieve the voltage dependent magnesium block of the NMDA receptor channel, but again the data were not significantly different between the +/+ and the -/- mice (data not shown).

6.3.2. Mossy fibre EPSCs evoked by repetitive stimulation, recorded at 37^{O}C in external solution containing magnesium

To see whether knocking-out GLAST would influence synaptic transmission at the mossy fibre – granule cell synapse during repetitive stimulation, I recorded EPSCs in wild-type (+/+) or GLAST knock-out (-/-) mice in response to 10 stimuli at 100 Hz at 37^{O}C in a solution containing 1.2 mM magnesium, as described in section 6.2.3 for mice lacking GLT-1. Figure 6.9 shows specimen traces of such recordings for a wild-type (A) and a knock-out (B) mouse. I analysed these data in the same way as described in section 6.2.3, i.e. for the last (10^{th}) EPSC in the train I measured the peak amplitude (Figure 6.10 A), the amplitude 10 ms after the peak (Figure 6.10 B), the ratio I_{10ms}/I_{peak} (Figure 6.10 C) and the total charge transfer after the 10^{th} stimulus (Figure 6.10 D). The bar graphs in Figure 6.10 show the averaged data for such an analysis, with the data from the wild-type mice (+/+) shown as black bars (n = 2 cells) and the data from the knock-out mice (-/-) shown as white bars (n = 4 cells).

Figure 6.9: The shape of the mossy fibre to granule cell EPSC evoked by repetitive stimulation is not altered in mice lacking GLAST (1.2 mM magnesium, at 37^{O}C)

A and B: Specimen traces of synaptic currents recorded in cerebellar granule cells of (A) a wild type and (B) a GLAST knock-out mouse, in response to repetitive stimulation (10 stimuli at 100 Hz) delivered to the mossy fibres. The recordings were at 37^{O}C, in 1.2 mM magnesium external solution containing 20 μM bicuculline and 10 μM glycine (Table 4, solution C), at a holding potential of –60 mV.

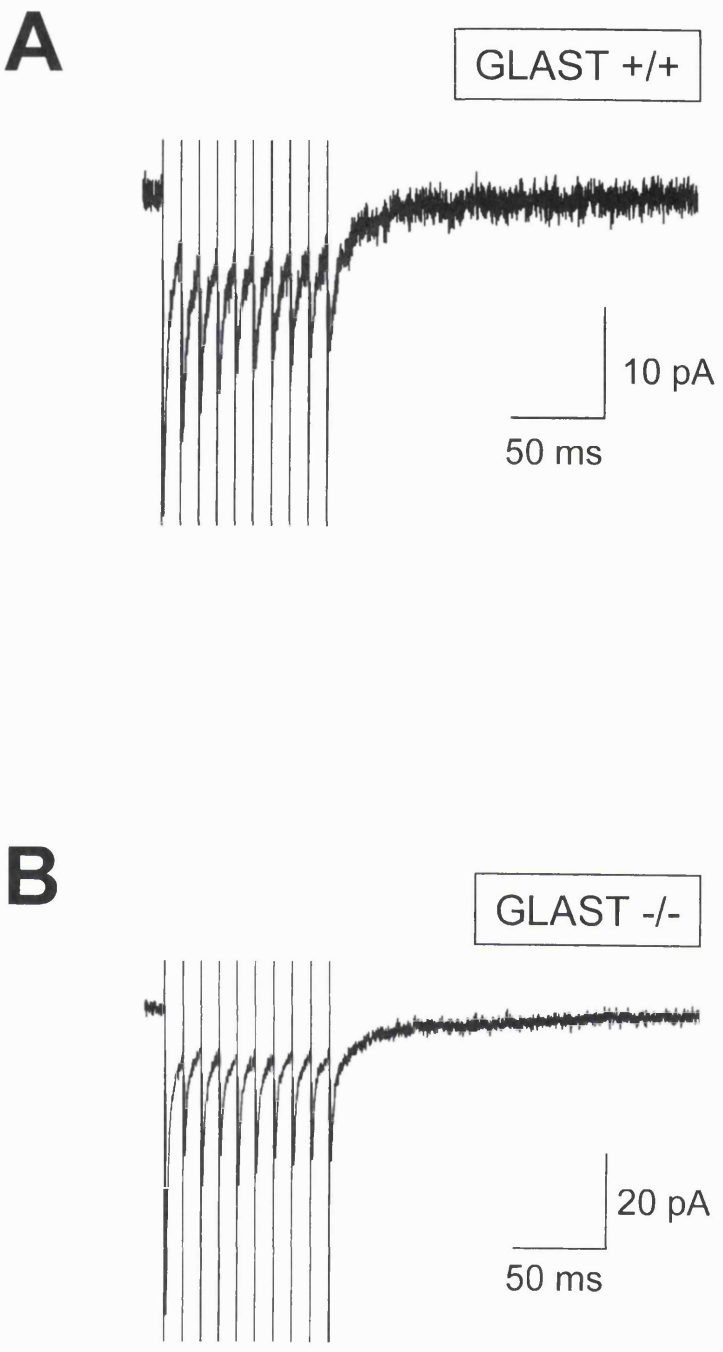
A
GLAST +/+
10 pA
50 ms
B
GLAST -/-
20 pA
50 ms

Figure 6.10: Comparison of the properties of the EPSC evoked by repetitive stimulation in wild type and GLAST knock-out mice (1.2 mM magnesium, at 37^{O}C)

Bar graphs of (A) the amplitude of the peak of the 10th EPSC (I_{peak}), (B) the amplitude measured 10 ms after the 10th peak (I_{10ms}), (C) the ratio of I_{10ms} to I_{peak}, and (D) the area of the EPSC after the 10th peak in wild type (black; n = 2 cells) and GLAST knock-out (white; n = 4 cells) mice. Specimen traces and recording conditions are in Figure 6.9.

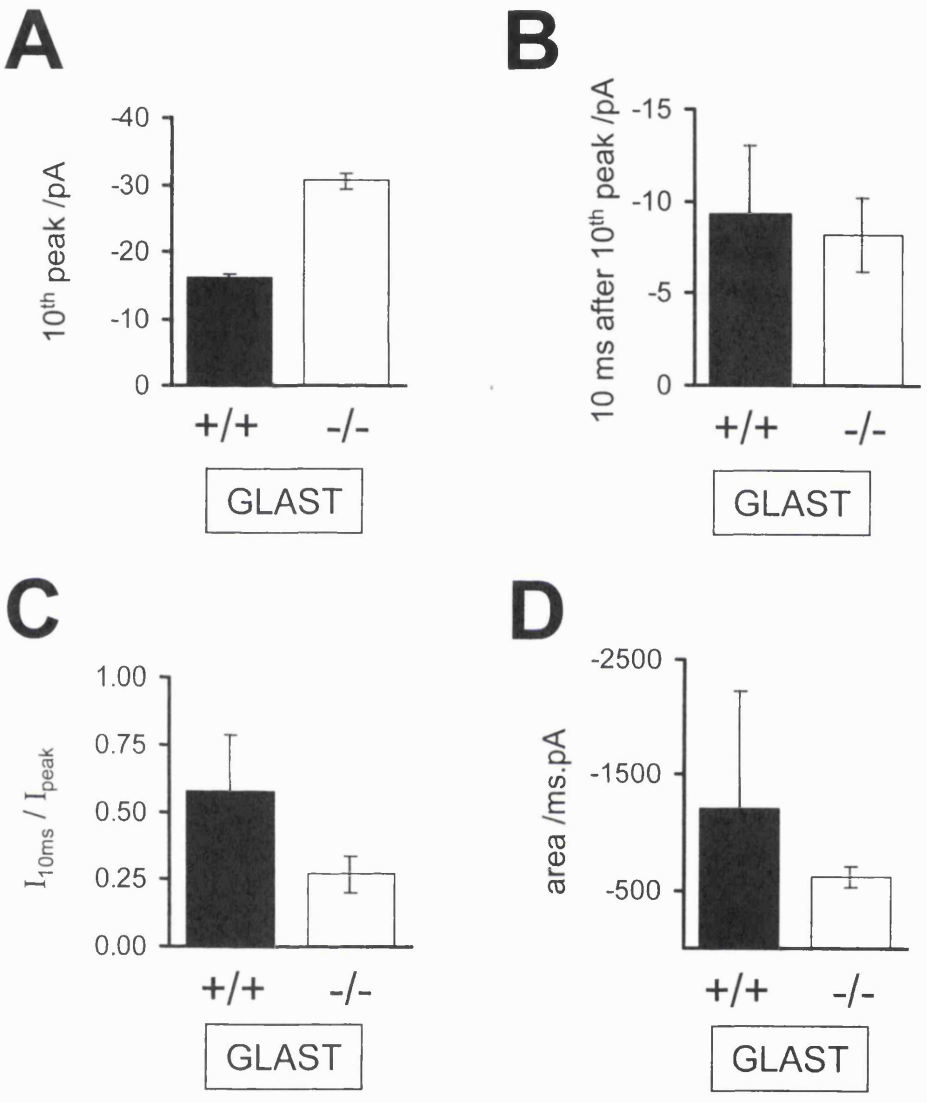
A
10th peak /pA
-40
-30
-20
-10
0
+/+
-/-
GLAST
B
10 ms after 10th peak /pA
-15
-10
-5
0
+/+
-/-
GLAST
C
I10ms / Ipeak
1.00
0.75
0.50
0.25
0.00
+/+
-/-
GLAST
D
area /ms.pA
-2500
-1500
-500
+/+
-/-
GLAST

The amplitude of the 10th peak (I_{peak}) was significantly different between the two genotypes (p = 0.001; unpaired t-test), but may simply reflect variability in EPSC size and the small sample number (i.e. only 2 and 4 cells from +/+ and -/- respectively). None of the other parameters showed a significant difference between the wild-type and the knock-out mice. P values for unpaired t-tests comparing the amplitude of the EPSC 10 ms after the 10th peak (I_{10ms}), the ratio I_{10ms}/I_{peak} and the total area after the 10th peak were 0.41, 0.78 and 0.14 respectively. I also recorded EPSCs from a few cells for each genotype at –30 mV (n = 1 (+/+) and 3 (-/-) cells) and +30 mV (n = 2 (+/+) and 3 (-/-) cells), but as before the data were not significantly different between the +/+ and the -/- mice (data not shown).

These data suggest that the glial glutamate transporter GLAST does not contribute to shaping the EPSC at the mossy fibre granule cell in the adult mouse, even during repetitive stimulation, and also that there are no developmental consequences of deleting GLAST (at least as far as the mossy fibre to granule cell synapse is concerned), despite this probably resulting in the granule cells experiencing a higher glutamate concentration and calcium influx as they migrate across the molecular layer (Komuro and Rakic, 1993; Rossi and Slater, 1993).

6.4 Synaptic transmission at the parallel fibre – Purkinje cell synapse in mice lacking the glutamate transporter GLAST

The following two sections describe experiments to investigate the role of the glial glutamate transporter GLAST in shaping synaptic transmission at the parallel fibre – Purkinje cell synapse. These experiments were carried out on P16-P20 day old mice, at room temperature and a holding potential of –70 mV, in collaboration with Paikan Marcaggi. All the data shown were obtained by myself. At P16-P20, GLAST is expressed at ~ 40% of its adult level, at least in rats (Furuta et al., 1997a; Ullensvang et al., 1997), and as mice develop faster than rats the percentage is

probably higher in mice.

6.4.1. Parallel fibre EPSCs evoked by single stimulation

To see whether knocking-out GLAST would influence synaptic transmission at the parallel fibre – Purkinje cell synapse, I recorded EPSCs in wild-type (+/+) and GLAST knock-out (-/-) mice. Purkinje cells receive inputs from many parallel fibres and increasing the stimulation strength results in more fibres being activated, producing a larger EPSC (by contrast, climbing fibre stimulation evoked an all or none EPSC, since at this age only one climbing fibre innervates each Purkinje cell). I confirmed that I was stimulating the parallel fibres by observing the characteristic paired-pulse facilitation at this synapse and the gradual increase in EPSC amplitude when the stimulation strength was increased (Konnerth et al., 1990; Perkel et al., 1990; Llano et al., 1991). To make comparison of cells in the wild-type and knock-out animals easier, I adjusted the stimulation strength to produce an EPSC of about 500-600 pA peak amplitude. Figure 6.11 shows specimen traces of such recordings for a wild-type (A) and a knock-out (B) mouse.

I analysed these data using a different procedure to that described for the granule cell EPSCs, because Purkinje cells only express AMPA receptors and not functional NMDA receptors at this age (Konnerth et al., 1990; Perkel et al., 1990; Rosenmund et al., 1992). I fitted the EPSC decay with a single exponential, to compare the decay time constants between the two genotypes. The bar graph in Figure 6.12 shows the averaged data for such an analysis, with the data from the wild-type mice (+/+) shown as a black bar (n = 33 cells) and the data from the knock-out mice (-/-) shown as a white bar (n = 38 cells). The decay time constant is significantly larger ($p = 0.004$, unpaired t-test) in the knock-out mice (6.53 ± 0.35 ms) than in wild type (5.15 ± 0.29 ms), indicating that the current takes longer to decay when glutamate transport is impaired.

Figure 6.11: The parallel fibre to Purkinje cell EPSC evoked by a single stimulus is slower in mice lacking GLAST (at room temperature)

A and B: Specimen traces of synaptic currents recorded in cerebellar Purkinje cells of (A) a wild type and (B) a GLAST knock-out mouse, in response to a single stimulus delivered to the parallel fibres in the molecular layer. The dashed box corresponds to the region of the current that is shown at a faster time-scale below. The recordings were at room temperature, in external solution containing 10 μM Gabazine to block $GABA_A$ receptors (Table 4, solution F), at a holding potential of -70 mV. EPSC decay time constants for the cells in A and B were 4.19 and 9.71 ms respectively.

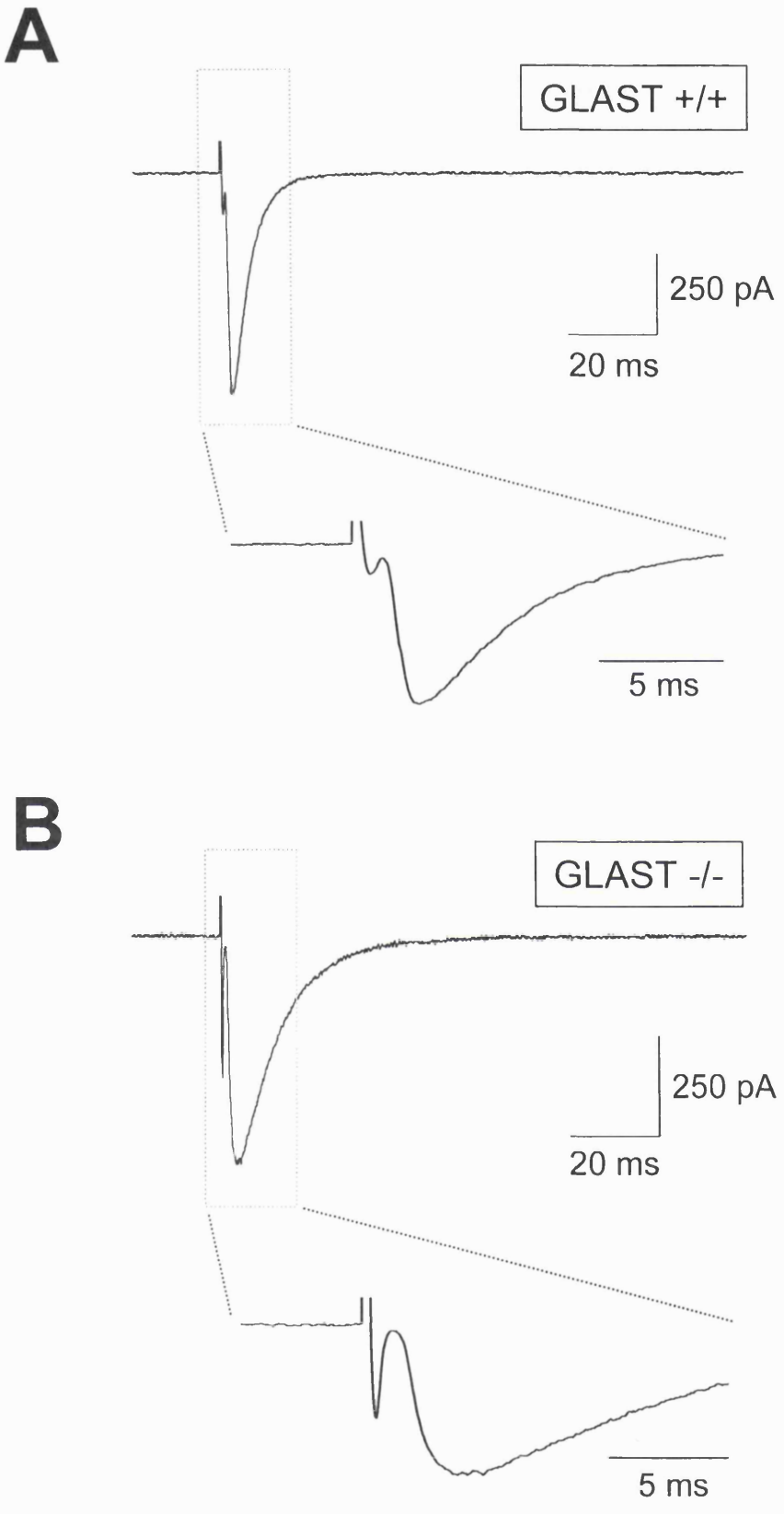
A
GLAST +/+
250 pA
20 ms
5 ms
B
GLAST -/-
250 pA
20 ms
5 ms

Figure 6.12: The parallel fibre to Purkinje cell EPSC evoked by a single stimulus decays more slowly in mice lacking GLAST (at room temperature)

Bar graphs of the decay time constants (single exponential fit) of the EPSCs in wild type (black; n = 33 cells) and GLAST knock-out (white; n = 38 cells) mice. Specimen traces and recording conditions are in Figure 6.11.

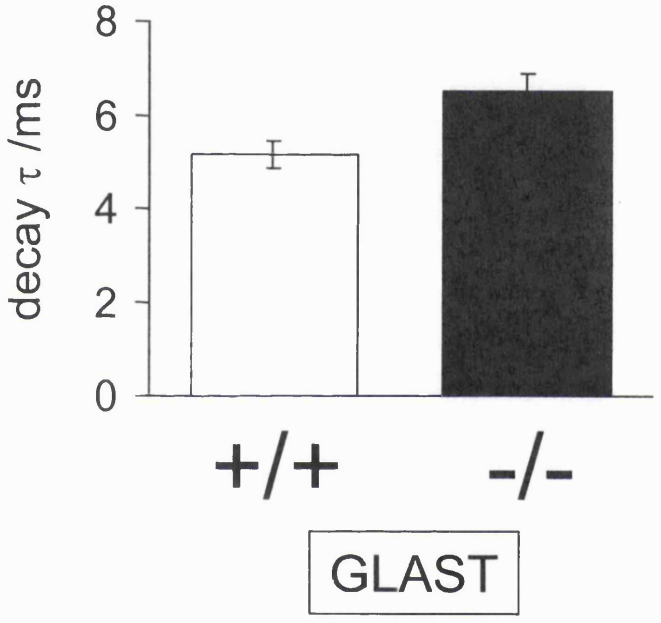
decay τ /ms
8
6
4
2
0
+/+
-/-
GLAST

These data suggest that the glial glutamate transporter GLAST contributes to shaping the EPSC at the parallel fibre Purkinje cell synapse, making the current decay faster.

6.4.2. Parallel fibre EPSCs evoked by repetitive stimulation

Parallel fibres can fire at frequencies up to several hundred hertz. During such high frequency activity, the extracellular glutamate concentration might build up, and glutamate transporters might then participate in shaping the postsynaptic response even more. To see whether knocking-out GLAST had a greater influence on synaptic transmission at the parallel fibre – Purkinje cell synapse during repetitive stimulation, I recorded EPSCs in wild-type (+/+) or GLT-1 knock-out (-/-) mice in response to 10 stimuli at 200 Hz. As before (section 6.4.1), I adjusted the stimulation strength to result in a single-stimulus evoked EPSC of around 500-600 pA peak amplitude. The parallel fibre – Purkinje cell synapse is facilitating (Konnerth et al., 1990; Perkel et al., 1990; Regehr and Atluri, 1995; Kreitzer and Regehr, 2000), so with each stimulus during the repetitive stimulation the current becomes larger. Because these large currents will reduce the voltage-clamp quality of the cell, I added 1 μM of the competitive non-NMDA receptor blocker NBQX to the bath solution to reduce the size of the postsynaptic current (this is unlikely to affect the EPSC decay kinetics: at the climbing fibre to Purkinje cell synapse a partly blocking dose of NBQX did not alter the EPSC kinetics: (Wadiche and Jahr, 2001); similarly, 1 μM CNQX, another AMPA receptor antagonist, did not alter the kinetics of the climbing fibre or parallel fibre to Purkinje cell EPSCs: (Barbour et al., 1994; Takahashi et al., 1995b)). Figure 6.13 shows specimen traces of such recordings for a wild-type (A) and a knock-out (B) mouse. The current after the last stimulation did not always decay straight away to baseline, but often continued to rise to a final peak about 20-50 ms after the end of the pulse train before decaying. This current was mediated by non-NMDA receptors since it could be blocked by 25 μM NBQX

Figure 6.13: The parallel-fibre – Purkinje cell EPSC evoked by repetitive stimulation in wild type mice and in mice lacking GLAST (at room temperature)

A and B: Specimen traces of synaptic currents recorded in cerebellar Purkinje cells of (A) a wild type and (B) a GLAST knock-out mouse, in response to repetitive stimulation (10 stimuli at 200 Hz) delivered to the parallel fibres in the molecular layer. The recordings were at room temperature, in external solution containing 1 μM NBQX and 10 μM Gabazine (Table 4, solution F), at a holding potential of –70 mV.

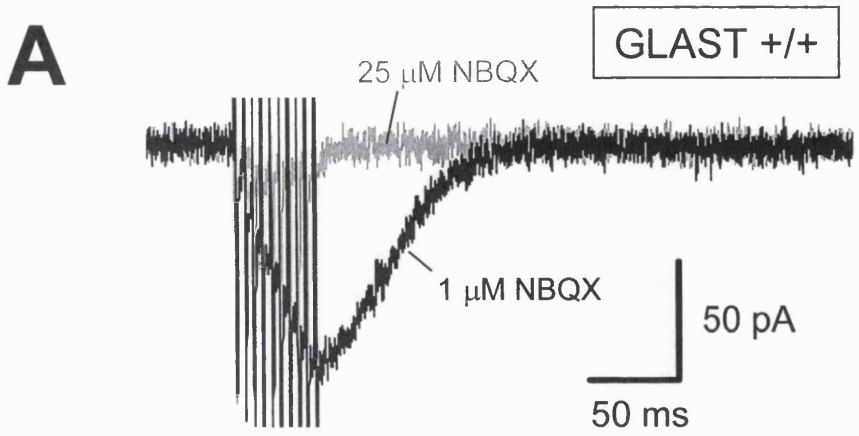
A
GLAST +/+
25 μM NBQX
1 μM NBQX
50 pA
50 ms

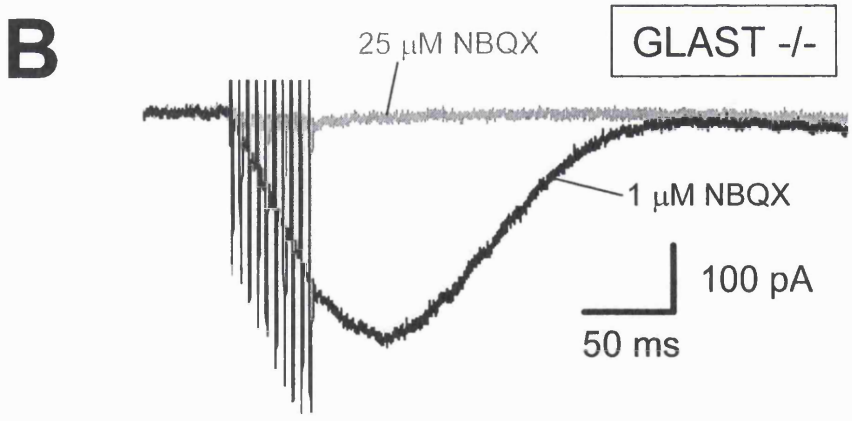
B
GLAST -/-
25 μM NBQX
1 μM NBQX
100 pA
50 ms

(grey traces). Whereas 4/6 cells obtained from the knock-out mice showed this delayed peak (see Figure 6.13B for an example with the peak), only 2/6 cells from wild-type animals showed the delayed peak (see Figure 6.13A for an example without the peak); however, this difference is not significant ($p = 0.56$ on χ^2 test with Yates correction for small sample numbers). Also, in some cases the EPSC decayed and was followed by a prominent, slowly rising, longer lasting (seconds) inward current, possibly mediated by metabotropic glutamate receptors (Batchelor and Garthwaite, 1993; Batchelor et al., 1994; Batchelor and Garthwaite, 1997; Tempia et al., 1998; Tempia et al., 2001). Half (3/6) of the cells obtained from the knock-out mice showed this late inward current (see Figure 6.15B (control trace, dotted box) for an example with the late current), but none (0/6) of the cells from wild-type animals showed it (see Figure 6.15A (control trace, dotted box) for an example without the late current; $p = 0.18$).

I analysed the data to obtain the peak current amplitude (i.e. at or after the last stimulus), the time for the EPSC needed to decay to half the value attained just after the 10^{th} stimulus ($T_{1/2}$) and the total charge transfer after the last stimulus. The charge transfer was integrated out to 3000 ms after the last stimulus, and so will include the putative metabotropic component when present, while the $T_{1/2}$ measurement reflects just the duration of the AMPA component (which is more than twice the size of the mGluR component under all conditions). The peak amplitude was -248 ± 52 pA for the wild-type ($n = 6$) and -261 ± 79 pA for the GLAST KO ($n = 6$) mouse, i.e. not significantly different ($p = 0.89$, unpaired t-test). The bar graphs in Figure 6.14A show the average data for the $T_{1/2}$ after the last stimulus, with the data from the wild-type mice (+/+) shown as a black bar ($n = 6$ cells) and the data from the knock-out mice (-/-) shown as a white bar ($n = 6$ cells). The $T_{1/2}$ were not statistically significantly different between the six +/+ and the six -/- cells ($p = 0.47$, unpaired t-test). The bar graphs in Figure 6.14B show the average data for the total charge transfer after the last stimulus, with the data from the wild-type mice (+/+) shown as

Figure 6.14: The parallel-fibre – Purkinje cell EPSC evoked by repetitive stimulation is not significantly longer lasting when GLAST is deleted

A: Bar graphs of the time needed for the EPSC to decay to half its value after the 10^{th} stimulus ($T_{1/2}$) in wild type (black; n = 6 cells) and GLAST knock-out (white; n = 6 cells) mice. Specimen traces and recording conditions are in Figure 6.13.

B: Bar graphs of the area of the EPSCs (after the 10^{th} peak) in wild type (black; n = 6 cells) and GLAST knock-out (white; n = 6 cells) mice. Specimen traces and recording conditions are in Figure 6.13.

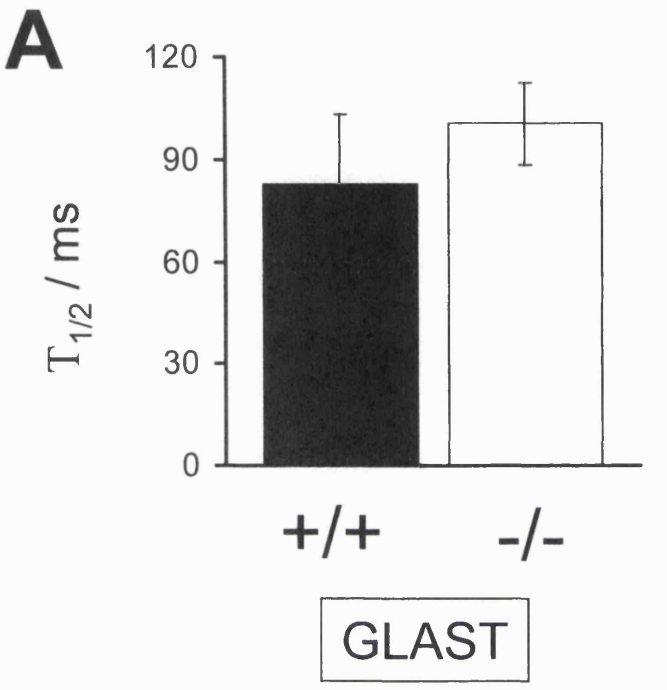
A
120
90
60
30
0
$T_{1/2}$ / ms
+/+
-/-
GLAST

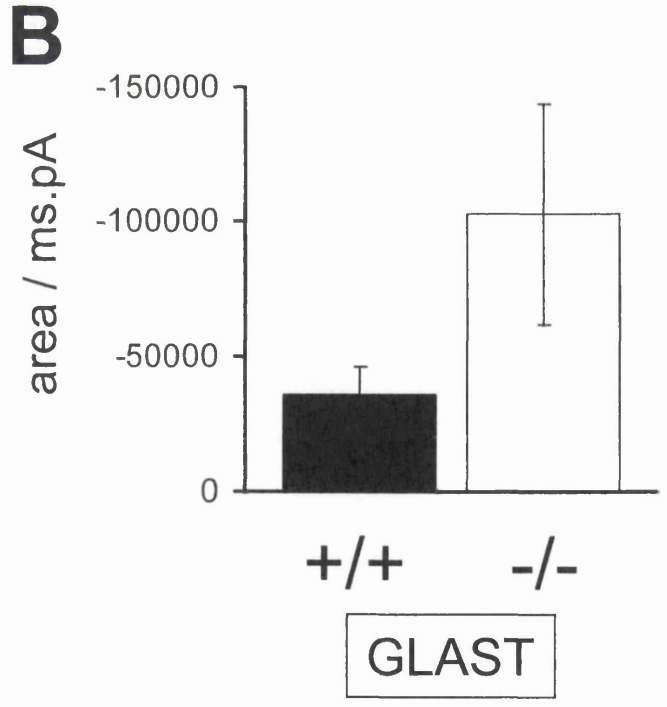
B
-150000
-100000
-50000
0
area / ms.pA
+/+
-/-
GLAST

black bar (n = 6 cells) and the data from the knock-out mice (-/-) shown as white bar (n = 6 cells). The total area was usually larger in the knock-out, but the data were not statistically significantly different between the six +/+ and the six -/- cells (p = 0.15, unpaired t-test). The lack of a significant difference between the wild type and the GLAST knock-out in the $T_{1/2}$ and charge transfer measurements is surprising, given the difference detected in the decay of the EPSC evoked by a single stimulus (see section 6.4.1). Since the mean values of $T_{1/2}$ and the charge transfer were larger in the knock-out mice, the lack of significance may reflect the small number of cells recorded for this study (6 compared to >33 for the single stimulus EPSC).

To investigate the function of the other glutamate transporter types present in the molecular layer (the glial GLT-1, and the neuronal EAAT-4 and EAAC-1) in shaping the synaptic response during repetitive stimulation, I recorded synaptic responses as described in the previous paragraph, in the absence or presence of either DHK, to block GLT-1, or (in wild-type cells only) DHK + TBOA, to block all known glutamate transporter types. Cells from the knock-out mice showed huge inward shifts of baseline current when DHK+TBOA was applied (presumably as a result of accumulation of extracellular glutamate) and usually died during the drug treatment, making it impossible to study the effect of these blockers with GLAST knocked-out. Figure 6.15 shows specimen traces of such recordings for a wild-type (A) and a knock-out (B) mouse.

Interestingly, blocking glutamate transport with either DHK or DHK+TBOA resulted in a larger fraction of cells, both wild-type and knock-out, exhibiting the delayed peak current after the end of the stimulus train (wild-type: control 2/6; +DHK 2/6; +DHK+TBOA 5/5 (p = 0.10 compared to control, χ^2 test with Yates correction); knock-out: control 4/6; +DHK 5/5 (not significantly different; p = 0.52)) and exhibiting the late putative metabotropic current (wild-type: control 0/6; +DHK 1/6; +DHK+TBOA 4/5 (significantly increased from control; p = 0.03); knock-out: control 3/6; +DHK 4/5 (not significantly different; p = 0.69)). I analysed these data

Figure 6.15: The parallel fibre to Purkinje cell EPSC is larger and longer lasting when more transporter types are blocked (repetitive stimulation, at room temperature)

A and B: Specimen traces of synaptic currents recorded in cerebellar Purkinje cells of (A) a wild type and (B) a GLAST knock-out mouse, in response to repetitive stimulation (10 stimuli at 200 Hz) delivered to the parallel fibres in the molecular layer, in the absence (black) or presence of 200 μM DHK (dark grey) or 200 μM DHK + 200 μM TBOA (light grey). The recordings were at room temperature, in external solution containing 1 μM NBQX and 10 μM Gabazine (Table 4, solution F), at a holding potential of –70 mV. The dotted box indicates the region of the putative mGluR component of the current.

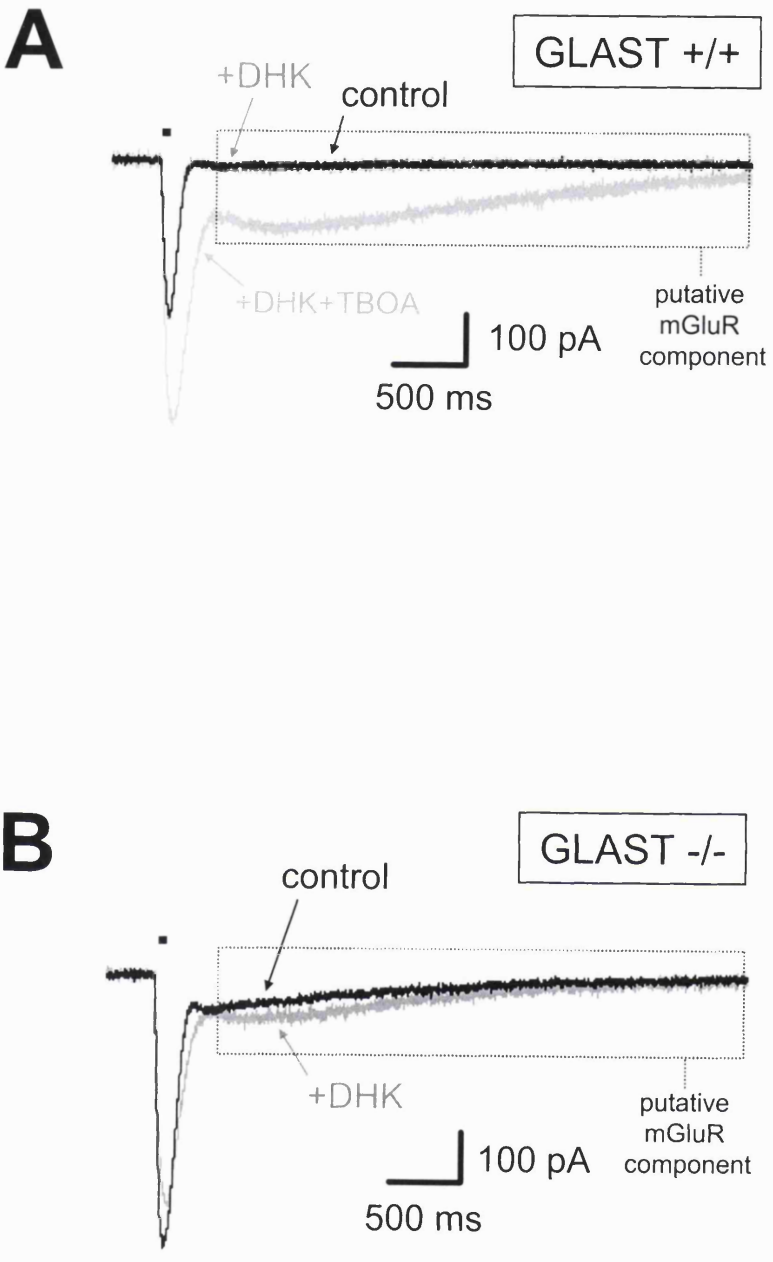
A
GLAST +/+
+DHK
control
+DHK+TBOA
putative
mGluR
component
100 pA
500 ms
B
GLAST -/-
control
+DHK
putative
mGluR
component
100 pA
500 ms

for the $T_{1/2}$ and the area after the last stimulus and normalized them in each cell to the value in control solution (i.e. without DHK or TBOA; raw values in control are shown in Figure 6.14). Figure 6.16A and 6.16B show the normalized $T_{1/2}$ and area respectively, of the currents for cells from wild-type (+/+) and knock-out (-/-) animals. The 1st (black) and 4th (white) bars are control for +/+ and -/- respectively, the 2nd (dark, dotted) and 5th (light, dotted) bars are in DHK for +/+ and -/- respectively and the 3rd (dark, striped) bar is in DHK and TBOA for +/+. The p values from paired t-tests on the normalized values for $T_{1/2}$ are 0.78 (comparing control and DHK in the +/+), 0.02 (comparing control and DHK+TBOA in the +/+), 0.02 (comparing DHK and DHK+TBOA in the +/+) and <0.01 (comparing control and DHK in the -/-). Similarly, the p values from paired t-tests on the normalized values for the area are 0.37 (comparing control and DHK for the +/+), 0.05 (comparing control and DHK+TBOA in the +/+), 0.04 (comparing DHK and DHK+TBOA in the +/+) and 0.20 (comparing control and DHK in the -/-). Interestingly, comparing the 3rd and the 5th bars with each other, i.e. with all glutamate transporters blocked (DHK+TBOA in the +/+) vs only the glial ones blocked (DHK in the -/-), shows a significant difference ($p = 0.02$), indicating that either the neuronal glutamate transporters play a prominent role in shaping the response after repetitive stimulation, or that the block of all transporters leads to a much greater accumulation of glutamate than occurs with just one set of transporters blocked.

To see how the GLAST KO mouse would cope with an even larger glutamate load, I stimulated the parallel fibres for different durations (10, 20 and 50 stimuli at 200 Hz). Figure 6.17 shows specimen traces of such recordings for a wild-type (A) and a knock-out (B) mouse stimulated with 10 (black trace), 20 (dark grey trace) or 50 (light grey trace) pulses. It appears that the KO mouse is more prone to glutamate accumulation, as can be seen by the larger and longer lasting current with increasing stimulation duration, but because of the small cell number ($n = 1$ for each genotype)

Figure 6.16: The parallel fibre to Purkinje cell EPSC is larger and longer lasting when more transporter types are blocked (repetitive stimulation, at room temperature)

A: Bar graphs of the $T_{1/2}$ of the EPSCs in wild type (black, +/+; n = 6 (1^{st} bar), 6 (2^{nd} bar) and 5 (3^{rd} bar)) Purkinje cells and GLAST knock-out (white, -/-; n = 6 (1^{st} bar) and 5 (2^{nd} bar)) Purkinje cells in control solution (1^{st} and 4^{th} bars), in 200 μM DHK (2^{nd} and 5^{th} bars) and in 200 μM DHK + 200 μM TBOA (3^{rd} bar). The $T_{1/2}$ in each cell was normalized to the $T_{1/2}$ obtained in control conditions (i.e. with no DHK or TBOA). Specimen traces and recording conditions are in Figure 6.15.

B: Bar graphs of the area of the EPSCs (after the peak of the response to the 10^{th} stimulus) in wild type (black, +/+; n = 6 (1^{st} bar), 6 (2^{nd} bar) and 5 (3^{rd} bar)) Purkinje cells and GLAST knock-out (white, -/-; n = 6 (1^{st} bar) and 5 (2^{nd} bar)) Purkinje cells, in control solution (1^{st} and 4^{th} bars), in 200 μM DHK (2^{nd} and 5^{th} bars) and in 200 μM DHK + 200 μM TBOA (3^{rd} bar). The area in each cell was normalized to the area obtained in control conditions (i.e. with no DHK or TBOA). Specimen traces and recording conditions are in Figure 6.15.

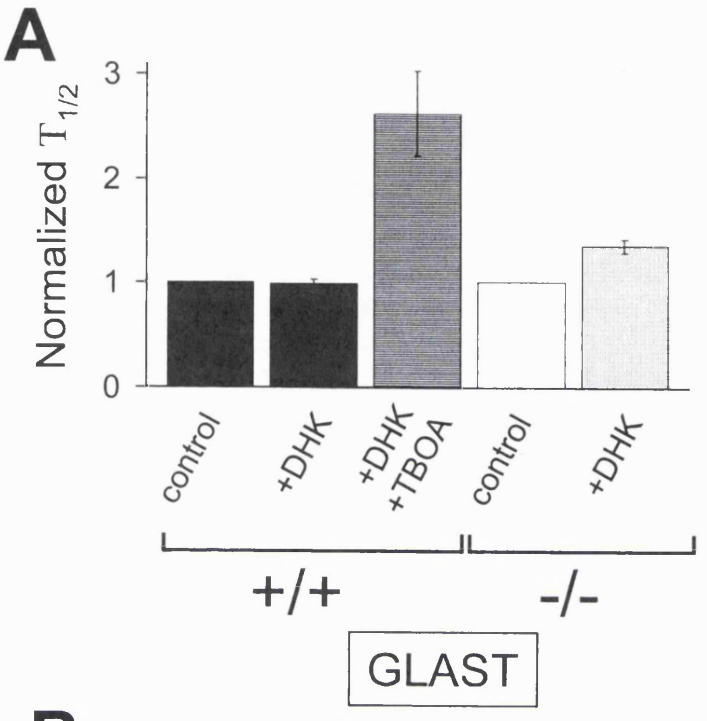
A
Normalized $T_{1/2}$
3
2
1
0
control
+DHK
+DHK +TBOA
control
+DHK
+/+
-/-
GLAST

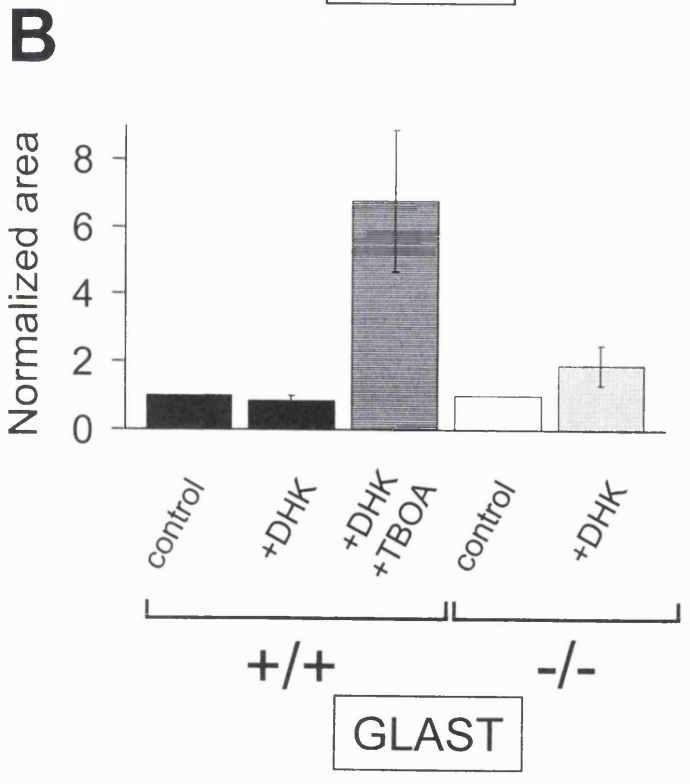
B
Normalized area
8
6
4
2
0
control
+DHK
+DHK +TBOA
control
+DHK
+/+
-/-
GLAST

Figure 6.17: The parallel fibre to Purkinje cell EPSC is larger and prolonged when more stimuli are given (repetitive stimulation, at room temperature)

A and B: Specimen traces of synaptic currents recorded in cerebellar Purkinje cells of (A) a wild type and (B) a GLAST knock-out mouse, in response to repetitive stimulation delivered to the parallel fibres in the molecular layer (black traces: 10 stimuli at 200 Hz; dark grey traces: 20 stimuli at 200 Hz; light grey traces: 50 stimuli at 200 Hz). The recordings were at room temperature, in external solution containing 1 μM NBQX and 10 μM Gabazine (Table 4, solution F), at a holding potential of -70 mV.

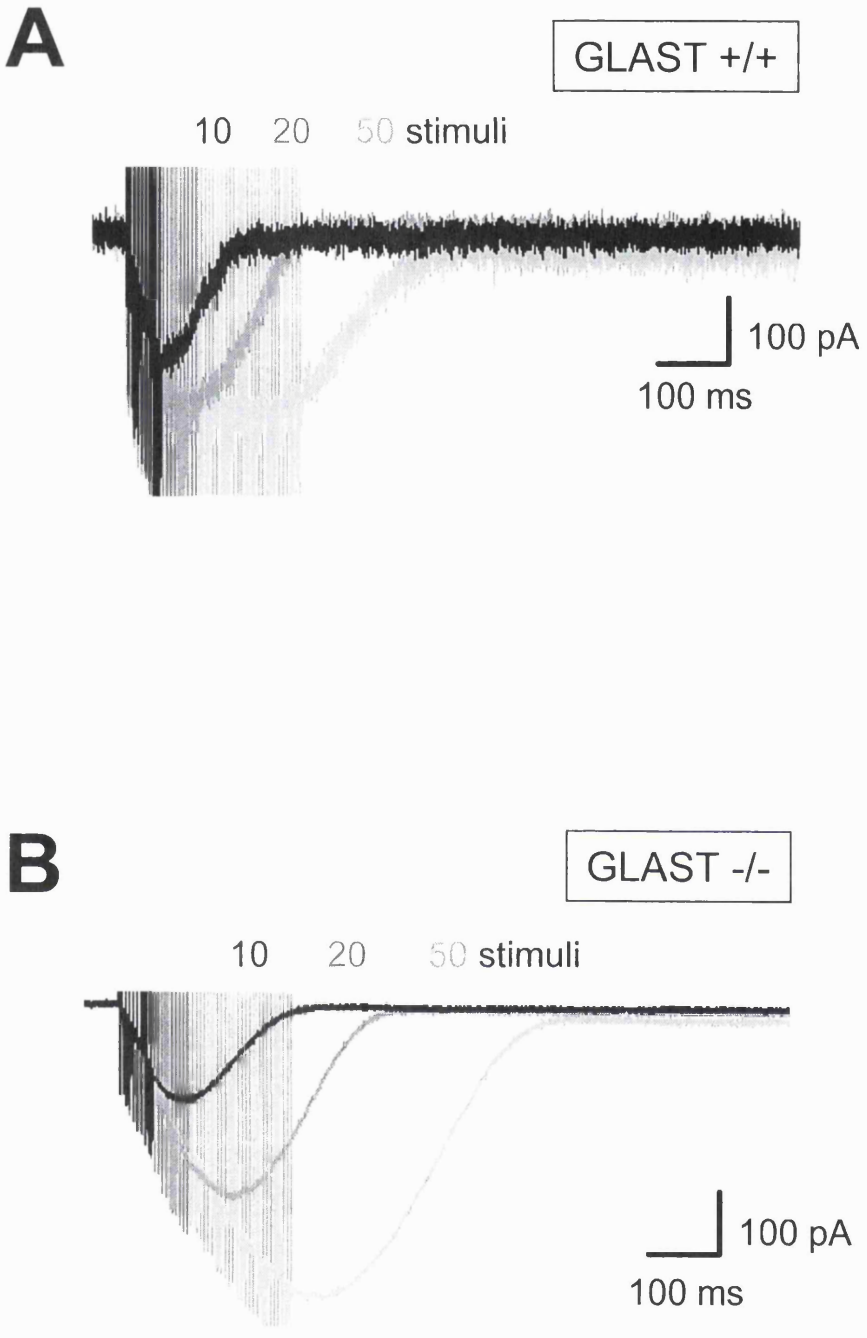
A
GLAST +/+
10 20 50 stimuli
100 pA
100 ms
B
GLAST -/-
10 20 50 stimuli
100 pA
100 ms

this is only a brief glimpse of a potentially interesting finding.

6.5 Discussion

To see whether the glial glutamate transporter GLT-1 and GLAST contribute to shaping synaptic transmission in the cerebellum, I recorded EPSCs in wild-type and knock-out mice.

6.5.1 The mossy fibre – granule cell synapse

Neither the lack of GLT-1 (in P11-P15 mice) nor the lack of GLAST (in P29-P30 mice) affected the synaptic current at the mossy fibre – granule cell synapse, either for single or repetitive stimulation, at room (24^{O}C) or at body (37^{O}C) temperature. This implies that the glial glutamate transporters do not contribute to shaping synaptic transmission at the mossy fibre – granule cell synapse in the cerebellum at the ages studied. For GLT-1 this might not be too surprising, because the animals express only around 5–40% of their adult level at the ages studied (P11-P15) (Furuta et al., 1997a; Ullensvang et al., 1997). This suggests that the EPSC is terminated either by EAAC-1 transporters (which are quite strongly expressed in the granule cell layer at the ages I examined: Furuta et al. (1997b; 1997a)), or by glutamate diffusing out of the synaptic cleft (if diffusion is slower than deactivation but faster than desensitization), or by AMPA receptor deactivation (if glutamate clearance from the cleft is faster than the deactivation kinetics) or by desensitization (though the two latter possibilities are unlikely, as the deactivation time constants of granule cell AMPA receptors are 0.66 ms (at 24^{O}C) and 0.23 ms (at 35^{O}C), significantly smaller than the EPSC decay time constants at the mossy fibre granule cell synapse (1.4 ms at 25^{O}C and 0.7 ms at 35^{O}C), and the desensitization time constants are 3.6 ms (at 25^{O}C) and 2.1 ms (at 35^{O}C), significantly larger than the EPSC decay time constant (Silver et al., 1996b)). I had planned to do experiments on

the EAAC-1 knock-out mouse (Peghini et al., 1997) to compare the relevance of GLT-1, GLAST and EAAC-1, but we were unable to obtain this mouse.

How do my data compare to the results obtained by others (Sarantis et al., 1993; Overstreet et al., 1999) at this synapse? As mentioned in section 1.3, Sarantis et al. (1993) and Overstreet et al. (1999) investigated the effect on the time-course of the mossy fibre – granule cell EPSC and EPSP of blocking glutamate transport pharmacologically. Consistent with my data, neither study showed an effect of PDC (which blocks all glutamate transporters) on the non-NMDA component of the EPSC evoked by a single stimulus, and Overstreet et al. (1999) saw no effect of the GLT-1 blocker DHK on the non-NMDA and NMDA components of the EPSC evoked by single or repetitive stimuli. However, Overstreet et al. (1999) reported that PDC caused: (1) a prolongation of the NMDA component of the EPSC during single stimulation, (2) a prolongation of the NMDA and non-NMDA components of the EPSC during repetitive stimulation, and (3) an increase of the EPSP area and an increase of the action potential firing (burst) duration. This demonstration of an effect of transporters contrasts with my results on the GLT-1 and GLAST knock-out mice, possibly for one of the following reasons. (1) The use of PDC can, as outlined in section 6.1, result in glutamate accumulation and an artificial prolongation of the EPSC time-course due to slowing of glutamate diffusion, which might cause problems in the interpretation of those two studies. However, Overstreet et al. (1999) used relatively low concentrations of PDC (30-100 μM) and did not observe an inward current (which would indicate accumulation of glutamate) when it was bath applied. (2) The use of knock-out mice in my work makes it necessary to compare data between cells taken from different animals. The variability of EPSC shape is very high between cells even within one genotype group, making it harder to detect a significant difference between genotypes. This was a major problem for the study described in this chapter. (3) There might be differences between species: I used mice in this study, while Sarantis et al. (1993) and Overstreet et al. (1999) used rats.

(4) The recording temperature will affect most processes involved in synaptic transmission, including speed of glutamate transport, speed of diffusion, receptor kinetics and presynaptic release machinery. I recorded most of my data at body temperature, whereas the other two studies recorded at room temperature. (5) Finally, all of the data might be reconciled if synaptic transmission at the mossy fibre synapse is terminated by the neuronal transporter EAAC-1 lowering the extracellular glutamate concentration. EAAC-1 is expressed in the granule cell layer (Furuta et al., 1997b; Furuta et al., 1997a), and would be blocked in the PDC experiments of Overstreet et al. (1999), but should be unaffected in my GLAST and GLT-1 knock-out mice.

6.5.2 The parallel fibre – Purkinje cell synapse

The glial transporter GLAST did affect the time-course of the parallel fibre – Purkinje cell EPSC (even the EPSC evoked by a single stimulus), making it slightly (21%) faster when transporters were functional. This implies that removal of glutamate by GLAST contributes to shaping the synaptic current at this synapse.

Interestingly, during repetitive stimulation of parallel fibres, a delayed peak to the AMPA receptor mediated EPSC occurred after the stimulus train particularly in conditions when transporter function was reduced, i.e. in cells from knock-out (compared with wild-type) mice, and in cells from all mice with glutamate transporters pharmacologically blocked using DHK or DHK+TBOA (e.g. Figure 6.13B). The origin of the delayed peak is unclear, but might be explained as follows. The current after repetitive stimulation is blocked by 25 μM NBQX (Figure 6.13), suggesting that it is mediated by AMPA (or kainate) receptors. The steady-state dose-response relation for glutamate acting on AMPA receptors has been shown to be bell-shaped in several preparations (Geoffroy et al., 1991; Raman and Trussell, 1992; Kinney et al., 1997), with an increase in glutamate concentration producing an increased current at low doses as more receptors are activated, but a decreased

current at high doses as more desensitization occurs. This property was used to explain the biphasic AMPA receptor mediated waveform of EPSCs at the large mossy fibre – unipolar brush cell (UBC) synapse in the cerebellar granule cell layer (Kinney et al., 1997). The bell-shaped glutamate dose-response relation for AMPA receptors might also explain the delayed peak seen at the parallel fibre – Purkinje cell synapse after repetitive stimulation. During the high frequency firing of parallel fibres (e.g. 10 stimuli at 200 Hz, which takes 50 ms), the extracellular glutamate level builds up before declining to resting levels after the stimulus train. If AMPA receptors are exposed to glutamate levels sufficiently elevated to go over the top of the bell-shaped curve, then when the glutamate concentration falls, the bell-shaped dose-response relation predicts an *in*crease in current before a final decrease. If the delayed peak in my experiments is due to this mechanism, it would also explain why this effect is more pronounced when glutamate transport is impaired (in the knock-out compared to the wild-type, or by application of DHK and TBOA compared to control), since less glutamate transport will lead to a higher glutamate concentration being reached.

Another other striking finding when glutamate transport was impaired was the occurrence of a slow current (Figure 6.15), possibly mediated by metabotropic glutamate receptors (Batchelor and Garthwaite, 1993; Batchelor et al., 1994; Batchelor and Garthwaite, 1997; Tempia et al., 1998; Tempia et al., 2001). This current was more pronounced in the knock-out (compared to the wild-type) mice and during application of DHK and TBOA (compared to control), suggesting that when transporters are non-functional the extracellular glutamate concentration rises more, activating more mGluRs for a longer period of time. There may also be more spill-over of glutamate to neighbouring synapses, producing activation of their receptors. In agreement with this, Brasnjo & Otis (2001) have recently demonstrated an important function of (neuronal) glutamate transporters in regulating mGluR activation and expression of long term depression (LTD) at the parallel fibre –

Purkinje cell synapse.

By comparing the effect of glutamate transport inhibitors with the effect of the knock-out of particular transporters, I attempted to assess the importance of glial vs neuronal transporters in shaping synaptic transmission at this synapse. Interestingly, TBOA, which blocks both neuronal and glial transporters (Shimamoto et al., 1998) had a huge effect on the parallel fibre EPSC peak amplitude, decay, delayed peak and slow (mGluR) current after repetitive stimulation compared to either DHK alone (to block GLT-1) or the GLAST knock-out mouse. It is tempting to suggest that this implies a major role in terminating synaptic transmission for neuronal glutamate transporters, such as EAAT-4 and EAAC-1, which are expressed by Purkinje cells (Furuta et al., 1997b; Furuta et al., 1997a). However, to test this it is necessary to measure the effect of blocking the neuronal transporters alone (e.g. by removing internal K+ as done by Brasnjo & Otis (2001)). It is possible that blocking neuronal transporters alone will have little effect on the EPSC, because glial transporters provide enough uptake to maintain a concentration gradient sufficient to drive glutamate diffusion out of the synaptic cleft. On this scenario the presence of either neuronal or glial transporters is sufficient for normal synaptic transmission, and it is only when all transporters are blocked that the EPSC becomes prolonged.

How do my data compare to the results (see Chapter 1) obtained by others (Barbour et al., 1994; Takahashi et al., 1995b; Brasnjo and Otis, 2001) at this synapse? Barbour et al. (1994) and Takahashi et al. (1995b) found that pharmacologically blocking glutamate transport prolonged the time-course of the parallel fibre – Purkinje cell EPSC, similar to the results described in section 6.4.1. Brasnjo & Otis (2001) reported that (non-transported) glutamate transport blockers potentiated the magnitude of the mGluR current, in agreement with my finding that impairing glutamate uptake increased the slow (mGluR) current. Finally, Wachtmann et al. (2000) and Watanase et al. (1998) investigated transmission at the parallel fibre – Purkinje cell synapse of glutamate transporter knock-out mice. Wachtmann et al.

(2000), using GLAST, EAAC-1 and GLAST/EAAC-1 double knock-out mice, reported a slight slowing of the EPSC in the GLAST and GLAST/EAAC-1 double knock-out, but not in the EAAC-1 knock-out mouse, suggesting that the glial and not the neuronal transporter terminates synaptic transmission at this synapse. This is consistent with my results. By contrast, Watanase et al. (1998), using GLAST knock-out mice, reported no effect on the time-course of the EPSC. This disagrees with the results in my study, but the reasons for the discrepancy are unclear.

CHAPTER 7

The glycine site of the NMDA receptor at the cerebellar mossy-fibre – granule cell synapse appears to be saturated

7.1 Introduction

As described in chapter 1, the opening of NMDA receptors is dependent on their co-agonist site being occupied by glycine or D-serine. At several central synapses the extracellular glycine level is not high enough to saturate the NMDA receptor glycine site (Thomson et al., 1989; Berger et al., 1998; Bergeron et al., 1998). The stoichiometry of the GLYT-2 transporter may allow glial cells to modulate the extracellular glycine concentration in the range where it alters NMDA receptor activation (Supplisson and Bergman, 1997; Roux and Supplisson, 2000; see sections 1.1.1.3.1 and 1.5), and in addition, in the developing cerebellum, D-serine may be an important agonist at the glycine site (Schell et al., 1997; see section 1.1.1.3.1). At present it is unknown to what extent the glycine site on cerebellar granule cells is activated.

This chapter describes experiments to determine whether the glycine site of the NMDA receptor in cerebellar granule cells is saturated after the cells have migrated to their final destination and synapse formation has occurred. To test this, I electrically stimulated mossy fibres in the internal granule cell layer, while recording postsynaptic currents in granule cells (using whole-cell patch-clamping) in the absence or presence of glycine (or D-serine). All experiments were performed on cerebellar slices of P14 old rats, in magnesium-free external solution at a holding potential of –60 mV.

7.2 Effect of exogenous glycine on the MF-gc EPSC at room temperature

To see whether the glycine site of the NMDA receptor at the mossy fibre – granule cell synapse in the cerebellum can be modulated by exogenous glycine or is already saturated, I recorded EPSCs with 0, 10 or 100 μM glycine added to the superfusion solution. Figure 7.1A shows specimen traces of such recordings, obtained at room temperature. It is obvious from these traces that the shape of the EPSC, with a rapid decaying AMPA component and a slowly decaying NMDA component, was not altered by exogenous glycine. To quantify the effects of glycine on the NMDA component of the EPSC, I measured the current amplitude 20 ms after the peak, at which time the AMPA receptor component of the EPSC is negligible, since it decays with a time constant of around 1-2 ms (Silver et al., 1992). The bar graph in Figure 7.1B shows the averaged data for such an analysis. The current amplitude at 20 ms after the peak in the absence of glycine was –24.1 ± 3.9 pA (n = 17 cells; black bar), in the presence of 10 μM glycine it was –24.4 ± 3.5 pA (n = 16; grey bar) and in the presence of 100 μM glycine it was –20.4 ± 3.6 pA (n = 13; white bar). Figure 7.1C shows the current amplitude measured at 20 ms after the peak when normalized to its value in the absence of glycine in each cell. In the presence of 10 μM glycine the normalized amplitude at 20 ms was 1.03 ± 0.03 (n = 16; p = 0.39 compared with 0 μM glycine (paired t-test); grey bar), and in the presence of 100 μM glycine the normalized amplitude at 20 ms was 1.00 ± 0.07 (n = 13; p = 0.95; white bar). Thus, the NMDA receptor component of the EPSC was not significantly altered when glycine was added to the bath solution.

The same EPSCs were also analysed for their peak amplitude, determined mainly by the AMPA component of the EPSC, and their total area, i.e. the total charge transfer during the EPSC. Both of these parameters showed no significant change when glycine was added, as shown in Figure 7.2, which shows the averaged values of the peak (A) and the area (C), and of the peak (B) and the area (D)

Figure 7.1: The NMDA receptor glycine site in cerebellar granule cells appears to be saturated

(A) Specimen traces of synaptic currents recorded in a rat cerebellar granule cell (mossy fibre – granule cell synapse) in the presence of different glycine concentrations (0, 10 or 100 μM) added to the superfusion solution. Arrow head indicates the location of the peak of the EPSCs. Vertical arrow points to the current 20 ms after the peak of the EPSCs, which was used to estimate its NMDA component. Dashed box corresponds to the region of the current which is shown at a faster time-scale below. The experiments were done at room temperature, in magnesium-free external solution at a holding potential of –60mV.

(B) Bar graph of the EPSC amplitude measured 20 ms after the peak (see vertical arrow in A) as a function of the glycine concentration added to the superfusate, i.e. in the absence of glycine (black, n = 17 cells), in the presence of 10 μM glycine (grey, n = 16 cells) and in the presence of 100 μM glycine (white, n = 13 cells).

(C) Bar graph of the EPSC amplitudes at 20 ms normalized in each cell to the value in the absence of glycine.

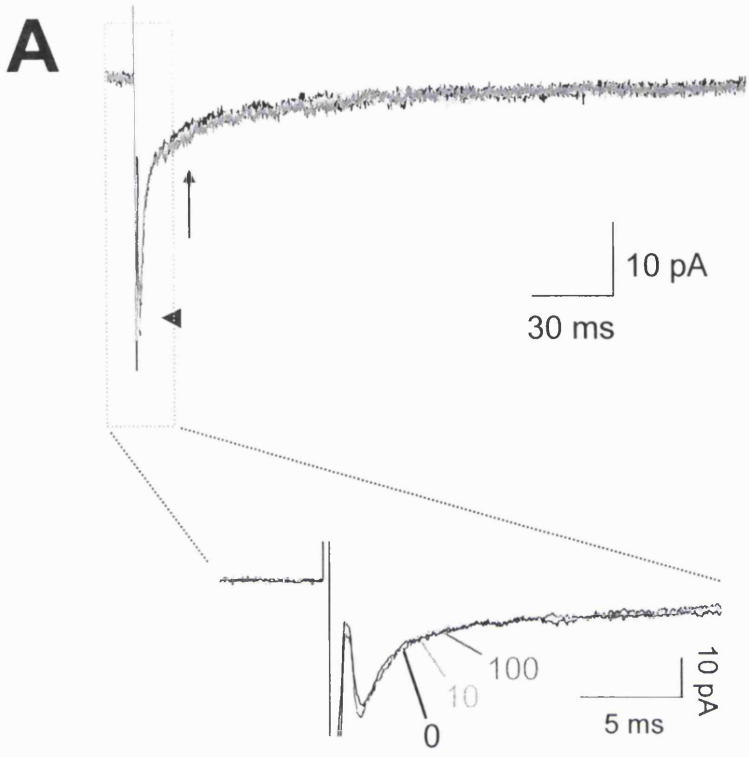
A
10 pA
30 ms
100
10
0
10 pA
5 ms

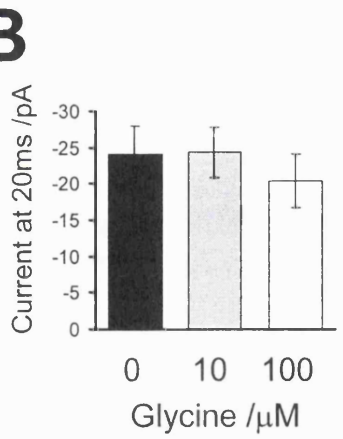
B
Current at 20ms /pA
-30
-25
-20
-15
-10
-5
0
0
10
100
Glycine /μM

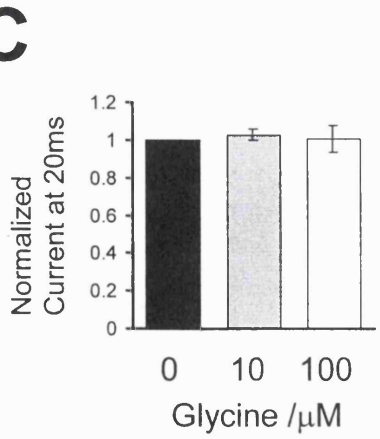
C
Normalized Current at 20ms
1.2
1
0.8
0.6
0.4
0.2
0
0
10
100
Glycine /μM

Figure 7.2: The effect of different glycine concentrations on the peak amplitude and the area of the EPSC

A and C: Bar graphs of (A) the peak amplitude (indicated as arrow head in Figure 7.1A), and (C) the area, of the EPSC as a function of the added glycine concentration. Data are from the same cells described in Figure 7.1 (n=17, n=16 and n=13 for 0, 10 and 100 μM added glycine, respectively).

B and D: Histograms of (B) the peak, and (D) the area, of the EPSCs, normalized in each cell to their values in the absence of added glycine.

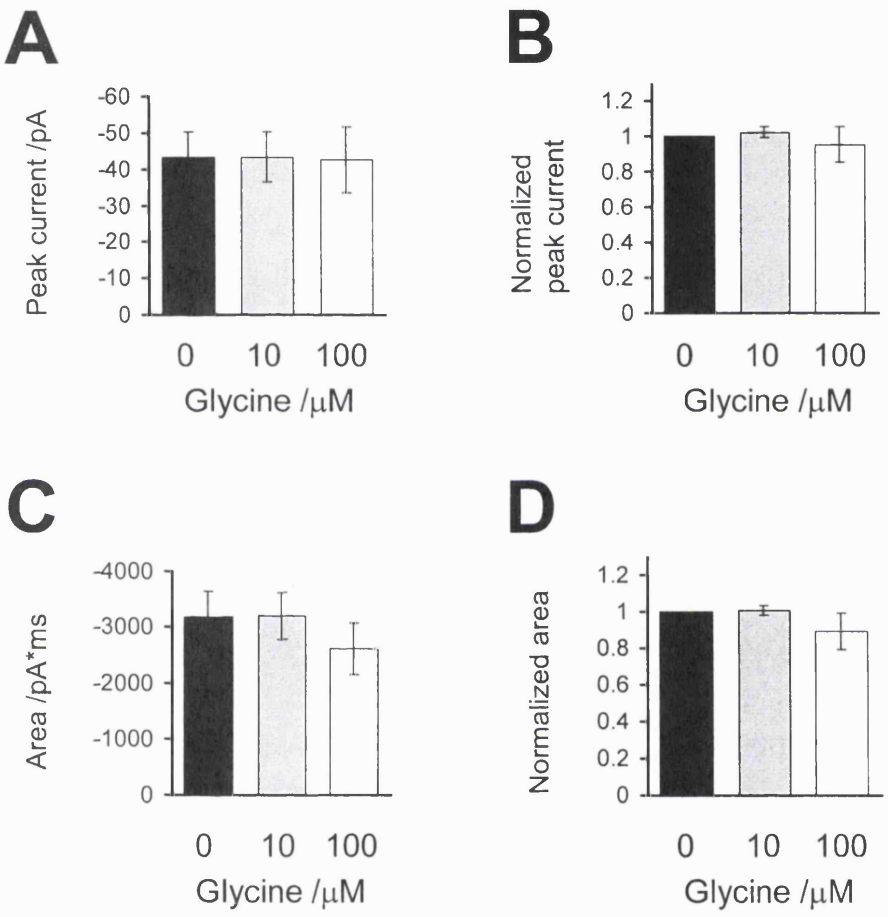
A
Peak current /pA
-60
-50
-40
-30
-20
-10
0
0 10 100
Glycine /μM
B
Normalized peak current
1.2
1
0.8
0.6
0.4
0.2
0
0 10 100
Glycine /μM
C
Area /pA*ms
-4000
-3000
-2000
-1000
0
0 10 100
Glycine /μM
D
Normalized area
1.2
1
0.8
0.6
0.4
0.2
0
0 10 100
Glycine /μM

normalized to their value with no added glycine. P values for paired t-tests comparing the normalized peak amplitude for 10 μM or 100 μM with that for 0 μM glycine were 0.41 (16 cells) and 0.65 (13 cells) respectively. Corresponding p values for the EPSC area were 0.85 and 0.60 respectively.

These data suggest that the glycine site of the NMDA receptor is saturated at room temperature.

7.3 Effect of 7-CK on the MF-gc EPSC

I considered the possibility that glycine did not change the shape of the MF-gc EPSC because the glycine site on the NMDA receptor is not functional. To test this, I applied the competitive glycine site antagonist 7-chloro kynurenic acid (7-CK; 100 μM). This antagonist did inhibit the NMDA component of the EPSC (Figure 7.3A). The average current amplitude at 20 ms after the peak (Figure 7.3B) with no added glycine was –12.5 ± 0.4 pA in the absence of 7-CK (n = 3 cells; 1st black bar), and –0.6 ± 0.1 pA in the presence of 100 μM 7-CK (n = 3 cells; 2nd black bar); in 10 μM superfused glycine it was –18.1 ± 5.6 pA in the absence of 7-CK (n = 4 cells; 1st grey bar), and –3.1 ± 0.9 pA in the presence of 100 μM 7-CK (n = 4 cells; 2nd grey bar); and in 100 μM glycine it was –26.9 pA in the absence of 7-CK (n = 1 cell; 1st white bar), and –12.2 pA in the presence of 100 μM 7-CK (n = 1 cell; 2nd white bar). Note that although the current values in the absence of 7-CK in Figure 7.3B increase with increasing superfused glycine concentration, the current measured at 10 μM glycine does not differ significantly from that seen with 0 μM glycine (p = 0.44) or 100 μM glycine (p = 0.53). The data without 7-CK in Figure 7.3B are included in the larger sample of Figure 7.1B which shows no effect of glycine on the NMDA component of the amplitude.

Figure 7.3C shows the EPSC current 20 ms after the peak at different external glycine concentrations in the presence of 100 μM 7-CK, normalized to the corresponding values in the absence of the inhibitor in each cell. The normalized

Figure 7.3: The NMDA receptor glycine site in cerebellar granule cells is functional

(A) Specimen traces of synaptic currents recorded in a rat cerebellar granule cell (mossy fibre – granule cell synapse) in the presence of 10 μM superfused glycine, in the absence (black) or presence (grey) of 100 μM 7-CK. Arrow head indicates the location of the peak of the control EPSCs. Vertical arrow points to the currents 20 ms after the peak of the EPSCs. Dashed box corresponds to the region of the current which is shown at a faster time-scale below. The experiments were done at room temperature, in magnesium-free external solution at a holding potential of -60mV.

(B) Bar graph of the EPSC amplitude measured 20 ms after the peak, as a function of the external glycine concentration, in the absence (-) or presence (+) of 100 μM 7-CK. Number of cells studied was as follows: in the absence of glycine (black) n = 3 cells; in the presence of 10 μM glycine (grey) n = 4 cells; and in the presence of 100 μM glycine (white) n = 1 cell.

(C) Bar graph of the EPSC amplitude at 20 ms in 7-CK normalized in each cell to its value in the absence of 7-CK.

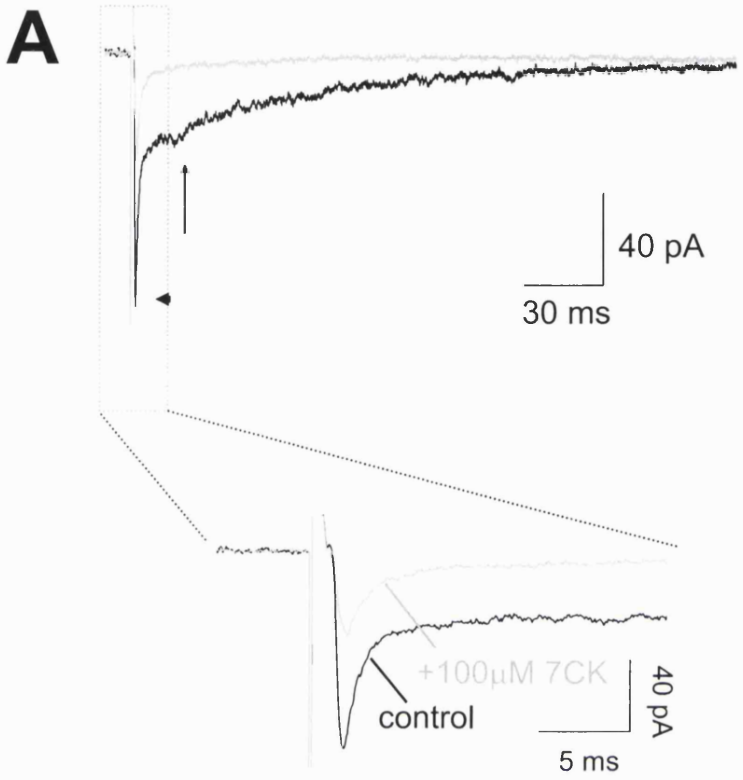
A
40 pA
30 ms
+100μM 7CK
control
40 pA
5 ms

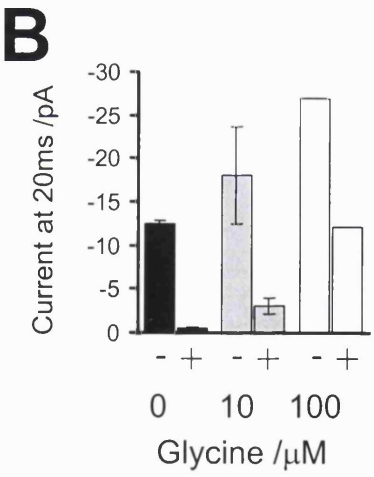
B
Current at 20ms /pA
-30
-25
-20
-15
-10
-5
0
- + - + - +
0 10 100
Glycine /μM

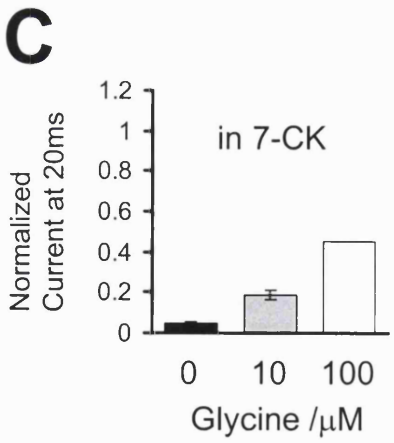
C
Normalized Current at 20ms
1.2
1
0.8
0.6
0.4
0.2
0
in 7-CK
0 10 100
Glycine /μM

Figure 7.4: The effect of 7-CK on the peak and the area of the EPSC

A and C: Bar graphs of (A) the peak amplitude, and (C) the area, of the EPSC as a function of the superfused glycine concentration, in the absence (-) or presence (+) of 100 μM 7-CK. Data are from the same cells as described in Figure 7.3 (n=3, n=4 and n=1 for 0, 10 and 100 μM glycine, respectively).

B and D: Bar graphs of (B) the peak, and (D) the area, of the EPSC in 7-CK, normalized in each cell to their values in the absence of 7-CK.

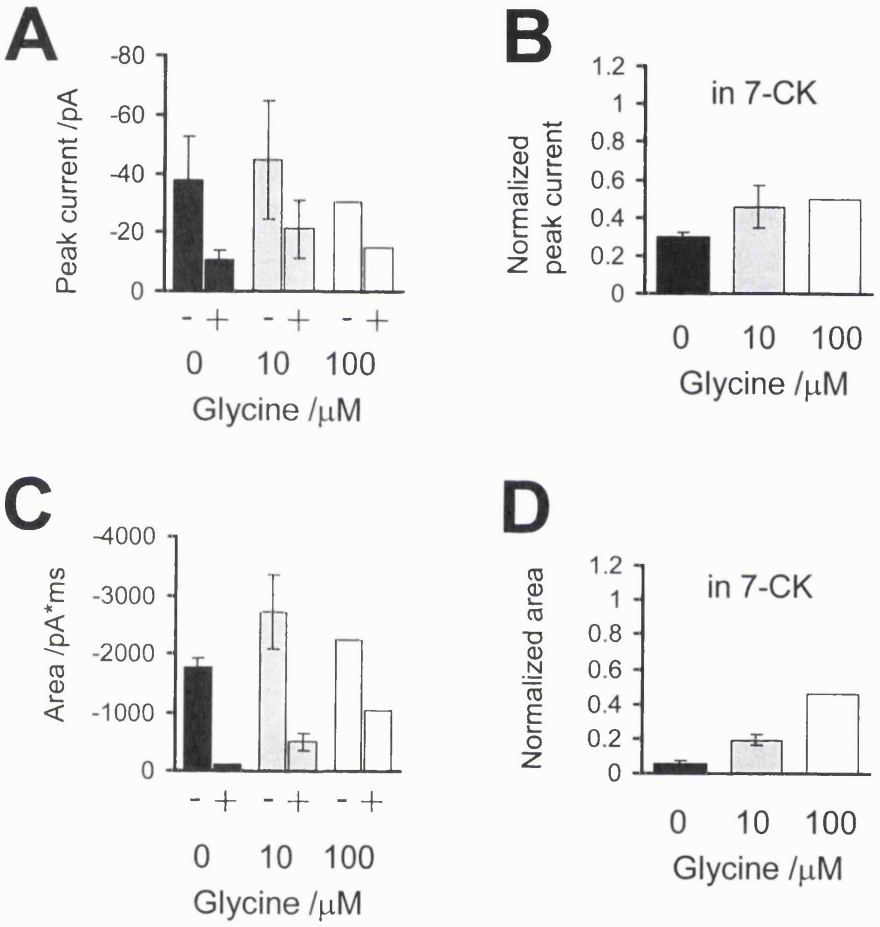
A
Peak current /pA
-80
-60
-40
-20
0
- + - + - +
0 10 100
Glycine /μM
B
Normalized peak current
in 7-CK
1.2
1
0.8
0.6
0.4
0.2
0
0 10 100
Glycine /μM
C
Area /pA*ms
-4000
-3000
-2000
-1000
0
- + - + - +
0 10 100
Glycine /μM
D
Normalized area
in 7-CK
1.2
1
0.8
0.6
0.4
0.2
0
0 10 100
Glycine /μM

current 20 ms after the peak was 0.046 ± 0.009 in the absence of glycine (n = 3 cells; p = 0.0001 compared with no 7-CK present (paired t-test); black bar), 0.186 ± 0.025 in the presence of 10 μM superfused glycine (n = 4 cells; p = 0.0001; grey bar) and 0.451 in the presence of 100 μM glycine (n = 1 cell; white bar). The fraction of the current remaining in 7-CK increases significantly with the superfused glycine concentration. As explained in the discussion, this is expected if 7-CK binds competitively to the glycine site on the NMDA receptor.

The same EPSCs were also analysed for their peak amplitude (largely mediated by AMPA receptors) and the total EPSC area. Figure 7.4 shows the averaged values of the peak (A) and the area (C). The peak amplitude (Figure 7.4A) in the absence of glycine was –37.6 ± 15.1 pA in the absence of 7-CK (n = 3 cells; 1st black bar) and –10.4 ± 3.4 pA in the presence of 100 μM 7-CK (n = 3 cells; 2nd black bar); in 10 μM superfused glycine it was –44.4 ± 20.2 pA in the absence of 7-CK (n = 4; 1st grey bar) and –20.9 ± 9.7 pA in the presence of 7-CK (n = 4; 2nd grey bar); in 100 μM glycine it was –30.0 pA and –14.9 pA, respectively, in the absence and presence of 100 μM 7-CK (n = 1; white bars). Figure 7.4B shows the peak amplitude (at different external glycine concentrations) in the presence of 100 μM 7-CK, normalized to the corresponding value in the absence of 7-CK in each cell. In the absence of glycine the normalized peak amplitude was 0.30 ± 0.03 (i.e. 70% block by 7-CK; n = 3 cells; p = 0.002 when compared to the value in the absence of 7-CK (paired t-test); black bar), in 10 μM glycine it was 0.46 ± 0.12 (n = 4 cells; p = 0.02 compared with no 7-CK; grey bar) and in 100 μM glycine it was 0.50 (n = 1 cell; white bar). Since NMDA receptors take about 9 msec to activate at this synapse (Silver et al., 1992) they should not contribute significantly to the peak of the EPSC, which is generated by AMPA receptors. This implies that 7-CK affects not only the slow (NMDA) but also the fast (AMPA) component of the EPSC. This could be due to a direct effect of 7-CK on the AMPA receptors, as has been described previously (Kemp et al., 1988; Oliver et al., 1990). The reduction of the EPSC peak amplitude

by 7-CK was not further investigated.

The EPSC area was also reduced by 7-CK (Figure 7.4C, D). Since most of the EPSC area is provided by the NMDA component, which 7-CK suppresses as shown in Figure 7.1, it is not surprising that 7-CK also suppresses the total area of the EPSC.

These data indicate that the glycine site at the NMDA receptor at this synapse is functional.

7.4 Effect of exogenous glycine on the MF-gc EPSC recorded at 37^{O}C

To see whether the lack of glycine modulation of the NMDA receptor EPSC described in section 7.1 occurred because of the recording conditions at room temperature, which may slow glycine uptake and thereby raise the extracellular glycine concentration, I repeated the experiments at 37°C. Figure 7.5A shows sample traces of such recordings. As for the recordings done at room temperature the shape of the EPSC was not altered by exogenous glycine. I quantified the effects of glycine on the NMDA component of the EPSC as described in section 7.1. The bar graph in Figure 7.5 B shows the averaged data for such an analysis. The current amplitude at 20 ms after the peak in the absence of glycine was –20.2 ± 4.3 pA (n = 6 cells; black bar) and in the presence of 100 μM glycine it was –20.2 ± 4.8 pA (n = 6; white bar). Figure 7.1C shows the corresponding current amplitudes when normalized to their value in the absence of glycine in each cell. In the presence of 100 μM glycine the normalized amplitude at 20 ms was 0.97 ± 0.14 (n = 6; p = 0.83 (paired t-test); white bar). This indicates that the NMDA receptor component of the EPSC is not altered when glycine was added to the bath solution, even when recorded at 37^{O}C.

The same EPSCs were also analysed for their peak amplitude and the total area, which similarly showed no significant change, whether analysed as simple averaged values of the peak (Figure 7.6A) and the area (Figure 7.6C), or as values

Figure 7.5: The NMDA receptor glycine site in cerebellar granule cells appears to be saturated, even when recorded at 37^{O}C

(A) Specimen traces of synaptic currents recorded in a rat cerebellar granule cell (mossy fibre – granule cell synapse) in the presence of different exogenously applied glycine concentrations (0, 10 or 100 μM glycine). Arrow head indicates the location of the peak of the EPSCs. Vertical arrow points to the currents 20 ms after the peak of the EPSCs, at which time the current amplitude was used to estimate its NMDA component. Dashed box corresponds to the region of the current which is shown on a faster time-scale below. The experiments were done at 37^{O}C, in magnesium-free external solution at a holding potential of –60mV.

(B) Bar graph of the EPSC amplitude measured 20 ms after the peak, in the absence (black) or presence of 100 μM glycine (white) (n = 6 cells).

(C) Bar graph of the EPSC amplitude at 20ms, normalized in each cell to its value in the absence of glycine.

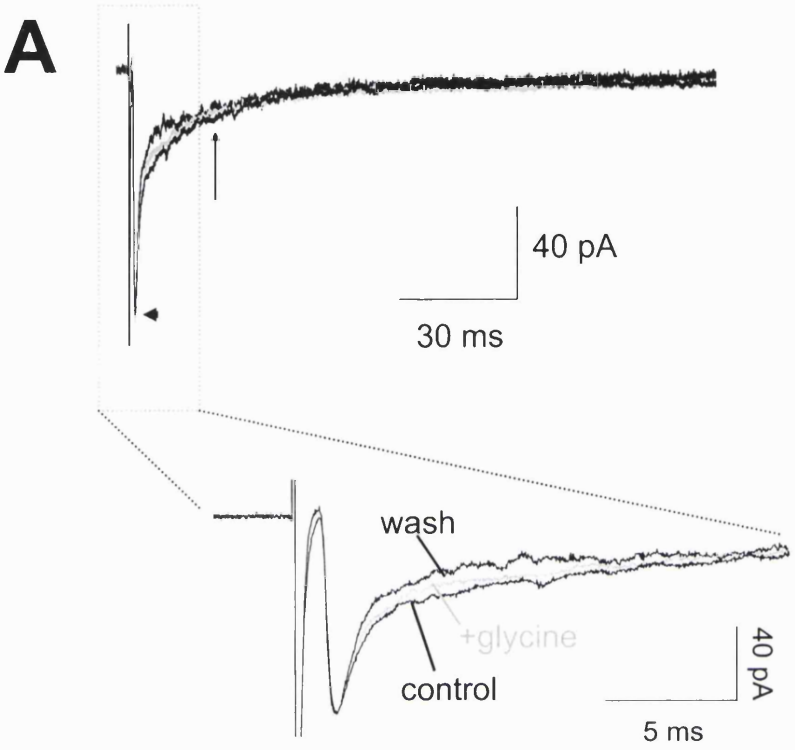
A
40 pA
30 ms
wash
+glycine
control
40 pA
5 ms

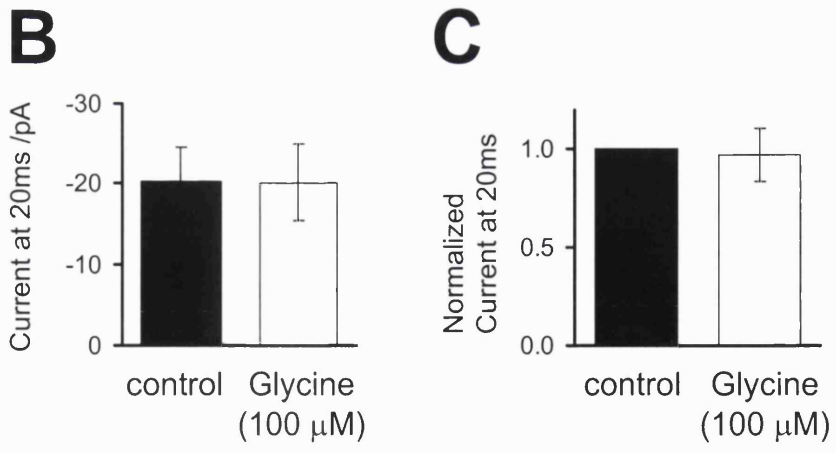
B
Current at 20ms /pA
-30
-20
-10
0
control
Glycine
(100 μM)
C
Normalized
Current at 20ms
1.0
0.5
0.0
control
Glycine
(100 μM)

Figure 7.6: The effect of different glycine concentrations on the peak and the area of the EPSC at 37^{O}C

A and C: Bar graphs of (A) the peak amplitude (indicated by the arrow head in Figure 7.5A), and (C) the area, of the EPSC in 0 (black) or 100 μM (white) external glycine. Data are from the same cells as described in Figure 7.5 (n = 6).

B and D: Bar graph of (B) the peak, and (D) the area, of the EPSC normalized in each cell to its value in the absence of glycine.

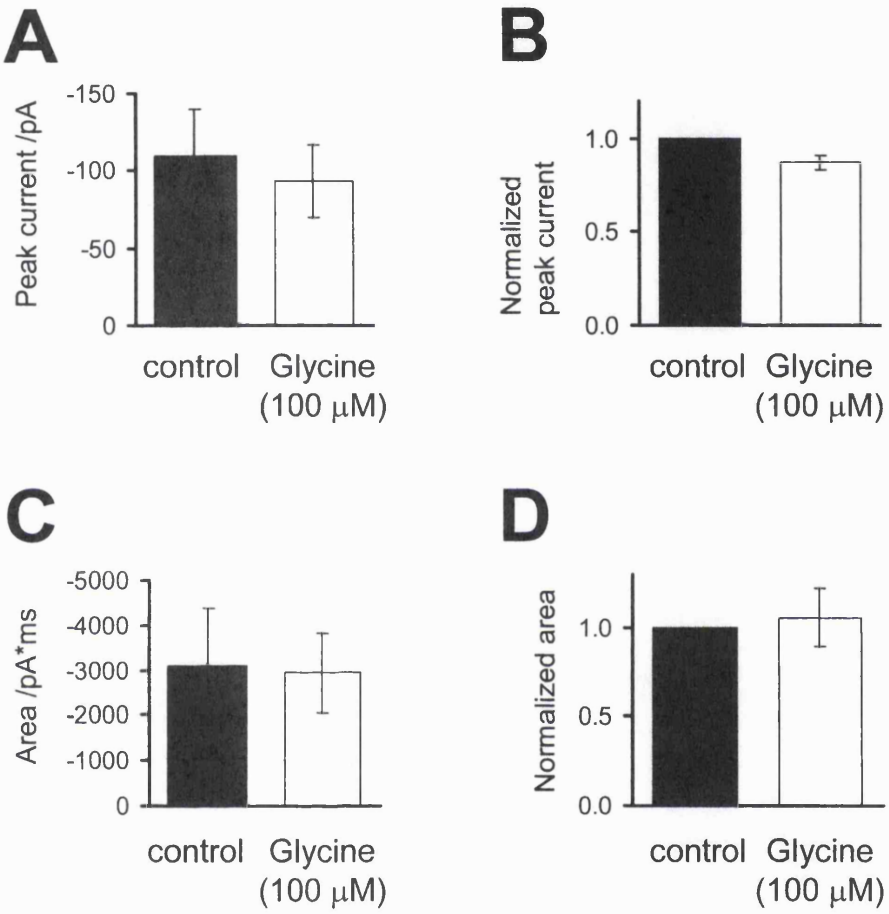
A
Peak current /pA
-150
-100
-50
0
control
Glycine
(100 μM)
B
Normalized
peak current
1.0
0.5
0.0
control
Glycine
(100 μM)
C
Area /pA*ms
-5000
-4000
-3000
-2000
-1000
0
control
Glycine
(100 μM)
D
Normalized area
1.0
0.5
0.0
control
Glycine
(100 μM)

normalized to the values in absence of glycine (Figure 7.6B and 7.6D). P values for paired t-tests comparing the EPSC peak amplitude and area in 100 μM glycine with their values in 0 μM glycine (in 6 cells) were 0.1 and 0.74 respectively.

These data indicate that bath applied glycine does not alter the shape of the EPSC at this synapse even when recorded at 37^{O}C and suggest that the glycine site of the NMDA receptor is saturated even at normal body temperature.

7.5 Effect of exogenous D-serine on the MF-gc EPSC recorded at 37°C

To see whether another agonist at the NMDA receptor glycine site that is not taken up by glycine transporters, i.e. D-serine, could modulate the EPSC at this synapse, I recorded mossy fibre – granule cell EPSCs in the absence and presence of 100 μM D-serine, at 37°C. Figure 7.7A shows specimen traces of such recordings. As for glycine the shape of the EPSC was not altered by exogenous D-serine. I quantified the effects of D-serine on the NMDA component of the EPSC as described in section 7.1. The current amplitude at 20 ms after the peak in the absence of D-serine was –30.8 ± 10.0 pA (n = 2 cells; black bar) and in the presence of 100 μM D-serine it was –29.9 ± 6.2 pA (n = 2; white bar). In the presence of 100 μM D-serine the normalized amplitude at 20 ms was 1.01 ± 0.13 (n = 2; white bar; p = 0.94 compared with 0 μM D-serine). This indicates that the NMDA receptor component of the EPSC was not modulated when D-serine was added to the bath solution.

The same EPSCs were also analysed for their peak and the total area, which similarly showed no significant change when D-serine was added (Figure 7.8). P values for paired t-tests comparing the amplitude and area of the EPSC in 100 μM and 0 μM D-serine were 0.1 and 0.16 respectively.

These data indicate that bath applied D-serine does not alter the shape of the EPSC at this synapse when recorded at 37^{O}C and suggests that the glycine site of the NMDA receptor is saturated even at normal body temperature.

Figure 7.7: Exogenous D-serine does not affect the MF-gc EPSC at 37^{O}C

(A) Specimen traces of synaptic currents recorded in a rat cerebellar granule cell (mossy fibre – granule cell synapse) in the absence (black trace) or presence (grey trace) of 100 μM D-serine. Arrow head indicates the location of the peak of the EPSCs. Vertical arrow points to the currents 20 ms after the peak of the EPSCs, at which time the current amplitude was used to estimate its NMDA component. Dashed box corresponds to the region of the current which is shown on a faster time-scale below. The experiments were done at 37^{O}C, in magnesium-free external solution at a holding potential of –60mV.

(B) Bar graph of the EPSC amplitude measured 20 ms after the peak, in the absence (black) or presence (white) of 100 μM D-serine (n = 2 cells).

(C) Bar graph of the EPSC amplitude at 20ms, normalized in each cell to its value in the absence of D-serine.

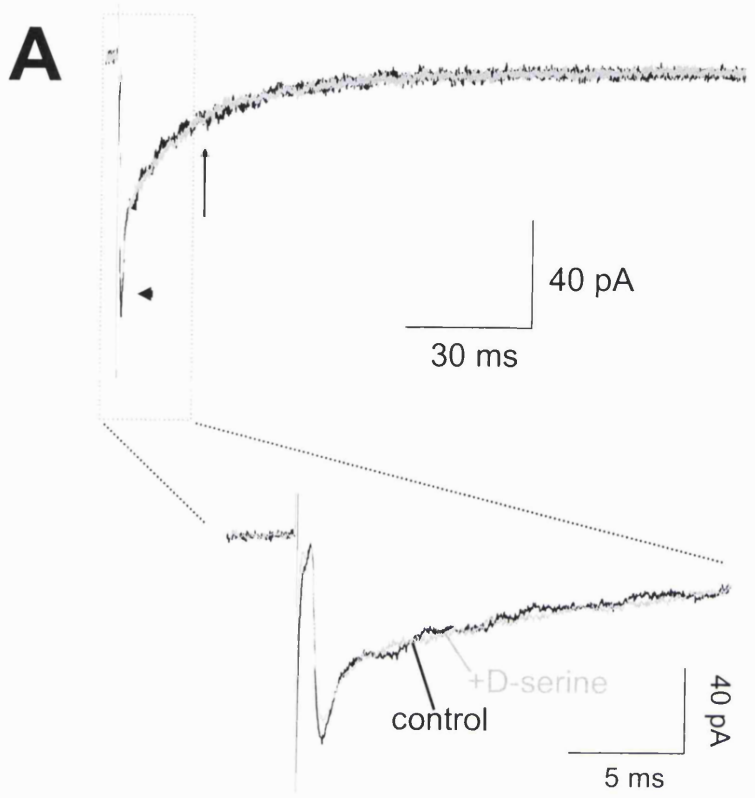
A
40 pA
30 ms
+D-serine
control
40 pA
5 ms

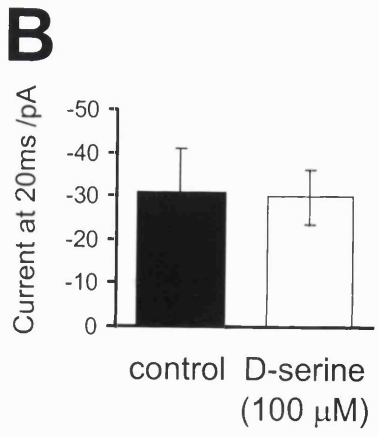
B
Current at 20ms /pA
-50
-40
-30
-20
-10
0
control
D-serine
(100 μM)

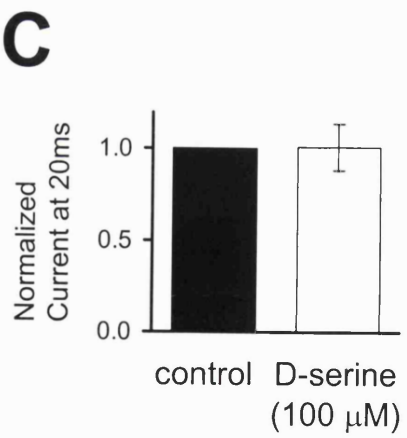
C
Normalized
Current at 20ms
1.0
0.5
0.0
control
D-serine
(100 μM)

Figure 7.8: The effect of D-serine on the peak and the area of the EPSC at 37^{o}C

A and C: Bar graphs of (A) the peak amplitude (indicated as arrow head in Figure 7.7A), and (C) the area, of the EPSC in 0 (black) or 100 μM (white) added D-serine. Data are from the same cells as described in Figure 7.7 (n = 2).

B and D: Bar graph of (B) the peak amplitude, and (D) the area, of the EPSC normalized in each cell to its value in the absence of D-serine.

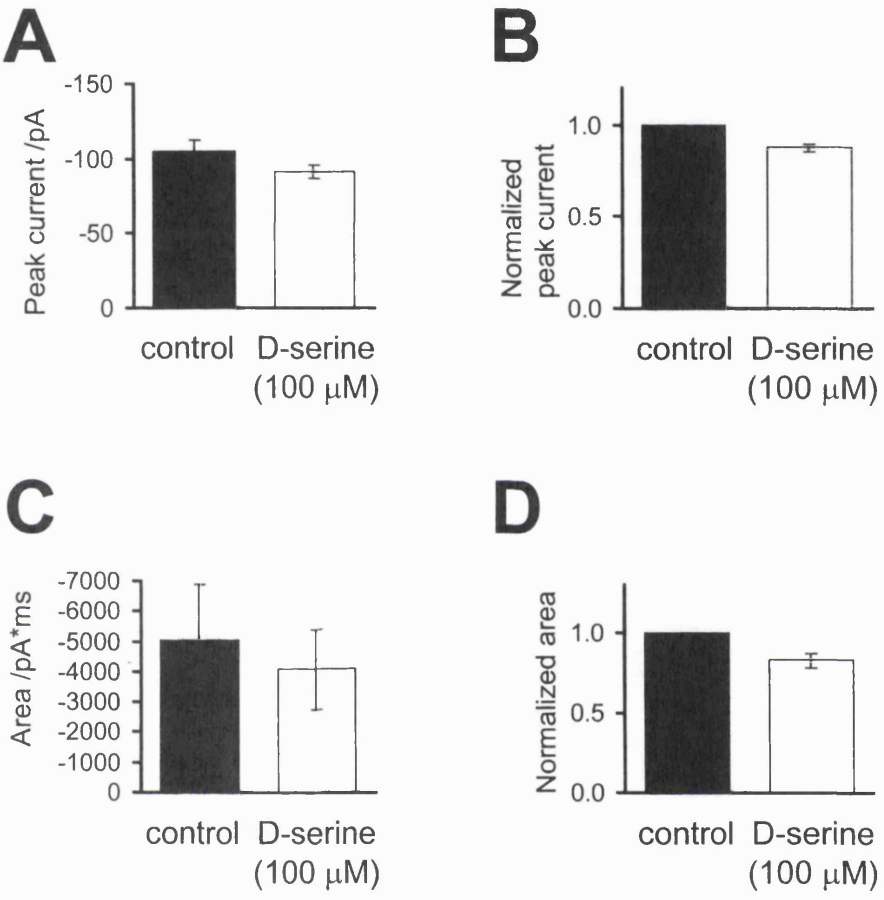
A
-150
-100
-50
0
Peak current /pA
control
D-serine
(100 μM)
B
1.0
0.5
0.0
Normalized
peak current
control
D-serine
(100 μM)
C
-7000
-6000
-5000
-4000
-3000
-2000
-1000
0
Area /pA*ms
control
D-serine
(100 μM)
D
1.0
0.5
0.0
Normalized area
control
D-serine
(100 μM)

7.6 Discussion

To see whether the glycine site of the NMDA receptor at the mossy-fibre – granule cell synapse is saturated, I recorded EPSCs in the absence or presence of bath applied glycine or D-serine. Neither glycine nor D-serine affected the shape of the EPSC, suggesting that this site is saturated both at room temperature and at 37 ^{o}C. A glycine site inhibitor, 7-chloro-kynurenic acid, did block the NMDA component though, suggesting that the glycine site at these receptors is functional. It is possible that the high concentration of 7-CK (100 μM) used for competing with glycine could act partly by inhibiting the glutamate binding site of the NMDA receptor (Kemp et al., 1988), but the relief of block by high glycine concentrations shows that it is acting (competitively) via the glycine binding site of the NMDA receptor.

From the effect of 7-CK on the NMDA receptor current, one can estimate the resting glycine concentration in the slice, $[gly]_o$. I will do this first crudely using the Hill equation, and then using a more rigorous model. If the dependence of the NMDA receptor current on glycine is described by a Hill equation:

$$I_{control} = \frac{I_{max} \cdot [gly]_o^{\,n}}{[gly]_o^{\,n} + EC_{50}^{\,n}} \qquad (7.1)$$

where I is the measured current, I_{max} is the maximal evoked current, n is the Hill coefficient, EC_{50} is the glycine concentration which produces a half maximal current, then in the presence of the competitive blocker 7-CK, if [7CK] is the concentration of 7-CK used and K_{7CK} is the dissociation constant for 7-CK:

$$I_{7CK} = \frac{I_{max} \cdot [gly]_o^{\,n}}{[gly]_o^{\,n} + EC_{50}^{\,n} \cdot \left(1 + \frac{[7CK]}{K_{7CK}}\right)^n} \qquad (7.2)$$

The ratio of current in the presence and absence of 7-CK is therefore:

$$\frac{I_{7CK}}{I_{control}} = \frac{[gly]_o^{\,n} + EC_{50}^{\,n}}{[gly]_o^{\,n} + EC_{50}^{\,n} \cdot \left(1 + \frac{[7CK]}{K_{7CK}}\right)^n} \qquad (7.3)$$

and solving for $[gly]_o$ gives:

$$[gly]_o = \sqrt[n]{\frac{EC_{50}^{\,n} \cdot \left(1 - \frac{I_{7CK}}{I_{control}} \cdot \left(1 + \frac{[7CK]}{K_{7CK}}\right)^n\right)}{\left(\frac{I_{7CK}}{I_{control}} - 1\right)}} \qquad (7.4)$$

If the Hill coefficient is n = 1.5 and EC_{50} = 170 nM (Woodward et al., 1995b), K_{7CK} is 0.14 μM (Benveniste and Mayer, 1991) and the concentration of 7-CK is 100 μM (as used in my experiments), the data for no added glycine in Figure 7.3C (i.e. $\frac{I_{7CK}}{I_{control}} = 0.046$) suggest a resting glycine concentration in the slice above 16 μM.

For a more accurate estimate of the resting glycine concentration under these recording conditions, I used the two binding site model proposed by Benveniste & Mayer (1991), in which two glycine molecules must bind to the receptor in order for gating to occur:

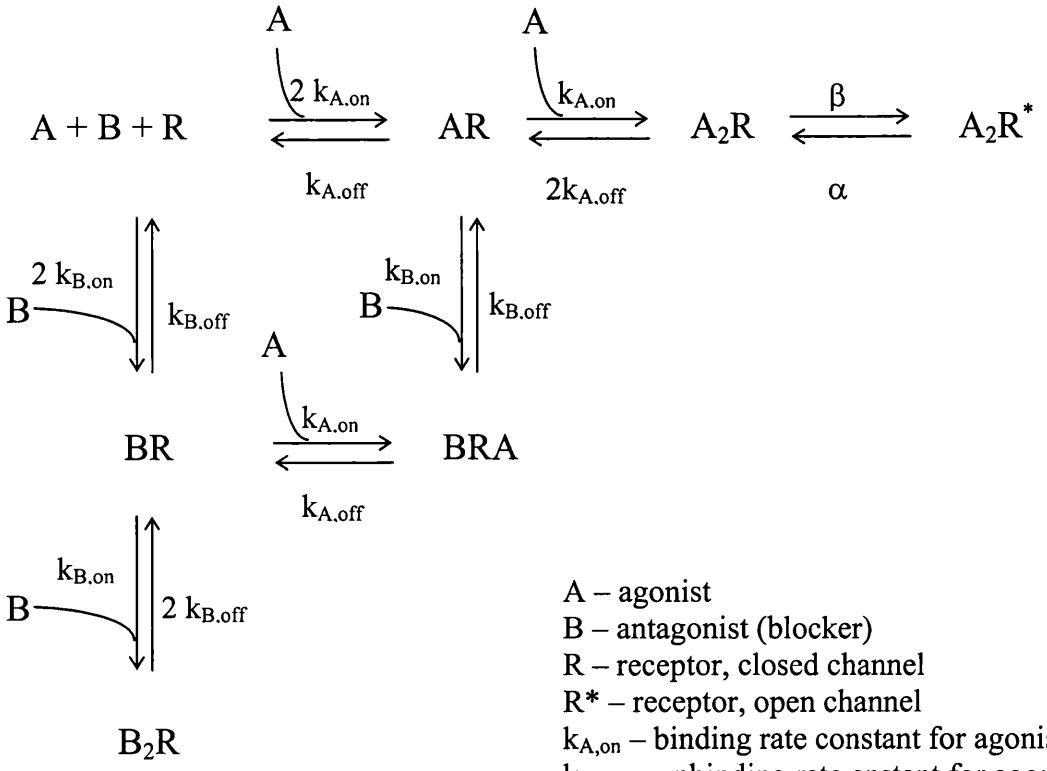

A – agonist
B – antagonist (blocker)
R – receptor, closed channel
R* – receptor, open channel
$k_{A,on}$ – binding rate constant for agonist
$k_{A,off}$ – unbinding rate cnstant for agonist
$k_{B,on}$ – binding rate constant for blocker
$k_{B,off}$ – unbinding rate cnstant for blocker
α – closing rate constant
β – opening rate constant

Benveniste & Mayer (1991) determined the rate constants for such a kinetic scheme from their experimental data on cultured hippocampal neurones of mice, which I will use for the calculations below. The fraction of receptors in each state will be abbreviated as:

A_2R^* – **x** (fraction of receptors in state A_2R^* – channel open)

A_2R – **y** (fraction of receptors in state A_2R – channel closed)

AR – **z** (fraction of receptors in state AR)

BRA – **w** (fraction of receptors in state BRA)

BR – **v** (fraction of receptors in state BR)

B_2R – **u** (fraction of receptors in state B_2R)

R – **1-x-y-z-u-v-w** (fraction of receptors in state R – no glycine bound)

In equilibrium:

(a) $\beta \cdot y = \alpha \cdot x$

(b) $k_{A,on} \cdot A \cdot z = 2 \cdot k_{A,off} \cdot y$

(c) $k_{B,off} \cdot w = k_{B,on} \cdot B \cdot z$

(d) $k_{A,on} \cdot A \cdot v = k_{A,off} \cdot w$

(e) $2 \cdot k_{B,off} \cdot u = k_{B,on} \cdot B \cdot v$

(f) $2 \cdot k_{B,on} \cdot B \cdot (1 - x - y - z - u - v - w) = k_{B,off} \cdot v$

with $\frac{k_{A,off}}{k_{A,on}} = K_A$ and $\frac{k_{B,off}}{k_{B,on}} = K_B$

and with (a), (b), (c), (d) and (e) put into (f), and solving for x:

$$x = \frac{\frac{\beta}{\alpha}}{\frac{\beta}{\alpha} + \left(1 + \frac{K_A}{A}\right)^2 + 2 \cdot \frac{K_A}{A} \cdot \frac{B}{K_B} \cdot \left(1 + \frac{1}{2} \cdot \frac{K_A}{A} \cdot \left(2 + \frac{B}{K_B}\right)\right)} \tag{7.5}$$

The glycine site is saturated in the absence of 7-CK, even with no added glycine, so in the absence of 7-CK x has its maximum value:

$$x_{max} = \frac{\frac{\beta}{\alpha}}{\frac{\beta}{\alpha} + 1} \tag{7.6}$$

Thus, the ratio of currents seen in the presence and absence of 7-CK is:

$$\frac{I_{7CK}}{I_{control}} = \frac{\frac{\beta}{\alpha} + 1}{\frac{\beta}{\alpha} + \left(1 + \frac{K_A}{A}\right)^2 + 2 \cdot \frac{K_A}{A} \cdot \frac{B}{K_B} \cdot \left(1 + \frac{1}{2} \cdot \frac{K_A}{A} \cdot \left(2 + \frac{B}{K_B}\right)\right)} \tag{7.7}$$

solving (7.7) for K_A/A gives:

$$\frac{K_A}{A} = \frac{-1+\sqrt{\frac{\beta}{\alpha}\cdot\left(\frac{I_{control}}{I_{7CK}}-1\right)+\frac{I_{control}}{I_{7CK}}}}{\left(1+\frac{B}{K_B}\right)} \tag{7.8}$$

so:

$$A = \frac{K_A\cdot\left(1+\frac{B}{K_B}\right)}{-1+\sqrt{\frac{\beta}{\alpha}\cdot\left(\frac{I_{control}}{I_{7CK}}-1\right)+\frac{I_{control}}{I_{7CK}}}} \tag{7.9}$$

Using $K_{glycine} = K_A = 0.073$ μM (Woodward et al., 1995b), $K_{7CK} = K_B = 0.14$ μM (Benveniste and Mayer, 1991), B = [7CK] = 100 μM as the 7-CK concentration used and $I_{7CK}/I_{control} = 0.046$ (from Figure 7.3C with no added glycine), this implies that in the absence of added glycine the glycine concentration present is $A = [gly]_o = 14.3$, 9.5, 7.5 or 6.4 μM for $\frac{\beta}{\alpha} = 0, 1, 2 \text{ or } 3$ respectively, corresponding to maximum channel open probability ($p_{open} = \frac{\beta}{\alpha+\beta}$ (see equation 7.6)) of 0, 0.5, 0.67 or 0.75 (different combinations of NMDA subunits are reported to produce maximum open probabilities between 0.04 and 0.36 (Wyllie et al., 1998; Chen et al., 1999)). Using these values of the residual glycine, which is assumed to be present in the absence of added glycine and is assumed to add to the glycine concentration in the superfusate, I plotted equation 7.7 through the data in Figure 7.3C, which shows the fraction of NMDA current remaining in 7-CK when 0, 10 and 100 μM glycine are added to the perfusion solution. Figure 7.9 shows the predicted fraction of current in 7-CK for different concentrations of added glycine, with $\frac{\beta}{\alpha} = 0, 1, 2 \text{ or } 3$. A reasonable fit (bearing in mind that only one cell was studied for the 100 μM glycine point) is

Figure 7.9: Estimating the residual glycine concentration in the slice

Filled circles show the measured currents in 7-CK relative to control (mean of the data shown in Figure 7.3C) when 0, 10 or 100 μM glycine were added to the perfusion medium. The lines show the predicted fractional currents in 7-CK for different values of β/α in equation 7.9:

$$\frac{I_{7CK}}{I_{control}} = \frac{1+\frac{\beta}{\alpha}}{\frac{\beta}{\alpha}+\left(1+\frac{K_A}{A}\right)^2+2\cdot\frac{K_A}{A}\cdot\frac{B}{K_B}\cdot\left(1+\frac{1}{2}\cdot\frac{K_A}{A}\cdot\left(2+\frac{B}{K_B}\right)\right)}$$

with $A = [gly]_{added} + [gly]_{residual}$

$K_A = K_{gly} = 0.073$

$K_B = K_{7CK} = 0.14$

$B = [7CK] = 100\ \mu M$

and $\beta/\alpha = 0$, 1, 2 or 3 with

$[gly]_{residual} = 14.3$, 9.5, 7.5 or 6.4 μM respectively

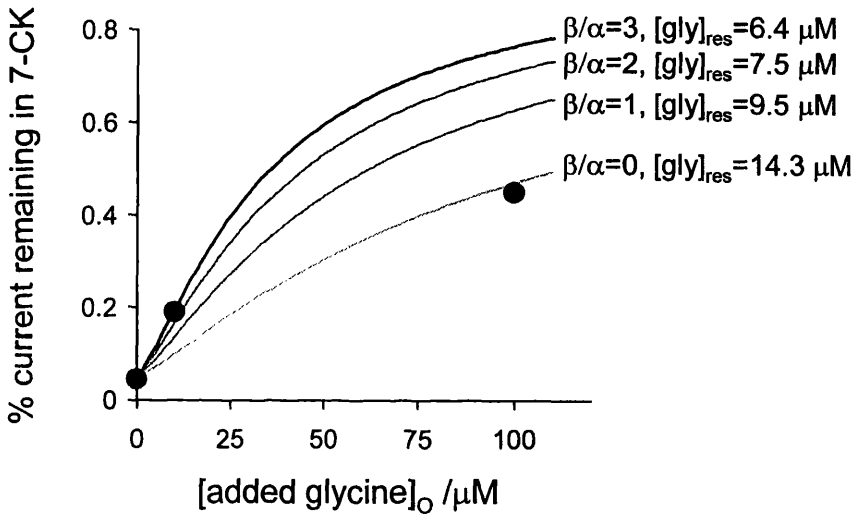
% current remaining in 7-CK
0.8
0.6
0.4
0.2
0
0
25
50
75
100
[added glycine]$_o$ /μM
β/α=3, [gly]$_{res}$=6.4 μM
β/α=2, [gly]$_{res}$=7.5 μM
β/α=1, [gly]$_{res}$=9.5 μM
β/α=0, [gly]$_{res}$=14.3 μM

obtained with $\frac{\beta}{\alpha}=1$, implying a glycine concentration in the slice of 9.5 μM even in the absence of added glycine – a value which would indeed, as seen in my experiments, saturate the glycine site at the NMDA receptor.

The question arises as to whether the glycine site is also saturated *in vivo*, or whether my experimental conditions resulted in a saturation. To assess this, one needs to know the normal source of extracellular glycine (or D-serine), and several scenarios come to mind.

(1) It might indeed be that the resting level of extracellular glycine (or D-serine) maintained by transporters (Attwell et al., 1993) is high enough to tonically saturate the NMDA receptor glycine site at this synapse.

(2) Glycine or D-serine might be released from nearby neurones and spill-over to activate the NMDA receptor at the neighbouring excitatory synapse. These neurones (possibly Golgi cells) could be spontaneously active or might be stimulated to release glycine/D-serine each time I stimulate the mossy fibre electrically, masking a further modulation by exogenous glycine/D-serine.

(3) Similarly, my electrical stimulation might activate release of glycine or D-serine from nearby glial cells. During neuronal activity the extracellular potassium concentration may rise and depolarize glial cells, leading to glycine transporters reversing (GLYT-1 being particularly prone to this: see section 1.5 and section 7.1) and pumping glycine out of the cells. The extracellular glycine concentration might then rise to levels high enough to saturate the NMDA receptor glycine site. If electrical stimulation results in this happening, it could mask a modulation by exogenously applied glycine/D-serine.

(4) The glycine site at the NMDA receptor might be saturated by endogenous release mechanism at the age of animal used, even if they are not saturated at older ages. The granule cells I recorded from in this project at P14 had migrated to their final destination and formed functional synapses. However, at this time the cerebellar glomeruli are not fully formed. The D-serine concentration in this region is at a peak

at P14, and it has been suggested that D-serine promotes cell migration and synapse formation in these cells (Schell et al., 1997). If D-serine is released at nearby forming synapses, it might spillover to formed synapses and result in the NMDA receptor glycine site on the recorded cell being saturated at this age.

Whatever the cause, however, these experiments show that when there is mossy fibre activation, the glycine or D-serine concentration is sufficiently high to evoke a maximal NMDA component of the EPSC at the mossy-fibre to granule cell synapse.

CHAPTER 8

Conclusion

In this thesis I report experiments investigating the modulation of synaptic transmission by intracellular proteins and transporters. The projects can broadly be divided into modulation of GABAergic (Chapters 3 and 4) and modulation of glutamatergic (Chapters 5, 6 and 7) synaptic transmission. In Chapters 3, 4 and 5, I took an indirect approach to studying modulation of synaptic transmission, by investigating the modulation of neurotransmitter transporter and receptor properties and intracellular chloride homeostasis, whereas in Chapters 6 and 7 I took the direct approach of recording synaptic currents in cells of cerebellar slices. A detailed discussion of the results and their physiological relevance is given at the end of each chapter. In this final chapter I will briefly summarize the aim and the main findings of each project and give some suggestions for future work.

8.1 Chapter 3

The aim of this project was to find out whether the microtubule-associated-protein MAP-1B, which has been shown to interact and co-localize with $GABA_C$ receptors (Hanley et al., 1999), influences $GABA_C$ receptor properties. The approach taken was to whole-cell patch-clamp retinal bipolar cells, which possess those proteins endogenously, and competitively disrupt the MAP-1B – $GABA_C$ receptor interaction by including a peptide (matching the MAP-1B binding site sequence of the $GABA_C$ receptor ρ1 subunit) in the patch pipette, while recording GABA dose-response curves. Non-specific effects of the peptide were checked by control experiments done with a scrambled peptide in the pipette.

Disrupting the MAP-1B – $GABA_C$ receptor interaction increased the GABA sensitivity of the receptor (the EC_{50} was decreased), with no change in the number of

functional receptors in the membrane (I_{max} remained the same). A change in agonist sensitivity produced by modulation of the MAP-1B – $GABA_C$ receptor interaction could profoundly influence the time course of synaptic transmission mediated by these receptors and alter retinal information processing, as discussed in section 3.17.

To advance our understanding of the physiological role of this interaction further, one could investigate (1) how disrupting the MAP-1B – $GABA_C$ receptor interaction in bipolar cells affects the amacrine cell – bipolar cell IPSC, (2) whether disrupting the interaction declusters $GABA_C$ receptors, allows them to leave the synaptic area and changes the ratio of $GABA_A$ and $GABA_C$ receptor mediated currents at the bipolar cell axon terminal, and (3) whether and how this interaction modulates the output of photoreceptor axon terminals, where $GABA_C$ receptors and MAP-1B have also been shown to co-localize (Pattnaik et al., 2000).

8.2 Chapter 4

The purpose of this project was to explore how the GABA response polarity is controlled by transporters mediating chloride homeostasis, and to explore the possibility of a chloride concentration gradient existing in the cytoplasm of retinal bipolar cells, as suggested by the different distribution of the two chloride transporters KCC-2 and NKCC-1 (Vardi et al., 2000a). To investigate this, I gramicidin perforated-patch-clamped bipolar cells in retinal slices, recorded the reversal potential of the GABA evoked current at the outer and the inner plexiform layers and used this information to calculate the chloride concentrations at the two ends.

Despite the distinct chloride transporter localization in the bipolar cell, the reversal potential of the GABA evoked (chloride mediated) current was only slightly more positive in the dendrites than in the axon terminal. Chloride transporters, the membrane potential and the external potassium concentration all appeared to actively regulate the internal chloride concentration and thus GABA response polarity in

these cells. These results have important implications for our understanding of lateral inhibition and response transience generation in the outer retina, as discussed in section 4.9.

It would be interesting to (1) investigate the relative importance of the two different chloride transporters (KCC-2 and NKCC-1) in regulating the internal chloride concentration, for example by using bumetanide which at low doses selectively blocks NKCC-1, and (2) examine the GABA response polarity and internal chloride regulation when bicarbonate is present.

8.3 Chapter 5

The aim was to see whether Ajuba, a protein that has been shown to interact and co-localize with the glutamate transporter GLT-1, affects the properties of the transporter. I used COS cells (a mammalian cell line) expressing either GLT-1, or GLT-1 and Ajuba, for patch-clamp experiments, to see whether co-expression of Ajuba altered some of the transporters properties.

Ajuba did not alter the EC_{50} for glutamate (in whole cell or perforated patch mode), the maximum uptake rate of the carrier (although the errors on these measurements are large), or the anion channel behaviour of the transporter. It seems therefore that Ajuba does not regulate the transporter properties, and the purpose of the Ajuba – GLT-1 interaction might lie in transporter localization, mediation of intracellular signalling, or in controlling Ajuba function.

To further investigate the role of the Ajuba – GLT-1 interaction in cells, one could (1) record GLT-1 mediated synaptic transporter currents in astrocytes in the presence of a binding site peptide to see whether disrupting the GLT-1 – Ajuba interaction alters the transporter current, e.g. by allowing GLT-1 to move further from the synapse and (2) investigate whether external glutamate application results in Ajuba unbinding from the transporter and activating intracellular signalling pathways. It would also be useful to study the recently developed Ajuba knock-out

mouse.

8.4 Chapter 6

The purpose of this project was to find out whether the glial glutamate transporters GLT-1 and GLAST contribute to shaping synaptic transmission at two cerebellar synapses. I investigate this by patch-clamping cells in cerebellar slices of the different mice and comparing the synaptic properties of the knock-out and wild-type mice.

The EPSC kinetics at the mossy-fibre granule cell synapse (evoked by single or repetitive stimulation, at room temperature and 37°C) did not differ in the GLT-1 and GLAST knock-out vs. wild type mice. The EPSC decay at the parallel fibre to Purkinje cell synapse (evoked by single stimulation, at room temperature) was slightly slower in the GLAST knock-out mice. The EPSC at the parallel fibre to Purkinje cell synapse (evoked by repetitive stimulation, at room temperature) also seemed to show a slow (mGluR) mediated current in the GLAST knock-out mice (but more cells are needed to confirm this).

To continue on this project, one could (1) investigate further the appearance of the slow (mGluR) current after repetitive stimulation, (2) see whether presynaptic NMDA receptor activation on the parallel fibre terminals is altered in the GLAST wild-type vs. knock-out mice, (3) examine whether the Purkinje cell firing in response to parallel fibre stimulation (input-output relation) is different in the mice lacking GLAST and (4) explore whether EAAC-1 is indeed the glutamate transporter important for shaping the mossy-fibre to granule cell EPSC, as suggested in section 6.5.

8.5 Chapter 7

The aim of these experiments was to investigate whether glycine or D-serine

modulates synaptic transmission at the mossy-fibre granule cell synapse in the cerebellum. To see whether the glycine site on the NMDA receptor is already saturated, I bath applied glycine or D-serine and recorded the mossy fibre – granule cell EPSC.

Neither glycine nor D-serine altered the EPSC duration or amplitude (at –60 mV, in magnesium free solution, at 37°C), suggesting that this site is saturated under these recording conditions. A glycine site inhibitor (7-CK) did block the currents though, suggesting that the glycine sites on the receptors are fully functional, and from the data recorded in 7-CK the extracellular glycine concentration was estimated to be about 10 μM.

To advance this project one could (1) examine whether the glycine site is only saturated as a result of glycine being released from Golgi cells activated by electrical stimulation (e.g. by measuring responses to superfused NMDA or glutamate released spontaneously (mEPSCs), instead of electrical stimulation), and (2) study whether blocking serine racemase, the synthesising enzyme for D-serine, affects the EPSC.

References

Abe K, Saito H (2001) Possible linkage between glutamate transporter and mitogen-activated protein kinase cascade in cultured rat cortical astrocytes. J Neurochem 76:217-223.

Akaike N (1996) Gramicidin perforated patch recording and intracellular chloride activity in excitable cells. Prog Biophys Mol Biol 65:251-264.

Akazawa C, Shigemoto R, Bessho Y, Nakanishi S, Mizuno N (1994) Differential expression of five N-methyl-D-aspartate receptor subunit mRNAs in the cerebellum of developing and adult rats. J Comp Neurol 347:150-160.

Altman J (1972a) Postnatal development of the cerebellar cortex in the rat. I. The external germinal layer and the transitional molecular layer. J Comp Neurol 145:353-397.

Altman J (1972b) Postnatal development of the cerebellar cortex in the rat. 3. Maturation of the components of the granular layer. J Comp Neurol 145:465-513.

Amato A, Barbour B, Szatkowski M, Attwell D (1994) Counter-transport of potassium by the glutamate uptake carrier in glial cells isolated from the tiger salamander retina. J Physiol (Lond) 479:371-380.

Anson LC, Chen PE, Wyllie DJ, Colquhoun D, Schoepfer R (1998) Identification of amino acid residues of the NR2A subunit that control glutamate potency in recombinant NR1/NR2A NMDA receptors. J Neurosci 18:581-589.

Araki K, Meguro H, Kushiya E, Takayama C, Inoue Y, Mishina M (1993) Selective expression of the glutamate receptor channel delta 2 subunit in cerebellar Purkinje cells. Biochem Biophys Res Commun 197:1267-1276.

Armano S, Rossi P, Taglietti V, D'Angelo E (2000) Long-term potentiation of intrinsic excitability at the mossy fiber- granule cell synapse of rat cerebellum. J Neurosci 20:5208-5216.

Arnold DB, Clapham DE (1999) Molecular determinants for subcellular localization of PSD-95 with an interacting K^+ channel. Neuron 23:149-157.

Arriza JL, Eliasof S, Kavanaugh MP, Amara SG (1997) Excitatory amino acid transporter 5, a retinal glutamate transporter coupled to a chloride conductance. Proc Natl Acad Sci U S A 94:4155-4160.

Arriza JL, Fairman WA, Wadiche JI, Murdoch GH, Kavanaugh MP, Amara SG (1994) Functional comparisons of three glutamate transporter subtypes cloned from human motor cortex. J Neurosci 14:5559-5569.

Ascher P, Nowak L (1988) The role of divalent cations in the N-methyl-D-aspartate responses of mouse central neurones in culture. J Physiol 399:247-266.

Ascher P, Bregestovski P, Nowak L (1988) N-methyl-D-aspartate-activated channels of mouse central neurones in magnesium-free solutions. J Physiol 399:207-226.

Atluri PP, Regehr WG (1996) Determinants of the time course of facilitation at the granule cell to Purkinje cell synapse. J Neurosci 16:5661-5671.

Attwell D, Barbour B, Szatkowski M (1993) Nonvesicular release of neurotransmitter. Neuron 11:401-407.

Auger C, Attwell D (2000) Fast removal of synaptic glutamate by postsynaptic transporters. Neuron 28:547-558.

Bach I (2000) The LIM domain: regulation by association. Mech Dev 91:5-17.

Backus KH, Deitmer JW, Friauf E (1998) Glycine-activated currents are changed by coincident membrane depolarization in developing rat auditory brainstem neurones. J Physiol 507:783-794.

Bader CR, Macleish PR, Schwartz EA (1979) A voltage-clamp study of the light response in solitary rods of the tiger salamander. J Physiol 296:1-26.

Ballanyi K, Grafe P (1985) An intracellular analysis of gamma-aminobutyric-acid-associated ion movements in rat sympathetic neurones. J Physiol 365:41-58.

Barbour B (1993) Synaptic currents evoked in Purkinje cells by stimulating individual granule cells. Neuron 11:759-769.

Barbour B (2001) An evaluation of synapse independence. J Neurosci 21:7969-7984.

Barbour B, Brew H, Attwell D (1988) Electrogenic glutamate uptake in glial cells is activated by intracellular potassium. Nature 335:433-435.

Barbour B, Szatkowski M, Ingledew N, Attwell D (1989) Arachidonic acid induces a prolonged inhibition of glutamate uptake into glial cells. Nature 342:918-920.

Barbour B, Keller BU, Llano I, Marty A (1994) Prolonged presence of glutamate during excitatory synaptic transmission to cerebellar Purkinje cells. Neuron 12:1331-1343.

Barnard EA, Skolnick P, Olsen RW, Mohler H, Sieghart W, Biggio G, Braestrup C, Bateson AN, Langer SZ (1998) International Union of Pharmacology. XV. Subtypes of gamma-aminobutyric acidA receptors: classification on the basis of subunit structure and receptor function. Pharmacol Rev 50:291-313.

Batchelor AM, Garthwaite J (1993) Novel synaptic potentials in cerebellar Purkinje cells: probable mediation by metabotropic glutamate receptors. Neuropharmacology 32:11-20.

Batchelor AM, Garthwaite J (1997) Frequency detection and temporally dispersed synaptic signal association through a metabotropic glutamate receptor pathway. Nature 385:74-77.

Batchelor AM, Madge DJ, Garthwaite J (1994) Synaptic activation of metabotropic glutamate receptors in the parallel fibre-Purkinje cell pathway in rat cerebellar slices. Neuroscience 63:911-915.

Bedford FK, Kittler JT, Uren JM, Thomas P, Smart TG, Moss SJ (2000) Membrane insertion of GABAA-R is regulated by interactions with GRUB1, a ubiquitin related protein. Society for Neuroscience 26:621.625.

Bedford FK, Kittler JT, Muller E, Thomas P, Uren JM, Merlo D, Wisden W, Triller A, Smart TG, Moss SJ (2001) GABA(A) receptor cell surface number and subunit stability are regulated by the ubiquitin-like protein Plic-1. Nat Neurosci 4:908-916.

Bekkers JM, Stevens CF (1989) NMDA and non-NMDA receptors are co-localized at individual excitatory synapses in cultured rat hippocampus. Nature 341:230-233.

Ben-Ari Y, Tseeb V, Raggozzino D, Khazipov R, Gaiarsa JL (1994) gamma-Aminobutyric acid (GABA): a fast excitatory transmitter which may regulate the development of hippocampal neurones in early postnatal life. Prog Brain Res 102:261-273.

Bennett JA, Dingledine R (1995) Topology profile for a glutamate receptor: three transmembrane domains and a channel-lining reentrant membrane loop. Neuron 14:373-384.

Benveniste M, Mayer ML (1991) Kinetic analysis of antagonist action at N-methyl-D-aspartic acid receptors. Two binding sites each for glutamate and glycine. Biophys J 59:560-573.

Berger AJ, Dieudonne S, Ascher P (1998) Glycine uptake governs glycine site occupancy at NMDA receptors of excitatory synapses. J Neurophysiol 80:3336-3340.

Bergeron R, Meyer TM, Coyle JT, Greene RW (1998) Modulation of N-methyl-D-aspartate receptor function by glycine transport. Proc Natl Acad Sci U S A 95:15730-15734.

Bergles DE, Jahr CE (1997) Synaptic activation of glutamate transporters in hippocampal astrocytes. Neuron 19:1297-1308.

Bergles DE, Dzubay JA, Jahr CE (1997) Glutamate transporter currents in bergmann glial cells follow the time course of extrasynaptic glutamate. Proc Natl Acad Sci U S A 94:14821-14825.

Billups B, Attwell D (1996) Modulation of non-vesicular glutamate release by pH. Nature 379:171-174.

Billups B, Rossi D, Attwell D (1996) Anion conductance behavior of the glutamate uptake carrier in salamander retinal glial cells. J Neurosci 16:6722-6731.

Billups D, Hanley JG, Orme M, Attwell D, Moss SJ (2000) $GABA_C$ receptor sensitivity is modulated by interaction with MAP1B. J Neurosci 20:8643-8650.

Bloomfield SA, Dowling JE (1985a) Roles of aspartate and glutamate in synaptic transmission in rabbit retina. I. Outer plexiform layer. J Neurophysiol 53:699-713.

Bloomfield SA, Dowling JE (1985b) Roles of aspartate and glutamate in synaptic transmission in rabbit retina. II. Inner plexiform layer. J Neurophysiol 53:714-725.

Bloomfield SA, Miller RF (1986) A functional organization of ON and OFF pathways in the rabbit retina. J Neurosci 6:1-13.

Bloomfield SA, Xin D (2000) Surround inhibition of mammalian AII amacrine cells is generated in the proximal retina. J Physiol 523 Pt 3:771-783.

Bloomfield SA, Dacheux RF (2001) Rod vision: pathways and processing in the mammalian retina. Prog Retin Eye Res 20:351-384.

Borden LA, Murali Dhar TG, Smith KE, Weinshank RL, Branchek TA, Gluchowski C (1994) Tiagabine, SK&F 89976-A, CI-966, and NNC-711 are selective for the cloned GABA transporter GAT-1. Eur J Pharmacol 269:219-224.

Bormann J, Feigenspan A (1995) $GABA_C$ receptors. Trends Neurosci 18:515-519.

Bormann J, Hamill OP, Sakmann B (1987) Mechanism of anion permeation through channels gated by glycine and gamma-aminobutyric acid in mouse cultured spinal neurones. J Physiol 385:243-286.

Boue-Grabot E, Roudbaraki M, Bascles L, Tramu G, Bloch B, Garret M (1998) Expression of GABA receptor rho subunits in rat brain. J Neurochem 70:899-907.

Boulter J, Hollmann M, O'Shea-Greenfield A, Hartley M, Deneris E, Maron C, Heinemann S (1990) Molecular cloning and functional expression of glutamate receptor subunit genes. Science 249:1033-1037.

Bouvier M, Szatkowski M, Amato A, Attwell D (1992) The glial cell glutamate uptake carrier countertransports pH-changing anions. Nature 360:471-474.

Bowery N (1989) $GABA_B$ receptors and their significance in mammalian pharmacology. Trends Pharmacol Sci 10:401-407.

Brakeman PR, Lanahan AA, O'Brien R, Roche K, Barnes CA, Huganir RL, Worley PF (1997) Homer: a protein that selectively binds metabotropic glutamate receptors. Nature 386:284-288.

Brandon NJ, Uren JM, Kittler JT, Wang H, Olsen R, Parker PJ, Moss SJ (1999) Subunit-specific association of protein kinase C and the receptor for activated C kinase with GABA type A receptors. J Neurosci 19:9228-9234.

Brandstatter JH, Koulen P, Wassle H (1997) Selective synaptic distribution of kainate receptor subunits in the two plexiform layers of the rat retina. J Neurosci 17:9298-9307.

Brandstatter JH, Hartveit E, Sassoe-Pognetto M, Wassle H (1994) Expression of NMDA and high-affinity kainate receptor subunit mRNAs in the adult rat retina. Eur J Neurosci 6:1100-1112.

Brasnjo G, Otis TS (2001) Neuronal glutamate transporters control activation of postsynaptic metabotropic glutamate receptors and influence cerebellar long-term depression. Neuron 31:607-616.

Brecha NC, Weigmann C (1994) Expression of GAT-1, a high-affinity gamma-aminobutyric acid plasma membrane transporter in the rat retina. J Comp Neurol 345:602-611.

Brenman JE, Chao DS, Gee SH, McGee AW, Craven SE, Santillano DR, Wu Z, Huang F, Xia H, Peters MF, Froehner SC, Bredt DS (1996) Interaction of nitric oxide synthase with the postsynaptic density protein PSD-95 and alpha1-syntrophin mediated by PDZ domains. Cell 84:757-767.

Brew H, Attwell D (1987) Electrogenic glutamate uptake is a major current carrier in the membrane of axolotl retinal glial cells [published erratum appears in Nature 1987 Aug 20-26;328(6132):742]. Nature 327:707-709.

Burnashev N, Villarroel A, Sakmann B (1996) Dimensions and ion selectivity of recombinant AMPA and kainate receptor channels and their dependence on Q/R site residues. J Physiol 496:165-173.

Burnashev N, Monyer H, Seeburg PH, Sakmann B (1992) Divalent ion permeability of AMPA receptor channels is dominated by the edited form of a single subunit. Neuron 8:189-198.

Calvo DJ, Miledi R (1995) Activation of GABA rho 1 receptors by glycine and beta-alanine. Neuroreport 6:1118-1120.

Calvo DJ, Vazquez AE, Miledi R (1994) Cationic modulation of rho 1-type gamma-aminobutyrate receptors expressed in Xenopus oocytes. Proc Natl Acad Sci U S A 91:12725-12729.

Canepari M, Papageorgiou G, Corrie JE, Watkins C, Ogden D (2001) The conductance underlying the parallel fibre slow EPSP in rat cerebellar Purkinje neurones studied with photolytic release of L- glutamate. J Physiol 533:765-772.

Carpenter MB, Sutin J (1983) Human Neuroanatomy, 8th Edition: Williams and Wilkins.

Carter AG, Regehr WG (2000) Prolonged synaptic currents and glutamate spillover at the parallel fiber to stellate cell synapse. J Neurosci 20:4423-4434.

Carter AG, Vogt KE, Foster KA, Regehr WG (2002) Assessing the role of calcium-induced calcium release in short-term presynaptic plasticity at excitatory central synapses. J Neurosci 22:21-28.

Casado M, Dieudonne S, Ascher P (2000) Presynaptic N-methyl-D-aspartate receptors at the parallel fiber- Purkinje cell synapse. Proc Natl Acad Sci U S A 97:11593-11597.

Casado M, Isope P, Ascher P (2002) Involvement of presynaptic N-methyl-d-aspartate receptors in cerebellar long-term depression. Neuron 33:123-130.

Casado M, Bendahan A, Zafra F, Danbolt NC, Aragon C, Gimenez C, Kanner BI (1993) Phosphorylation and modulation of brain glutamate transporters by protein kinase C. J Biol Chem 268:27313-27317.

Cathala L, Misra C, Cull-Candy S (2000) Developmental profile of the changing properties of NMDA receptors at cerebellar mossy fiber-granule cell synapses. J Neurosci 20:5899-5905.

Chang Y, Weiss DS (1999) Channel opening locks agonist onto the $GABA_C$ receptor. Nat Neurosci 2:219-225.

Chaudhry FA, Lehre KP, van Lookeren Campagne M, Ottersen OP, Danbolt NC, Storm-Mathisen J (1995) Glutamate transporters in glial plasma membranes: highly differentiated localizations revealed by quantitative ultrastructural immunocytochemistry. Neuron 15:711-720.

Chazot PL, Coleman SK, Cik M, Stephenson FA (1994) Molecular characterization of N-methyl-D-aspartate receptors expressed in mammalian cells yields evidence for the coexistence of three subunit types within a discrete receptor molecule. J Biol Chem 269:24403-24409.

Chen G, Trombley PQ, van den Pol AN (1996) Excitatory actions of GABA in developing rat hypothalamic neurones. J Physiol 494:451-464.

Chen L, Wang H, Vicini S, Olsen RW (2000a) The gamma-aminobutyric acid type A ($GABA_A$) receptor-associated protein (GABARAP) promotes $GABA_A$ receptor clustering and modulates the channel kinetics. Proc Natl Acad Sci U S A 97:11557-11562.

Chen L, Chetkovich DM, Petralia RS, Sweeney NT, Kawasaki Y, Wenthold RJ, Bredt DS, Nicoll RA (2000b) Stargazing regulates synaptic targeting of AMPA receptors by two distinct mechanisms. Nature 408:936-943.

Chen N, Luo T, Raymond LA (1999) Subtype-dependence of NMDA receptor channel open probability. J Neurosci 19:6844-6854.

Chen W, Aoki C, Gruber C, Harley R, Wang GJ, Blitzblau R, Volpe JJ, Irwin N, Rosenberg PA (2000c) Molecular cloning, functional characterization, and neuronal characterization of a variant form of the glutamate transporter GLT-1. Society for Neuroscience 26:593.515.

Cherubini E, Gaiarsa JL, Ben-Ari Y (1991) GABA: an excitatory transmitter in early postnatal life. Trends Neurosci 14:515-519.

Cherubini E, Rovira C, Gaiarsa JL, Corradetti R, Ben Ari Y (1990) GABA mediated excitation in immature rat CA3 hippocampal neurons. Int J Dev Neurosci 8:481-490.

Chiba C, Saito T (1994) APB (2-amino-4-phosphonobutyric acid) activates a chloride conductance in ganglion cells isolated from newt retina. Neuroreport 5:489-492.

Choi DW, Maulucci-Gedde M, Kriegstein AR (1987) Glutamate neurotoxicity in cortical cell culture. J Neurosci 7:357-368.

Ciabarra AM, Sullivan JM, Gahn LG, Pecht G, Heinemann S, Sevarino KA (1995) Cloning and characterization of chi-1: a developmentally regulated member of a novel class of the ionotropic glutamate receptor family. J Neurosci 15:6498-6508.

Clark BA, Barbour B (1997) Currents evoked in Bergmann glial cells by parallel fibre stimulation in rat cerebellar slices. J Physiol 502:335-350.

Clark JA, Amara SG (1994) Stable expression of a neuronal gamma-aminobutyric acid transporter, GAT-3, in mammalian cells demonstrates unique pharmacological properties and ion dependence. Mol Pharmacol 46:550-557.

Clements JD (1996) Transmitter timecourse in the synaptic cleft: its role in central synaptic function. Trends Neurosci 19:163-171.

Clements JD, Lester RA, Tong G, Jahr CE, Westbrook GL (1992) The time course of glutamate in the synaptic cleft. Science 258:1498-1501.

Collingridge GL, Lester RA (1989) Excitatory amino acid receptors in the vertebrate central nervous system. Pharmacol Rev 41:143-210.

Colquhoun D, Jonas P, Sakmann B (1992) Action of brief pulses of glutamate on AMPA/kainate receptors in patches from different neurones of rat hippocampal slices. J Physiol 458:261-287.

Conradt M, Stoffel W (1997) Inhibition of the high-affinity brain glutamate transporter GLAST-1 via direct phosphorylation. J Neurochem 68:1244-1251.

Conti F, DeBiasi S, Minelli A, Rothstein JD, Melone M (1998) EAAC1, a high-affinity glutamate tranporter, is localized to astrocytes and gabaergic neurons besides pyramidal cells in the rat cerebral cortex. Cereb Cortex 8:108-116.

Cubitt AB, Heim R, Adams SR, Boyd AE, Gross LA, Tsien RY (1995) Understanding, improving and using green fluorescent proteins. Trends Biochem Sci 20:448-455.

Cull-Candy SG, Brickley SG, Misra C, Feldmeyer D, Momiyama A, Farrant M (1998) NMDA receptor diversity in the cerebellum: identification of subunits contributing to functional receptors. Neuropharmacology 37:1369-1380.

Cutting GR, Curristin S, Zoghbi H, O'Hara B, Seldin MF, Uhl GR (1992) Identification of a putative gamma-aminobutyric acid (GABA) receptor subunit rho2 cDNA and colocalization of the genes encoding rho2 (GABRR2) and rho1 (GABRR1) to human chromosome 6q14-q21 and mouse chromosome 4. Genomics 12:801-806.

Cutting GR, Lu L, O'Hara BF, Kasch LM, Montrose-Rafizadeh C, Donovan DM, Shimada S, Antonarakis SE, Guggino WB, Uhl GR, et al. (1991) Cloning of the gamma-aminobutyric acid (GABA) rho 1 cDNA: a GABA receptor subunit highly expressed in the retina. Proc Natl Acad Sci U S A 88:2673-2677.

Dacey D, Packer OS, Diller L, Brainard D, Peterson B, Lee B (2000) Center surround receptive field structure of cone bipolar cells in primate retina. Vision Res 40:1801-1811.

Dallwig R, Deitmer JW, Backus KH (1999) On the mechanism of GABA-induced currents in cultured rat cortical neurons. Pflugers Arch 437:289-297.

Danbolt NC (2001) Glutamate uptake. Prog Neurobiol 65:1-105.

D'Angelo E, Rossi P, Taglietti V (1993) Different proportions of N-methyl-D-aspartate and non-N-methyl-D- aspartate receptor currents at the mossy fibre-granule cell synapse of developing rat cerebellum. Neuroscience 53:121-130.

D'Angelo E, De Filippi G, Rossi P, Taglietti V (1995) Synaptic excitation of individual rat cerebellar granule cells in situ: evidence for the role of NMDA receptors. J Physiol 484:397-413.

D'Angelo E, Rossi P, Armano S, Taglietti V (1999) Evidence for NMDA and mGlu receptor-dependent long-term potentiation of mossy fiber-granule cell transmission in rat cerebellum. J Neurophysiol 81:277-287.

Danysz W, Parsons AC (1998) Glycine and N-methyl-D-aspartate receptors: physiological significance and possible therapeutic applications. Pharmacol Rev 50:597-664.

Das S, Sasaki YF, Rothe T, Premkumar LS, Takasu M, Crandall JE, Dikkes P, Conner DA, Rayudu PV, Cheung W, Chen HS, Lipton SA, Nakanishi N (1998) Increased NMDA current and spine density in mice lacking the NMDA receptor subunit NR3A. Nature 393:377-381.

Davis KE, Straff DJ, Weinstein EA, Bannerman PG, Correale DM, Rothstein JD, Robinson MB (1998) Multiple signaling pathways regulate cell surface expression and activity of the excitatory amino acid carrier 1 subtype of Glu transporter in C6 glioma. J Neurosci 18:2475-2485.

Dawid IB, Breen JJ, Toyama R (1998) LIM domains: multiple roles as adapters and functional modifiers in protein interactions. Trends Genet 14:156-162.

De Blasi A, Conn PJ, Pin J, Nicoletti F (2001) Molecular determinants of metabotropic glutamate receptor signaling. Trends Pharmacol Sci 22:114-120.

DeFazio RA, Keros S, Quick MW, Hablitz JJ (2000) Potassium-coupled chloride cotransport controls intracellular chloride in rat neocortical pyramidal neurons. J Neurosci 20:8069-8076.

Dehnes Y, Chaudhry FA, Ullensvang K, Lehre KP, Storm-Mathisen J, Danbolt NC (1998) The glutamate transporter EAAT4 in rat cerebellar Purkinje cells: a glutamate-gated chloride channel concentrated near the synapse in parts of the dendritic membrane facing astroglia. J Neurosci 18:3606-3619.

Delpire E (2000) Cation-Chloride Cotransporters in Neuronal Communication. News Physiol Sci 15:309-312.

DeVries SH, Schwartz EA (1999) Kainate receptors mediate synaptic transmission between cones and 'Off' bipolar cells in a mammalian retina. Nature 397:157-160.

Diamond JS (2001) Neuronal glutamate transporters limit activation of NMDA receptors by neurotransmitter spillover on CA1 pyramidal cells. J Neurosci 21:8328-8338.

Diamond JS, Jahr CE (1997) Transporters buffer synaptically released glutamate on a submillisecond time scale. J Neurosci 17:4672-4687.

Diana MA, Levenes C, Mackie K, Marty A (2002) Short-term retrograde inhibition of GABAergic synaptic currents in rat Purkinje cells is mediated by endogenous cannabinoids. J Neurosci 22:200-208.

Diaz-Nido J, Serrano L, Avila J (1988) Differential phosphorylation of microtubule proteins by ATP and GTP. Mol Cell Biochem 79:73-79.

Dieudonne S, Dumoulin A (2000) Serotonin-driven long-range inhibitory connections in the cerebellar cortex. J Neurosci 20:1837-1848.

Dingledine R, Borges K, Bowie D, Traynelis SF (1999) The glutamate receptor ion channels. Pharmacol Rev 51:7-61.

Dino MR, Nunzi MG, Anelli R, Mugnaini E (2000a) Unipolar brush cells of the vestibulocerebellum: afferents and targets. Prog Brain Res 124:123-137.

Dino MR, Schuerger RJ, Liu Y, Slater NT, Mugnaini E (2000b) Unipolar brush cell: a potential feedforward excitatory interneuron of the cerebellum. Neuroscience 98:625-636.

Dittman JS, Regehr WG (1996) Contributions of calcium-dependent and calcium-independent mechanisms to presynaptic inhibition at a cerebellar synapse. J Neurosci 16:1623-1633.

Dittman JS, Regehr WG (1997) Mechanism and kinetics of heterosynaptic depression at a cerebellar synapse. J Neurosci 17:9048-9059.

Dmitriev AV, Govardovskii VI, Schwahn HN, Steinberg RH (1999) Light-induced changes of extracellular ions and volume in the isolated chick retina-pigment epithelium preparation. Vis Neurosci 16:1157-1167.

Dong CJ, Werblin FS (1995) Zinc downmodulates thf $GABA_C$ receptor current in cone horizontal cells acutely isolated from the catfish retina. J Neurophysiol 73:916-919.

Dong CJ, Werblin FS (1998) Temporal contrast enhancement via $GABA_C$ feedback at bipolar terminals in the tiger salamander retina. J Neurophysiol 79:2171-2180.

Dong H, O'Brien RJ, Fung ET, Lanahan AA, Worley PF, Huganir RL (1997) GRIP: a synaptic PDZ domain-containing protein that interacts with AMPA receptors. Nature 386:279-284.

Drew CA, Johnston GA (1992) Bicuculline- and baclofen-insensitive gamma-aminobutyric acid binding to rat cerebellar membranes. J Neurochem 58:1087-1092.

Drew CA, Johnston GA, Weatherby RP (1984) Bicuculline-insensitive GABA receptors: studies on the binding of (-)- baclofen to rat cerebellar membranes. Neurosci Lett 52:317-321.

Duan S, Anderson CM, Stein BA, Swanson RA (1999) Glutamate induces rapid upregulation of astrocyte glutamate transport and cell-surface expression of GLAST. J Neurosci 19:10193-10200.

Dumoulin A, Triller A, Dieudonne S (2001) IPSC kinetics at identified GABAergic and mixed GABAergic and glycinergic synapses onto cerebellar Golgi cells. J Neurosci 21:6045-6057.

Ebihara S, Shirato K, Harata N, Akaike N (1995) Gramicidin-perforated patch recording: GABA response in mammalian neurones with intact intracellular chloride. J Physiol 484:77-86.

Eccles JC, Ito M, Szentagothai J (1967) The Cerebellum as a Neuronal Machine: Springer-Verlag.

Edelmann W, Zervas M, Costello P, Roback L, Fischer I, Hammarback JA, Cowan N, Davies P, Wainer B, Kucherlapati R (1996) Neuronal abnormalities in microtubule-associated protein 1B mutant mice. Proc Natl Acad Sci U S A 93:1270-1275.

Edwards FA, Konnerth A, Sakmann B, Takahashi T (1989) A thin slice preparation for patch clamp recordings from neurones of the mammalian central nervous system. Pflugers Arch 414:600-612.

Egebjerg J, Heinemann SF (1993) Ca^{2+} permeability of unedited and edited versions of the kainate selective glutamate receptor GluR6. Proc Natl Acad Sci U S A 90:755-759.

Ehrlich I, Lohrke S, Friauf E (1999) Shift from depolarizing to hyperpolarizing glycine action in rat auditory neurones is due to age-dependent Cl^- regulation. J Physiol 520 Pt 1:121-137.

Eliasof S, Jahr CE (1996) Retinal glial cell glutamate transporter is coupled to an anionic conductance. Proc Natl Acad Sci U S A 93:4153-4158.

Eliasof S, Arriza JL, Leighton BH, Kavanaugh MP, Amara SG (1998a) Excitatory amino acid transporters of the salamander retina: identification, localization, and function. J Neurosci 18:698-712.

Eliasof S, Arriza JL, Leighton BH, Amara SG, Kavanaugh MP (1998b) Localization and function of five glutamate transporters cloned from the salamander retina. Vision Res 38:1443-1454.

Enz R, Bormann J (1995) A single point mutation decreases picrotoxinin sensitivity of the human GABA receptor rho 1 subunit. Neuroreport 6:1569-1572.

Enz R, Cutting GR (1998) Molecular composition of $GABA_C$ receptors. Vision Res 38:1431-1441.

Enz R, Cutting GR (1999) $GABA_C$ receptor rho subunits are heterogeneously expressed in the human CNS and form homo- and heterooligomers with distinct physical properties. Eur J Neurosci 11:41-50.

Enz R, Ross BJ, Cutting GR (1999) Expression of the voltage-gated chloride channel ClC-2 in rod bipolar cells of the rat retina. J Neurosci 19:9841-9847.

Enz R, Brandstatter JH, Wassle H, Bormann J (1996) Immunocytochemical localization of the $GABA_C$ receptor rho subunits in the mammalian retina. J Neurosci 16:4479-4490.

Enz R, Brandstatter JH, Hartveit E, Wassle H, Bormann J (1995) Expression of GABA receptor rho 1 and rho 2 subunits in the retina and brain of the rat. Eur J Neurosci 7:1495-1501.

Erecinska M, Wantorsky D, Wilson DF (1983) Aspartate transport in synaptosomes from rat brain. J Biol Chem 258:9069-9077.

Eskandari S, Kreman M, Kavanaugh MP, Wright EM, Zampighi GA (2000) Pentameric assembly of a neuronal glutamate transporter. Proc Natl Acad Sci U S A 97:8641-8646.

Euler T, Wassle H (1995) Immunocytochemical identification of cone bipolar cells in the rat retina. J Comp Neurol 361:461-478.

Euler T, Wassle H (1998) Different contributions of $GABA_A$ and $GABA_C$ receptors to rod and cone bipolar cells in a rat retinal slice preparation. J Neurophysiol 79:1384-1395.

Euler T, Masland RH (2000) Light-evoked responses of bipolar cells in a mammalian retina. J Neurophysiol 83:1817-1829.

Euler T, Schneider H, Wassle H (1996) Glutamate responses of bipolar cells in a slice preparation of the rat retina. J Neurosci 16:2934-2944.

Fairman WA, Vandenberg RJ, Arriza JL, Kavanaugh MP, Amara SG (1995) An excitatory amino-acid transporter with properties of a ligand-gated chloride channel. Nature 375:599-603.

Farrant M, Feldmeyer D, Takahashi T, Cull-Candy SG (1994) NMDA-receptor channel diversity in the developing cerebellum. Nature 368:335-339.

Feigenspan A, Bormann J (1994a) Differential pharmacology of $GABA_A$ and $GABA_C$ receptors on rat retinal bipolar cells. Eur J Pharmacol 288:97-104.

Feigenspan A, Bormann J (1994b) Modulation of $GABA_C$ receptors in rat retinal bipolar cells by protein kinase C. J Physiol 481:325-330.

Feigenspan A, Bormann J (1998) GABA-gated Cl^- channels in the rat retina. Prog Retin Eye Res 17:99-126.

Feigenspan A, Wassle H, Bormann J (1993) Pharmacology of GABA receptor Cl^- channels in rat retinal bipolar cells. Nature 361:159-162.

Fenwick EM, Marty A, Neher E (1982) A patch-clamp study of bovine chromaffin cells and of their sensitivity to acetylcholine. J Physiol 331:577-597.

Figiel M, Engele J (2000) Pituitary adenylate cyclase-activating polypeptide (PACAP), a neuron-derived peptide regulating glial glutamate transport and metabolism. J Neurosci 20:3596-3605.

Filippova N, Dudley R, Weiss DS (1999) Evidence for phosphorylation-dependent internalization of recombinant human rho1 $GABA_C$ receptors. J Physiol 518:385-399.

Finch EA, Augustine GJ (1998) Local calcium signalling by inositol-1,4,5-trisphosphate in Purkinje cell dendrites. Nature 396:753-756.

Fischer F, Kneussel M, Tintrup H, Haverkamp S, Rauen T, Betz H, Wassle H (2000) Reduced synaptic clustering of GABA and glycine receptors in the retina of the gephyrin null mutant mouse. J Comp Neurol 427:634-648.

Fletcher EL, Koulen P, Wassle H (1998) $GABA_A$ and $GABA_C$ receptors on mammalian rod bipolar cells. J Comp Neurol 396:351-365.

Forsythe ID, Westbrook GL, Mayer ML (1988) Modulation of excitatory synaptic transmission by glycine and zinc in cultures of mouse hippocampal neurons. J Neurosci 8:3733-3741.

Frech MJ, Deitmer JW, Backus KH (1999) Intracellular chloride and calcium transients evoked by gamma- aminobutyric acid and glycine in neurons of the rat inferior colliculus. J Neurobiol 40:386-396.

Frishman LJ, Yamamoto F, Bogucka J, Steinberg RH (1992) Light-evoked changes in $[K^+]_o$ in proximal portion of light-adapted cat retina. J Neurophysiol 67:1201-1212.

Furuta A, Rothstein JD, Martin LJ (1997a) Glutamate transporter protein subtypes are expressed differentially during rat CNS development. J Neurosci 17:8363-8375.

Furuta A, Martin LJ, Lin CL, Dykes-Hoberg M, Rothstein JD (1997b) Cellular and synaptic localization of the neuronal glutamate transporters excitatory amino acid transporter 3 and 4. Neuroscience 81:1031-1042.

Gaal L, Roska B, Picaud SA, Wu SM, Marc R, Werblin FS (1998) Postsynaptic response kinetics are controlled by a glutamate transporter at cone photoreceptors. J Neurophysiol 79:190-196.

Gadea A, Lopez-Colome AM (2001a) Glial transporters for glutamate, glycine, and GABA III. Glycine transporters. J Neurosci Res 64:218-222.

Gadea A, Lopez-Colome AM (2001b) Glial transporters for glutamate, glycine, and GABA: II. GABA transporters. J Neurosci Res 63:461-468.

Ganguly K, Schinder AF, Wong ST, Poo M (2001) GABA itself promotes the developmental switch of neuronal GABAergic responses from excitation to inhibition. Cell 105:521-532.

Garner CC, Kindler S, Gundelfinger ED (2000) Molecular determinants of presynaptic active zones. Curr Opin Neurobiol 10:321-327.

Garthwaite J, Brodbelt AR (1989) Synaptic activation of N-methyl-D-aspartate and non-N-methyl-D-aspartate receptors in the mossy fibre pathway in adult and immature rat cerebellar slices. Neuroscience 29:401-412.

Geoffroy M, Lambolez B, Audinat E, Hamon B, Crepel F, Rossier J, Kado RT (1991) Reduction of desensitization of a glutamate ionotropic receptor by antagonists. Mol Pharmacol 39:587-591.

Gibb AJ, Colquhoun D (1991) Glutamate activation of a single NMDA receptor-channel produces a cluster of channel openings. Proc R Soc Lond B Biol Sci 243:39-45.

Gibb AJ, Colquhoun D (1992) Activation of N-methyl-D-aspartate receptors by L-glutamate in cells dissociated from adult rat hippocampus. J Physiol 456:143-179.

Glanville M, Kingscote S, Thwaites DT, Simmons NL (2001) Expression and role of sodium, potassium, chloride cotransport (NKCC1) in mouse inner medullary collecting duct (mIMCD-K2) epithelial cells. Pflugers Arch 443:123-131.

Goldberg JM, Fernandez C (1971) Physiology of peripheral neurons innervating semicircular canals of the squirrel monkey. I. Resting discharge and response to constant angular accelerations. J Neurophysiol 34:635-660.

Goyal RK, Lin P, Kanungo J, Payne AS, Muslin AJ, Longmore GD (1999) Ajuba, a novel LIM protein, interacts with Grb2, augments mitogen- activated protein kinase activity in fibroblasts, and promotes meiotic maturation of Xenopus oocytes in a Grb2- and Ras-dependent manner. Mol Cell Biol 19:4379-4389.

Greferath U, Grunert U, Muller F, Wassle H (1994) Localization of $GABA_A$ receptors in the rabbit retina. Cell Tissue Res 276:295-307.

Greferath U, Grunert U, Fritschy JM, Stephenson A, Mohler H, Wassle H (1995) $GABA_A$ receptor subunits have differential distributions in the rat retina: in situ hybridization and immunohistochemistry. J Comp Neurol 353:553-571.

Grunewald M, Kanner BI (2000) The accessibility of a novel reentrant loop of the glutamate transporter GLT-1 is restricted by its substrate. J Biol Chem 275:9684-9689.

Grunewald M, Bendahan A, Kanner BI (1998) Biotinylation of single cysteine mutants of the glutamate transporter GLT-1 from rat brain reveals its unusual topology. Neuron 21:623-632.

Gundelfinger ED, tom Dieck S (2000) Molecular organization of excitatory chemical synapses in the mammalian brain. Naturwissenschaften 87:513-523.

Hackam AS, Wang TL, Guggino WB, Cutting GR (1998) Sequences in the amino termini of GABA rho and GABA(A) subunits specify their selective interaction in vitro. J Neurochem 70:40-46.

Hamill OP, Marty A, Neher E, Sakmann B, Sigworth FJ (1981) Improved patch-clamp techniques for high-resolution current recording from cells and cell-free membrane patches. Pflugers Arch 391:85-100.

Hammarback JA, Obar RA, Hughes SM, Vallee RB (1991) MAP1B is encoded as a polyprotein that is processed to form a complex N- terminal microtubule-binding domain. Neuron 7:129-139.

Hamori J, Somogyi J (1983) Differentiation of cerebellar mossy fiber synapses in the rat: a quantitative electron microscope study. J Comp Neurol 220:365-377.

Hamori J, Jakab RL, Takacs J (1997) Morphogenetic plasticity of neuronal elements in cerebellar glomeruli during deafferentation-induced synaptic reorganization. J Neural Transplant Plast 6:11-20.

Hanley JG, Jones EM, Moss SJ (2000) GABA receptor rho1 subunit interacts with a novel splice variant of the glycine transporter, GLYT-1. J Biol Chem 275:840-846.

Hanley JG, Koulen P, Bedford F, Gordon-Weeks PR, Moss SJ (1999) The protein MAP-1B links GABA(C) receptors to the cytoskeleton at retinal synapses. Nature 397:66-69.

Hansel C, Linden DJ, D'Angelo E (2001) Beyond parallel fiber LTD: the diversity of synaptic and non-synaptic plasticity in the cerebellum. Nat Neurosci 4:467-475.

Harada T, Harada C, Watanabe M, Inoue Y, Sakagawa T, Nakayama N, Sasaki S, Okuyama S, Watase K, Wada K, Tanaka K (1998) Functions of the two glutamate transporters GLAST and GLT-1 in the retina. Proc Natl Acad Sci U S A 95:4663-4666.

Hare WA, Owen WG (1996) Receptive field of the retinal bipolar cell: a pharmacological study in the tiger salamander. J Neurophysiol 76:2005-2019.

Hartveit E (1997) Functional organization of cone bipolar cells in the rat retina. J Neurophysiol 77:1716-1730.

Hashimoto A, Oka T (1997) Free D-aspartate and D-serine in the mammalian brain and periphery. Prog Neurobiol 52:325-353.

Haugeto O, Ullensvang K, Levy LM, Chaudhry FA, Honore T, Nielsen M, Lehre KP, Danbolt NC (1996) Brain glutamate transporter proteins form homomultimers. J Biol Chem 271:27715-27722.

Haverkamp S, Grunert U, Wassle H (2000) The cone pedicle, a complex synapse in the retina. Neuron 27:85-95.

Heidelberger R, Matthews G (1991) Inhibition of calcium influx and calcium current by gamma-aminobutyric acid in single synaptic terminals. Proc Natl Acad Sci U S A 88:7135-7139.

Heim R, Cubitt AB, Tsien RY (1995) Improved green fluorescence. Nature 373:663-664.

Hertz L (1979) Functional interactions between neurons and astrocytes I. Turnover and metabolism of putative amino acid transmitters. Prog Neurobiol 13:277-323.

Hestrin S (1992) Developmental regulation of NMDA receptor-mediated synaptic currents at a central synapse. Nature 357:686-689.

Hestrin S, Sah P, Nicoll RA (1990) Mechanisms generating the time course of dual component excitatory synaptic currents recorded in hippocampal slices. Neuron 5:247-253.

Heuss C, Gerber U (2000) G-protein-independent signaling by G-protein-coupled receptors. Trends Neurosci 23:469-475.

Hibino H, Inanobe A, Tanemoto M, Fujita A, Doi K, Kubo T, Hata Y, Takai Y, Kurachi Y (2000) Anchoring proteins confer G protein sensitivity to an inward-rectifier K($^{+}$) channel through the GK domain. Embo J 19:78-83.

Higgs MH, Lukasiewicz PD (1999) Glutamate uptake limits synaptic excitation of retinal ganglion cells. J Neurosci 19:3691-3700.

Hollmann M, Heinemann S (1994) Cloned glutamate receptors. Annu Rev Neurosci 17:31-108.

Hollmann M, Hartley M, Heinemann S (1991) Ca^{2+} permeability of KA-AMPA--gated glutamate receptor channels depends on subunit composition. Science 252:851-853.

Hollmann M, Maron C, Heinemann S (1994) N-glycosylation site tagging suggests a three transmembrane domain topology for the glutamate receptor GluR1. Neuron 13:1331-1343.

Honda S, Yamamoto M, Saito N (1995) Immunocytochemical localization of three subtypes of GABA transporter in rat retina. Brain Res Mol Brain Res 33:319-325.

Horn R, Marty A (1988) Muscarinic activation of ionic currents measured by a new whole-cell recording method. J Gen Physiol 92:145-159.

Howe JR, Cull-Candy SG, Colquhoun D (1991) Currents through single glutamate receptor channels in outside-out patches from rat cerebellar granule cells. J Physiol 432:143-202.

Hubner CA, Lorke DE, Hermans-Borgmeyer I (2001a) Expression of the Na-K-2Cl-cotransporter NKCC1 during mouse development. Mech Dev 102:267-269.

Hubner CA, Stein V, Hermans-Borgmeyer I, Meyer T, Ballanyi K, Jentsch TJ (2001b) Disruption of KCC2 reveals an essential role of K-Cl cotransport already in early synaptic inhibition. Neuron 30:515-524.

Huggett J, Vaughan-Thomas A, Mason D (2000) The open reading frame of the Na(+)-dependent glutamate transporter GLAST-1 is expressed in bone and a splice variant of this molecule is expressed in bone and brain. FEBS Lett 485:13-18.

Hume RI, Dingledine R, Heinemann SF (1991) Identification of a site in glutamate receptor subunits that controls calcium permeability. Science 253:1028-1031.

Husi H, Ward MA, Choudhary JS, Blackstock WP, Grant SG (2000) Proteomic analysis of NMDA receptor-adhesion protein signaling complexes. Nat Neurosci 3:661-669.

Isaacson JS, Nicoll RA (1993) The uptake inhibitor L-trans-PDC enhances responses to glutamate but fails to alter the kinetics of excitatory synaptic currents in the hippocampus. J Neurophysiol 70:2187-2191.

Isenring P, Jacoby SC, Forbush B, 3rd (1998) The role of transmembrane domain 2 in cation transport by the Na-K-Cl cotransporter. Proc Natl Acad Sci U S A 95:7179-7184.

Ito M (2001) Cerebellar long-term depression: characterization, signal transduction, and functional roles. Physiol Rev 81:1143-1195.

Ito M, Kano M (1982) Long-lasting depression of parallel fiber-Purkinje cell transmission induced by conjunctive stimulation of parallel fibers and climbing fibers in the cerebellar cortex. Neurosci Lett 33:253-258.

Jackson M, Song W, Liu MY, Jin L, Dykes-Hoberg M, Lin CI, Bowers WJ, Federoff HJ, Sternweis PC, Rothstein JD (2001) Modulation of the neuronal glutamate transporter EAAT4 by two interacting proteins. Nature 410:89-93.

Jacobs AL, Werblin FS (1998) Spatiotemporal patterns at the retinal output. J Neurophysiol 80:447-451.

Jakab RL (1989) Three-dimensional reconstruction and synaptic architecture of cerebellar glomeruli in the rat. Acta Morphol Hung 37:11-20.

Jakab RL, Hamori J (1988) Quantitative morphology and synaptology of cerebellar glomeruli in the rat. Anat Embryol 179:81-88.

Jeromin A, Huganir RL, Linden DJ (1996) Suppression of the glutamate receptor delta 2 subunit produces a specific impairment in cerebellar long-term depression. J Neurophysiol 76:3578-3583.

Johnson J, Chen TK, Rickman DW, Evans C, Brecha NC (1996) Multiple gamma-Aminobutyric acid plasma membrane transporters (GAT-1, GAT-2, GAT-3) in the rat retina. J Comp Neurol 375:212-224.

Johnson JW, Ascher P (1987) Glycine potentiates the NMDA response in cultured mouse brain neurons. Nature 325:529-531.

Johnston GA, Curtis DR, Beart PM, Game CJ, McCulloch RM, Twitchin B (1975) Cis- and trans-4-aminocrotonic acid as GABA analogues of restricted conformation. J Neurochem 24:157-160.

Jonas P, Racca C, Sakmann B, Seeburg PH, Monyer H (1994) Differences in Ca^{2+} permeability of AMPA-type glutamate receptor channels in neocortical neurons caused by differential GluR-B subunit expression. Neuron 12:1281-1289.

Jones MV, Sahara Y, Dzubay JA, Westbrook GL (1998) Defining affinity with the $GABA_A$ receptor. J Neurosci 18:8590-8604.

Kaila K (1994) Ionic basis of $GABA_A$ receptor channel function in the nervous system. Prog Neurobiol 42:489-537.

Kaila K, Pasternack M, Saarikoski J, Voipio J (1989) Influence of GABA-gated bicarbonate conductance on potential, current and intracellular chloride in crayfish muscle fibres. J Physiol 416:161-181.

Kakazu Y, Akaike N, Komiyama S, Nabekura J (1999) Regulation of intracellular chloride by cotransporters in developing lateral superior olive neurons. J Neurosci 19:2843-2851.

Kanai Y, Hediger MA (1992) Primary structure and functional characterization of a high-affinity glutamate transporter. Nature 360:467-471.

Kaneda M, Andrasfalvy B, Kaneko A (2000) Modulation by Zn^{2+} of GABA responses in bipolar cells of the mouse retina. Vis Neurosci 17:273-281.

Kaneda M, Mochizuki M, Aoki K, Kaneko A (1997) Modulation of $GABA_C$ response by Ca^{2+} and other divalent cations in horizontal cells of the catfish retina. J Gen Physiol 110:741-747.

Kaneko A (1970) Physiological and morphological identification of horizontal, bipolar and amacrine cells in goldfish retina. J Physiol 207:623-633.

Kanungo J, Pratt SJ, Marie H, Longmore GD (2000) Ajuba, a cytosolic LIM protein, shuttles into the nucleus and affects embryonal cell proliferation and fate decisions. Mol Biol Cell 11:3299-3313.

Karschin A, Wassle H (1990) Voltage- and transmitter-gated currents in isolated rod bipolar cells of rat retina. J Neurophysiol 63:860-876.

Kashiwabuchi N, Ikeda K, Araki K, Hirano T, Shibuki K, Takayama C, Inoue Y, Kutsuwada T, Yagi T, Kang Y, et al. (1995) Impairment of motor coordination, Purkinje cell synapse formation, and cerebellar long-term depression in GluR delta 2 mutant mice. Cell 81:245-252.

Katagiri H, Tanaka K, Manabe T (2001) Requirement of appropriate glutamate concentrations in the synaptic cleft for hippocampal LTP induction. Eur J Neurosci 14:547-553.

Kaupmann K, Huggel K, Heid J, Flor PJ, Bischoff S, Mickel SJ, McMaster G, Angst C, Bittiger H, Froestl W, Bettler B (1997) Expression cloning of GABA(B) receptors uncovers similarity to metabotropic glutamate receptors. Nature 386:239-246.

Kaupmann K, Malitschek B, Schuler V, Heid J, Froestl W, Beck P, Mosbacher J, Bischoff S, Kulik A, Shigemoto R, Karschin A, Bettler B (1998) GABA(B)-receptor subtypes assemble into functional heteromeric complexes. Nature 396:683-687.

Keller BU, Konnerth A, Yaari Y (1991) Patch clamp analysis of excitatory synaptic currents in granule cells of rat hippocampus. J Physiol 435:275-293.

Kemp JA, Foster AC, Leeson PD, Priestley T, Tridgett R, Iversen LL, Woodruff GN (1988) 7-Chlorokynurenic acid is a selective antagonist at the glycine modulatory site of the N-methyl-D-aspartate receptor complex. Proc Natl Acad Sci U S A 85:6547-6550.

Kennedy MB (2000) Signal-processing machines at the postsynaptic density. Science 290:750-754.

Kennelly PJ, Krebs EG (1991) Consensus sequences as substrate specificity determinants for protein kinases and protein phosphatases. J Biol Chem 266:15555-15558.

Kidd FL, Isaac JT (2001) Kinetics and activation of postsynaptic kainate receptors at thalamocortical synapses: role of glutamate clearance. J Neurophysiol 86:1139-1148.

Kinney GA, Overstreet LS, Slater NT (1997) Prolonged physiological entrapment of glutamate in the synaptic cleft of cerebellar unipolar brush cells. J Neurophysiol 78:1320-1333.

Kirsch J, Wolters I, Triller A, Betz H (1993) Gephyrin antisense oligonucleotides prevent glycine receptor clustering in spinal neurons. Nature 366:745-748.

Kleckner NW, Dingledine R (1988) Requirement for glycine in activation of NMDA-receptors expressed in Xenopus oocytes. Science 241:835-837.

Kleckner NW, Dingledine R (1989) Selectivity of quinoxalines and kynurenines as antagonists of the glycine site on N-methyl-D-aspartate receptors. Mol Pharmacol 36:430-436.

Kneussel M, Helmut Brandstatter J, Gasnier B, Feng G, Sanes JR, Betz H (2001) Gephyrin-independent clustering of postsynaptic gaba(a) receptor subtypes. Mol Cell Neurosci 17:973-982.

Kneussel M, Haverkamp S, Fuhrmann JC, Wang H, Wassle H, Olsen RW, Betz H (2000) The gamma-aminobutyric acid type A receptor (GABAAR)-associated protein GABARAP interacts with gephyrin but is not involved in receptor anchoring at the synapse. Proc Natl Acad Sci U S A 97:8594-8599.

Kolb H (1979) The inner plexiform layer in the retina of the cat: electron microscopic observations. J Neurocytol 8:295-329.

Komuro H, Rakic P (1993) Modulation of neuronal migration by NMDA receptors. Science 260:95-97.

Kondo H, Toyoda J (1983) GABA and glycine effects on the bipolar cells of the carp retina. Vision Res 23:1259-1264.

Konnerth A, Llano I, Armstrong CM (1990) Synaptic currents in cerebellar Purkinje cells. Proc Natl Acad Sci U S A 87:2662-2665.

Koulen P, Brandstatter JH, Enz R, Bormann J, Wassle H (1998a) Synaptic clustering of GABA(C) receptor rho-subunits in the rat retina. Eur J Neurosci 10:115-127.

Koulen P, Brandstatter JH, Kroger S, Enz R, Bormann J, Wassle H (1997) Immunocytochemical localization of the GABA(C) receptor rho subunits in the cat, goldfish, and chicken retina. J Comp Neurol 380:520-532.

Koulen P, Malitschek B, Kuhn R, Bettler B, Wassle H, Brandstatter JH (1998b) Presynaptic and postsynaptic localization of GABA(B) receptors in neurons of the rat retina. Eur J Neurosci 10:1446-1456.

Kreitzer AC, Regehr WG (2000) Modulation of transmission during trains at a cerebellar synapse. J Neurosci 20:1348-1357.

Kreitzer AC, Regehr WG (2001) Retrograde Inhibition of Presynaptic Calcium Influx by Endogenous Cannabinoids at Excitatory Synapses onto Purkinje Cells. Neuron 29:717-727.

Krishek BJ, Moss SJ, Smart TG (1996) A functional comparison of the antagonists bicuculline and picrotoxin at recombinant $GABA_A$ receptors. Neuropharmacology 35:1289-1298.

Krupp JJ, Vissel B, Heinemann SF, Westbrook GL (1996) Calcium-dependent inactivation of recombinant N-methyl-D-aspartate receptors is NR2 subunit specific. Mol Pharmacol 50:1680-1688.

Krupp JJ, Vissel B, Thomas CG, Heinemann SF, Westbrook GL (1999) Interactions of calmodulin and alpha-actinin with the NR1 subunit modulate Ca^{2+}-dependent inactivation of NMDA receptors. J Neurosci 19:1165-1178.

Kuffler SW (1953) Discharge patterns and functional organization of mammalian retina. Journal of Neurophysiology 16:37-68.

Kusama T, Sakurai M, Kizawa Y, Uhl GR, Murakami H (1995) GABA rho1 receptor: inhibition by protein kinase C activators. Eur J Pharmacol 291:431-434.

Kyrozis A, Reichling DB (1995) Perforated-patch recording with gramicidin avoids artifactual changes in intracellular chloride concentration. J Neurosci Methods 57:27-35.

Laine J, Axelrad H (1996) Morphology of the Golgi-impregnated Lugaro cell in the rat cerebellar cortex: a reappraisal with a description of its axon. J Comp Neurol 375:618-640.

Laine J, Axelrad H (1998) Lugaro cells target basket and stellate cells in the cerebellar cortex. Neuroreport 9:2399-2403.

Landsend AS, Amiry-Moghaddam M, Matsubara A, Bergersen L, Usami S, Wenthold RJ, Ottersen OP (1997) Differential localization of delta glutamate receptors in the rat cerebellum: coexpression with AMPA receptors in parallel fiber-spine synapses and absence from climbing fiber-spine synapses. J Neurosci 17:834-842.

Langkopf A, Hammarback JA, Muller R, Vallee RB, Garner CC (1992) Microtubule-associated proteins 1A and LC2. Two proteins encoded in one messenger RNA. J Biol Chem 267:16561-16566.

Laube B, Kuhse J, Betz H (1998) Evidence for a tetrameric structure of recombinant NMDA receptors. J Neurosci 18:2954-2961.

Laube B, Hirai H, Sturgess M, Betz H, Kuhse J (1997) Molecular determinants of agonist discrimination by NMDA receptor subunits: analysis of the glutamate binding site on the NR2B subunit. Neuron 18:493-503.

Laurie DJ, Seeburg PH (1994) Regional and developmental heterogeneity in splicing of the rat brain NMDAR1 mRNA. J Neurosci 14:3180-3194.

Laurie DJ, Putzke J, Zieglgansberger W, Seeburg PH, Tolle TR (1995) The distribution of splice variants of the NMDAR1 subunit mRNA in adult rat brain. Brain Res Mol Brain Res 32:94-108.

Law R, Rothstein JD (2000) Identification and characterization of an excitatory amino acid 4 (EAAT-4) interacting protein. Society for Neuroscience 26:150.152.

Lehre KP, Danbolt NC (1998) The number of glutamate transporter subtype molecules at glutamatergic synapses: chemical and stereological quantification in young adult rat brain. J Neurosci 18:8751-8757.

Lehre KP, Levy LM, Ottersen OP, Storm-Mathisen J, Danbolt NC (1995) Differential expression of two glial glutamate transporters in the rat brain: quantitative and immunocytochemical observations. J Neurosci 15:1835-1853.

Lester RA, Jahr CE (1992) NMDA channel behavior depends on agonist affinity. J Neurosci 12:635-643.

Lester RA, Clements JD, Westbrook GL, Jahr CE (1990) Channel kinetics determine the time course of NMDA receptor-mediated synaptic currents. Nature 346:565-567.

Levy LM, Warr O, Attwell D (1998) Stoichiometry of the glial glutamate transporter GLT-1 expressed inducibly in a Chinese hamster ovary cell line selected for low endogenous Na^+-dependent glutamate uptake. J Neurosci 18:9620-9628.

Lim S, Naisbitt S, Yoon J, Hwang JI, Suh PG, Sheng M, Kim E (1999) Characterization of the Shank family of synaptic proteins. Multiple genes, alternative splicing, and differential expression in brain and development. J Biol Chem 274:29510-29518.

Lin CI, Orlov I, Ruggiero AM, Dykes-Hoberg M, Lee A, Jackson M, Rothstein JD (2001) Modulation of the neuronal glutamate transporter EAAC1 by the interacting protein GTRAP3-18. Nature 410:84-88.

Linberg KA, Fisher SK (1988) Ultrastructural evidence that horizontal cell axon terminals are presynaptic in the human retina. J Comp Neurol 268:281-297.

Liu G, Choi S, Tsien RW (1999) Variability of neurotransmitter concentration and nonsaturation of postsynaptic AMPA receptors at synapses in hippocampal cultures and slices. Neuron 22:395-409.

Llano I, Marty A, Armstrong CM, Konnerth A (1991) Synaptic- and agonist-induced excitatory currents of Purkinje cells in rat cerebellar slices. J Physiol 434:183-213.

Lomeli H, Sprengel R, Laurie DJ, Kohr G, Herb A, Seeburg PH, Wisden W (1993) The rat delta-1 and delta-2 subunits extend the excitatory amino acid receptor family. FEBS Lett 315:318-322.

Lomeli H, Mosbacher J, Melcher T, Hoger T, Geiger JR, Kuner T, Monyer H, Higuchi M, Bach A, Seeburg PH (1994) Control of kinetic properties of AMPA receptor channels by nuclear RNA editing. Science 266:1709-1713.

Lu J, Karadsheh M, Delpire E (1999) Developmental regulation of the neuronal-specific isoform of K-Cl cotransporter KCC2 in postnatal rat brains. J Neurobiol 39:558-568.

Luddens H, Wisden W (1991) Function and pharmacology of multiple $GABA_A$ receptor subunits. Trends Pharmacol Sci 12:49-51.

Luddens H, Korpi ER, Seeburg PH (1995) $GABA_A$/benzodiazepine receptor heterogeneity: neurophysiological implications. Neuropharmacology 34:245-254.

Lukasiewicz PD, Werblin FS (1994) A novel GABA receptor modulates synaptic transmission from bipolar to ganglion and amacrine cells in the tiger salamander retina. J Neurosci 14:1213-1223.

Lukasiewicz PD, Wong RO (1997) $GABA_C$ receptors on ferret retinal bipolar cells: a diversity of subtypes in mammals? Vis Neurosci 14:989-994.

Lukasiewicz PD, Shields CR (1998) Different combinations of $GABA_A$ and $GABA_C$ receptors confer distinct temporal properties to retinal synaptic responses. J Neurophysiol 79:3157-3167.

Lukasiewicz PD, Maple BR, Werblin FS (1994) A novel GABA receptor on bipolar cell terminals in the tiger salamander retina. J Neurosci 14:1202-1212.

Maejima T, Hashimoto K, Yoshida T, Aiba A, Kano M (2001) Presynaptic inhibition caused by retrograde signal from metabotropic glutamate to cannabinoid receptors. Neuron 31:463-475.

Mager S, Naeve J, Quick M, Labarca C, Davidson N, Lester HA (1993) Steady states, charge movements, and rates for a cloned GABA transporter expressed in Xenopus oocytes. Neuron 10:177-188.

Mainen ZF, Malinow R, Svoboda K (1999) Synaptic calcium transients in single spines indicate that NMDA receptors are not saturated. Nature 399:151-155.

Mano I, Teichberg VI (1998) A tetrameric subunit stoichiometry for a glutamate receptor-channel complex. Neuroreport 9:327-331.

Marc RE (1999) Kainate activation of horizontal, bipolar, amacrine, and ganglion cells in the rabbit retina. J Comp Neurol 407:65-76.

Marie H, Attwell D (1999) C-terminal interactions modulate the affinity of GLAST glutamate transporters in salamander retinal glial cells. J Physiol (Lond) 520 Pt 2:393-397.

Marie H, Billups D, Bedford F, Dumoulin A, Goyal RK, Longmore GD, Moss SJ, Attwell D (2002) The amino terminus of the glial glutamate transporter GLT-1 interacts with the LIM protein Ajuba. Molecular and Cellular Neuroscience in press.

Marr D (1969) A theory of cerebellar cortex. J Physiol 202:437-470.

Marr D, Hildreth E (1980) Theory of edge detection. Proc R Soc Lond B Biol Sci 207:187-217.

Marshall FH, Jones KA, Kaupmann K, Bettler B (1999) $GABA_B$ receptors - the first 7TM heterodimers. Trends Pharmacol Sci 20:396-399.

Martina M, Strata F, Cherubini E (1995) Whole cell and single channel properties of a new GABA receptor transiently expressed in the Hippocampus. J Neurophysiol 73:902-906.

Martina M, Royer S, Pare D (2001) Cell-Type-Specific GABA Responses and Chloride Homeostasis in the Cortex and Amygdala. J Neurophysiol 86:2887-2895.

Masland RH (2001a) The fundamental plan of the retina. Nat Neurosci 4:877-886.

Masland RH (2001b) Neuronal diversity in the retina. Curr Opin Neurobiol 11:431-436.

Masson J, Sagne C, Hamon M, El Mestikawy S (1999) Neurotransmitter transporters in the central nervous system. Pharmacol Rev 51:439-464.

Matsui K, Hosoi N, Tachibana M (1999) Active role of glutamate uptake in the synaptic transmission from retinal nonspiking neurons. J Neurosci 19:6755-6766.

Matsui K, Hasegawa J, Tachibana M (2001) Modulation of excitatory synaptic transmission by GABA(C) receptor- mediated feedback in the mouse inner retina. J Neurophysiol 86:2285-2298.

Matsui T, Sekiguchi M, Hashimoto A, Tomita U, Nishikawa T, Wada K (1995) Functional comparison of D-serine and glycine in rodents: the effect on cloned NMDA receptors and the extracellular concentration. J Neurochem 65:454-458.

Matthews G, Ayoub GS, Heidelberger R (1994) Presynaptic inhibition by GABA is mediated via two distinct GABA receptors with novel pharmacology. J Neurosci 14:1079-1090.

Mayat E, Petralia RS, Wang YX, Wenthold RJ (1995) Immunoprecipitation, immunoblotting, and immunocytochemistry studies suggest that glutamate receptor delta subunits form novel postsynaptic receptor complexes. J Neurosci 15:2533-2546.

Mayer ML, Westbrook GL (1987a) The physiology of excitatory amino acids in the vertebrate central nervous system. Prog Neurobiol 28:197-276.

Mayer ML, Westbrook GL (1987b) Permeation and block of N-methyl-D-aspartic acid receptor channels by divalent cations in mouse cultured central neurones. J Physiol 394:501-527.

Mayer ML, Westbrook GL, Guthrie PB (1984) Voltage-dependent block by Mg^{2+} of NMDA responses in spinal cord neurones. Nature 309:261-263.

McBain CJ, Mayer ML (1994) N-methyl-D-aspartic acid receptor structure and function. Physiol Rev 74:723-760.

Mennerick S, Dhond RP, Benz A, Xu W, Rothstein JD, Danbolt NC, Isenberg KE, Zorumski CF (1998) Neuronal expression of the glutamate transporter GLT-1 in hippocampal microcultures. J Neurosci 18:4490-4499.

Meyer G, Kirsch J, Betz H, Langosch D (1995) Identification of a gephyrin binding motif on the glycine receptor beta subunit. Neuron 15:563-572.

Meyer T, Munch C, Knappenberger B, Liebau S, Volkel H, Ludolph AC (1998) Alternative splicing of the glutamate transporter EAAT2 (GLT-1). Neurosci Lett 241:68-70.

Michaelis EK (1998) Molecular biology of glutamate receptors in the central nervous system and their role in excitotoxicity, oxidative stress and aging. Prog Neurobiol 54:369-415.

Miller B, Sarantis M, Traynelis SF, Attwell D (1992) Potentiation of NMDA receptor currents by arachidonic acid. Nature 355:722-725.

Miller HL, Peachey NS, McCall MA (2000) Construction and characterization of $GABA_C$/rho1/GFP transgenic and $GABA_C$/rho1 null-mice. Society for Neuroscience 26:248.242.

Mitchell SJ, Silver RA (2000a) GABA spillover from single inhibitory axons suppresses low-frequency excitatory transmission at the cerebellar glomerulus. J Neurosci 20:8651-8658.

Mitchell SJ, Silver RA (2000b) Glutamate spillover suppresses inhibition by activating presynaptic mGluRs. Nature 404:498-502.

Mitrovic AD, Plesko F, Vandenberg RJ (2001) Zn(2+) inhibits the anion conductance of the glutamate transporter EEAT4. J Biol Chem 276:26071-26076.

Mohler H, Fritschy JM (1999) $GABA_B$ receptors make it to the top--as dimers. Trends Pharmacol Sci 20:87-89.

Momiyama A, Feldmeyer D, Cull-Candy SG (1996) Identification of a native low-conductance NMDA channel with reduced sensitivity to Mg^{2+} in rat central neurones. J Physiol 494:479-492.

Monyer H, Seeburg PH, Wisden W (1991) Glutamate-operated channels: developmentally early and mature forms arise by alternative splicing. Neuron 6:799-810.

Monyer H, Burnashev N, Laurie DJ, Sakmann B, Seeburg PH (1994) Developmental and regional expression in the rat brain and functional properties of four NMDA receptors. Neuron 12:529-540.

Moriyoshi K, Masu M, Ishii T, Shigemoto R, Mizuno N, Nakanishi S (1991) Molecular cloning and characterization of the rat NMDA receptor. Nature 354:31-37.

Mosbacher J, Schoepfer R, Monyer H, Burnashev N, Seeburg PH, Ruppersberg JP (1994) A molecular determinant for submillisecond desensitization in glutamate receptors. Science 266:1059-1062.

Moss SJ, Smart TG (2001) Constructing inhibitory synapses. Nat Rev Neurosci 2:240-250.

Mothet JP, Parent AT, Wolosker H, Brady RO, Jr., Linden DJ, Ferris CD, Rogawski MA, Snyder SH (2000) D-serine is an endogenous ligand for the glycine site of the N-methyl-D- aspartate receptor. Proc Natl Acad Sci U S A 97:4926-4931.

Mugnaini E, Dino MR, Jaarsma D (1997) The unipolar brush cells of the mammalian cerebellum and cochlear nucleus: cytology and microcircuitry. Prog Brain Res 114:131-150.

Naisbitt S, Kim E, Tu JC, Xiao B, Sala C, Valtschanoff J, Weinberg RJ, Worley PF, Sheng M (1999) Shank, a novel family of postsynaptic density proteins that binds to the NMDA receptor/PSD-95/GKAP complex and cortactin. Neuron 23:569-582.

Nawy S (1999) The metabotropic receptor mGluR6 may signal through G(o), but not phosphodiesterase, in retinal bipolar cells. J Neurosci 19:2938-2944.

Nawy S, Jahr CE (1990) Suppression by glutamate of cGMP-activated conductance in retinal bipolar cells. Nature 346:269-271.

Nawy S, Jahr CE (1991) cGMP-gated conductance in retinal bipolar cells is suppressed by the photoreceptor transmitter. Neuron 7:677-683.

Neal MJ, Cunningham JR, James TA, Joseph M, Collins JF (1981) The effect of 2-amino-4-phosphonobutyrate (APB) on acetylcholine release from the rabbit retina: evidence for on-channel input to cholinergic amacrine cells. Neurosci Lett 26:301-305.

Nelson R, Famiglietti EV, Jr., Kolb H (1978) Intracellular staining reveals different levels of stratification for on- and off-center ganglion cells in cat retina. J Neurophysiol 41:472-483.

Nishi M, Hinds H, Lu HP, Kawata M, Hayashi Y (2001) Motoneuron-specific expression of NR3B, a novel NMDA-type glutamate receptor subunit that works in a dominant-negative manner. J Neurosci 21:RC185.

Nishimune A, Isaac JT, Molnar E, Noel J, Nash SR, Tagaya M, Collingridge GL, Nakanishi S, Henley JM (1998) NSF binding to GluR2 regulates synaptic transmission. Neuron 21:87-97.

Nistri A, Sivilotti L (1985) An unusual effect of gamma-aminobutyric acid on synaptic transmission of frog tectal neurones in vitro. Br J Pharmacol 85:917-921.

Noel J, Ralph GS, Pickard L, Williams J, Molnar E, Uney JB, Collingridge GL, Henley JM (1999) Surface expression of AMPA receptors in hippocampal neurons is regulated by an NSF-dependent mechanism. Neuron 23:365-376.

Nowak L, Bregestovski P, Ascher P, Herbet A, Prochiantz A (1984) Magnesium gates glutamate-activated channels in mouse central neurones. Nature 307:462-465.

Nunzi MG, Birnstiel S, Bhattacharyya BJ, Slater NT, Mugnaini E (2001) Unipolar brush cells form a glutamatergic projection system within the mouse cerebellar cortex. J Comp Neurol 434:329-341.

Ogurusu T, Shingai R (1996) Cloning of a putative gamma-aminobutyric acid (GABA) receptor subunit rho 3 cDNA. Biochim Biophys Acta 1305:15-18.

Ogurusu T, Taira H, Shingai R (1995) Identification of $GABA_A$ receptor subunits in rat retina: cloning of the rat $GABA_A$ receptor rho 2-subunit cDNA. J Neurochem 65:964-968.

Oliet SH, Piet R, Poulain DA (2001) Control of glutamate clearance and synaptic efficacy by glial coverage of neurons. Science 292:923-926.

Oliver MW, Kessler M, Larson J, Schottler F, Lynch G (1990) Glycine site associated with the NMDA receptor modulates long-term potentiation. Synapse 5:265-270.

Otis T, Zhang S, Trussell LO (1996a) Direct measurement of AMPA receptor desensitization induced by glutamatergic synaptic transmission. J Neurosci 16:7496-7504.

Otis TS, Jahr CE (1998) Anion currents and predicted glutamate flux through a neuronal glutamate transporter. J Neurosci 18:7099-7110.

Otis TS, Kavanaugh MP (2000) Isolation of current components and partial reaction cycles in the glial glutamate transporter EAAT2. J Neurosci 20:2749-2757.

Otis TS, Wu YC, Trussell LO (1996b) Delayed clearance of transmitter and the role of glutamate transporters at synapses with multiple release sites. J Neurosci 16:1634-1644.

Otis TS, Kavanaugh MP, Jahr CE (1997) Postsynaptic glutamate transport at the climbing fiber-Purkinje cell synapse. Science 277:1515-1518.

Overstreet LS, Kinney GA, Liu YB, Billups D, Slater NT (1999) Glutamate transporters contribute to the time course of synaptic transmission in cerebellar granule cells. J Neurosci 19:9663-9673.

Owens DF, Boyce LH, Davis MB, Kriegstein AR (1996) Excitatory GABA responses in embryonic and neonatal cortical slices demonstrated by gramicidin perforated-patch recordings and calcium imaging. J Neurosci 16:6414-6423.

Ozawa S, Kamiya H, Tsuzuki K (1998) Glutamate receptors in the mammalian central nervous system. Prog Neurobiol 54:581-618.

Palay SL, Chan-Palay V (1974) Cerebellar Cortex: Cytology and Organization: Springer Verlag.

Pan ZH, Lipton SA (1995) Multiple GABA receptor subtypes mediate inhibition of calcium influx at rat retinal bipolar cell terminals. J Neurosci 15:2668-2679.

Pan ZH, Zhang D, Zhang X, Lipton SA (2000) Evidence for coassembly of mutant $GABA_C$ rho1 with $GABA_A$ gamma2S, glycine alpha1 and glycine alpha2 receptor subunits in vitro [In Process Citation]. Eur J Neurosci 12:3137-3145.

Pasternack M, Boller M, Pau B, Schmidt M (1999) GABA(A) and GABA(C) receptors have contrasting effects on excitability in superior colliculus. J Neurophysiol 82:2020-2023.

Patneau DK, Mayer ML (1990) Structure-activity relationships for amino acid transmitter candidates acting at N-methyl-D-aspartate and quisqualate receptors. J Neurosci 10:2385-2399.

Pattnaik B, Jellali A, Sahel J, Dreyfus H, Picaud S (2000) $GABA_C$ receptors are localized with microtubule-associated protein 1B in mammalian cone photoreceptors. J Neurosci 20:6789-6796.

Payne JA (1997) Functional characterization of the neuronal-specific K-Cl cotransporter: implications for $[K^+]_o$ regulation. Am J Physiol 273:C1516-1525.

Payne JA, Stevenson TJ, Donaldson LF (1996) Molecular characterization of a putative K-Cl cotransporter in rat brain. A neuronal-specific isoform. J Biol Chem 271:16245-16252.

Pedrotti B, Ulloa L, Avila J, Islam K (1996) Characterization of microtubule-associated protein MAP1B: phosphorylation state, light chains, and binding to microtubules. Biochemistry 35:3016-3023.

Peghini P, Janzen J, Stoffel W (1997) Glutamate transporter EAAC-1-deficient mice develop dicarboxylic aminoaciduria and behavioral abnormalities but no neurodegeneration. Embo J 16:3822-3832.

Perez-Otano I, Schulteis CT, Contractor A, Lipton SA, Trimmer JS, Sucher NJ, Heinemann SF (2001) Assembly with the NR1 subunit is required for surface expression of NR3A-containing NMDA receptors. J Neurosci 21:1228-1237.

Perkel DJ, Hestrin S, Sah P, Nicoll RA (1990) Excitatory synaptic currents in Purkinje cells. Proc R Soc Lond B Biol Sci 241:116-121.

Peters S, Koh J, Choi DW (1987) Zinc selectively blocks the action of N-methyl-D-aspartate on cortical neurons. Science 236:589-593.

Picaud SA, Larsson HP, Grant GB, Lecar H, Werblin FS (1995) Glutamate-gated chloride channel with glutamate-transporter-like properties in cone photoreceptors of the tiger salamander. J Neurophysiol 74:1760-1771.

Pines G, Danbolt NC, Bjoras M, Zhang Y, Bendahan A, Eide L, Koepsell H, Storm-Mathisen J, Seeberg E, Kanner BI (1992) Cloning and expression of a rat brain L-glutamate transporter. Nature 360:464-467.

Plachez C, Danbolt NC, Recasens M (2000) Transient expression of the glial glutamate transporters GLAST and GLT in hippocampal neurons in primary culture. J Neurosci Res 59:587-593.

Plotkin MD, Snyder EY, Hebert SC, Delpire E (1997) Expression of the Na-K-2Cl cotransporter is developmentally regulated in postnatal rat brains: a possible mechanism underlying GABA's excitatory role in immature brain. J Neurobiol 33:781-795.

Polenzani L, Woodward RM, Miledi R (1991) Expression of mammalian gamma-aminobutyric acid receptors with distinct pharmacology in Xenopus oocytes. Proc Natl Acad Sci U S A 88:4318-4322.

Pow DV, Hendrickson AE (1999) Distribution of the glycine transporter glyt-1 in mammalian and nonmammalian retinae. Vis Neurosci 16:231-239.

Pow DV, Barnett NL (2000) Developmental expression of excitatory amino acid transporter 5: a photoreceptor and bipolar cell glutamate transporter in rat retina. Neurosci Lett 280:21-24.

Premkumar LS, Auerbach A (1997) Stoichiometry of recombinant N-methyl-D-aspartate receptor channels inferred from single-channel current patterns. J Gen Physiol 110:485-502.

Prybylowski K, Rumbaugh G, Wolfe BB, Vicini S (2000) Increased exon 5 expression alters extrasynaptic NMDA receptors in cerebellar neurons. J Neurochem 75:1140-1146.

Qian H, Dowling JE (1993) Novel GABA responses from rod-driven retinal horizontal cells. Nature 361:162-164.

Qian H, Dowling JE (1995) $GABA_A$ and $GABA_C$ receptors on hybrid bass retinal bipolar cells. J Neurophysiol 74:1920-1928.

Qian H, Ripps H (1999) Response kinetics and pharmacological properties of heteromeric receptors formed by coassembly of GABA rho- and gamma 2-subunits. Proc R Soc Lond B Biol Sci 266:2419-2425.

Qian H, Ripps H (2001) The $GABA_C$ receptors of retinal neurons. Prog Brain Res 131:295-308.

Qin P, Pourcho RG (2001) Immunocytochemical localization of kainate-selective glutamate receptor subunits GluR5, GluR6, and GluR7 in the cat retina. Brain Res 890:211-221.

Rae J, Cooper K, Gates P, Watsky M (1991) Low access resistance perforated patch recordings using amphotericin B. J Neurosci Methods 37:15-26.

Ragozzino D, Woodward RM, Murata Y, Eusebi F, Overman LE, Miledi R (1996) Design and in vitro pharmacology of a selective gamma-aminobutyric acidC receptor antagonist. Mol Pharmacol 50:1024-1030.

Raman IM, Trussell LO (1992) The kinetics of the response to glutamate and kainate in neurons of the avian cochlear nucleus. Neuron 9:173-186.

Rauen T (2000) Diversity of glutamate transporter expression and function in the mammalian retina. Amino Acids 19:53-62.

Rauen T, Kanner BI (1994) Localization of the glutamate transporter GLT-1 in rat and macaque monkey retinae. Neurosci Lett 169:137-140.

Rauen T, Rothstein JD, Wassle H (1996) Differential expression of three glutamate transporter subtypes in the rat retina. Cell Tissue Res 286:325-336.

Regehr WG, Atluri PP (1995) Calcium transients in cerebellar granule cell presynaptic terminals. Biophys J 68:2156-2170.

Reichling DB, Kyrozis A, Wang J, MacDermott AB (1994) Mechanisms of GABA and glycine depolarization-induced calcium transients in rat dorsal horn neurons. J Physiol 476:411-421.

Risso S, DeFelice LJ, Blakely RD (1996) Sodium-dependent GABA-induced currents in GAT1-transfected HeLa cells. J Physiol 490:691-702.

Rivera C, Wegelius K, Reeben M, Kaila K, Michael P (2000) Different sensitivities of human and rat rho(1) GABA receptors to extracellular pH. Neuropharmacology 39:977-989.

Rivera C, Voipio J, Payne JA, Ruusuvuori E, Lahtinen H, Lamsa K, Pirvola U, Saarma M, Kaila K (1999) The K^+/Cl^- co-transporter KCC2 renders GABA hyperpolarizing during neuronal maturation. Nature 397:251-255.

Robert A, Irizarry SN, Hughes TE, Howe JR (2001) Subunit interactions and AMPA receptor desensitization. J Neurosci 21:5574-5586.

Rosenmund C, Westbrook GL (1993a) Rundown of N-methyl-D-aspartate channels during whole-cell recording in rat hippocampal neurons: role of Ca^{2+} and ATP. J Physiol 470:705-729.

Rosenmund C, Westbrook GL (1993b) Calcium-induced actin depolymerization reduces NMDA channel activity. Neuron 10:805-814.

Rosenmund C, Legendre P, Westbrook GL (1992) Expression of NMDA channels on cerebellar Purkinje cells acutely dissociated from newborn rats. J Neurophysiol 68:1901-1905.

Rosenmund C, Stern-Bach Y, Stevens CF (1998) The tetrameric structure of a glutamate receptor channel. Science 280:1596-1599.

Roska B, Werblin F (2001) Vertical interactions across ten parallel, stacked representations in the mammalian retina. Nature 410:583-587.

Roska B, Gaal L, Werblin FS (1998) Voltage-dependent uptake is a major determinant of glutamate concentration at the cone synapse: an analytical study. J Neurophysiol 80:1951-1960.

Roska B, Nemeth E, Orzo L, Werblin FS (2000) Three levels of lateral inhibition: A space-time study of the retina of the tiger salamander. J Neurosci 20:1941-1951.

Rossi DJ, Slater NT (1993) The developmental onset of NMDA receptor-channel activity during neuronal migration. Neuropharmacology 32:1239-1248.

Rossi DJ, Oshima T, Attwell D (2000) Glutamate release in severe brain ischaemia is mainly by reversed uptake. Nature 403:316-321.

Rossi DJ, Alford S, Mugnaini E, Slater NT (1995) Properties of transmission at a giant glutamatergic synapse in cerebellum: the mossy fiber-unipolar brush cell synapse. J Neurophysiol 74:24-42.

rossi P, D'Angelo E, Taglietti V (1996) Differential long-lasting potentiation of the NMDA and non-NMDA synaptic currents induced by metabotropic and NMDA receptor coactivation in cerebellar granule cells. Eur J Neurosci 8:1182-1189.

Rothstein JD, Martin L, Levey AI, Dykes-Hoberg M, Jin L, Wu D, Nash N, Kuncl RW (1994) Localization of neuronal and glial glutamate transporters. Neuron 13:713-725.

Rothstein JD, Dykes-Hoberg M, Pardo CA, Bristol LA, Jin L, Kuncl RW, Kanai Y, Hediger MA, Wang Y, Schielke JP, Welty DF (1996) Knockout of glutamate transporters reveals a major role for astroglial transport in excitotoxicity and clearance of glutamate. Neuron 16:675-686.

Roux MJ, Supplisson S (2000) Neuronal and glial glycine transporters have different stoichiometries. Neuron 25:373-383.

Ruiz M, Egal H, Sarthy V, Qian X, Sarkar HK (1994) Cloning, expression, and localization of a mouse retinal gamma- aminobutyric acid transporter. Invest Ophthalmol Vis Sci 35:4039-4048.

Rumbaugh G, Vicini S (1999) Distinct synaptic and extrasynaptic NMDA receptors in developing cerebellar granule neurons. J Neurosci 19:10603-10610.

Rumbaugh G, Prybylowski K, Wang JF, Vicini S (2000) Exon 5 and spermine regulate deactivation of NMDA receptor subtypes. J Neurophysiol 83:1300-1306.

Russell JM (2000) Sodium-potassium-chloride cotransport. Physiol Rev 80:211-276.

Sabatini BL, Regehr WG (1996) Timing of neurotransmission at fast synapses in the mammalian brain. Nature 384:170-172.

Salin PA, Malenka RC, Nicoll RA (1996) Cyclic AMP mediates a presynaptic form of LTP at cerebellar parallel fiber synapses. Neuron 16:797-803.

Sarantis M, Everett K, Attwell D (1988) A presynaptic action of glutamate at the cone output synapse. Nature 332:451-453.

Sarantis M, Ballerini L, Miller B, Silver RA, Edwards M, Attwell D (1993) Glutamate uptake from the synaptic cleft does not shape the decay of the non-NMDA component of the synaptic current. Neuron 11:541-549.

Sather W, Johnson JW, Henderson G, Ascher P (1990) Glycine-insensitive desensitization of NMDA responses in cultured mouse embryonic neurons. Neuron 4:725-731.

Satoh H, Kaneda M, Kaneko A (2001) Intracellular chloride concentration is higher in rod bipolar cells than in cone bipolar cells of the mouse retina. Neurosci Lett 310:161-164.

Sato-Yoshitake R, Shiomura Y, Miyasaka H, Hirokawa N (1989) Microtubule-associated protein 1B: molecular structure, localization, and phosphorylation-dependent expression in developing neurons. Neuron 3:229-238.

Schell MJ, Molliver ME, Snyder SH (1995) D-serine, an endogenous synaptic modulator: localization to astrocytes and glutamate-stimulated release. Proc Natl Acad Sci U S A 92:3948-3952.

Schell MJ, Brady RO, Jr., Molliver ME, Snyder SH (1997) D-serine as a neuromodulator: regional and developmental localizations in rat brain glia resemble NMDA receptors. J Neurosci 17:1604-1615.

Schlag BD, Vondrasek JR, Munir M, Kalandadze A, Zelenaia OA, Rothstein JD, Robinson MB (1998) Regulation of the glial Na+-dependent glutamate transporters by cyclic AMP analogs and neurons. Mol Pharmacol 53:355-369.

Schmidt M, Boller M, Ozen G, Hall WC (2001) Disinhibition in rat superior colliculus mediated by $GABA_C$ receptors. J Neurosci 21:691-699.

Schmitt A, Asan E, Lesch KP, Kugler P (2002) A splice variant of glutamate transporter GLT1/EAAT2 expressed in neurons: cloning and localization in rat nervous system. Neuroscience 109:45-61.

Schoenfeld TA, McKerracher L, Obar R, Vallee RB (1989) MAP 1A and MAP 1B are structurally related microtubule associated proteins with distinct developmental patterns in the CNS. J Neurosci 9:1712-1730.

Schwartz EA (1982) Calcium-independent release of GABA from isolated horizontal cells of the toad retina. J Physiol 323:211-227.

Seal RP, Amara SG (1998) A reentrant loop domain in the glutamate carrier EAAT1 participates in substrate binding and translocation. Neuron 21:1487-1498.

Seal RP, Leighton BH, Amara SG (2000) A model for the topology of excitatory amino acid transporters determined by the extracellular accessibility of substituted cysteines. Neuron 25:695-706.

Sheng M (2001a) The postsynaptic NMDA-receptor?PSD-95 signaling complex in excitatory synapses of the brain. J Cell Sci 114:1251-1252.

Sheng M (2001b) Molecular organization of the postsynaptic specialization. Proc Natl Acad Sci U S A 98:7058-7061.

Sheng M, Pak DT (2000) Ligand-gated ion channel interactions with cytoskeletal and signaling proteins. Annu Rev Physiol 62:755-778.

Sheng M, Kim E (2000) The Shank family of scaffold proteins. J Cell Sci 113:1851-1856.

Sheng M, Lee SH (2000) Growth of the NMDA receptor industrial complex. Nat Neurosci 3:633-635.

Sheng M, Sala C (2001) Pdz domains and the organization of supramolecular complexes. Annu Rev Neurosci 24:1-29.

Sheng M, Cummings J, Roldan LA, Jan YN, Jan LY (1994) Changing subunit composition of heteromeric NMDA receptors during development of rat cortex. Nature 368:144-147.

Shepherd GM (1998) The synaptic organization of the brain, 4 Edition: Oxford University Press.

Shields CR, Tran MN, Wong RO, Lukasiewicz PD (2000) Distinct ionotropic GABA receptors mediate presynaptic and postsynaptic inhibition in retinal bipolar cells. J Neurosci 20:2673-2682.

Shiells RA, Falk G (1990) Glutamate receptors of rod bipolar cells are linked to a cyclic GMP cascade via a G-protein. Proc R Soc Lond B Biol Sci 242:91-94.

Shimada S, Cutting G, Uhl GR (1992) gamma-Aminobutyric acid A or C receptor? gamma-Aminobutyric acid rho 1 receptor RNA induces bicuculline-, barbiturate-, and benzodiazepine- insensitive gamma-aminobutyric acid responses in Xenopus oocytes. Mol Pharmacol 41:683-687.

Shimamoto K, Lebrun B, Yasuda-Kamatani Y, Sakaitani M, Shigeri Y, Yumoto N, Nakajima T (1998) DL-threo-beta-benzyloxyaspartate, a potent blocker of excitatory amino acid transporters. Mol Pharmacol 53:195-201.

Shingai R, Yanagi K, Fukushima T, Sakata K, Ogurusu T (1996) Functional expression of GABA rho 3 receptors in Xenopus oocytes. Neurosci Res 26:387-390.

Sieghart W, Fuchs K, Tretter V, Ebert V, Jechlinger M, Hoger H, Adamiker D (1999) Structure and subunit composition of GABA(A) receptors. Neurochem Int 34:379-385.

Silver RA, Traynelis SF, Cull-Candy SG (1992) Rapid-time-course miniature and evoked excitatory currents at cerebellar synapses in situ. Nature 355:163-166.

Silver RA, Cull-Candy SG, Takahashi T (1996a) Non-NMDA glutamate receptor occupancy and open probability at a rat cerebellar synapse with single and multiple release sites. J Physiol 494:231-250.

Silver RA, Colquhoun D, Cull-Candy SG, Edmonds B (1996b) Deactivation and desensitization of non-NMDA receptors in patches and the time course of EPSCs in rat cerebellar granule cells. J Physiol 493:167-173.

Sims KD, Straff DJ, Robinson MB (2000) Platelet-derived growth factor rapidly increases activity and cell surface expression of the EAAC1 subtype of glutamate transporter through activation of phosphatidylinositol 3-kinase. J Biol Chem 275:5228-5237.

Sivilotti L, Nistri A (1989) Pharmacology of a novel effect of gamma-aminobutyric acid on the frog optic tectum in vitro. Eur J Pharmacol 164:205-212.

Slater NT, Rossi DJ, Kinney GA (1997) Physiology of transmission at a giant glutamatergic synapse in cerebellum. Prog Brain Res 114:151-163.

Slaughter MM, Miller RF (1981) 2-amino-4-phosphonobutyric acid: a new pharmacological tool for retina research. Science 211:182-185.

Slaughter MM, Miller RF (1983) The role of excitatory amino acid transmitters in the mudpuppy retina: an analysis with kainic acid and N-methyl aspartate. J Neurosci 3:1701-1711.

Slaughter MM, Miller RF (1985) Characterization of an extended glutamate receptor of the on bipolar neuron in the vertebrate retina. J Neurosci 5:224-233.

Smith KE, Borden LA, Hartig PR, Branchek T, Weinshank RL (1992) Cloning and expression of a glycine transporter reveal colocalization with NMDA receptors. Neuron 8:927-935.

Smith TC, Howe JR (2000) Concentration-dependent substate behavior of native AMPA receptors. Nat Neurosci 3:992-997.

Sommer B, Kohler M, Sprengel R, Seeburg PH (1991) RNA editing in brain controls a determinant of ion flow in glutamate- gated channels. Cell 67:11-19.

Sommer B, Keinanen K, Verdoorn TA, Wisden W, Burnashev N, Herb A, Kohler M, Takagi T, Sakmann B, Seeburg PH (1990) Flip and flop: a cell-specific functional switch in glutamate-operated channels of the CNS. Science 249:1580-1585.

Southan AP, Robertson B (1998) Patch-clamp recordings from cerebellar basket cell bodies and their presynaptic terminals reveal an asymmetric distribution of voltage- gated potassium channels. J Neurosci 18:948-955.

Spiridon M, Kamm D, Billups B, Mobbs P, Attwell D (1998) Modulation by zinc of the glutamate transporters in glial cells and cones isolated from the tiger salamander retina. J Physiol (Lond) 506:363-376.

Srivastava S, Ziff EB (1999) ABP: a novel AMPA receptor binding protein. Ann N Y Acad Sci 868:561-564.

Srivastava S, Osten P, Vilim FS, Khatri L, Inman G, States B, Daly C, DeSouza S, Abagyan R, Valtschanoff JG, Weinberg RJ, Ziff EB (1998) Novel anchorage of GluR2/3 to the postsynaptic density by the AMPA receptor-binding protein ABP. Neuron 21:581-591.

Staley KJ, Soldo BL, Proctor WR (1995) Ionic mechanisms of neuronal excitation by inhibitory $GABA_A$ receptors. Science 269:977-981.

Steinberg RH, Oakley B, 2nd, Niemeyer G (1980) Light-evoked changes in $[K^+]_o$ in retina of intact cat eye. J Neurophysiol 44:897-921.

Stern P, Behe P, Schoepfer R, Colquhoun D (1992) Single-channel conductances of NMDA receptors expressed from cloned cDNAs: comparison with native receptors. Proc R Soc Lond B Biol Sci 250:271-277.

Stone S, Schutte M (1991) Physiological and morphological properties of off- and on-center bipolar cells in the Xenopus retina: effects of glycine and GABA. Vis Neurosci 7:363-376.

Storck T, Schulte S, Hofmann K, Stoffel W (1992) Structure, expression, and functional analysis of a $Na(^+)$-dependent glutamate/aspartate transporter from rat brain. Proc Natl Acad Sci U S A 89:10955-10959.

Strata F, Cherubini E (1994) Transient expression of a novel type of GABA response in rat CA3 hippocampal neurones during development. J Physiol 480:493-503.

Strettoi E, Dacheux RF, Raviola E (1990) Synaptic connections of rod bipolar cells in the inner plexiform layer of the rabbit retina. J Comp Neurol 295:449-466.

Strettoi E, Raviola E, Dacheux RF (1992) Synaptic connections of the narrow-field, bistratified rod amacrine cell (AII) in the rabbit retina. J Comp Neurol 325:152-168.

Strettoi E, Dacheux RF, Raviola E (1994) Cone bipolar cells as interneurons in the rod pathway of the rabbit retina. J Comp Neurol 347:139-149.

Sucher NJ, Akbarian S, Chi CL, Leclerc CL, Awobuluyi M, Deitcher DL, Wu MK, Yuan JP, Jones EG, Lipton SA (1995) Developmental and regional expression pattern of a novel NMDA receptor- like subunit (NMDAR-L) in the rodent brain. J Neurosci 15:6509-6520.

Sung KW, Kirby M, McDonald MP, Lovinger DM, Delpire E (2000) Abnormal $GABA_A$ receptor-mediated currents in dorsal root ganglion neurons isolated from Na-K-2Cl cotransporter null mice. J Neurosci 20:7531-7538.

Supplisson S, Bergman C (1997) Control of NMDA receptor activation by a glycine transporter co-expressed in Xenopus oocytes. J Neurosci 17:4580-4590.

Swanson RA, Liu J, Miller JW, Rothstein JD, Farrell K, Stein BA, Longuemare MC (1997) Neuronal regulation of glutamate transporter subtype expression in astrocytes. J Neurosci 17:932-940.

Szatkowski M, Attwell D (1994) Triggering and execution of neuronal death in brain ischaemia: two phases of glutamate release by different mechanisms. Trends Neurosci 17:359-365.

Szatkowski M, Barbour B, Attwell D (1990) Non-vesicular release of glutamate from glial cells by reversed electrogenic glutamate uptake. Nature 348:443-446.

Tachibana M, Kaneko A (1987) gamma-Aminobutyric acid exerts a local inhibitory action on the axon terminal of bipolar cells: evidence for negative feedback from amacrine cells. Proc Natl Acad Sci U S A 84:3501-3505.

Takahashi K, Miyoshi S, Kaneko A, Copenhagen DR (1995a) Actions of nipecotic acid and SKF89976A on GABA transporter in cone- driven horizontal cells dissociated from the catfish retina. Jpn J Physiol 45:457-473.

Takahashi M, Kovalchuk Y, Attwell D (1995b) Pre- and postsynaptic determinants of EPSC waveform at cerebellar climbing fiber and parallel fiber to Purkinje cell synapses. J Neurosci 15:5693-5702.

Takahashi M, Sarantis M, Attwell D (1996a) Postsynaptic glutamate uptake in rat cerebellar Purkinje cells. J Physiol (Lond) 497:523-530.

Takahashi T, Feldmeyer D, Suzuki N, Onodera K, Cull-Candy SG, Sakimura K, Mishina M (1996b) Functional correlation of NMDA receptor epsilon subunits expression with the properties of single-channel and synaptic currents in the developing cerebellum. J Neurosci 16:4376-4382.

Takechi H, Eilers J, Konnerth A (1998) A new class of synaptic response involving calcium release in dendritic spines. Nature 396:757-760.

Takei Y, Teng J, Harada A, Hirokawa N (2000) Defects in axonal elongation and neuronal migration in mice with disrupted tau and map1b genes. J Cell Biol 150:989-1000.

Takei Y, Kondo S, Harada A, Inomata S, Noda T, Hirokawa N (1997) Delayed development of nervous system in mice homozygous for disrupted microtubule-associated protein 1B (MAP1B) gene. J Cell Biol 137:1615-1626.

Tanaka K, Watase K, Manabe T, Yamada K, Watanabe M, Takahashi K, Iwama H, Nishikawa T, Ichihara N, Kikuchi T, Okuyama S, Kawashima N, Hori S, Takimoto M, Wada K (1997) Epilepsy and exacerbation of brain injury in mice lacking the glutamate transporter GLT-1. Science 276:1699-1702.

Tang CM, Dichter M, Morad M (1990) Modulation of the N-methyl-D-aspartate channel by extracellular H+. Proc Natl Acad Sci U S A 87:6445-6449.

Tang CM, Margulis M, Shi QY, Fielding A (1994) Saturation of postsynaptic glutamate receptors after quantal release of transmitter. Neuron 13:1385-1393.

Tempia F, Miniaci MC, Anchisi D, Strata P (1998) Postsynaptic current mediated by metabotropic glutamate receptors in cerebellar Purkinje cells. J Neurophysiol 80:520-528.

Tempia F, Alojado ME, Strata P, Knopfel T (2001) Characterization of the mGluR(1)-Mediated Electrical and Calcium Signaling in Purkinje Cells of Mouse Cerebellar Slices. J Neurophysiol 86:1389-1397.

Tessier-Lavigne M, Attwell D, Mobbs P, Wilson M (1988) Membrane currents in retinal bipolar cells of the axolotl. J Gen Physiol 91:49-72.

Thompson SM, Deisz RA, Prince DA (1988) Relative contributions of passive equilibrium and active transport to the distribution of chloride in mammalian cortical neurons. J Neurophysiol 60:105-124.

Thomson AM, Walker VE, Flynn DM (1989) Glycine enhances NMDA-receptor mediated synaptic potentials in neocortical slices. Nature 338:422-424.

Tian N, Slaughter MM (1994) Pharmacological similarity between the retinal APB receptor and the family of metabotropic glutamate receptors. J Neurophysiol 71:2258-2268.

Tong G, Jahr CE (1994a) Block of glutamate transporters potentiates postsynaptic excitation. Neuron 13:1195-1203.

Tong G, Jahr CE (1994b) Multivesicular release from excitatory synapses of cultured hippocampal neurons. Neuron 12:51-59.

Traynelis SF, Cull-Candy SG (1990) Proton inhibition of N-methyl-D-aspartate receptors in cerebellar neurons. Nature 345:347-350.

Trotti D, Rizzini BL, Rossi D, Haugeto O, Racagni G, Danbolt NC, Volterra A (1997) Neuronal and glial glutamate transporters possess an SH-based redox regulatory mechanism. Eur J Neurosci 9:1236-1243.

Trussell LO, Fischbach GD (1989) Glutamate receptor desensitization and its role in synaptic transmission. Neuron 3:209-218.

Trussell LO, Zhang S, Raman IM (1993) Desensitization of AMPA receptors upon multiquantal neurotransmitter release. Neuron 10:1185-1196.

Tu JC, Xiao B, Naisbitt S, Yuan JP, Petralia RS, Brakeman P, Doan A, Aakalu VK, Lanahan AA, Sheng M, Worley PF (1999) Coupling of mGluR/Homer and PSD-95 complexes by the Shank family of postsynaptic density proteins. Neuron 23:583-592.

Tucker RP, Garner CC, Matus A (1989) In situ localization of microtubule-associated protein mRNA in the developing and adult rat brain. Neuron 2:1245-1256.

Turecek R, Trussell LO (2000) Control of synaptic depression by glutamate transporters. J Neurosci 20:2054-2063.

Ullensvang K, Lehre KP, Storm-Mathisen J, Danbolt NC (1997) Differential developmental expression of the two rat brain glutamate transporter proteins GLAST and GLT. Eur J Neurosci 9:1646-1655.

Vandenberg RJ, Mitrovic AD, Johnston GA (1998) Molecular basis for differential inhibition of glutamate transporter subtypes by zinc ions. Mol Pharmacol 54:189-196.

Vardi N, Sterling P (1994) Subcellular localization of $GABA_A$ receptor on bipolar cells in macaque and human retina. Vision Res 34:1235-1246.

Vardi N, Morigiwa K (1997) ON cone bipolar cells in rat express the metabotropic receptor mGluR6. Vis Neurosci 14:789-794.

Vardi N, Zhang LL, Payne JA, Sterling P (2000a) Evidence that different cation chloride cotransporters in retinal neurons allow opposite responses to GABA. J Neurosci 20:7657-7663.

Vardi N, Duvoisin R, Wu G, Sterling P (2000b) Localization of mGluR6 to dendrites of ON bipolar cells in primate retina. J Comp Neurol 423:402-412.

Verdoorn TA, Burnashev N, Monyer H, Seeburg PH, Sakmann B (1991) Structural determinants of ion flow through recombinant glutamate receptor channels. Science 252:1715-1718.

Vetter P, Garthwaite J, Batchelor AM (1999) Regulation of synaptic transmission in the mossy fibre-granule cell pathway of rat cerebellum by metabotropic glutamate receptors. Neuropharmacology 38:805-815.

Vicini S, Wang JF, Li JH, Zhu WJ, Wang YH, Luo JH, Wolfe BB, Grayson DR (1998) Functional and pharmacological differences between recombinant N-methyl- D-aspartate receptors. J Neurophysiol 79:555-566.

Volterra A, Bezzi P, Rizzini BL, Trotti D, Ullensvang K, Danbolt NC, Racagni G (1996) The competitive transport inhibitor L-trans-pyrrolidine-2, 4- dicarboxylate triggers excitotoxicity in rat cortical neuron-astrocyte co-cultures via glutamate release rather than uptake inhibition. Eur J Neurosci 8:2019-2028.

Vu TQ, Payne JA, Copenhagen DR (2000) Localization and developmental expression patterns of the neuronal K-Cl cotransporter (KCC2) in the rat retina. J Neurosci 20:1414-1423.

Vyklicky L, Jr., Benveniste M, Mayer ML (1990) Modulation of N-methyl-D-aspartic acid receptor desensitization by glycine in mouse cultured hippocampal neurones. J Physiol 428:313-331.

Wachtmann D, Koerner M, Stoffel W, Keller B (2000) Excitatory synaptic transmission in cerebellar Purkinje cells od defined glutamate transporter knock-out mice. Eur J Neurosci Suppl (FENS meeting 2000, UK) 12.

Wadiche JI, Jahr CE (2001) Multivesicular release at climbing fiber-Purkinje cell synapses. Neuron 32:301-313.

Wadiche JI, Amara SG, Kavanaugh MP (1995a) Ion fluxes associated with excitatory amino acid transport. Neuron 15:721-728.

Wadiche JI, Arriza JL, Amara SG, Kavanaugh MP (1995b) Kinetics of a human glutamate transporter. Neuron 14:1019-1027.

Wafford KA, Bain CJ, Le Bourdelles B, Whiting PJ, Kemp JA (1993) Preferential co-assembly of recombinant NMDA receptors composed of three different subunits. Neuroreport 4:1347-1349.

Wafford KA, Kathoria M, Bain CJ, Marshall G, Le Bourdelles B, Kemp JA, Whiting PJ (1995) Identification of amino acids in the N-methyl-D-aspartate receptor NR1 subunit that contribute to the glycine binding site. Mol Pharmacol 47:374-380.

Wang H, Olsen RW (2000) Binding of the GABA(A) receptor-associated protein (GABARAP) to microtubules and microfilaments suggests involvement of the cytoskeleton in GABARAP-GABA(A) receptor interaction. J Neurochem 75:644-655.

Wang H, Bedford FK, Brandon NJ, Moss SJ, Olsen RW (1999) GABA(A)-receptor-associated protein links GABA(A) receptors and the cytoskeleton. Nature 397:69-72.

Wang TL, Guggino WB, Cutting GR (1994) A novel gamma-aminobutyric acid receptor subunit (rho 2) cloned from human retina forms bicuculline-insensitive homooligomeric receptors in Xenopus oocytes. J Neurosci 14:6524-6531.

Wang YH, Bosy TZ, Yasuda RP, Grayson DR, Vicini S, Pizzorusso T, Wolfe BB (1995) Characterization of NMDA receptor subunit-specific antibodies: distribution of NR2A and NR2B receptor subunits in rat brain and ontogenic profile in the cerebellum. J Neurochem 65:176-183.

Wassle H, Koulen P, Brandstatter JH, Fletcher EL, Becker CM (1998) Glycine and GABA receptors in the mammalian retina. Vision Res 38:1411-1430.

Watanabe M, Mishina M, Inoue Y (1994) Distinct spatiotemporal expressions of five NMDA receptor channel subunit mRNAs in the cerebellum. J Comp Neurol 343:513-519.

Watase K, Hashimoto K, Kano M, Yamada K, Watanabe M, Inoue Y, Okuyama S, Sakagawa T, Ogawa S, Kawashima N, Hori S, Takimoto M, Wada K, Tanaka K (1998) Motor discoordination and increased susceptibility to cerebellar injury in GLAST mutant mice. Eur J Neurosci 10:976-988.

Watkins JC (2000) l-glutamate as a central neurotransmitter: looking back. Biochem Soc Trans 28:297-309.

Wegelius K, Reeben M, Rivera C, Kaila K, Saarma M, Pasternack M (1996) The rho 1 GABA receptor cloned from rat retina is down-modulated by protons. Neuroreport 7:2005-2009.

Wegelius K, Pasternack M, Hiltunen JO, Rivera C, Kaila K, Saarma M, Reeben M (1998) Distribution of GABA receptor rho subunit transcripts in the rat brain. Eur J Neurosci 10:350-357.

Werblin FS, Dowling JE (1969) Organization of the retina of the mudpuppy, Necturus maculosus. II. Intracellular recording. J Neurophysiol 32:339-355.

Westbrook GL, Mayer ML (1987) Micromolar concentrations of Zn^{2+} antagonize NMDA and GABA responses of hippocampal neurons. Nature 328:640-643.

Wiche G, Oberkanins C, Himmler A (1991) Molecular structure and function of microtubule-associated proteins. Int Rev Cytol 124:217-273.

Williams K, Romano C, Molinoff PB (1989) Effects of polyamines on the binding of [3H]MK-801 to the N-methyl-D- aspartate receptor: pharmacological evidence for the existence of a polyamine recognition site. Mol Pharmacol 36:575-581.

Wolosker H, Blackshaw S, Snyder SH (1999) Serine racemase: a glial enzyme synthesizing D-serine to regulate glutamate-N-methyl-D-aspartate neurotransmission. Proc Natl Acad Sci U S A 96:13409-13414.

Woodward RM, Polenzani L, Miledi R (1992a) Characterization of bicuculline/baclofen-insensitive gamma-aminobutyric acid receptors expressed in Xenopus oocytes. I. Effects of Cl^- channel inhibitors. Mol Pharmacol 42:165-173.

Woodward RM, Polenzani L, Miledi R (1992b) Effects of steroids on gamma-aminobutyric acid receptors expressed in Xenopus oocytes by poly(A)+ RNA from mammalian brain and retina. Mol Pharmacol 41:89-103.

Woodward RM, Polenzani L, Miledi R (1993) Characterization of bicuculline/baclofen-insensitive (rho-like) gamma- aminobutyric acid receptors expressed in Xenopus oocytes. II. Pharmacology of gamma-aminobutyric acidA and gamma-aminobutyric acidB receptor agonists and antagonists. Mol Pharmacol 43:609-625.

Woodward RM, Huettner JE, Guastella J, Keana JF, Weber E (1995a) In vitro pharmacology of ACEA-1021 and ACEA-1031: systemically active quinoxalinediones with high affinity and selectivity for N-methyl-D- aspartate receptor glycine sites. Mol Pharmacol 47:568-581.

Woodward RM, Huettner JE, Tran M, Guastella J, Keana JF, Weber E (1995b) Pharmacology of 5-chloro-7-trifluoromethyl-1,4-dihydro-2,3- quinoxalinedione: a novel systemically active ionotropic glutamate receptor antagonist. J Pharmacol Exp Ther 275:1209-1218.

Wotring VE, Chang Y, Weiss DS (1999) Permeability and single channel conductance of human homomeric rho1 $GABA_C$ receptors. J Physiol (Lond) 521 Pt 2:327-336.

Wu SM, Maple BR (1998) Amino acid neurotransmitters in the retina: a functional overview. Vision Res 38:1371-1384.

Wyllie DJ, Behe P, Colquhoun D (1998) Single-channel activations and concentration jumps: comparison of recombinant NR1a/NR2A and NR1a/NR2D NMDA receptors. J Physiol 510:1-18.

Xia J, Zhang X, Staudinger J, Huganir RL (1999) Clustering of AMPA receptors by the synaptic PDZ domain-containing protein PICK1. Neuron 22:179-187.

Yamada K, Watanabe M, Shibata T, Tanaka K, Wada K, Inoue Y (1996) EAAT4 is a post-synaptic glutamate transporter at Purkinje cell synapses. Neuroreport 7:2013-2017.

Yamazaki M, Araki K, Shibata A, Mishina M (1992) Molecular cloning of a cDNA encoding a novel member of the mouse glutamate receptor channel family. Biochem Biophys Res Commun 183:886-892.

Yang XL, Wu SM (1991) Feedforward lateral inhibition in retinal bipolar cells: input-output relation of the horizontal cell-depolarizing bipolar cell synapse. Proc Natl Acad Sci U S A 88:3310-3313.

Yeh HH, Grigorenko EV, Veruki ML (1996) Correlation between a bicuculline-resistant response to GABA and $GABA_A$ receptor rho 1 subunit expression in single rat retinal bipolar cells. Vis Neurosci 13:283-292.

Zafra F, Aragon C, Olivares L, Danbolt NC, Gimenez C, Storm-Mathisen J (1995) Glycine transporters are differentially expressed among CNS cells. J Neurosci 15:3952-3969.

Zerangue N, Kavanaugh MP (1996) Flux coupling in a neuronal glutamate transporter. Nature 383:634-637.

Zerangue N, Arriza JL, Amara SG, Kavanaugh MP (1995) Differential modulation of human glutamate transporter subtypes by arachidonic acid. J Biol Chem 270:6433-6435.

Zhang D, Pan Z, Awobuluyi M, Lipton SA (2001) Structure and function of GABA(C) receptors: a comparison of native versus recombinant receptors. Trends Pharmacol Sci 22:121-132.

Zhang D, Pan ZH, Zhang X, Brideau AD, Lipton SA (1995) Cloning of a gamma-aminobutyric acid type C receptor subunit in rat retina with a methionine residue critical for picrotoxinin channel block. Proc Natl Acad Sci U S A 92:11756-11760.

Zhao HM, Wenthold RJ, Wang YX, Petralia RS (1997) Delta-glutamate receptors are differentially distributed at parallel and climbing fiber synapses on Purkinje cells. J Neurochem 68:1041-1052.